UNIVERSITEIT GENT

Ozonation and UV/hydrogen peroxide treatment of natural water and secondary wastewater effluent: experimental study and mathematical modelling

ing. Wim Audenaert

Thesis submitted in fulfillment of the requirements for the degree of Doctor (PhD) of Applied Biological Sciences

BIOMATH

ENBICHEM RESEARCH GROUP

I love the smell of ozone in the morning

Examination Committee
Prof. dr. ir. Paul Van der Meeren (Chair, Ghent University)
Prof. dr. ir. Kristof Demeestere (Ghent University)
Prof. dr. ir. Arne Verliefde (Ghent University)
Prof. dr. Santi Esplugas (University of Barcelona, Spain)
Prof. dr. ir. Luuk Rietveld (Delft University of Technology, the Netherlands)
dr. ir. Jochen Türk (Institut für Energie- und Umwelttechnik e.V., Germany)

Promotors
Prof. dr. ir. Ingmar Nopens
Department of Mathematical Modelling, Statistics and Bioinformatics
BIOMATH research group: Model-based analysis and optimization of bioprocesses
Faculty of Bioscience Engineering
Ghent University

Prof. dr. ir. Stijn Van Hulle
ENBICHEM research group
University College West Flanders

Dean
Prof. dr. ir. Guido Van Huylenbroeck

Rector
Prof. dr. Paul Van Cauwenberge

ing. Wim Audenaert

Ozonation and UV/hydrogen peroxide treatment of natural water and secondary wastewater effluent: experimental study and mathematical modelling

Thesis submitted in fulfillment of the requirements for the degree of Doctor (PhD) of Applied Biological Sciences

Dutch translation of the title:
Ozonisatie en UV/waterstofperoxide behandeling van natuurlijk water en secundair effluent: experimentele studie en wiskundige modellering

Please refer to this work as follows:
Audenaert, W.T.M., 2012. Ozonation and UV/hydrogen peroxide treatment of natural water and secondary wastewater effluent: experimental study and mathematical modelling. PhD thesis, Ghent University, Belgium.

ISBN: 978-90-5989-565-2

Dankwoord

Om nu eens met een echt cliché te beginnen: wat vliegt de tijd. In 1998 (einde van mijn lagere schoolopleiding) zaten mijn ouders met de handen in het haar. “Wat doen we met die jongen die niet wil leren?” Gelukkig werd opgemerkt dat ik het toch op één vak goed deed: natuurkennis. De beslissing om mij in de richting van de wetenschappen te sturen zou later een goede keuze blijken te zijn. In januari 2009 begon ik aan een echte uitdaging: een doctoraat. Ik kende zeer weinig van oxidatieve waterbehandeling, niets van geavanceerde oxidatie, laat staan van de wiskundige modellering van deze processen. Vandaag finaliseer ik hierover mijn proefschrift, iets wat mij toen nog heel ver weg leek. Ik ben zeer blij dat ik dit gedaan heb en niet alleen omdat ik het werk heel graag deed, maar ook omdat er talrijke toffe mensen direct of indirect bijdroegen tot dit resultaat. Dit zou dan ook geen dankwoord zijn als ik deze mensen hier niet oprecht zou bedanken.

Ik begin bij mijn promotoren: Ingmar Nopens en Stijn Van Hulle. Ingmar en Stijn, bedankt voor jullie hulp, steun, gedrevenheid en goedlachsheid. Jullie professionalisme en doelgerichte aanpak stimuleerden continue vooruitgang in het onderzoek. Als het “serieus” moest zijn, was het ook zo, als er mocht gelachen worden, werd er ook gelachen. Dit perfect evenwicht tussen productiviteit en ontspanning brengen jullie met succes over op jullie onderzoeksteams. Bedankt voor de unieke kans die jullie mij gaven.

Op wetenschappelijk vlak werkte ik samen met meerdere fantastische mensen. Ik wil Hans Pattyn van het VTI Poperinge oprecht bedanken omdat ik enkele weken met de UV-reactor mocht ‘spelen’. Dat lassersoog ben ik al vergeten. Verder bedank ik Jan Cromphout van de VMW voor de vlotte gegevensuitwisseling en de mogelijkheid om een studie uit te voeren op de mooie site in Kluizen. Graag bedank ik ook Petra Ross en Luuk Rietveld van TU Delft omdat ik hen mocht vergezellen naar Riga waar ik de kans kreeg om enkele staalnames uit te voeren. Voor DOC-analyses kon ik op elk moment terecht op de KHBO. Daarom bedank ik met plezier Annick Monballiu, Evelyn Desmidt en Boudewijn Meesschaert. Tenslotte wil ik nog een woordje van dank richten naar alle mensen die hun steentje bijdroegen in de organisatie van de afgelopen YWP Benelux conferenties.

Gewoonweg fantastisch om met Arne Verliefde als ‘trekker’ een conferentie te organiseren. Arne, bedankt voor de onvergetelijke momenten (en kebab).

Mijn collega’s op de beide departementen waar ik werkte, zorgden altijd voor een fantastische atmosfeer (met of zonder ozon erin). Ik start met de groep van de HOWEST in Kortrijk. Het was fantastisch om deel uit te maken van het Kernteam Chemie met Joël, Yannick en Pascal. Joël, bescherm uw pompoenplanten voor Betty; Yannick, uw druivenplanten groeien weelderig op mijn muur en pas op voor trolley’s op publieke plaatsen; Pascal, bedankt voor de ochtendlijke koffiekletsen met José ten gunste van het ozonkot. Kevin, Sam, Dries, Ellen, Ann (V), Kathelijne, Han, Veerle, Michael, Bjorge, Annelies, Justine, Kristof, Imca, Katleen, Jan, Diederik, Ann (D), bedankt voor talrijke zeer uiteenlopende zaken. Caroline bedankt voor de ondersteuning i.v.m. de practica’s chemie. Nele, bedankt voor de ondersteuning in Leuven. Bernard, bedankt dat ik beroep mocht doen op de zuurstofprobe en koelcel. VLAKWA-babes Charlotte en Veerle, bedankt voor jullie aanmoedigingen. Gerdi en Xavier, bedankt voor het soldeerwerk, het uitlenen van de boormachine en andere technische zaken. Lieven, ik apprecieerde uw pogingen om mij te converteren in tjeef, maar helaas is het niet gelukt. Manly, Yoshi, Michael, Mathieu, Liselot en Dieter: het was meer dan aangenaam jullie als thesisstudenten te begeleiden.

BIOMATH-weekends, BIOMATH-feestjes, BIOMATCHEN, ..., één voor één waren ze onvergetelijk en resulteerden ze in talrijke anekdotes die, indien ik ze hier zou vermelden, de printkosten zouden doen verdubbelen. Buurman Stijn, bedankt voor de ambiance in het simulatielab en voor uw hulp op diverse gebieden. Van ondersteuning in software tot ondersteuning op de weg, je stond altijd klaar! Katrijn, je bent altijd bezig met onzekerheid. Wees van één ding zeker: je was een fantastische collega met een permanente lach. Thomas, of je nu geel of groen bent, ik dank je voor uw fantastische humor. Ons optimaal experimenteel ontwerp i.v.m. het aansteken van een sigaar zal ik nooit vergeten. Elena, het was de max om met jou samen te werken, iets minder om met jou een fles La Chouffe leeg te drinken. Youri, Wouter, Webbey, Lorenzo, Ward, Karel, Séverine, grote Giacomo, kleine Giacomo, Abhishek, Mehul, Andres, Tarad en Ashish, bedankt voor uiteenlopende werk- en niet-werkgerelateerde zaken. Timpe, Roos, Viv, Annie, bedankt om de administratieve zaken te regelen. Ronny, bedankt voor jouw Dana Winner-hits. Tinne, uw taarten en andere baksels waren veel beter dan deze van de bakker, bedankt hiervoor. BIOMATCH, vergeet nooit onze succesvolle voetbalkern en laat jullie goed managen bij de nakende transfers naar topclubs.

Dit doctoraat was niet tot stand gekomen zonder mijn goede familie en vrienden. Papa en mama, bedankt voor de talrijke kansen die jullie mij gaven en voor de onvoorwaardelijke steun. Mijn toffe broeremannen Piet, Jan en Bert met jullie mooie gezinnetjes, ook bedankt voor jullie support! Pepe Fiel en Meme Monique, bedankt om de T en de M van Wim T.M. te zijn. Schoonbroer Koen, bedankt voor de technische tekening van mijn reactor. Beste schoonfamilie, bedankt voor jullie steun. Vrienden, bedankt voor de toffe ontspanningsmomenten tussendoor.

Als laatste wil ik nog mijn Katrientje bedanken omdat ze van mij zo'n gelukkig persoon maakt. Zonder haar dagdagelijkse steun was dit nooit mogelijk geweest. En lieve kleine Leonie, je bent zo'n schattige meid die mij elke dag doet glunderen van plezier. Jij en je broertje of zusje (dat tijdens dit schrijven de laatste voorbereidingen treft voor zijn of haar geboorte) geven mij de motivatie om er elke dag volop voor te gaan. Dit doctoraat draag ik dan ook grotendeels op aan ons gezinnetje.

Gent, 23 november 2012

Table of contents

List of abbreviations and symbols

a	specific interfacial area of gas bubbles ($m^2\ m^{-3}$)
A	absorbance (-)
AMW	apparent molecular weight (Da)
AWTP	advanced water treatment plant
AOC	assimilable organic carbon
AOP	advanced oxidation process
ASF	absolute sensitivity function
ASI	absorbance slope index
b	optical path length (cm)
bDOC	biodegradable fraction of DOC
BGAC	biological granular activated carbon
BOD	biochemical oxygen demand (mg L^{-1})
CAGR	compound annual growth rate (%)
CAS	conventional activated sludge
CAPEX	capital expenditure
CSTR	completely stirred tank reactor
CFD	computational fluid dynamics
CFU	colony forming unit
CHA	charged hydrophilic fraction
C_i	concentration of compound i (M)
C_{O2_L}	oxygen concentration in the liquid phase (mg L^{-1})
C_{O2_L0}	initial dissolved oxygen concentration (mg L^{-1})
$C_{O2\_L}^*$	equilibrium concentration of oxygen in the liquid phase (mg L^{-1})
C_{O3_G}	ozone concentration in the gas phase (mol L^{-1})
C_{O3_L}	ozone concentration in the liquid phase (mg L^{-1})
$C_{O3\_L}^*$	equilibrium concentration of ozone in the liquid phase (mg L^{-1})
C_T	total inorganic carbon (mM)
COD	chemical oxygen demand (mg L^{-1})
D_a	diffusion coefficient of gas a ($m^2\ s^{-1}$)
Da	Dalton (unit of AMW)
DAEs	differential and algebraic equations

DAS	differential absorbance spectra
DBCP	1,2-Dibromo-3-chloropropane
DBPs	disinfection by products
D_{O2}	diffusion coefficient of oxygen ($m^2 s^{-1}$)
D_{O3}	diffusion coefficient of ozone ($m^2 s^{-1}$)
DOC	dissolved organic carbon (mg L^{-1})
DOM	dissolved organic matter
E_0	UV fluence rate (mW cm^{-2})
EA_3G	European, African, Asian, Australasian group of the IOA
EDCs	endocrine disrupting compounds
EfOM	effluent organic matter
E(t')	dimensionless hydraulic residence time distribution (-)
f_i	fraction of UV absorbed by compound i (-)
GAC	granular activated carbon
GWRS	Groundwater Replenishment System
H	UV fluence (mJ cm^{-2})
h^+	electron hole
H_e	Henry's constant (L atm mol^{-1})
HGE	hierarchical graphical editor
$HO^{\bullet}$	hydroxyl radical
HPSEC	high performance size exclusion chromatography
HRT	hydraulic residence time (h)
I_0	incident (volume based) photon flux (Einsteins $L^{-1} s^{-1}$)
IOA	International Ozone Association
IOD	instantaneous ozone demand
IPR	indirect potable reuse
J(θ)	objective function
k	first or second order reaction rate constant (s^{-1} or $M^{-1} s^{-1}$)
k_L	individual liquid phase mass transfer coefficient (m s^{-1})
k_La	volumetric mass-transfer coefficient (s^{-1})
k_La_{O2}	volumetric mass-transfer coefficient for oxygen (s^{-1})
k_La_{O3}	volumetric mass-transfer coefficient for ozone (s^{-1})
$k_{O3/Br}$	reaction rate constant for reaction between ozone and bromide ($m^3.g^{-1} s^{-1}$)
$k_{O3/P}$	2nd order rate constant for reaction of pollutant P with ozone ($M^{-1} s^{-1}$)
$k_{O3/UV254}$	second order rate constant for the reaction of UV_{254} with ozone ($m^3 g^{-1} s^{-1}$)

$k_{O3/X}$	ozone inactivation rate constant for a particular microorganism ($m^3\ g^{-1}\ s^{-1}$)
$k_{HO•/P}$	2nd order rate constant for reaction of pollutant P with hydroxyl radicals ($M^{-1}\ s^{-1}$)
k'_{app}	apparent first order ozone decomposition rate constant (s^{-1})
k'_d	pseudo-first order rate constant for direct photolysis (s^{-1})
k'_T	overall pseudo first order rate constant (s^{-1})
k'^D_d	fluence based pseudo-first order rate constant for direct photolysis ($cm^2\ mJ^{-1}$)
k'^D_T	fluence based overall pseudo first order rate constant ($cm^2\ mJ^{-1}$)
LHS	Latin Hypercube Sampling
LOX	liquid oxygen
LP-HO	low pressure high output
LP-UV	low pressure UV
LSA	local sensitivity analysis
M	molecular mass ($g\ mol^{-1}$)
MCL	maximum contaminant level
MF	microfiltration
MIB	2 methyl isoborneol
MP-UV	medium pressure UV
MSL	model specification language
MTBE	methyl tertiary butyl ether
MW	molecular weight (Da)
N	number of data points
NDMA	N-nitrosodimethylamine
NEU	neutral hydrophilic fraction
NOM	natural organic matter
OCD	organic carbon detection
ODE	ordinary differential equation
OPEX	operational expenditure
P	a certain target pollutant
PAC	powdered activated carbon
pCBA	para-chlorobenzoic acid
PCE	perchloroethylene
PDF	probability density function
p.e.	person equivalents
P_{O3}	partial pressure of ozone in the gas phase (atm)
PPCPs	pharmaceuticals and personal care products

PSA	pressure swing adsorption
Q	water flow rate (L h^{-1})
R	ideal gas constant (L atm K^{-1} mol^{-1})
R_{CT}	ratio of hydroxyl radical exposure and ozone exposure (-)
RO	reverse osmosis
$R_{OH,UV}$	ratio of hydroxyl radical exposure and UV fluence (M s cm^2 mJ^{-1})
RSF	relative sensitivity function
RWPF	raw water production facility
SA	sensitivity analysis
SF	sensitivity function
SHA	slightly hydrophobic acid fraction
SHB	Staehelin Hoigné Bühler
S_i	scavenger species i
SMPs	soluble microbial products
SOM	self-organizing map
SRC	standardized regression coefficient
SRT	sludge residence time (d)
SS	steady-state
SUVA	specific UV absorbance ((mg C/L)$^{-1}$ cm^{-1})
TCE	trichloroethene
TFG	Tomiyasu, Fukutomi and Gordon
THM	trihalomethane
THMFP	trihalomethane formation potential
TIC	Theil's inequality coefficient (-)
TIS	tanks-in-series
TOC	total organic carbon (mg L^{-1})
TOD	transferred ozone dose (mg L^{-1})
tSRC	t-statistic value of standardized regression coefficients (-)
T&O	taste and odour
t'	dimensionless time (-)
U_{254}	energy per mole of photons (J $Einstein^{-1}$)
UV	ultraviolet
UV_{254}	decadic UV absorption coefficient at 254 nm (cm^{-1})
UV_{254}^{S}	soluble fraction of UV_{254} (cm^{-1})
UV_{254}^{X}	particulate fraction of UV_{254} (cm^{-1})
UV_{310}	decadic UV absorption coefficient at 310 nm (cm^{-1})
UV_{310}^{S},	soluble fraction of UV_{310} (cm^{-1})
UV_{310}^{X}	particulate fraction of UV_{310} (cm^{-1})

UV-VIS	UV-visible
V	volume (L)
VHA	very hydrophobic acid fraction
VMW	Flemish Water Supply Company
VOCs	volatile organic chemicals
w_j	weight factor for variable j (-)
WRF	water reclamation facility
WSSE	weighted sum of squared errors
WTP	water treatment plant
WWTP	municipal wastewater treatment plant
x	solvent association parameter (-)
X_{bact}	viable micro-organisms
$Y_{A/B}$	stoichiometry factor for the reaction between species A and B
$y_{cond,m}(t)$	measured conductivity as function of time
y_j	output variable j
$y_{ij}(\theta)$	model prediction of variable j at time i
$\hat{y}_{ij}$	experimental data of variable j at time i
α_λ	decadic absorption coefficient (cm^{-1})
δ_L	thickness of liquid film layer (m)
ε_{UV310S}	molar absorption coefficient of $UV_{310}{}^S$ at 254 nm (cm^{-1}/cm^{-1})
ε_{UV310X}	molar absorption coefficient of $UV_{310}{}^X$ at 254 nm (cm^{-1}/cm^{-1})
$\varepsilon_{\lambda,i}$	molar absorption coefficient of compound i at wavelength λ (M^{-1} cm^{-1})
ζ	perturbation factor (-)
η	dynamic viscosity of a solution (centipoise)
θ_n	nominal parameter value
$\hat{\theta}$	optimized parameter values
λ	wavelength (nm)
ρ	density ($g\ L^{-1}$)
ϕ	primary quantum yield (-)
Φ	overall quantum yield (-)

Chapter 1

Introduction, objectives and outline

1.1 Introduction

Multiple factors impose severe stress on the global water system and urban water supplies. These factors include worldwide population growth, depletion of groundwater resources, uneven geographical spread of water resources, population growth in water scarce areas and increasing water consumption per capita (Jiménez et al., 2008). Additionally, the occurrence of emerging contaminants such as endocrine disrupting compounds (EDCs), pharmaceuticals and personal care products (PPCPs) is a potential risk for both the environment and human health (Daughton and Ternes, 1999; Heberer, 2002; Kolpin et al., 2002; Gerrity and Snyder, 2011).

Hence, the interest in advanced water and wastewater treatment systems in view of water reuse and the removal of these harmful compounds is significantly increasing. Technologies that have found to be effective in this context include membrane filtration (Drewes et al., 2003) and (advanced) oxidation processes (Malley, 2010; Gerrity and Snyder, 2011; Loeb et al., 2012).

Oxidation processes, and especially ozonation and ultraviolet (UV) irradiation in combination with hydrogen peroxide (H_2O_2) will be the topics of interest in this PhD dissertation. The UV/H_2O_2 process is generally called an advanced oxidation process (AOP) as it relies on the production of the reactive hydroxyl radical ($HO^{\bullet}$). The main advantage that these processes hold over other techniques is that target pollutants are (partially) destroyed, rather than transferred to another phase which is the case during adsorption or membrane filtration processes (Parsons, 2004).

Ozone is applied as a drinking water disinfectant for already more than a century with early applications in France (Le Paulouë and Langlais, 1999). Currently, thousands of drinking water applications exist worldwide (Oneby et al., 2010). Very recently, the use of ozone for advanced municipal wastewater treatment

and/or water reuse prevailed (Mielcke and Ried, 2012; Loeb et al., 2012). These applications rely on both the disinfecting and oxidative power of the ozone molecule.

In contrast to ozonation, the UV/H_2O_2 process has only few drinking water applications with all of them being installed during the last decade. Often, this AOP is applied to remove unwanted organic compounds (Sarathy and Mohseni, 2006) or to restrict bromate formation (Kruithof et al., 2007). The latter is an important drawback of the ozonation process as bromide which is naturally present in the water will be oxidized to the carcinogenic bromate by ozone. With respect to advanced municipal wastewater treatment, the UV/H_2O_2 technology (often preceded by membrane filtration) has several large-scale project applications (Leach et al., 2006).

According to a report published by Global Water Intelligence, the global water industry is expected to grow at a slow rate of 5.6% between 2007 and 2016. However, as shown in Figure 1.1, the markets of ozone and AOP applications are expected to grow much faster at compound annual growth rates (CAGRs) of 7.6 and 31.9%, respectively. New applications of these oxidation technologies are expected to arise especially in developed countries (Loeb et al., 2012).

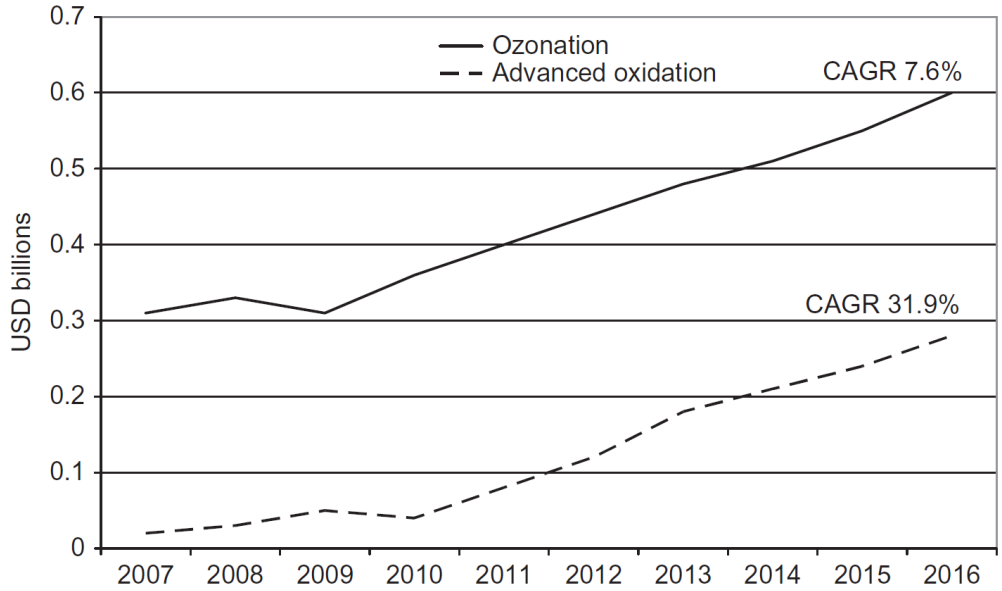

Figure 1.1: Expected growth for ozone and AOP market (Loeb et al., 2012)

Despite the current interest and rapidly growing number of applications, the design and operation of ozone and UV/H_2O_2 processes for advanced water and wastewater treatment still have to be optimized. In this context, mathematical models can be of great value as they allow for prediction of process efficiency at different

operational and water quality conditions and hence, allow for virtually testing a multitude of scenarios before actual implementation in practice. However, despite extensive research on the reactions taking place during oxidation, the chemical complexity of the processes currently impedes modelling efforts. This knowledge gap has to be filled in order to enable optimal process design and operation and hence, cost effective advanced water treatment.

1.2 Aims and objectives

A thorough understanding of ozonation and UV/H_2O_2 processes is of vital importance for their effective and optimal application. The oxidation pathways in pure water systems (in the absence of inorganic and organic matter) are very well known and many of the elementary reactions have been described in literature. This knowledge gave rise to well defined kinetic models. However, real system applications deal with water that contains numerous organic and inorganic compounds. In those cases, the degree of complexity severely restricts the level of detail that kinetic models can reach. Hence, in many cases empirical approaches are used to cope with the lack of mechanistic knowledge. Nevertheless, the development of adequate (semi-)mechanistic models is essential as these models are much more valuable during process design, control and optimization compared to the empirical ones. The model structure of mechanistic models is to a certain degree a reflection of the real system and hence, these models are more flexible and robust if the system conditions change.

As shown in Figure 1.2, micropollutants such as EDCs or PPCPs will be transformed during oxidative water treatment. On the other hand, an important fraction of the oxidant (ozone and $HO^{\bullet}$) will be consumed by dissolved organic matter (DOM). The concentration and properties of DOM are highly source dependent and a major part of its content consists of very complex molecules such as natural organic matter (NOM). The presence of DOM is the main reason for the system complexity associated with "real water" oxidation. Figure 1.2 also illustrates the difference between ozonation and UV/H_2O_2 treatment. During ozonation, ozone will react with organic compounds after which transformation products are formed. Some of the reactions between DOM and ozone will give rise to free radicals ($O_3^{\bullet-}$ and $O_2^{\bullet-}$) which in their turn directly or indirectly give rise to $HO^{\bullet}$ production. Hence, the importance of $HO^{\bullet}$ induced oxidation during an ozonation process depends on both the concentration and properties of DOM. In most of the cases, the reaction between ozone and the hydroxyl ion is of minor importance. Contrastingly, the UV/H_2O_2 process only relies on $HO^{\bullet}$ attack and due

to the absence of ozone, the process is somewhat less complex. Noteworthy, however, is that Figure 1.2 depicts a highly simplified reaction scheme and only the most important reactions with regard to organic compound oxidation are included. Furthermore, the transformation products in their turn will react with the oxidants, which is not indicated in the scheme.

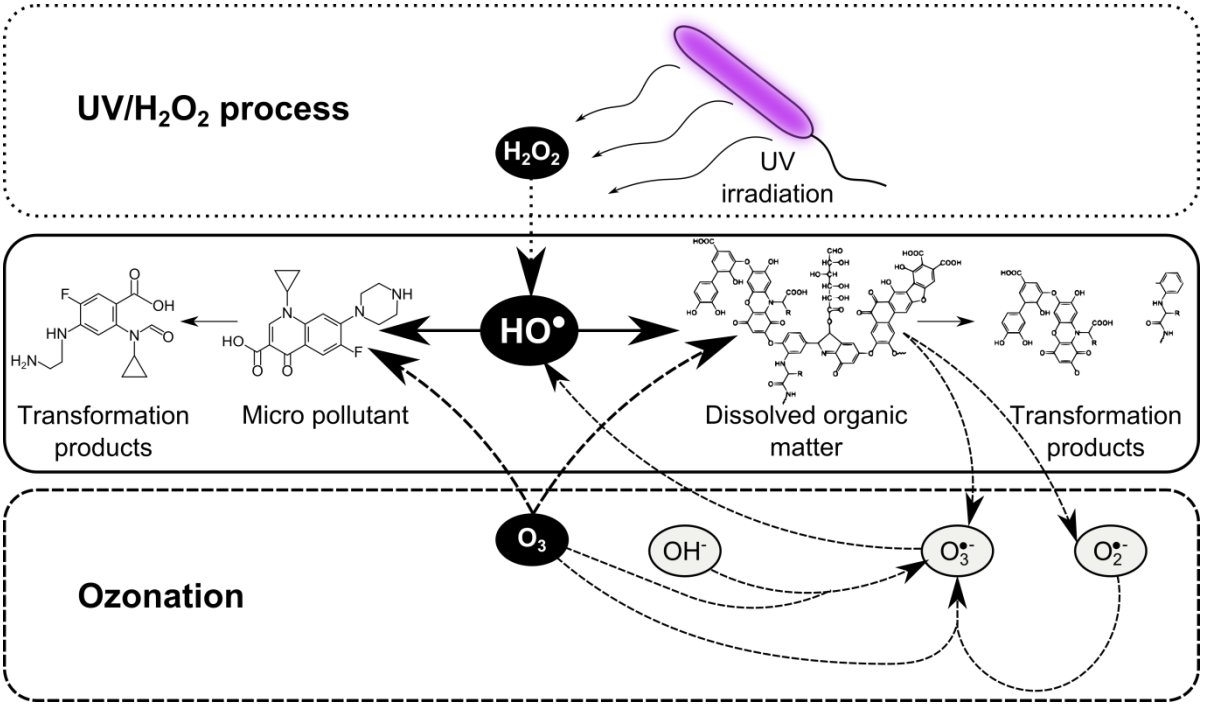

Figure 1.2: Major reaction pathways of organic contaminant attack during ozonation and UV/H_2O_2 treatment

In this PhD dissertation, ozonation and UV/H_2O_2 treatment of "real water" are studied. Several reactors (lab-scale or full-scale) treating natural water or secondary treated wastewater are used to calibrate and validate mechanistic models. As such, a combination of practical experimentation and mathematical modelling at various operational and water quality conditions is the major scientific contribution of the work performed during this study. The main objectives are to:

(i) evaluate the performance of existing mechanistic models using real water matrices

(ii) determine the key elementary reactions and parameters of the models in order to reveal possible improvements of the existing model structures

(iii) gather insight into the reaction mechanisms

(iv) study and compare ozone and $HO^{\bullet}$ induced conversions of DOM using multiple surrogates

(v) evaluate the usage of several surrogates for DOM in mathematical models and to propose new surrogates for future model development

1.3 Outline

The outline of this thesis and the relation between the different chapters is presented in Figure 1.3. The chapters involve mathematical simulation (in the figure denoted as "virtual world"), practical experimentation (in the figure denoted as "real world") as well as combinations of both. Chapters 2 and 3, respectively dealing with the state-of-the-art and description of adopted methods in this work are not included in the figure.

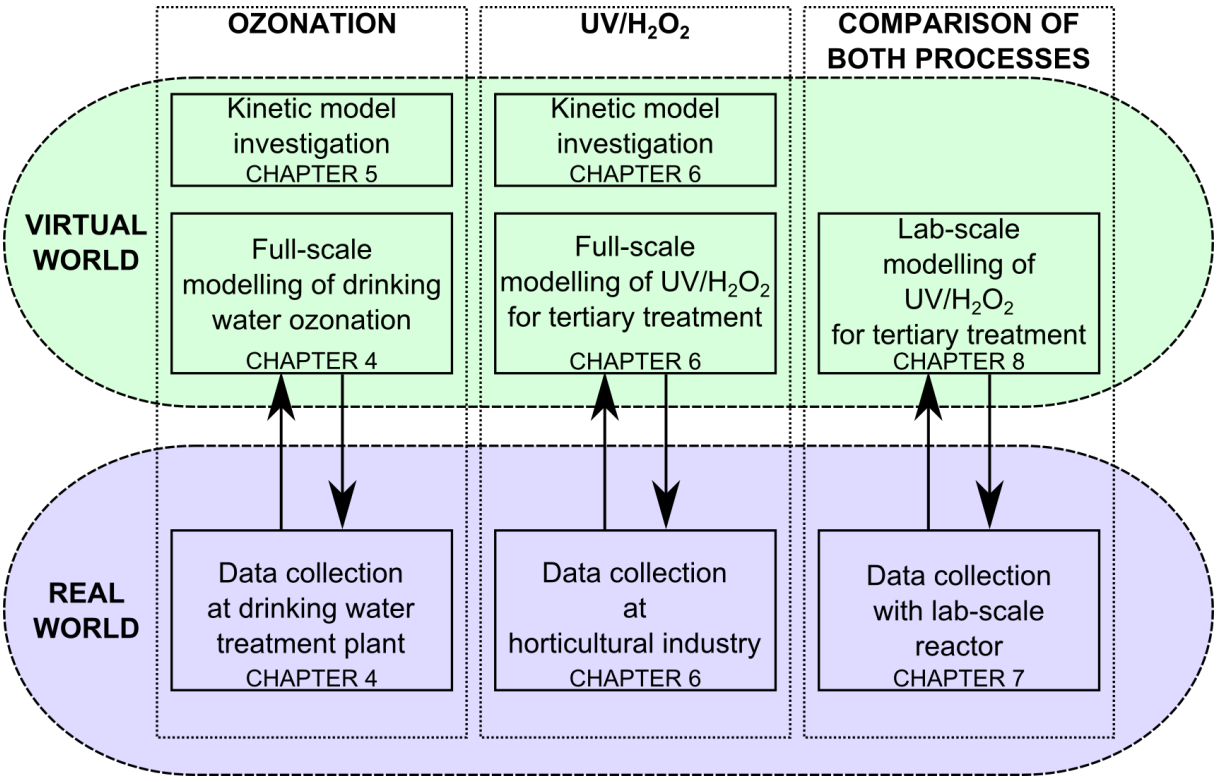

Figure 1.3: Outline of this dissertation

Chapter 2 is a literature review consisting of two major parts. The first part involves fundamentals of ozonation and UV/H_2O_2 treatment of water and wastewater. The second part describes important trends and developments related to the practical application of both processes.

Chapter 3 provides information on the methods used to perform the simulations.

Chapter 4 describes the application of a relatively simple ozone model at a drinking water treatment plant for prediction of disinfection efficiency, bromate formation, ozone decomposition and oxidation of the unsaturated part of DOM.

Chapter 5 is related to a theoretical study of an extensive mechanistic ozone decomposition model. A sensitivity analysis was used to determine the most important model parameters and to provide further insight in the reaction mechanism.

Chapter 6 presents the application of a mechanistic UV/H_2O_2 model at full-scale. Model calibration and validation was performed and the most important process parameters were determined.

Chapter 7 discusses a lab-scale investigation of ozone and $HO^{\bullet}$ driven conversion of effluent organic matter present in secondary effluent of a municipal wastewater treatment plant. Multiple properties of the organic matrix were studied and both processes were compared.

Chapter 8 involves the application of the model used in Chapter 6 to the UV/H_2O_2 experiments performed in Chapter 7. The model was calibrated and validated using the lab-scale data.

Chapter 9 contains the final conclusions of this thesis combined with some perspectives and opportunities for future research.

Chapter 2

Literature review

2.1 Introduction

Recent developments regarding water scarcity and water pollution have led to an increased interest in advanced water and wastewater treatment technologies such as membrane filtration and oxidation processes. Especially oxidation technologies such as ozonation and UV/H_2O_2 treatment are considered as promising technologies which implies that the number of full-scale applications is rapidly growing (Leach et al., 2006; Sarathy and Mohseni, 2006; Ried et al., 2009; Oneby et al., 2010; Gerrity and Snyder, 2011; Loeb et al., 2012). Ozone is used for drinking water disinfection for already more than one century and UV/ H_2O_2 treatment has proven to be an effective technology for industrial wastewater treatment. Further, some important trends with respect to advanced (municipal) wastewater treatment and water reuse arose recently. Secondary effluent originating from municipal wastewater treatment plants is more often tertiary treated using oxidation technologies and in some cases, the treatment is performed in separate advanced water treatment facilities that are especially designed for water reuse (Leach et al., 2006; Loeb et al., 2012).

Due to these recent and rapid developments, there are still some knowledge gaps that have to be filled in order to design and operate these advanced treatment steps in an efficient way. This is of major importance, as advanced treatment is cost intensive. An important need is the construction of mathematical models that can be of significant value during process design and operation. Currently, some models are used for process design (Li et al., 2008; Alpert et al., 2010), but the modelling knowledge does not allow for model predictive control. Consequently, the control strategies that are currently applied for ozonation and UV/H_2O_2 processes are relatively simple and often, oxidant dosage is only based on the flow rate of the water to be treated, which is often suboptimal. Future improved models

based on a better understanding of the processes should allow the process control to be also affected by the water composition.

The first part of this chapter explains the fundamentals of oxidative treatment of water and wastewater. In a second part, the historical development, current applications and shortcomings and future growth potential of ozonation and UV/H_2O_2 processes for advanced water and wastewater treatment will be discussed.

2.2 Fundamentals of oxidation and advanced oxidation for water and wastewater treatment

2.2.1 Oxidation and advanced oxidation

If oxidation is applied for water in wastewater treatment, the aim is to oxidize pollutants to form relatively harmless transformation products. This transformation is called partial oxidation. If extensive oxidation is applied, mineralization can take place after which only inorganic compounds are left. The latter, however, is rarely applied as excessive oxidant doses are required. Oxidation of inorganic compounds implies the removal of electrons to reach a higher oxidation state, while oxidation of organic compounds is associated with the formation of more oxygen rich moieties (Parsons, 2004). Table 2.1 contains some common oxidizing agents with their relative strengths.

Table 2.1: Oxidative power of common oxidizing species (Parsons, 2004)

Oxidizing species	Oxidation potential (V)
Fluorine (F)	3.03
Hydroxyl radical ($HO^{\bullet}$)	2.80
Atomic oxygen (O)	2.42
Ozone (O_3)	2.07
Hydrogen peroxide (H_2O_2)	1.78
Hydroperoxyl radical ($HO_2^{\bullet}$)	1.70
Permanganate (MnO_4^-)	1.68
Hypobromous acid (HOBr)	1.59
Chlorine dioxide (ClO_2)	1.57
Hypochlorous acid (HOCl)	1.49
Chlorine (Cl_2)	1.36

Table 2.1 reveals that $HO^{\bullet}$ is the strongest oxidant after fluorine. Using this compound (*advanced oxidation*) virtually any compound present in the water matrix can be oxidized. Also ozone has a relatively high oxidation potential,

although this is significantly less than that of $HO^{\bullet}$. As a consequence, ozone reacts selectively with organic compounds with reaction rate constants spreading over more than nine orders of magnitude (<0.1 M^{-1} s^{-1} - $7x10^{9}$ M^{-1} s^{-1}). In contrast, $HO^{\bullet}$ is unselective due to its reactivity and rate constants vary over four orders of magnitude, with the major part of the values being in the order of 10^{9} M^{-1} s^{-1} (von Gunten, 2003a).

2.2.2 Advanced oxidation processes

If the $HO^{\bullet}$ is of significance during water or wastewater treatment, the process is called an *advanced oxidation process (AOP).* Numerous technologies exist to produce this reactive species, although few of them currently have practical applications (Parsons, 2004).

$HO^{\bullet}$ generation of AOPs is based on the use of oxidants (e.g. ozone, hydrogen peroxide), radiation sources (gamma rays, UV irradiation), ultrasound waves or catalysts (metal salts, metal oxides, semiconductors) (Parsons, 2004). In most of the cases, one of these elements is used in combination with one or more of the others.

The processes that are of importance in this dissertation are (1) the combination of UV-C irradiation with hydrogen peroxide (the UV/H_2O_2 process) and (2) ozonation. Although ozonation is not often called an AOP, significant $HO^{\bullet}$ production can occur in the presence of dissolved organic matter as will be discussed further in this work. These two technologies were chosen as they have already proven to be effective and practically and economically feasible technologies (Leach et al., 2006; Loeb et al., 2012).

Two other processes will be shortly discussed to illustrate the different ways of generating $HO^{\bullet}$: (1) UV-A irradiation in combination with a semiconductor (semiconductor photocatalysis) and (2) combination of hydrogen peroxide with Fe(II) (Fenton process). The initiation of these processes relies on completely different mechanisms.

2.2.2.1 Semiconductor photocatalysis

Production of $HO^{\bullet}$ during semiconductor photocatalysis relies on irradiation of the semiconductor catalyst surface. If the semiconductor is TiO_2 (the most frequently used semiconductor), UV light with a wavelength (λ) smaller than 380 nm is used (UV light energy exceeds the band gap energy). Electrons of the valence band become excited and can reach the conduction band energy level. The electron holes (h^{+}) can readily oxidize electron donors such as pollutants that are adsorbed at the catalyst surface. If the holes subtract electrons from adsorbed water molecules, $HO^{\bullet}$

is being formed, as shown in Figure 2.1. The free electrons react with an electron acceptor, which is oxygen (Beltrán, 2004; Parsons, 2004). Electrons of the conduction band, however, can recombine with the holes, which can significantly lower the efficiency of the process.

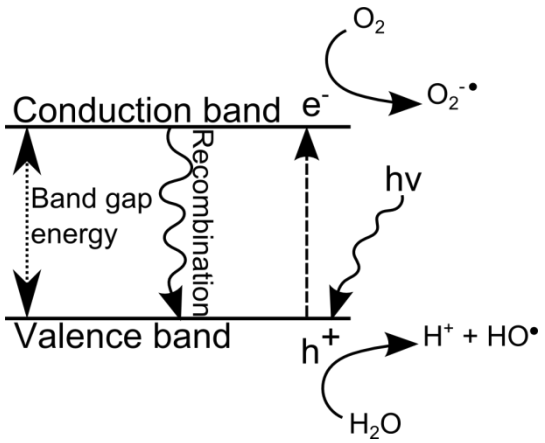

Figure 2.1: Schematic illustration of hydroxyl radical production during semiconductor photocatalysis

Today, no commercial applications of photocatalytic oxidation exist. Main problems that impede the application of this technology are the recombination of electrons and holes, poor absorption of solar light and the adsorption of water that hinders mobility of organics to the hydrophilic TiO_2 surface (Pichat, 2012).

2.2.2.2 The Fenton process

The Fenton process is based on decomposition of hydrogen peroxide catalysed by Fe(II) in acidic pH according to the following reaction (Pignatello et al., 2006):

$$Fe^{II} + H_2O_2 \rightarrow Fe^{III} + HO^{\bullet} + OH^- \quad (2.1)$$

Key parameters of this process include the Fe(II)/H_2O_2 ratio, pH and temperature (Neyens and Baeyens, 2003). At a pH value of around 3, process efficiency will be maximized. Although the $HO^{\bullet}$ production is efficient, an important drawback of this process is the precipitation of amorphous ferric oxylhydroxides from Fe(III) if the pH is increased (Pignatello et al., 2006).

This process has proven to be efficient in the destruction of refractory compounds and has some applications for the treatment of highly contaminated wastewaters such as textile wastewater containing dyes, pulp bleaching wastewater, effluents originating from wine and olive oil industry, landfill leachates and industrial wastewater (Pignatello et al., 2006). As such, wastewaters with a relatively high dissolved organic carbon (DOC) content can be treated by the Fenton process.

2.2.3 Fundamentals of ozonation

In most of the cases, ozone is known because of its presence in the stratosphere, where it protects the living species by absorbing UV-B and UV-C irradiation. This is merely one of numerous unique properties that can be addressed to the ozone molecule. Important physical-chemical properties of ozone are given in Table 2.2.

Table 2.2: Physical-chemical properties of ozone (Beltrán, 2004)

Property	Value
Melting point (°C)	-251
Boiling point	-112
Critical pressure (atm)	54.62
Critical temperature (°C)	-12.1
Specific gravity	1.658
Critical density (kg m^{-3})	436
Heat of vaporization (cal mol^{-1})	2,980
Heat of formation (cal mol^{-1})	33,880
Free energy of formation (cal mol^{-1})	38,860

Addition of ozone to a water system gives rise to a very complex reaction sequence and the complexity of the system significantly increases if dissolved organic matter is present. To date, numerous studies are focusing on the mechanisms of ozone decomposition in different water matrices.

2.2.3.2 Reactivity of the ozone molecule

The ozone molecule consists of three oxygen atoms, each having the following electronic configuration: $1s^2\ 2s^2\ 2p_x^2\ 2p_y^1\ 2p_z^1$. As a result of sp^2 hybridization, the oxygen atoms have three sp^2 orbitals and one 2p orbital (Figure 2.2).

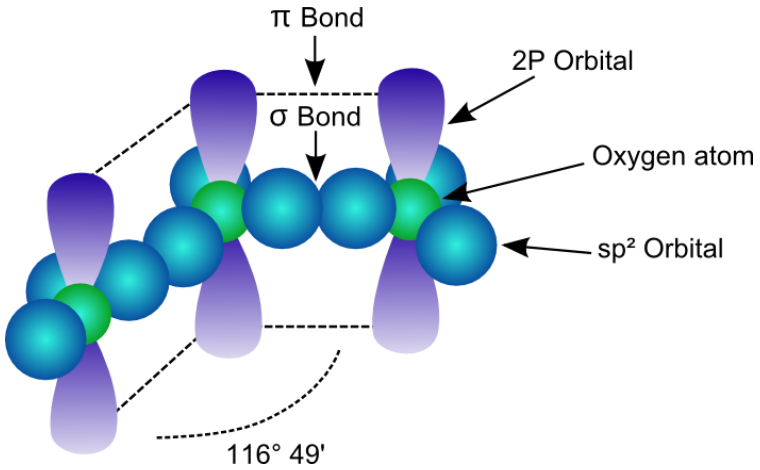

Figure 2.2: Electronic configuration of ozone (Beltrán, 2004)

The 2p orbitals of the outer oxygen atoms combine with the $2sp^2$ orbital of the central oxygen atom which gives rise to two π orbitals. As in these orbitals electrons can move along the ozone molecule, different resonance structures are possible (Figure 2.3). In some cases, one of the outer oxygen atoms can be positively charged, which explains the strong electrophilic nature of ozone. The resonance structure implies that ozone can react via three different ways with compounds present in the water matrix: oxidation-reduction reactions, cycloaddition reactions and electrophilic substitution reactions (Beltrán, 2004).

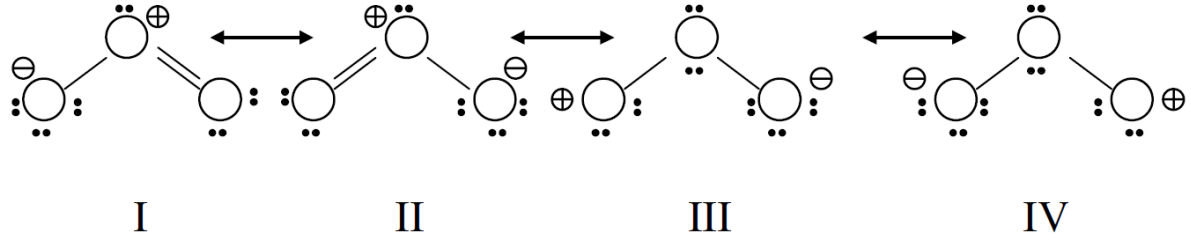

Figure 2.3: Resonance structures of the ozone molecule (Beltrán, 2004)

An example of an oxidation-reduction reaction which involves an electron transfer is the reaction between ozone and the hydroperoxyl anion (deprotonated form of hydrogen peroxide). The ozone and hydroperoxyl radicals are formed (von Gunten, 2003a):

$$O_3 + HO_2^- \rightarrow O_3^{-\bullet} + HO_2^{\bullet} \qquad (2.2)$$

Cycloaddition reactions require the presence of olefinic compounds which have one or more carbon double bonds. The general reaction pathway is called the Criegee mechanism which involves the formation of a temporal cyclic ozonide structure (Beltrán, 2004), as shown in Figure 2.4.

An example of electrophilic substitution is given in Figure 2.5. Ozone attacks a nucleophilic site of phenol and first adds to the molecule. Finally, after singlet oxygen formation and hydrogen addition, catechol is formed (this is just one of several possible pathways) (Mvula and von Sonntag, 2003). Phenolic compounds react via electrophilic substitution rather than cyclo-addition as resonance phenomena in the aromatic rings will stabilize local charges (Beltrán, 2004).

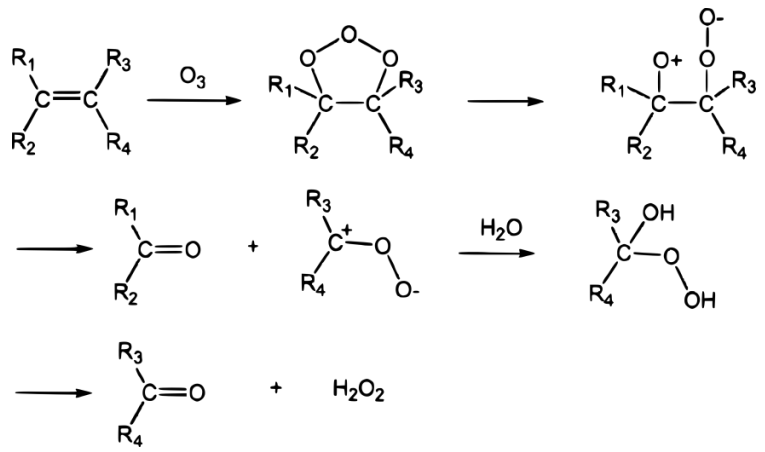

Figure 2.4: Dipolar cycloaddition reaction: the Criegee mechanism involving olefins (von Gunten, 2003a)

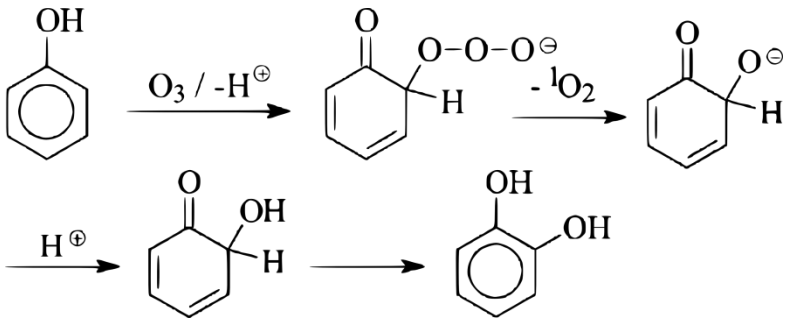

Figure 2.5: Electrophilic substitution: reaction between ozone and phenol which leads to catechol formation (Mvula and von Sonntag, 2003)

Detailed information regarding the possible reactions of ozone can be found elsewhere (Mvula and von Sonntag, 2003; von Gunten, 2003a; Beltrán, 2004).

2.2.3.3 Autocatalytic decomposition of ozone in aqueous solution

The decomposition of ozone in pure water proceeds through a complex chain of reactions which give rise to multiple free radical species. For already more than one century, the decomposition chain is subject of fundamental research on ozone. A first model was proposed by Weiss in 1935, which included the following reactions:

Initiation: $O_3 + OH^- \rightarrow HO_2^{\bullet} + O_2^{-\bullet}$ (2.3)

Propagation: $O_2^{-\bullet} + O_3 \rightarrow 2O_2 + HO^{\bullet}$ (2.4)

$HO^{\bullet} + O_3 \rightarrow HO_2^{\bullet} + O_2$ (2.5)

In that period, researchers were searching for evidence on the existence of the hydroperoxyl radical ($HO_2^{\bullet}$) and some used ozone for this purpose (Weiss, 1935).

The chain mechanism was further extended in the 1980s. By using pulse radiolysis, some of the reactions could be studied in more detail by selectively initiating the chain with electrons. As such, the model of Weiss (1935) was further developed by adding new reactions and radical species. Two different mechanisms were proposed in literature: a first model for near neutral pH (Buhler et al., 1984; Staehelin et al., 1984), a second for acidic pH (Tomiyasu et al., 1985). The first model (neutral pH) is most commonly used and is often referred to as the SHB mechanism, according to the names of the authors (Beltrán, 2004).

A last modification was made in 1994 by Hoigné (as cited in Beltrán, 2004) by making a change in the chain initiation (Equation 2.3). The final ozone SHB decomposition mechanism is given in Table 2.3.

Table 2.3: Ozone decomposition mechanism in pure water; normal text: first model of Weiss (1938), italic: extensions by Buhler et al (1984), bold: extensions by Staehelin et al., 1984, underlined: modifications by Hoigné in 1994 (as cited in Beltrán, 2004)

Reaction	Rate constant	Reaction No.
	Initiation	
$O_3+OH^- \rightarrow \underline{HO_2^- + O_2}$	$k=70\ M^{-1}s^{-1}$	(2.6)
$\underline{O_3+ HO_2^- \rightarrow HO_2^\bullet + O_2^{-\bullet}}$	$\underline{k=2.2x10^6\ M^{-1}s^{-1}}$	(2.7)
	Propagation	
$HO_2^\bullet \leftrightarrow O_2^{-\bullet} + H^+$	$k_f=7.9x10^5\ s^{-1}$ $k_r=5x10^{10}\ M^{-1}s^{-1}$	(2.8)
$O_2^{-\bullet} + O_3 \rightarrow O_3^{-\bullet} + O_2$	$k=1.6x10^9\ M^{-1}s^{-1}$	(2.9)
$\mathbf{HO^\bullet + O_3 \leftrightarrow HO_4^\bullet}$	$\mathbf{k_f=(2.0\pm0.5)\ x10^9\ M^{-1}s^{-1}}$ $\mathbf{k_r}$**=negligible**	(2.10)
$\mathbf{HO_4^\bullet \rightarrow HO_2^\bullet + O_2}$	$\mathbf{k=2.8x10^4\ M^{-1}s^{-1}}$	(2.11)
$O_3^{-\bullet} + H^+ \leftrightarrow HO_3^\bullet$	$k_f=(5.2\pm0.6)x10^{10}\ M^{-1}s^{-1}$ $k_r=(3.3\pm0.3)x10^2\ s^{-1}$	(2.12)
$HO_3^\bullet \rightarrow HO^\bullet + O_2$	$k=(1.09\pm0.06)x10^5\ s^{-1}$	(2.13)
$\underline{HO_2^- + H^+ \leftrightarrow H_2O_2}$	$\underline{k_f=5x10^{10}\ M^{-1}s^{-1}}$ $\underline{kr=0.25\ s^{-1}}$	(2.14)
$\underline{HO^\bullet + H_2O_2 \rightarrow HO_2^\bullet + H_2O}$	$\underline{k=2.7\ x10^7\ M^{-1}s^{-1}}$	(2.15)
$\underline{HO^\bullet + HO_2^- \rightarrow HO_2^\bullet + OH^-}$	$\underline{k=7.5\ x10^9\ M^{-1}s^{-1}}$	(2.16)
	Termination	
$\mathbf{HO_4^\bullet + HO_4^\bullet \rightarrow H_2O_2 + 2O_3}$	$\mathbf{k=5\ x10^9\ M^{-1}s^{-1}}$	(2.17)
$\mathbf{HO_4^\bullet + HO_3^\bullet \rightarrow H_2O_2 + O_2 + O_3}$	$\mathbf{k_f=5\ x10^9\ M^{-1}s^{-1}}$	(2.18)

2.2.3.4 Ozone decomposition in natural water and wastewater

If ozone is added to water containing dissolved organic matter, the reaction system becomes highly complex in nature. In that case, the scheme presented in Table 2.3 is not sufficient to describe the ozone and $HO^\bullet$ concentrations.

Additionally, a significant difference exists between the ozonation of natural water and secondary effluent. This is due to differences in DOC concentration and the

properties of the organic matrix. If an economical ozone dose is applied to both waters using a batch reactor, the observed ozone decomposition profile will be totally different (Buffle et al., 2006b), as shown in Figure 2.6. In both systems, a phase of rapid ozone decomposition prior to 20 s is observed. The amount of ozone decomposed during that phase is often called instantaneous ozone demand (IOD) and can be attributed to compounds that have very high reaction rates with ozone (Buffle and von Gunten, 2006). During that phase, the apparent first order decay constant of ozone (k'_{app}) can be described using a power function (Buffle et al., 2006a), (see also Chapter 7). During a second phase, which does not occur in secondary effluent as all ozone is consumed during phase one, a significantly slower and first order ozone decomposition takes place (von Gunten, 2003a).

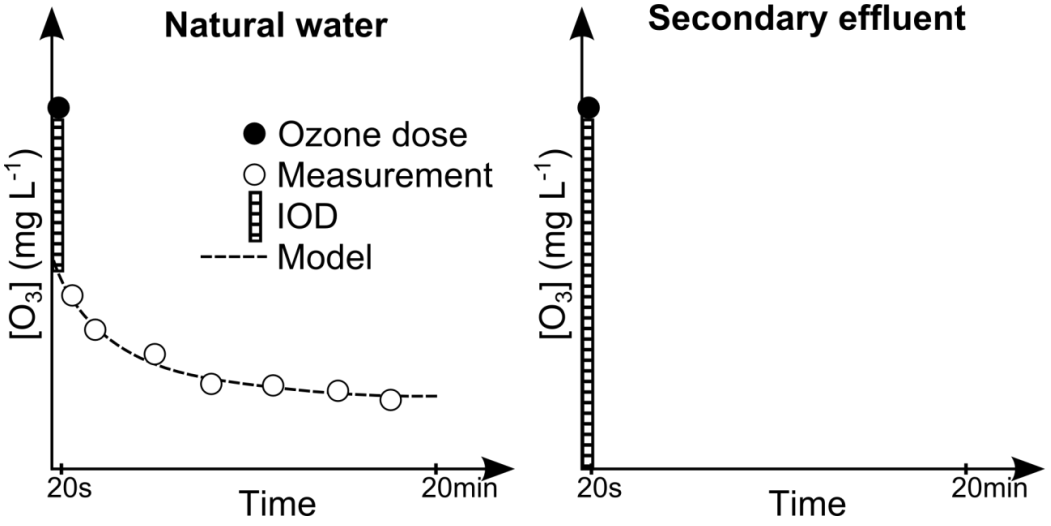

Figure 2.6: Observed ozone decomposition in a batch reactor containing natural water (left) and secondary effluent (right) (Buffle et al., 2006b)

As such, ozonation of secondary effluent is highly comparable to the first phase of natural water ozonation (Buffle et al., 2006a). It has to be noticed, however, that depending on the effluent composition and ozone dose applied, a second phase might be observed during ozonation of secondary effluent. To study ozone decomposition during the fast initial phase, reactor systems other than batch have to be used. Due to the instantaneous addition of all ozone and significant ozone consumption within the millisecond timeframe, a typical batch set-up does not allow for sampling at very low ozone exposures. Additionally, using a batch set-up, the addition of ozone stock solution comprises some dilution of the sample water which is not the case in the semi-batch system. To cope with most of the disadvantages of a batch system and to avoid the use of a more complex heterogeneous system, some researchers used stopped-flow systems (Noethe et al.,

2009) or quench systems (Buffle et al., 2006b) to study ozonation during the first milliseconds of reaction. Both systems are based on nearly instantaneous mixing of ozone stock solution and sample water rapidly followed by measurements. The stopped-flow system starts acquiring absorbance data at high frequency directly after the mixing. Typically, a wavelength of 260 nm is used to record the ozone concentration profile (Noethe et al., 2009). Buffle et al. (2006b) developed a continuous quench system to cope with the interfering absorption of DOM and its transformation products in the UV region. The reactor consisted of eight flow loops with volumes varying between 0.016 and 3.872 mL. By using a fixed flow-rate and different loops, reaction times between 0.35 and 21.38 s (in a conventional batch system the first sample is taken after 20 s) could be applied. Directly upon reaction, ozone was quenched (with e.g. indigo reagent) and indirectly measured. As higher volumes were used compared to stopped-flow techniques, additional chromatographic measurements could be performed (Buffle et al., 2006b).

Reactions between DOM and ozone are complex and can affect ozone stability in several ways (Figure 2.7). Some DOM moieties directly react with ozone and part of these reactions can give rise to superoxide radical anions or ozone radicals and as such initiate the chain reaction (von Gunten, 2003a; Buffle and von Gunten, 2006). As shown in Figure 2.7, DOM also indirectly affects ozone decomposition by interacting with $HO^{\bullet}$. Part of these reactions lead to carbon centred radicals which subsequently react with dissolved oxygen to finally produce superoxide radical anions. These radicals significantly promote ozone decomposition according to Equation 2.9. Examples of compounds that produce superoxide radical anions upon reaction with ozone are secondary amines (Buffle and von Gunten, 2006):

$$R_2NH + O_3 \rightarrow R_2NO^{\bullet} + H^+ + O_2^{-\bullet} \quad (2.19)$$

This reaction yields 80% superoxide radical anions and 20% singlet oxygen (Buffle and von Gunten, 2006). In contrast, tertiary amines will generate 10% ozone radicals and 90% singlet oxygen. Another compound that directly produces ozone radicals upon direct electron transfer is phenol (PhOH) (or its deprotonated form phenolate) (Mvula and von Sonntag, 2003):

$$PhO^-/PhOH + O_3 \rightarrow PhO^{\bullet}/PhOH^{\bullet+} + O_3^{-\bullet} \quad (2.20)$$

The phenoxyl radical ($PhO^{\bullet}$) can be directly produced or via instantaneous deprotonation of the phenol radical cation (pK_a=-2) (Mvula and von Sonntag, 2003). Subsequent reaction of the phenoxyl radical with $HO^{\bullet}$ can give rise to the superoxide radical anion that further accelerates ozone decomposition (Mvula and

von Sonntag, 2003; Buffle and von Gunten, 2006). Important to notice is that phenol reacts six orders of magnitude slower with ozone than phenolate. Consequently, ozone will react almost exclusively with the charged form, even though the pKa value is significantly higher than the pH (Mvula and von Sonntag, 2003).

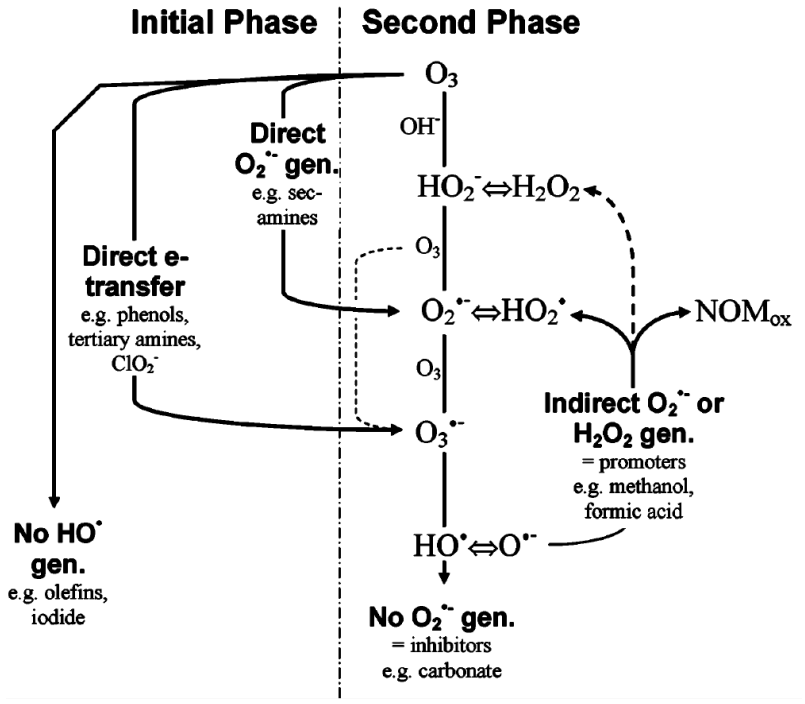

Figure 2.7: Influence of DOM on ozone decomposition (Buffle and von Gunten, 2006)

Especially during secondary effluent ozonation but also during the initial phase of natural water ozonation, hydroxyl radical production is significant (Buffle et al., 2006a; Noethe et al., 2009) (see also Chapter 7). This is especially due to the aromatic moieties of NOM and effluent organic matter (EfOM).

2.2.3.5 The R_{CT} concept by Elovitz and von Gunten (1999)

As discussed in previous section, $HO^{\bullet}$ production during ozonation of water that contains DOM (NOM or EfOM) is significant. For this reason, both the ozone and $HO^{\bullet}$ exposures should be known if accurate predictions of target pollutant degradations are sought. Two approaches can be used to model such systems. The first is to use a well-defined mechanistic model as the one presented in Table 2.3. By extending this model with reactions involving DOM (e.g. Figure 2.7), an attempt can be made to describe the system, provided that calibration is performed. The current lack of knowledge of these complex reactions, however, will impede the model extension and will finally give rise to models that become more empirical in nature and that have a low predictive power in real systems (Elovitz

and von Gunten, 1999). A second and semi-empirical approach was developed by Elovitz and von Gunten (1999). These researchers correlated the ozone exposure ($\int[O_3]dt$) to the $HO^{\bullet}$ exposure ($\int[HO^{\bullet}]dt$) in natural water. Ozone exposure was calculated from the surface under the ozone concentration profile, while the $HO^{\bullet}$ exposure was indirectly measured using p-chlorobenzoic acid (pCBA) as a probe compound:

$$ln\left(\frac{[pCBA]}{[pCBA]_0}\right) = -k_{HO^{\bullet}/pCBA} \int [HO^{\bullet}]dt \quad (2.21)$$

in which $k_{HO^{\bullet}/pCBA}$ represents the second order rate constant for reaction between pCBA and $HO^{\bullet}$.

The R_{CT} value was defined as the ratio of $HO^{\bullet}$ exposure and ozone exposure (and hence, $HO^{\bullet}$ and ozone concentration ratio). During the second phase of natural water ozonation, R_{CT} was found to be a constant and water specific value. As such, the $HO^{\bullet}$ exposure for a specific water could be derived from the ozone exposure and R_{CT} value. Degradation of a certain target compound (P) during ozonation is mostly due to both ozone and $HO^{\bullet}$ attack:

$$\frac{-d[P]}{dt} = k_{HO^{\bullet}/P}[HO^{\bullet}][P] + k_{O_3/P}[O_3][P] \quad (2.22)$$

Values for R_{CT} during natural water ozonation typically vary between 10^{-7} and 10^{-9} (von Gunten, 2003a) but can easily exceed 10^{-6} during ozonation of secondary effluent (Buffle et al., 2006a). Using the R_{CT} concept, Equation 2.22 becomes:

$$\frac{-d[P]}{dt} = [O_3][P]\left(k_{HO^{\bullet}/P}\, R_{CT} + k_{O_3/P}\right) \quad (2.23)$$

As such, by knowing the ozone concentration, the rate constants for reaction with ozone ($k_{O3/P}$) and $HO^{\bullet}$ ($k_{HO^{\bullet}/P}$) and the R_{CT} value, the degradation of a given pollutant can be predicted without needing a separate mass balance for $HO^{\bullet}$. The mass balance for ozone during the second phase of natural water can be simply constructed using a first order kinetic law (von Gunten, 2003a).

The R_{CT} concept can also be used to assess the relative importance (f) of $HO^{\bullet}$ and ozone attack during degradation of a given compound:

$$f_{HO^{\bullet}} = \frac{k_{HO^{\bullet}/P}\, R_{CT}}{k_{HO^{\bullet}/P}\, R_{CT} + k_{O_3/P}} \quad (2.24)$$

As it is now, the R_{CT} concept is not suitable to describe ozonation of secondary effluent as it is not a constant value throughout the process (Buffle et al., 2006a; b). Additionally, it was proven that the R_{CT} value significantly impacts the prediction

of compounds that slowly react with ozone and hence, very accurate determination of this value is required (Neumann et al., 2009; Zimmermann et al., 2011).

Currently, a lot of research is performed to find a way to assess the $HO^{\bullet}$ exposure during secondary effluent ozonation. At present however, no suitable models exist.

2.2.4 Fundamentals of the UV/hydrogen peroxide process

2.2.4.1 UV photolysis and hydroxyl radical production

UV light is electromagnetic radiation with a wavelength below 400 nm and depending on the wavelength range, UV-A (400-315 nm), UV-B (315-280 nm) UV-C (280-200 nm) and vacuum UV (<200 nm) are defined. In the UV/H_2O_2 process, low pressure (LP) or medium pressure (MP) UV lamps are generally used. LP-UV lamps are monochromatic light sources that emit at 253.7 nm, while MP-UV lamps are polychromatic light sources emitting in the whole UV region and partially in the visible region (Masschelein, 2002).

If an aqueous solution is irradiated with UV light, a fraction will be absorbed by the compounds present in the water. According to the first law of photochemistry, only the light that is absorbed by a molecule can be effective in producing photochemical changes in that molecule (Parsons, 2004). The efficiency of this photolysis for a given compound is determined by the primary *quantum yield* (ϕ) of that compound. ϕ corresponds to the fraction of photon absorption events that actually give rise to photolysis and is wavelength dependent. The fraction of the total absorption of UV light that is absorbed by a specific compound i is associated with the decadic *molar absorption coefficient* ($\varepsilon_{\lambda,i}$) of the compound, expressed in $M^{-1}cm^{-1}$. The decadic absorption coefficient (α_λ) of the solution is given by the Beer-Lambert expression:

$$\alpha_\lambda = \sum_i \varepsilon_{\lambda,i} C_i \qquad (2.25)$$

where C_i is the concentration of compound i (M).

Often, the decadic absorption coefficient at 254 nm (α_{254}, further in this thesis referred to as UV_{254}) is related to the presence of DOM (see further). The decadic absorption coefficient (unit m^{-1} or cm^{-1}) is thus defined as the absorbance (A) divided by the optical path length of the solution (Braslavsky, 2007):

$$\alpha_\lambda = \frac{A}{b} \qquad (2.26)$$

In which b represents the optical path length (cm).

In the case of hydrogen peroxide photolysis, homolytic bond cleavage of the O-O bond leads to the production of two $HO^{\bullet}$ species:

$$H_2O_2 + hv \rightarrow HO^{\bullet} + HO^{\bullet} \quad (2.27)$$

LP-UV lamps (254 nm) are the most commonly used UV sources in UV/H_2O_2 systems (Parsons, 2004). The primary quantum yield of H_2O_2 at this wavelength is 0.5. However, the overall observed quantum yield (Φ) is 1 as hydrogen peroxide is also decomposed by the free radicals produced (Song et al., 2008). The molar absorption coefficient is 19.6 $M^{-1}cm^{-1}$, which is a relatively low value e.g. compared to ozone (3,300 $M^{-1}cm^{-1}$). This implies that relatively high doses of hydrogen peroxide are required to achieve sufficient $HO^{\bullet}$ production. The overall hydrogen peroxide photolysis rate is expressed as follows (Parsons, 2004):

$$\frac{d[H_2O_2]}{dt} = -\phi_{H_2O_2} I_0 f_{H_2O_2} (1 - 10^{-A}) \quad (2.28)$$

Where I_0 is the incident (volume based) photon flux (Einsteins $L^{-1}s^{-1}$) and f_{H2O2} is the fraction of the UV light that is absorbed by hydrogen peroxide. One Einstein equals one mole of photons.

During the UV/H_2O_2 process, direct photolysis of trace pollutants can be significant, especially if MP-UV lamps are used. Consequently, both direct photolysis and $HO^{\bullet}$ attack have to be considered during kinetic investigation of trace pollutant removal (Audenaert et al., 2011):

$$\frac{d[P]}{dt} = -\phi_M I_0 f_M (1 - 10^{-A}) - k_{HO^{\bullet}/P}[HO^{\bullet}][P] \quad (2.29)$$

where the first and second term at the right side represent the photolysis and $HO^{\bullet}$ oxidation rates of a given pollutant P, respectively.

Hence, the three key properties of a pollutant that determine its conversion rate are the quantum yield, molar extinction coefficient and second order rate constant for the reaction with $HO^{\bullet}$ (Wols and Hofman-Caris, 2012). A solid review on these properties was performed by Wols and Hofman-Caris (2012). An extensive list of target pollutants together with their photochemical parameters was provided. Furthermore, these researchers used self-organizing maps (SOMs) to cluster pollutants with similar properties. As shown in Figure 2.8 the SOMs consisted of cells with each separate cell representing a cluster containing zero or more compounds. A set of three values (one value for each of the three key photochemical properties) was assigned to each cell. Each organic compound was added to the cluster (cell) with the most similar properties. It was found that the

quantum yield and molar absorption coefficient were inversely correlated in horizontal direction. Contrastingly, the SOM associated with the $HO^{\bullet}$ rate constants was layered vertically. Compounds belonging to the same chemical family were generally found in the same or nearby clusters. The cell belonging to N-nitrosodimethylamine (NDMA) was surrounded by several empty cells due to its low $HO^{\bullet}$ reaction rate constant (Wols and Hofman-Caris, 2012).

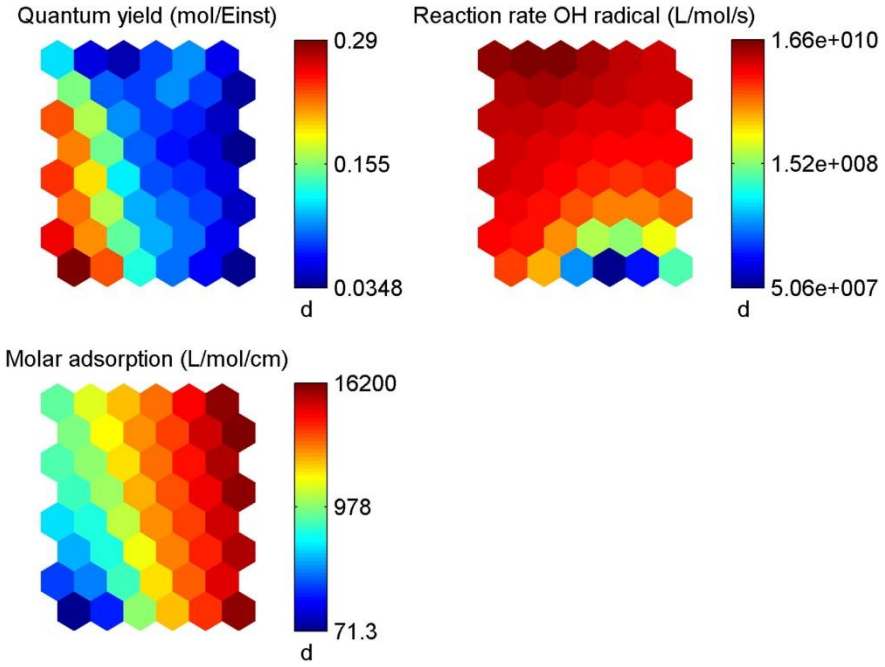

Figure 2.8: Self-organizing maps analysis to visualize the coherence between the three key parameters of photochemical conversion: quantum yield, molar absorption coefficient and rate constant for reaction with $HO^{\bullet}$ (Wols and Hofman-Caris, 2012)

A detailed kinetic scheme of the UV/H_2O_2 process including the main process parameters and elementary reactions involved will be presented in Chapter 6.

2.2.4.2 The $R_{OH,UV}$ concept by Rosenfeldt and Linden (2007)

In analogy with the R_{CT} concept that was developed to simplify the modelling of natural water ozonation (see Section 2.2.3.4), Rosenfeldt and Linden (2007) developed the $R_{OH,UV}$ concept. The R_{CT} concept involves that a certain ozone exposure corresponds to a certain $HO^{\bullet}$ exposure. Analogically, the $R_{OH,UV}$ concept assumes that a certain UV exposure corresponds to a certain $HO^{\bullet}$ exposure. The experimental determination of $R_{OH,UV}$ for a given water is also very similar to that of R_{CT}. After spiking a known pCBA concentration to a water sample, the oxidation process is started and the pCBA concentration profile is recorded.

If Equation 2.21 is extended with a first order rate term for direct photolysis, the following expression is obtained:

$$ln\left(\frac{[pCBA]_0}{[pCBA]}\right) = k'_d.t + k_{HO^\bullet/pCBA}\int[HO^\bullet]dt \quad (2.30)$$

in which k'_d represents the pseudo-first order rate constant for direct photolysis of pCBA.

If both direct photolysis and $HO^\bullet$ oxidation are lumped into a single pseudo first order kinetic rate law, the overall pseudo first order rate constant (k'_T) can be described as follows:

$$k'_T = k'_d + \frac{k_{HO^\bullet/pCBA}\int_0^t[HO^\bullet]dt}{t} \quad (2.31)$$

The first order rate constants given in Equation 2.31 are time based (with unit s^{-1}) and are converted to "fluence based" rate constants. The incident photon flux (I_0) of Equation 2.28 in this case is expressed in power per unit of surface area (e.g. mW cm^{-2}) and is called "fluence rate" (E_0). This terminology originates from the experimental collimated beam set-up that is often used to set up dose-response curves for disinfection (Bolton and Linden, 2003). In this set-up, a petri dish with known surface area is irradiated for a given time. The volume of the solution is negligible and as such, E_0 is volume independent. The conversion is performed by dividing all terms of Equation 2.31 by E_0 (mW s^{-1} cm^{-2}):

$$k'^D_T - k'^D_d = \frac{k_{HO^\bullet/pCBA}\int_0^t[HO^\bullet]dt}{E_0 t} \quad (2.32)$$

The superscript "D" indicates that the rate constants are fluence based with unit cm^2 mJ^{-1}.

The UV fluence H (mJ cm^{-2}) corresponds to the UV exposure and is the product of E_0 and time. Finally, $R_{OH,UV}$ is defined as follows:

$$R_{OH,UV} = \frac{\int_0^t[HO^\bullet]dt}{H} = \frac{k'^D_T - k'^D_d}{k_{HO^\bullet/pCBA}} \quad (2.33)$$

Rate constants k'^D_T and k'^D_d can be determined after combining Equations 2.30-2.32:

$$ln\left(\frac{[pCBA]_0}{[pCBA]}\right) = k'_T.H \quad (2.34)$$

k'^D_d is determined from the slope of the ln([pCBA]/$[pCBA]_0$) vs. H plot in the absence of hydrogen peroxide. In the presence of hydrogen peroxide, this slope equals k'^D_T. After considering $k_{HO^\bullet/pCBA}$ ($5x10^9$ M^{-1} s^{-1}), $R_{OH,UV}$ is calculated according to Equation 2.33. It is useful to obtain $R_{OH,UV}$ values at different hydrogen peroxide concentrations after which a $R_{OH,UV}$ vs. $[H_2O_2]$ plot can be made

(see further). Values of $R_{OH,UV}$ are typically in the order of 10^{-12} M s cm² mJ^{-1} (Rosenfeldt and Linden, 2007).

To make this concept useful for modelling practices, the $HO^{\bullet}$ concentration must be assumed to be at steady state. In that case, the $R_{OH,UV}$ value can be used to assess the $HO^{\bullet}$ concentration:

$$R_{OH,UV} = \frac{[HO^{\bullet}]_{ss}}{E_0} \tag{2.35}$$

Using a conventional steady state modelling approach, $[HO^{\bullet}]_{ss}$ is calculated as follows:

$$[HO^{\bullet}]_{ss} = \frac{E_0 \varepsilon_{H_2O_2} [H_2O_2] \phi_{H_2O_2}}{U_{254}\left(\sum k_{HO^{\bullet}/S_i}[S]_i + k_{HO^{\bullet}/pCBA}[pCBA] + k_{HO^{\bullet}/H_2O_2}[H_2O_2]\right)} \tag{2.36}$$

in which U_{254} represents the energy per mole of photons (J $Einstein^{-1}$) and $k_{HO\bullet/Si}$ is the second order rate constant for reaction between a certain scavenger S_i and $HO^{\bullet}$. S_i can be DOC, carbonate, bicarbonate and/or another species.

The major drawback of this commonly used approach is that the uncertainty related to the scavenging term ($\sum k_{HO^{\bullet}/S}[S]_i$) negatively impacts the accuracy of the model prediction. Especially for reactions involving DOM assumptions have to be made and/or surrogates have to be used.

Using the $R_{OH,UV}$ concept, these assumptions can be avoided by deriving the scavenging term directly from the measured pCBA decay profiles. First, Equation 2.36 has to be rearranged as follows:

$$\frac{E_0}{[HO^{\bullet}]_{ss}} = \frac{U_{254}\left(\sum k_{HO^{\bullet}/S_i}[S]_i + k_{HO^{\bullet}/pCBA}[pCBA]\right)}{\varepsilon_{H_2O_2}\phi_{H_2O_2}}\left(\frac{1}{[H_2O_2]}\right) + \frac{U_{254}k_{HO^{\bullet}/H_2O_2}}{\varepsilon_{H_2O_2}\phi_{H_2O_2}} \tag{2.37}$$

If the left term (the inverse of the $R_{OH,UV}$ value, according to Equation 2.35) is plotted against the inverse of the hydrogen peroxide concentration, a straight line is obtained with slope m and intercept b. After m and b have been determined, the scavenging term can be calculated (after rearrangement of Equation 2.37):

$$\sum k_{HO^{\bullet}/S_i}[S]_i = k_{HO^{\bullet}/H_2O_2}\frac{m}{b} - k_{HO^{\bullet}/pCBA}[pCBA] \tag{2.38}$$

After re-introducing this term into Equation 2.36, the steady state $HO^{\bullet}$ concentration can be obtained without the influencing effect of pCBA scavenging ($[HO^{\bullet}]_{ss}$ of Equation 2.35 can be affected by the addition of pCBA).

Rosenfeldt and Linden (2007) showed that model predictions of micropollutant oxidation were significantly better using the $R_{OH,UV}$ concept compared to the conventional mechanistic approach.

However, a similar remark as for the R_{CT} concept can be made: the concept was developed using natural water and it is largely unknown whether it has the same potential for the modelling of secondary effluent oxidation. The dynamic character of effluent will certainly impede its implementation and may require future extension of the concept.

2.3 Towards advanced water treatment and water reuse

An increasing world population implies that water and wastewater treatment plants are facing new challenges. Population growth inherently leads to both an increasing water demand and wastewater production and, if treatment technologies do not advance in parallel, this will have a negative impact on both the quantity and quality of the natural water resources. More and more water treatment facilities therefore include *advanced treatment* steps in their treatment train and the number of *water reuse* projects is increasing.

A wide variety of factors act as driving forces for the application of water reuse, including population growth in regions facing severe droughts and over-pumping of groundwater resources leading to salt water intrusion (Malley, 2010) and decreasing ground water levels. Even in regions with a reasonable annual rainfall, these problems can occur. For example, the region of West Flanders (Belgium) (annual rainfall 800 mm, (KMI, 2012)) is highly dependent on groundwater as the main industrial activities involve vegetable processing, textile and chemical industry and agriculture. Overexploitation of the aquifer resulted in a deterioration of both the quantity and quality of the groundwater. The overall water extraction now needs to be reduced by 75% and hence, the use of alternative water sources and/or water reuse is becoming primordial (SERR/RESOC, 2007).

On the other hand, the occurrence of emerging contaminants such as EDCs and PPCPs (Daughton and Ternes, 1999; Heberer, 2002; Kolpin et al., 2002) or other synthetic organic chemicals such as pesticides, solvents and additives (von Gunten, 2003a) is well recognized. Due to recent developments in analytical techniques, trace levels of these compounds can be detected leading to a continuously growing public awareness of these contaminants in the water supply. Water contamination with trace pollutants is rather complex and can occur via different routes as shown in Figure 2.9, which is a specific example for pharmaceuticals (Ikehata et al., 2006). Together with more stringent regulations and the need to protect both public health and natural water resources, this leads to a growing interest in advanced water and wastewater treatment and in particular in ozone and AOPs (Comninellis et al., 2008; Malley, 2010; Oneby et al., 2010; Oller et al., 2011). Important driving forces that are responsible for the increasing interest in advanced treatment technologies such as ozone and AOPs are presented in Figure 2.10. Global trends such as a worldwide population growth and unequal geographical spread of water resources are directly responsible for the growing need for water reuse. Together with the occurrence of persistent organic pollutants in combination with more

stringent regulations and increased public awareness with respect to these compounds, these trends are the main drivers for application of advanced water and wastewater treatment technologies.

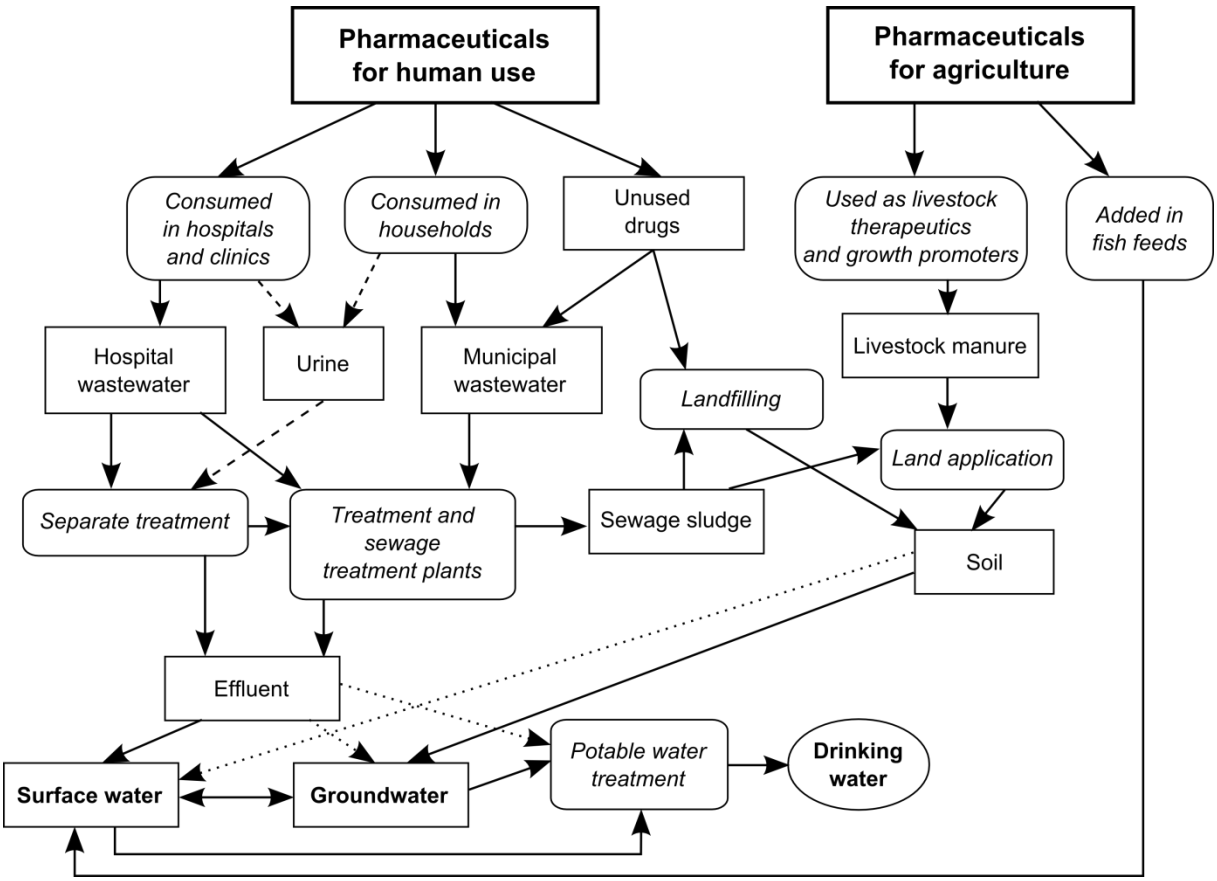

Figure 2.9: Occurrence and transportation of pharmaceuticals in the aquatic environment (Ikehata et al., 2006)

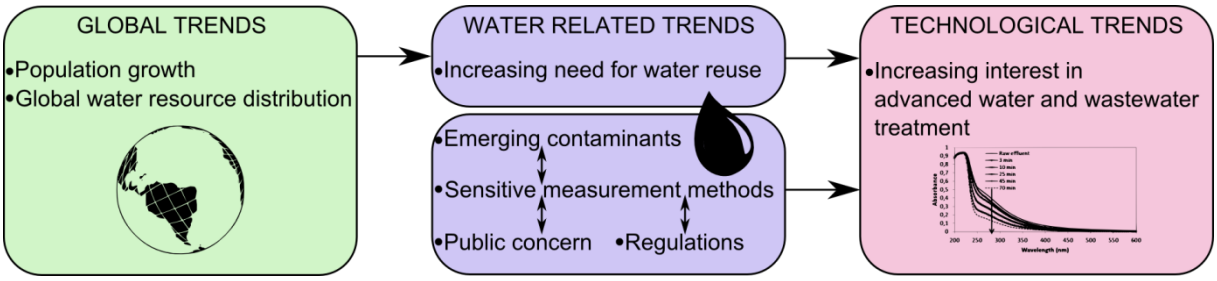

Figure 2.10: Driving forces responsible for increasing interest in advanced water treatment technologies

In many advanced water treatment applications AOPs play a major role as in most of the cases, the wastewater to be recycled or the (drinking) water to be treated contains organic (micro)pollutants that belong to one or more of the classes mentioned above. Some of these compounds are hard to remove with conventional

technologies (such as membrane filtration, air stripping or adsorption) as they have a low molecular weight (MW), low volatility and poor adsorption characteristics (Parsons, 2004). Using AOPs, the target compounds are being transformed or destroyed, rather than being transported to another phase.

Most of the existing water reuse applications that include ozone or AOPs focus on the reuse of secondary treated municipal wastewater. The tertiary treatment can be performed on-site at the municipal wastewater treatment plants (WWTPs) or in separate facilities, often called advanced water treatment plants (AWTPs), raw water production facilities (RWPFs) or water reclamation facilities (WRFs). The high quality reclaimed effluent is used for industrial or agricultural applications or for drinking water production. Water reuse can take many forms: potable or non-potable, direct or indirect, planned or unplanned (Oneby et al., 2010), as depicted in Figure 2.11. Indirect potable reuse

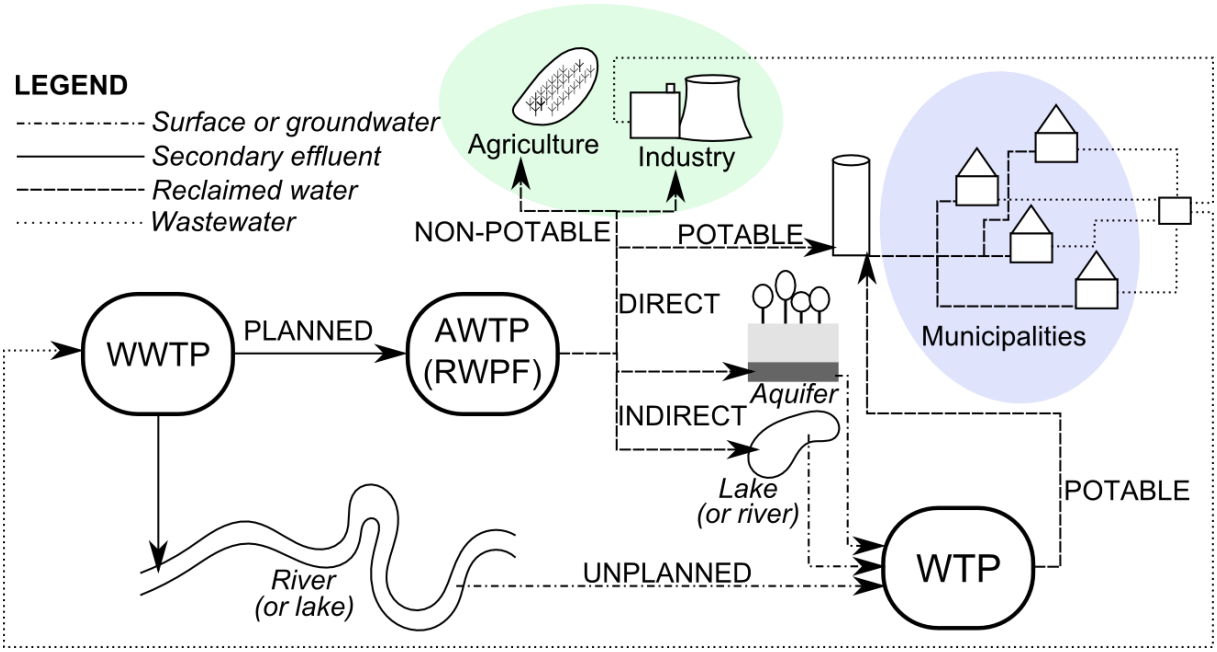

Figure 2.11: Different forms of water reuse

(IPR) involves the integration of wastewater treatment, water supply and drinking water treatment into a single management strategy. In that context, wastewater is becoming a reuse opportunity, instead of being a disposal problem. Although the oxidation process has several potential positions within the wastewater treatment train (Figure 2.12), the optimal location is after the biological treatment (Huber et al., 2005; Ikehata et al., 2006; Ried et al., 2009). Prior to the biological step, oxidant requirements are exceedingly high because of the high DOC caused by the biodegradable matter that is still present. Moreover, the limited UV transmittance of primary treated water limits the application of UV-based AOPs. Often, multiple

pretreatment steps are installed upstream of these technologies (see further). In the specific case of ozone, additional applications exist such as exhaust air treatment for odour control, sludge reduction or sludge treatment to enhance sludge settling properties (Ried et al., 2009). This is, however, beyond the scope of this work. As shown in Figure 2.12, ozonation and AOPs are also attractive technologies to be included in the water treatment train.

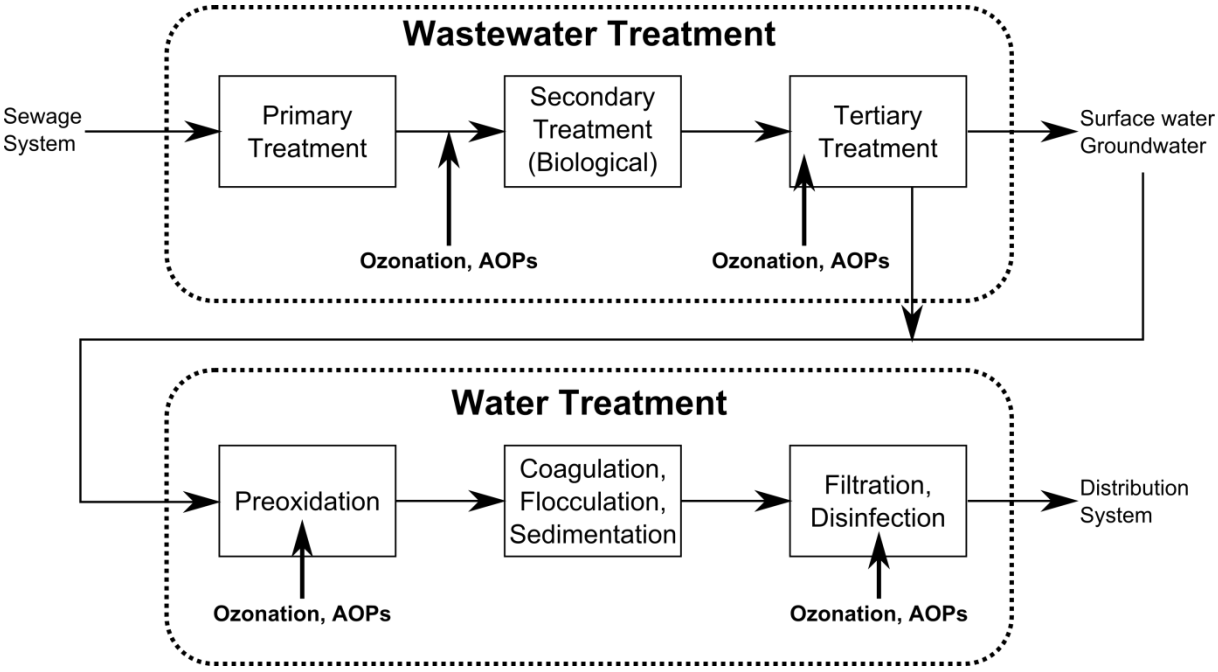

Figure 2.12: Possible points to apply ozone or AOPs to remove micropollutants (Ikehata et al., 2006)

The use of ozone for drinking water treatment is already established for more than a century and thousands of applications exist worldwide (Böhme, 1999; Geering, 1999; Kruithof and Masschelein, 1999; Larocque, 1999; Le Paulouë and Langlais, 1999; Lowndes, 1999; Matsumoto and Watanabe, 1999; Rice, 1999). Both pre-ozonation to enhance coagulation and final disinfection and oxidation (Figure 2.12) are applied. The implementation of advanced oxidation in the drinking water or advanced wastewater treatment train, however, prevailed this century. Hence, to date only few applications exist. This review will especially focus on applications of the UV/H_2O_2 process, as this AOP currently dominates the market of drinking water applications and this technology plays an important role in this dissertation. Furthermore, the (growing) use of ozone and UV/H_2O_2 for advanced municipal wastewater treatment and water reuse will be discussed.

2.3.1 Removal efficiency of trace pollutants at WWTPs

WWTPs are regarded as the main sources of trace pollutants in the environment (Daughton and Ternes, 1999; Heberer, 2002; Kolpin et al., 2002). This is due to the poor removal of these compounds during the conventionally applied primary and secondary treatment steps (Daughton and Ternes, 1999). Upgrading these plants with an oxidative tertiary treatment step can significantly improve the removal efficiency as (advanced) oxidation techniques have proven to be effective for the destruction of a wide range of organic compounds (Ikehata et al., 2006).

Municipal wastewater consists of several compound classes such as solids, trace pollutants, nutrients and biodegradable and non-biodegradable carbon (mainly NOM). WWTPs provided with primary and secondary treatment steps are especially designed for the removal of solids, nutrients and biodegradable carbon. As a result, EfOM will mainly consist of NOM, soluble microbial products (SMPs) originating from the activated sludge and trace pollutants (Shon et al., 2006).

The removal efficiency of trace pollutants at WWTPs is highly variable due to the wide variety of existing pollutants and the complex mechanisms that are responsible for their removal (Daughton and Ternes, 1999). Additionally, operational conditions and wastewater properties can significantly vary among different WWTPs. The unit processes applied (secondary treatment, filtration, disinfection) and operational variables such as sludge retention time (SRT) are determining for the removal or conversion rates of trace pollutants (Gerrity and Snyder, 2011). Trace pollutant removal can significantly increase with increased SRTs (Schaar et al., 2010). If removal occurs, two main mechanisms can be responsible: (1) microbial degradation and (2) sorption to particles that are later removed with the sludge (Daughton and Ternes, 1999).

Several factors can lead to poor removal rates. First, the concentrations of trace pollutants can be lower than the microbial affinity constants. In that case, no bacterial conversions can take place. Second, the constant introduction of new PPCPs requires continuous adaption of the microbial communities at WWTPs. This poses severe challenges to biodegradation. Third, some of the compounds that are able to adsorb to particles can also adsorb to colloids and can still be discharged with the effluent. Finally, even if removal efficiencies of some PPCPs are high, periods with changing influent dynamics (e.g. increased flow rates, seasonal variations,…) can have a dramatic effect on the removal. Several days can be needed for the system to recover (Daughton and Ternes, 1999).

In general, removal efficiencies of trace pollutants vary between 7 and 96%, with an average removal of 60% (Daughton and Ternes, 1999). Regarding pharmaceutical products, more than 80 compounds have been detected in secondary effluent or surface waters located downstream from WWTPs. In some cases, concentrations were in the µg L^{-1} range (Heberer, 2002).

2.3.2 Application of UV/H_2O_2 for advanced water treatment and reuse

2.3.2.1 Current situation

Although extensive research revealed that the UV/H_2O_2 process is efficient in removing target compounds such as NDMA, methyl tertiary butyl ether (MTBE) and other pollutants, the application of this process for advanced water treatment or water reuse only prevailed very recently. The first UV/H_2O_2 process for drinking water treatment applied at full-scale was commissioned in 1998 in Salt Lake City, USA (Sarathy and Mohseni, 2006). From then, the number of applications worldwide increased steadily with an average slope of 1.5 per year (Figure 2.13). At present, approximately 20 full-scale UV/H_2O_2 installations for municipal drinking water production or municipal water reuse have been installed. Figure 2.14 shows that starting from 2004, due to the installation or upgrade of larger plants, the production capacity increased significantly. From that period, some new AWTPs were constructed that were especially designed to treat secondary effluent originating from WWTPs. As shown in Table 2.4., most of the UV/H_2O_2 plants are located in North-America (twelve), three are located in Australia, two in Canada and one is located in Europe. At WTPs, the pretreatment processes upstream of the AOP reactor mostly consist of coagulation followed by filtration (rapid sand filtration or membrane filtration) or sedimentation. At the AWTPs, however, treatment processes prior to the oxidation step include successive membrane filtration with microfiltration (MF) and reverse osmosis (RO) (see Table 2.4). At present, the total production capacity of WTPs using UV/H_2O_2 is very little compared to the production capacity of drinking water facilities that have ozone reactors installed. E.g. the North-American plants using the UV-based AOP have a total production capacity of 364,000 $m^3\ d^{-1}$ (based on Table 2.4), while that of the ozone based plants is in the order of 55 million $m^3\ d^{-1}$ (Loeb et al., 2012). Worth noticing, however, is that ozone in the above mentioned plants in most of the cases is applied to accomplish disinfection, and far more less meant for oxidation. Contrarily, for water reuse applications, and in particular IPR, UV/H_2O_2 is more often applied than ozone. The combination of RO and UV/H_2O_2 treatment is

generally considered the standard for IPR (Gerrity and Snyder, 2011), at least for now.

All applications are intended for the removal of trace organic contaminants. These contaminants include nitrosamines such as NDMA, 1,4-dioxane, pesticides, taste and odour (T&O) compounds such as 2 methyl isoborneol (MIB) and geosmin, pharmaceuticals, volatile organic chemicals (VOCs) and algal toxins (Leach et al., 2006). Often, also inactivation of chlorine resistant waterborne organisms such as Cryptosporidium and Giardia is one of the major goals (Swaim et al., 2011). This is especially the case if surface water is used for drinking water production. Table 2.4 shows that especially NDMA, 1,4-dioxane, T&O compounds and micropollutants are the main target compounds. Most of them are hard to remove with conventional technologies. NDMA and 1,4-dioxane especially pose problems in (Southern) California. An example is the problem of contaminated groundwater the San Gabriel Basin aquifer, an important source of drinking water in Southern California. Besides NDMA and 1,4-dioxane, the most prevalent contaminants are trichloroethene (TCE), perchloroethylene (PCE), carbon tetrachloride and perchlorate (EPA, 2011). Four water utilities (La Puente Valley County Water District, Valley County Water District and San Gabriel Valley Water Company) used successive air stripping and ion exchange to remove the VOCs and the perchlorate, respectively. The last treatment step involves UV/H_2O_2 treatment to oxidize the remaining pollutants. More details of the oxidation facilities can be found in Table 2.4.

The recent interest in the UV/H_2O_2 process for (indirect) drinking water production is mostly driven by the effectiveness of the process to remove both chemical and microbial contaminants and by the low footprint which makes a retrofit in an existing WTP plant easier (Malley, 2010). Additionally, disinfection by products (DBPs) such as bromate are not formed. Bromate often restricts the ozone dose that can be applied in ozone based applications (typically 2 mg L^{-1}). In the case of T&O compound removal, the flexibility of the process is of added value. Some WTPs face the problem of seasonal occurrence of MIB and geosmin (caused by algal blooms). The Neshamini Falls, Cornwall and Lucerne WTPs only dose hydrogen peroxide during periods of increased algal activity in order to save costs (Leach et al., 2006; TrojanUV, 2012).

As mentioned in Section 2.3, there are several drivers that determine the need for water reuse. The best known (and world's largest) water reuse facility for IPR is the Groundwater Replenishment System (GWRS) in Orange County, California. Severe water scarcity in this region was an important accelerator for the project that

was intended for augmentation of regional groundwater supplies (Leach et al., 2006). The Big Spring RWPF in Colorado was constructed with the same purpose. Groundwater over-pumping in coastal areas can lead to intrusion of salt water into freshwater aquifers. To counteract this problem, the Water Replenishment District of Southern California and West Basin Municipal Water District (both located in California) have built RWPFs. Reclaimed water is injected into the sea water barrier to cope with the sea water intrusion (TrojanUV, 2012).

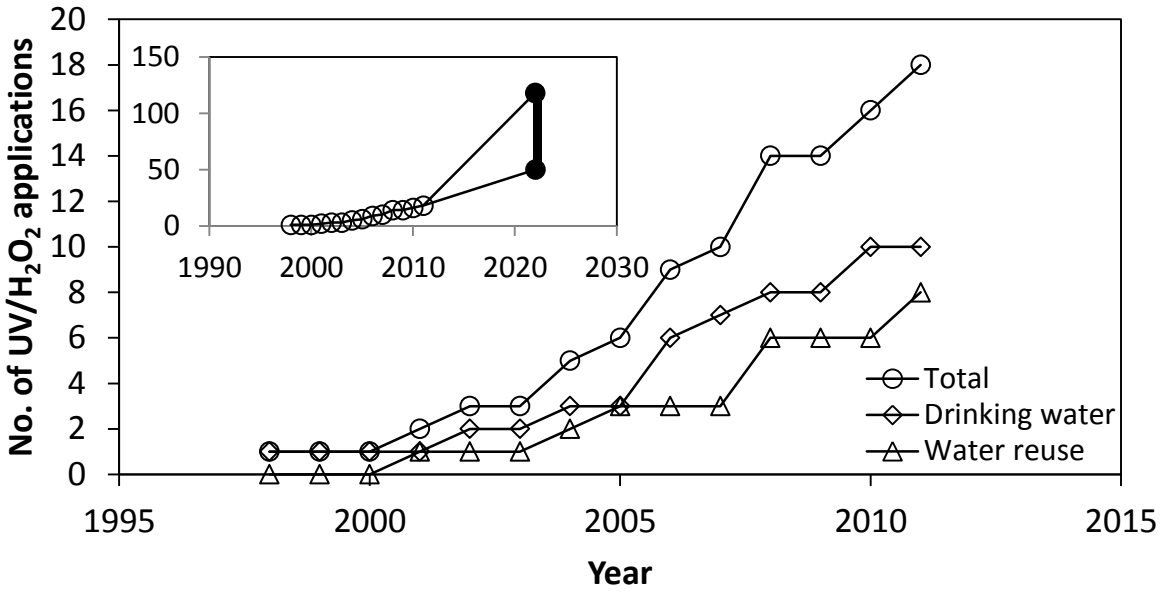

Figure 2.13: Number of UV/H_2O_2 applications worldwide for water treatment and water reuse during the last decade. Inset: prediction for next decade (between 50 and 100 new installations in next decade) based on Malley et al. (2010)

A remarkable case is that of a large water recycling project in Australia. As a result of extreme drought between 2001 and 2008, the fresh water resources of the south-eastern region of Queensland, one of the fastest growing regions in Australia, dropped drastically. As a reaction on the water scarcity, the Australian government initiated the Western Corridor Recycled Water Project one of world's largest water recycling projects. The $2.5 billion (AUS) (€2.1 billion) project involved the design and construction of three AWTPs and an underground water grid consisting of 200 km of pipeline (Rowe, 2009). The principal aim of the project was to help ensure the security of the water supply by reducing the reliance of industry and agriculture on fresh water. A maximum recycled water supply capacity of 230,000 $m^3\ d^{-1}$ is available for power plants and irrigation and, if needed, for recharge of drinking water sources.

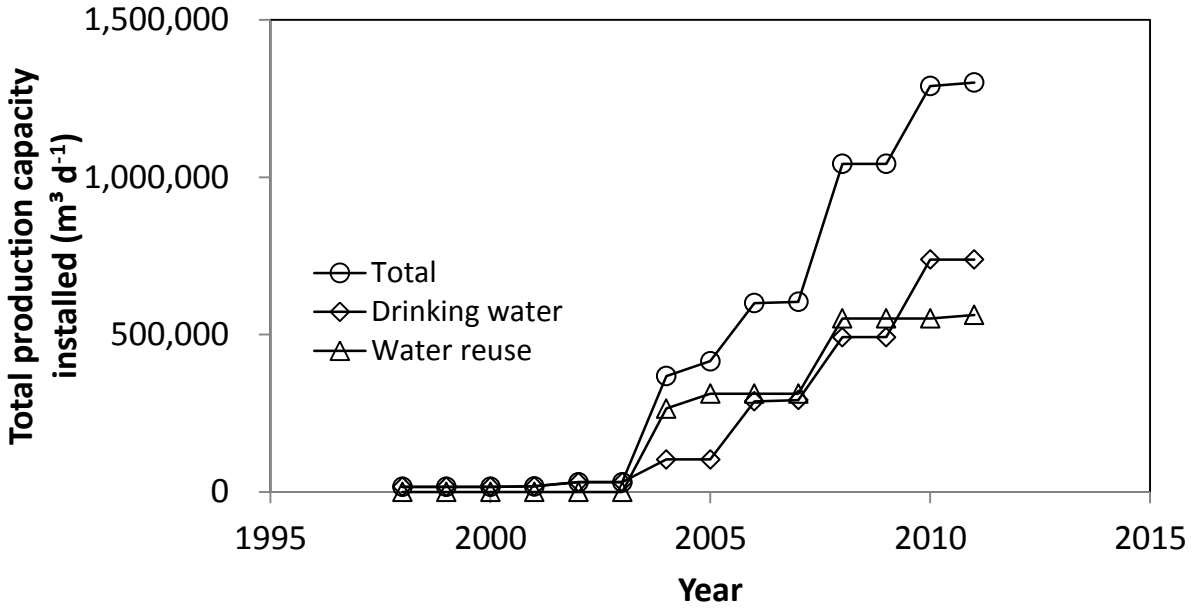

Figure 2.14: Cumulative production capacity of UV/H_2O_2 applications worldwide for water treatment and water reuse during the last decade.

The three AWTPs are located near Brisbane. A first plant was built at Bundamba, a second at Gibson Island and a third was constructed at Luggage Point (Rowe, 2009). The plants are designed to treat secondary effluent of nearby WWTPs and have a similar process setup, including UV/H_2O_2 treatment. Effluent is pretreated by coagulation and flocculation. The second step consists of membrane treatment with microfiltration followed by reverse osmosis. Finally, advanced oxidation with UV/H_2O_2 is applied (WaterSecure, 2012).

At the moment the project was finalized (2009), the drought mostly eased and the government of Queensland decided to use the recycled water as an emergency option only (Couriermail, 2008). Although the intentions of the Western Corridor Recycled Water Project initially included IPR, recycled water is now only used to supply power plants. As such, only a fraction of the production capacity is used (this was not accounted for in Figure 2.14).

Table 2.4: Full-scale UV/H_2O_2 applications for advanced water treatment or water reuse. GW=groundwater, SW=surface water, SE=secondary effluent

Water utility	Reactor (year)	Application	Target pollutant(s)	Water source	Pretreatment steps	Capacity (m^3 d^{-1})
Salt Lake City Department of Public Utilities, Utah, USA[a]	Calgon Rayox™ (1998)	Drinking water production	-PCE	GW	Unknown	16,350
City of Stockton (drinking water well), Stockton, California, USA[a,b,c]	TrojanUVPhox™ (2001)	Drinking water well protection (aquifer reinjection)	-1,4-dioxane	GW	Unknown	1,100
La Puente Valley County Water District (Baldwin Site), California, USA[a,d]	TrojanUVSwift™ECT (2002)	Drinking water production	-NDMA -1,4-dioxane	GW	-Air stripping -Ion exchange	13,600
PWN Water Supply Company North Holland (Andijk WTP), Netherlands [a,e]	TrojanUVSwift™ECT (2004)	Drinking water production	-Micropollutants	SW	-Coagulation -Rapid sand filtration	72,000
City of Cornwall, Ontario (Cornwall WTP), Canada[a,b]	TrojanUVSwift™ECT (2006) (AOP on demand)	Drinking water production	-NDMA -1,4-dioxane	SW	-Coagulation -Mixed-media filtration	100,000
Valley County Water District (Baldwin Site), California, USA[a,f]	TrojanUVSwift™ECT (2006)	Drinking water production	-NDMA -1,4-dioxane	SW	-Air stripping -Ion exchange	42,400
San Gabriel Valley Water Company (Baldwin Site), California, USA[a,c]	TrojanUVPhox™ (2006)	Drinking water production	-NDMA -1,4-dioxane	SW	-Air stripping -Granular activated carbon filtration -Ion exchange	42,400
California water service company (Lucerne WTP), California, USA[c]	TrojanUVSwift™ECT (2007) (AOP on demand)	Drinking water production	-MIB -Geosmin	SW	-Coagulation -Rapid sand filtration	3,800
Regional municipality of Peel (Lorne Park WTP), Ontario, Canada[c]	TrojanUVSwift™ECT (2008)	Drinking water production	-MIB -Geosmin	SW	-Coagulation -Ultrafiltration	200,000
Aurora Water (Peter Binney WTP), Colorado, USA[b,g]	TrojanUVPhox™ (2010)	Drinking water production	-NDMA and other nitrosamines -Micropollutants	SW	-River bank filtration -Coagulation -Sedimentation	190,000

Table 2.4 (continued)

Aqua Pennsylvania (Neshamini Falls WTP), Pennsylania, USA[c]	TrojanUVSwift™ECT (2010) (AOP on demand)	Drinking water production	-MIB -Geosmin	SW	-Coagulation -Rapid sand filtration	57,000
Orange County Water District (GWRS), California, USA[a,b,h]	TrojanUVPhox™ (2004)	Water reuse (aquifer injection)	-NDMA -1,4-dioxane	SE	-Microfiltration -Reverse osmosis	265,000
West Basin Municipal Water District (El Segundo RWPF), California, USA[a,i]	TrojanUVPhox™ (2005)	Water reuse (sea water barrier injection)	-NDMA	SE	-Microfiltration -Reverse osmosis	47,300
Queensland State Government (Bundamba AWTP), Queensland, Australia[j,k,l]	TrojanUVPhox™ (2008)	Water reuse (process water for power stations)	-Micropollutants	SE	-Coagulation -Microfiltration -Reverse osmosis	66,000
Queensland State Government (Gibson Island AWTP), Queensland, Australia[k,l]	TrojanUVPhox™ (2008)	Water reuse (process water for power plants)	-Micropollutants	SE	-Coagulation -Microfiltration -Reverse osmosis	100,000
Queensland State Government (Luggage Point AWTP), Queensland, Australia[k,l]	TrojanUVPhox™ (2008)	Water reuse (process water for power stations)	-Micropollutants	SE	-Coagulation -Microfiltration -Reverse osmosis	66,000
Colorado River Municipal Water District (Big Spring RWPF), Colorado, USA[c,m]	TrojanUVPhox™ (2011)	Water reuse (surface water injection)	-Micropollutants	SE	-Microfiltration -Reverse osmosis	6,800
Water Replenishment District of Southern California (Leo J. Vander Lans AWTP), California, USA[c]	TrojanUVPhox™ (2011)	Water reuse (sea water barrier injection)	-NDMA	SE	-Microfiltration -Reverse osmosis	11,300

[a]Sarathy and Mohseni, 2006; [b]Leach et al., 2006; [c]case studies provided online by Trojan Technologies inc. (TrojanUV, 2012); [d]La Puente Valley County WD, 2010; [e]Martijn et al., 2008; [f]VCWD, 2007; [g]Swaim et al., 2011; [h]Malley, 2010; [i]West Basin MWD, 2011; [j]water-technology.net, 2011; [k]Rowe, 2009; [l]WaterSecure, 2012; [m]CRMWD, 2009

In the Netherlands, other factors than water scarcity were drivers for the upgrade of the WTP in Andijk operated by PWN. The major goals of the introduction of advanced oxidation were to discard a breakpoint chlorination step, to provide an extra barrier against chlorine resistant micro-organisms, to enhance the overall disinfection capacity, to lower the health risk and finally, to remove micropollutants (Kruithof et al., 2007). The UV/H_2O_2 process was chosen as the use of ozone based processes led to excessive bromate formation in the bromide rich surface water, even if hydrogen peroxide was added. In the Netherlands, the proposed standard for bromate in drinking water is 5 µg L^{-1} (Loeb et al., 2012), which is relatively low compared to other countries (the EU and EPA standard is 10 µg L^{-1} (Audenaert et al., 2010)).

2.3.2.2 Process operation

Process design

In contrast to ozonation, the set-up of a UV/H_2O_2 system is relatively simple. A UV/H_2O_2 unit typically consists of a stainless steel reactor containing LP or MP-UV lamps surrounded by a quartz jacket. Furthermore, a power supply and hydrogen peroxide dosing system are required (Linden et al., 2005). If a plant is upgraded, the UV/H_2O_2 is mostly placed in-line of an existing water pipe.

The choice for LP or MP UV/H_2O_2 and the dimensions of the system are highly site dependent. Typically, extensive lab-scale research followed by pilot scale testing is used to assess the performance of the technique in the site-specific water matrix. Also the use of kinetic models whether or not in combination with computational fluid dynamics (CFD) can be of significance for the designing process (Alpert et al., 2010; Mohajerani et al., 2010; Wols et al., 2011). If lamp placement is optimized by means of CFD, 3D images of the UV reactor are used, as demonstrated in Figure 2.15. The simulation results, combined with plant specific

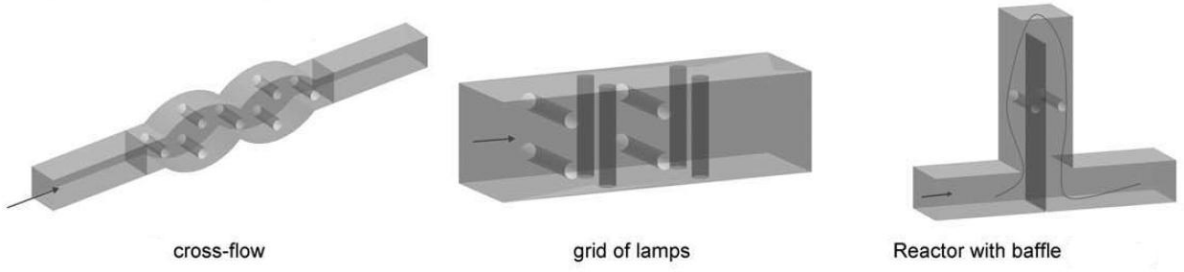

Figure 2.15: Three dimensional images of UV reactors used for CFD calculations to optimize lamp placement (Wols et al., 2011)

parameters (flow rate characteristics, down- and upstream processes, …) are used to design the full-scale installation. MP-UV lamps can operate at a higher power input than LP-UV lamps which makes that MP-UV reactors need fewer lamps than LP-UV reactors.

The market leader of UV/H_2O_2 applications for water treatment or water reuse is Trojan Technologies inc. In almost every WTP or RWPF included in Table 2.4, the AOP unit was designed and constructed by Trojan. Two commercially available UV/H_2O_2 units are supplied by this Canadian company: the TrojanUVPhox™ and TrojanUVSwift™ECT reactors (TrojanUV, 2012). The TrojanUVPhox™ relies on low pressure high output (LP-HO) amalgam UV lamps. This monochromatic light source is especially used in combination with hydrogen peroxide to accomplish advanced oxidation. The TrojanUVSwift™ECT system (Figure 2.16) consists of medium pressure UV lamps that enable UV-photolysis of organic contaminants. This system can also be used in combination with hydrogen peroxide (TrojanUV, 2012).

Figure 2.16: The polychromatic TrojanUVSwift™ECT system with cross-flow lamp configuration (PWN, 2012)

Process control

Most of the UV reactors are equipped with UV sensors that continuously measure the output of the lamps. This indicates whether scaling of the quartz sleeves is occurring and cleaning is needed. Cleaning can be automated using an automatic wiping system (TrojanUV, 2012).

To control the oxidation process, the lamp power, the number of lamps in operation and the H_2O_2 dosage are the main process parameters to be varied. However, often the UV dose and H_2O_2 concentration are set based on the worst case scenario, leading to cost intensive operation (Hofman-Caris et al., 2012). In some cases, UV absorbance measurements are used to control the process (TrojanUV, 2012), although it remains unclear how this is exactly performed.

More optimal operation can be achieved with the help of mathematical models that provide information on the scavenging capacity of the water that is treated. The use of such models for predictive process control has not yet been described in literature and research is still in full development. Nowadays, kinetic models are especially used to support reactor design (Kruithof et al., 2007; Li et al., 2008) and to help understand the process in non-synthetic water (Audenaert et al., 2011).

Costs

The major part of the operational costs of a UV/H_2O_2 system is related to the electrical energy consumption by the UV lamps and the dosage of hydrogen peroxide. As an example, the UV/H_2O_2 system in Andijk, the Netherlands will be considered. The energy requirement at normal operation in WTP Andijk is 0.56 kWh m^{-3} and the applied H_2O_2 dose is 6 mg L^{-1} (Martijn et al., 2008). If an energy cost of 0.07 €/kWh is assumed (Ried et al., 2009), the operational cost for energy is around 0.039 € m^{-3}. With a unit price for hydrogen peroxide of 1.5 \$ lb^{-1} (2.7 € kg^{-1}) (Li et al., 2008), the cost associated with hydrogen peroxide consumption is around 0.016 € m^{-3}. Hence, total operational costs attributed to energy and hydrogen peroxide vary around 0.055 € m^{-3}. Noteworthy, however is that significant regional differences exist in energy and hydrogen peroxide prices and thus this calculation is only an approximation. Additionally, an energy cost of 0.1€ kWh^{-1} currently is a more realistic value (Lucas et al., 2010). The (lower) energy cost mentioned above was applied to allow comparison with ozonation data further in this chapter. This calculation shows that especially the energy consumption determines the operational cost of the UV/H_2O_2 process. Compared to ozonation, where generally energy consumption varies around 0.1 kWh m^{-3} (Ried et al., 2009), the UV/H_2O_2 process is five times more energy intensive.

Regarding the combined operational and capital cost, a large range can be found in literature. The reported values are highly dependent on the scale of the plant, UV and hydrogen peroxide dose applied and the approximations made about energy and hydrogen peroxide cost. In general, total costs vary between 0.05 and 0.46 € m^{-3} water treated (Bolle and Pinnekamp, 2011).

2.3.3 Application of ozone for advanced water treatment and reuse

Besides its major use as a drinking water disinfectant, ozone is applied for a wide variety of other applications including industrial and municipal wastewater treatment, swimming pool disinfection, cooling water treatment, groundwater remediation and water reuse (Ried, 2012). E.g. the main use for ozone in Germany is the treatment of swimming pool water (Loeb et al., 2012). Besides the use in water and wastewater, ozone has numerous other applications. It is used in agricultural, food and electronic industry, for air treatment and for medicinal therapy (the so-called ozonotherapy) (Ried, 2012).

As mentioned in Section 2.3, the use of ozone for drinking water applications is an established technique for already one century. France is considered as the cradle of ozone for drinking water disinfection. Early water disinfection tests in 1886 lead to a first full-scale application in 1906 and by 1961, over 500 ozonation plants were already installed (Le Paulouë and Langlais, 1999). To make a comparison, the first significant ozone application in the USA was installed in 1940, and the technology had a real breakthrough in 1987 (Rice, 1999). Worldwide, the current number of applications in this field is estimated to be around 3,000 (Oneby et al., 2010). The primary goal in most of the cases is to achieve disinfection, although there are a lot of plants that also implemented ozone for oxidation of recalcitrant organic contaminants.

As a lot of literature is available on drinking water ozonation, this review will only focus on recent developments in the application of ozone for municipal wastewater treatment and water reuse.

In the specific case of ozone, multiple potential positions in the municipal wastewater treatment train exist (Figure 2.17) (Ried et al., 2009):

- Improvement of effluent quality (chemical and microbiological)
- Sludge treatment (foam reduction, enhancement of settling properties)
- Treatment of exhaust air (odour reduction)
- Treatment of highly contaminated side streams (decolorization, reduction of toxicity)

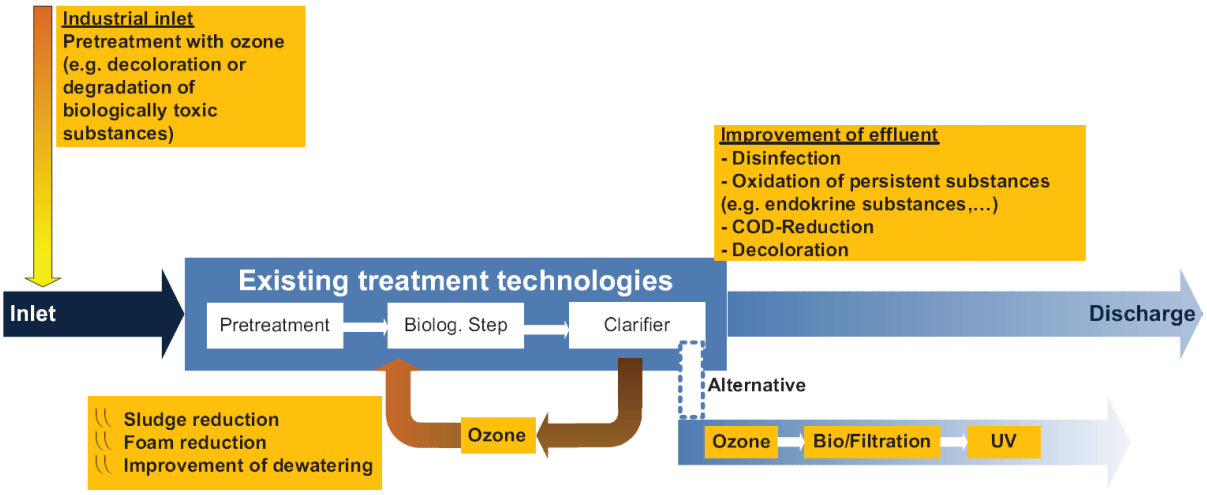

Figure 2.17: Potential applications of ozone in the municipal wastewater treatment train (Mielcke and Ried, 2012)

In this dissertation, the treatment of effluent is the ozone application of interest. As shown in Figure 2.18, the goal that will be achieved depends on the amount of ozone that is dosed to the secondary effluent. Significant differences in lower and upper bounds exist, as wastewater characteristics are highly variable and case dependent (Ried et al., 2009). This figure shows that ozone doses between 0.5 and 5 mg L^{-1} can be effective for disinfection. It is, however, likely to occur that applying these dosages does not result in a measurable aqueous ozone concentration due to the high rapid ozone demand of the effluent.

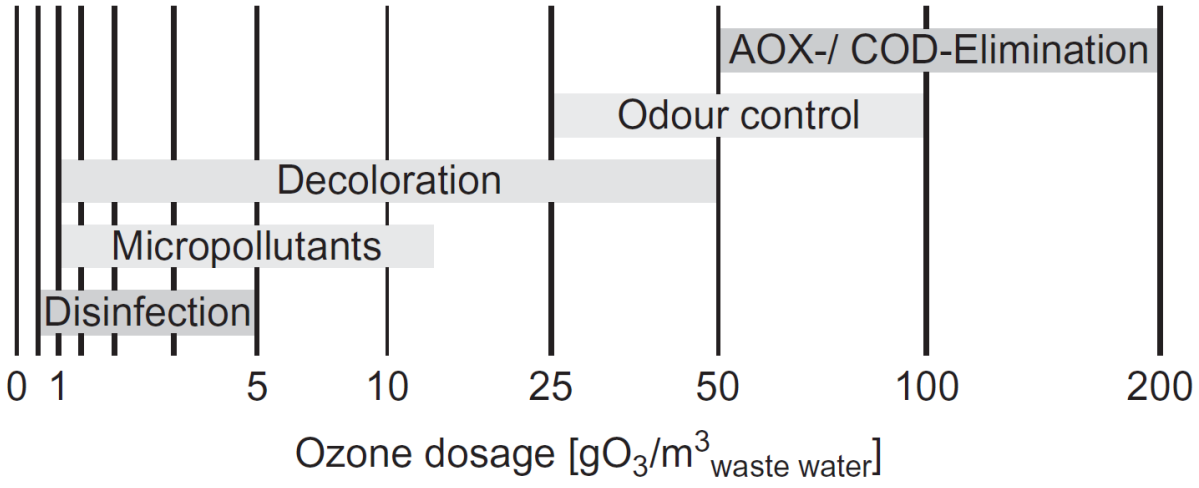

Figure 2.18: Goals to be reached with effluent ozonation as function of ozone dose (Ried et al., 2009)

Required doses to achieve measurable ozone can easily vary between 1 and 7 mg L^{-1} (Wert et al., 2009). It can thus be concluded that deactivation of bacteria

can occur in the absence of detectable ozone (Xu et al., 2002). For micropollutant reduction and decolorization, doses vary between 1 and 15 mg L^{-1} and 1 and 50 mg L^{-1}, respectively. Again, the applied dose is site dependent. In general, ozone dosages that are currently applied at full-scale plants vary between 5 and 10 mg L^{-1} for final discharge and 10 and 15 mg L^{-1} for reuse (Loeb et al., 2012). Reuse requires decolorization and hence, higher dosages (Figure 2.18).

2.3.3.1 Historical development

Tertiary treatment of municipal wastewater using ozone already exists for about forty years. However, after a strong initial interest during the early period, the number of wastewater applications declined, while ozone applications in drinking water grew exponentially. Since the 1990s, renewed interest resulted in a steady growth until today (Loeb et al., 2012).

The evolution described above can be illustrated using the USA as example. During the decade between 1975 and 1985, driven by USA EPA encouragement and government funds, the number of North-American WWTPs implementing ozone grew to 44 (Oneby et al., 2010). The major part of these plants introduced ozone for effluent disinfection. From the aforementioned plants, only five still use ozone today. The remaining facilities switched to alternative disinfectants such as chlorine and UV. To date, the number of new applications installed after 1985 that are still in operation today is only five. Three other plants discarded ozone in the meantime, one of the early plants re-introduced ozone. As such, the current number of applications in the USA is nine (Table 2.5).

The reason for the slow development of ozone technology for advanced wastewater treatment is twofold: (1) early ozone installations were inundated with operation and maintenance problems and (2) disinfection was much more important than oxidation in the past, making other alternatives more attractive.

Considering recent developments in ozone technology, the first issue can be addressed as follows: frequently occurring problems with early installations included prohibitive maintenance requirements, frequent breakdowns, material damage due to moisture and ozone and inefficient ozone production (Oneby et al., 2010). Due to the widespread experience with drinking water ozonation, all of these problems were addressed properly. The efficiency of ozone generation significantly improved, which is a key factor for raising applicability (Ried et al., 2009). Related to the second issue: nowadays, as stated in Section 2.3, advanced wastewater treatment including oxidation becomes more important, which partly

explains the renewed interest in ozone applications for municipal wastewater treatment.

2.3.3.2 Current situation

As mentioned in previous section, the total number of WWTPs using ozone that are currently in operation in the USA is about nine. In other continents, the current status of ozone use at WWTPs is also limited. Based on a recent survey of the European, African, Asian, Australasian group (EA_3G) of the International Ozone Association (IOA), the total number of ozone installations at WWTPs in the EA_3G region in 2004 was only nine (Loeb et al., 2012). Most likely, the major part of the (small-scale) applications can be found in Japan. The installations are used for final discharge (100,000 $m^3\ d^{-1}$ per plant on average) and to a less extend for water reuse at smaller scale (usually less than 10,000 $m^3\ d^{-1}$ per plant) (Loeb et al., 2012). Some full-scale WWTPs or AWTPs that use ozone are listed in Table 2.5. In contrast to Table 2.4, this table does not contain all of the existing ozonation plants as information about these applications is harder to find than that of the recent UV/H_2O_2 applications. This was also recognized in a recent review on worldwide ozone capacity by Loeb et al. (2012). The table, however, contains most of the existing water reuse facilities. In comparison with UV/H_2O_2 applications, the treatment train preceding the oxidation step is designed differently. Table 2.4, however only includes facilities designed for water reuse or drinking water production, while in Table 2.5 several projects for direct discharge were included (these applications often apply ozonation directly to the secondary effluent). Nevertheless, water reuse plants that make use of ozone apply micro- or ultrafiltration, rather than reverse osmosis and granular or powdered activated carbon adsorption is more often applied. Based on numerous lab-scale, pilot-scale and full-scale studies, the combination of ozone and granular activated carbon seems to be economically and technically feasible and can be considered as full-scale approved (Mielcke and Ried, 2012).

Table 2.5 reveals that the number and total capacity of water reuse projects using ozone is limited and smaller compared to UV/H_2O_2 applications (Table 2.4). This is especially the case for projects involving IPR. However, three larger scale projects started up recently: the F. Wayne Hill Water Reclamation Center (FWHWRC), the Clark County Water District AWTP and the Fred Hervey Water Reclamation Center (FHWRC). All three plants were constructed in densely populated regions with limited water availability due to climatological or geographical reasons (Oneby et al., 2010). The projects are included in Table 2.5 and will be shortly summarized below.

Table 2.5: Full-scale ozone applications for advanced wastewater treatment or water reuse

WWTP (year in which ozonation was installed) and/or location	Application	Targets	Treatment steps of secondary effluent	Ozone dose (mg O_3 L^{-1})	Capacity (m^3 d^{-1})
WWTP Ranica, Italy[a]	Final discharge	Decolorization (textile industrial activity) Disinfection	-Porous media filtration -Ozonation	6.6	48,000
Wuëri WWTP (2009), Regensdorf, Switzerland[a,b]	Final discharge	Micropollutant removal Disinfection	-Ozonation	3	5,550
Bad Sassendorf WWTP (2009), Germany[c]	Final discharge	Micropollutant removal	-Ozonation -Stabilization	2-7	7,200
Duisburg-Vierlinden WWTP (2011), Germany[c]	Final discharge	Micropollutant removal	-Ozonation -Biological post-treatment	2-7	9,600
Schwerte WWTP (2010), Germany[c,d]	Final discharge	Micropollutant removal	-Ozonation -PAC dosing	10	15,700
South Caboolture AWTP (1999), Queensland, Australia[b,e]	Water reuse (non-potable)	Micropollutant removal Disinfection	-Biological denitrification -Pre-ozonation -Coagulation -Dissolved air flotation -Sand filtration -Main ozonation -BGAC filtration -Final ozonation	2(pre)/ 5(main)/ 2(post)	10,000
Mahoning County WWTP (1995), Ohio, USA[f]	Final discharge	Disinfection	-Ozonation	unknown	31,200
Springfield, Missouri (2000), USA[f]	Final discharge	Disinfection	-Ozonation	unknown	112,800
Frankfort, Kentucky (2007), USA[f]	Final discharge	Disinfection	-Ozonation	unknown	26,400
Fred Hervey WRP (2008), Texas, USA[f]	Water reuse (irrigation, industrial cooling water, aquifer injection of IPR)	Disinfection	-Lime treatment -Recarbonatation -Granular media filtration -Ozonation -GAC adsorption	unknown	38,400
Trion (1997), Georgia, USA[f]	Final discharge	Color removal Disinfection	-Ozonation	27	31,200

Table 2.5 (continued)

F. Wayne Hill WRC (2006) Gwinnett County, Georgia, USA[f,g]	Water reuse (surface water injection for IPR)	Disinfection	-Coagulation -Ultrafiltration -Pre-ozonation -GAC adsorption -Post-ozonation	2.7(pre)/ 1.3 (post)	151,200
Belmont WWTP (2010), Indiana, USA[f]	Final discharge	Disinfection	-Porous media filtration -Ozonation	6	408,000
Southport WWTP (2010), Indiana, USA[f]	Final discharge	Disinfection	-Porous media filtration -Ozonation	6	408,000
Clark County Water Reclamation District Las Vegas (2006), Nevada, USA[f,h]	Water reuse (surface water injection for IPR)	Micropollutant removal Disinfection	-Ultrafiltration -Ozonation	8	112,800
Tokyo Bureau of Sewerage, Shibaura AWTP (2004), Tokyo, Japan[i]	Final discharge Water reuse (lavatory flushing and irrigation)	T&O Disinfection	-Biological filtration -Ozonation -Microfiltration -Chlorination	unknown	4,300
Tokyo Bureau of Sewerage, Ariake AWTP, Tokyo, Japan[i]	Final discharge (90%) Water reuse (lavoratory flushing and irrigation) (10%)	T&O Disinfection	-Biological filtration -Ozonation -Chlorination -Microfiltration	unknown	unknown

[a]Ried et al., 2009; [b]Gerrity and Snyder, 2011; [c]Grünebaum, 2011; [d]MKULNV.NRW; [e]Watertec Engineering, 2006; [f]Oneby et al., 2010; [g]Porter, 2010; [h]Drury and Snyder, 2007; [i]Yamashita and Kaya, 2009

The FWHWRC is an AWTP that discharges highly treated effluent into two different surface waters that serve for recreational purposes and drinking water production (Oneby et al., 2010). The plant is located in Gwinnett County, Georgia, USA and was developed stepwise. A first phase was completed in 2003, the second and final phase was completed in 2006. The design of the AWTP was based on multiple effluent quality goals to be met.

The AWTP of the Clark County Water District is located in the water scarce Las Vegas, Nevada, USA. The water district owns several WWTPs that discharge into the Las Vegas Wash, a channel that ends up in the primary drinking water source of the Las Vegas valley, Lake Mead. In fact, prior to the construction of the AWTP, unplanned IPR was occurring (since 1950s). Besides ozonation, this plant included ultrafiltration in its treatment train. This current combination of unit operations allows for enhanced phosphorus removal, multiple barrier removal of micro-organisms and removal of trace pollutants (Oneby et al., 2010). In contrast to the FWHRC, granular activated carbon (GAC) filtration is not applied.

The FHWRC is located in El Paso, Texas, USA. Although this facility has a significant smaller production capacity than the two previous mentioned AWTPs, it is worth to discuss it into more detail. The water produced by this AWTP meets the drinking water standards due to extensive treatment using multiple unit processes, as shown in Table 2.5. The secondary treatment (not included in the table) prior to the advanced treatment relies on a biophysical process combining conventional activated sludge (CAS) with powdered activated carbon (PAC) dosing (Oneby et al., 2010).

With respect to projects for final discharge, recent applications can especially be found in Europe (Germany and Switzerland) and the USA (Indiana), as shown in Table 2.5. The four European projects were especially designed for removal of trace pollutants, while the two plants in Indiana (Southport and Belmont WWTPs) were upgraded with ozonation for disinfection. The Southport and Belmont WWTPs replaced early ozonation systems by other techniques, but recently re-introduced ozone in their treatment train (Oneby et al., 2010). Recently, Montreal (Canada) announced that it plans to be world's first metropolis that disinfects all of its wastewater using ozone (Loeb et al., 2012). This project is expected to be of huge capacity.

2.3.3.3 Process operation

Process design

Integration of an ozone system into a WWTP implies that the following key elements have to be considered (Ried et al., 2009):

- Ozone dose range to be applied (case dependent)
- Calculation of the ozone demand (Ozone dose multiplied by the flow rate)
- Different elements of which the ozone unit exists
- Process control, online measurement

The ozone dose range is typically determined by preliminary lab-scale or pilot-scale research. Factors that especially determine the ozone consumption are both the influent composition and WWTP performance. These issues determine the quality of the secondary effluent at which the ozonation is applied.

Figure 2.19 presents the different building blocks of which a typical ozone process at a WWTP consists. These elements include the ozone generator (Figure 2.20), oxygen supply, cooling unit, power supply, reaction chamber and off gas handling.

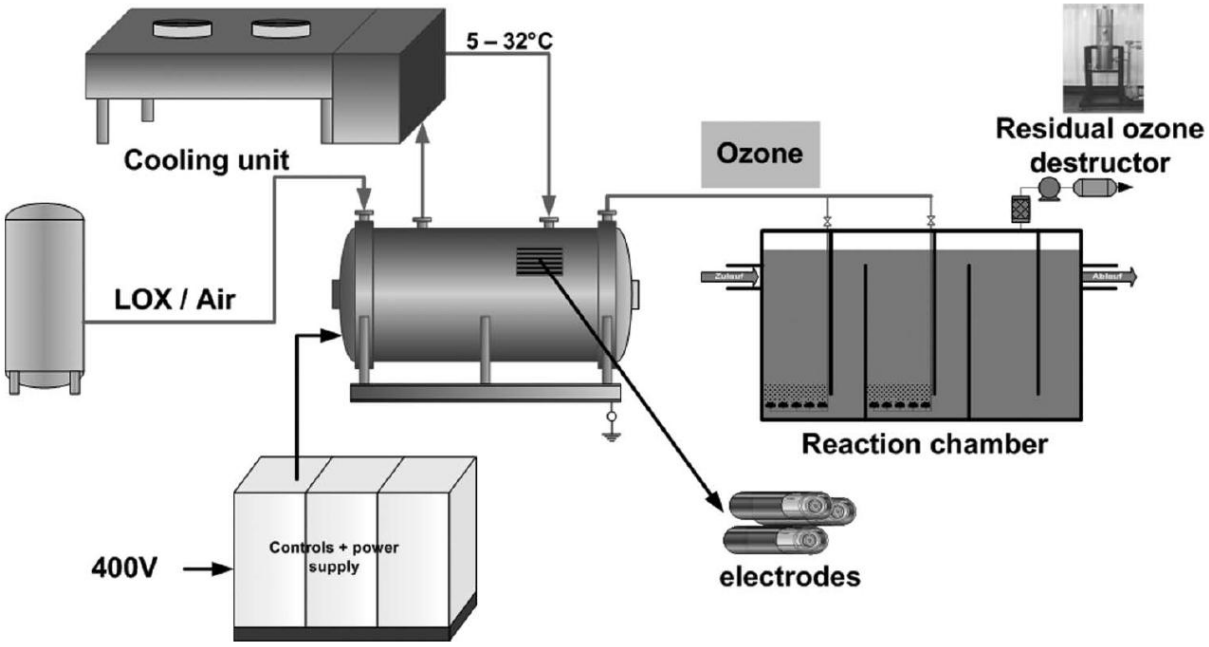

Figure 2.19: General layout of an ozone system integrated in a WWTP (Ried et al., 2009)

Oxygen supply can be either air, liquid oxygen (LOX) or oxygen that is produced on-site by pressure swing adsorption (PSA) (Ried et al., 2009). For the ozone reaction chamber, an existing concrete basin can be used to save costs. This was e.g. the case in WWTP Wüeri in Switzerland where a mixing chamber for final

flocculation was retrofitted to a full-scale six compartments ozone reactor (Zimmermann et al., 2011). Most of the current plant design is based on extrapolated knowledge from drinking water ozonation.

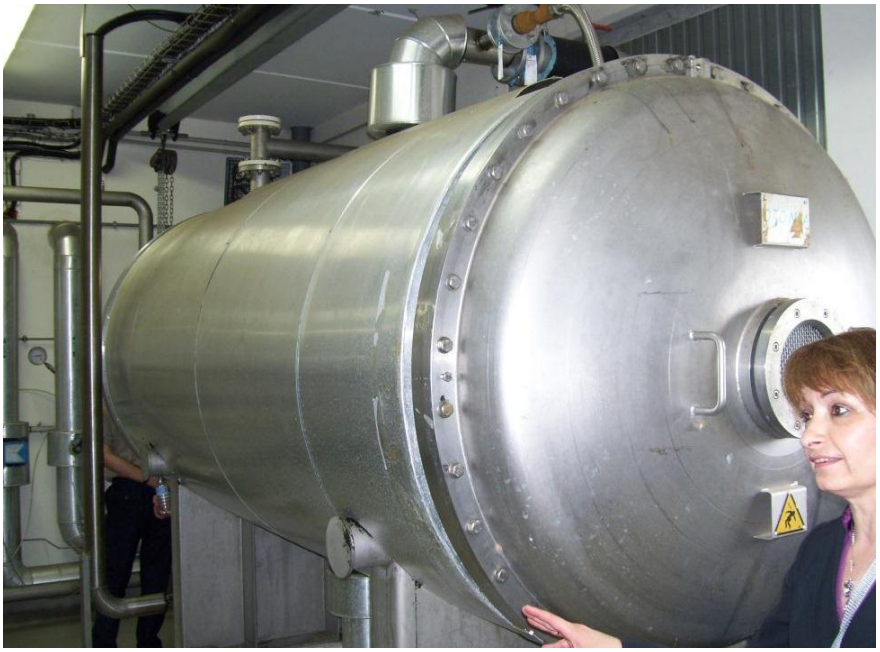

Figure 2.20: Ozone generator (30 kg h^{-1}) at WWTP of Laroque d'olmes, Ariège, France; the plant treats combined municipal and textile wastewater; ozone dose is 30 mg L^{-1}

Process control

For process control of the ozonation process, several measurements are readily available such as water flow rate, gaseous ozone concentration in both feed gas and off gas, feed gas flow rate and aqueous ozone concentration at the end of the reactor. These parameters can be controlled readily based on their measurements (Ried et al., 2009). However, as discussed earlier, aqueous ozone is often not detectable due to the rapid ozone demand that is inherent to secondary effluent. As such, the above mentioned measurements only allow for control of a fixed ozone dose based on both the water flow rate and ozone consumption rate (difference between feed gas mass flow rate and off gas mass flow rate).

Additional control strategies exist. E.g. in WWTP Bad Sassendorf (Germany), multiple strategies were tested (Grünebaum, 2011). As shown in Figure 2.21, three different approaches were used to obtain the desired ozone dose (the figure was translated to English). The first and most simple approach was based on a single set-point value for the ozone dose (e.g. 2 mg L^{-1}) and corresponds to the method described above. The second approach was based on a set point value of the specific ozone dose (mg O_3 mg DOC^{-1}). On-line absorbance measurements were

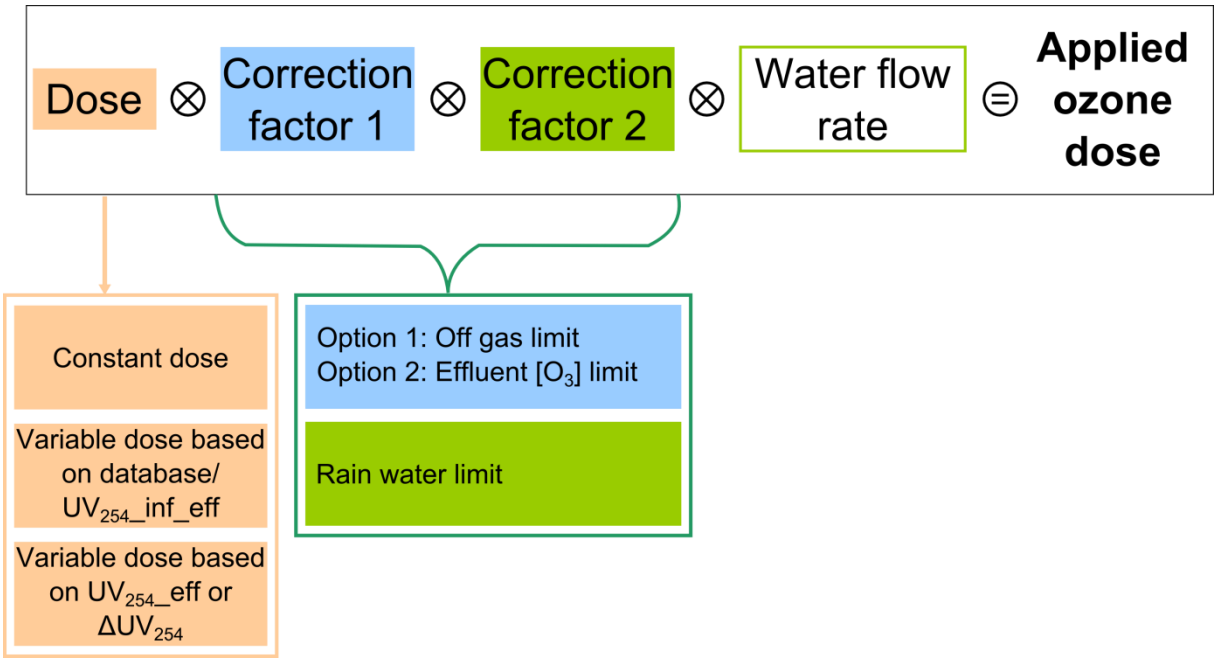

Figure 2.21: Control strategies that were tested in Bad Sassendorf, text translated to English (Grünebaum, 2011)

used to approximate the DOC by using a correlation between the DOC and UV_{254}. As such, the ozone dose applied was dependent on the DOC value prior or after ozonation. An on-line DOC sensor could allow for constant (re)evaluation of the existing correlation. The third strategy also relied on UV_{254} measurements. However, in this case, the ozone dose applied was function of (1) the absorption coefficient of the raw effluent or (2) the difference in absorption of the water before and after oxidation (Grünebaum, 2011).

Besides a strategy to set the ozone dose, some safety factors were considered. Threshold values for the off gas and aqueous ozone concentrations were built in that allowed for automatic correction (lowering) of the ozone dose if these values were exceeded. Also a correction that comes into action at rain events was applied. These safety measures imply that in some cases, the desired dose cannot be reached (Grünebaum, 2011).

Considering the oxidation of trace pollutants, which is one of the major goals of today's ozone plants, process control is much more difficult and still in full development. Analysis of trace pollutants requires expertise, proper instrumentation and is time, labour and cost intensive (Gerrity and Snyder, 2011). As such, on-line or frequent off-line measurement of these compounds is infeasible and hence, proper surrogates that can be measured on-line are needed. Recent research designated absorbance, color and fluorescence measurements as promising

surrogates to be used for process control (Wert et al., 2009; Nanaboina and Korshin, 2010) (see also Chapter 7).

In that context, process control of drinking water ozonation is much easier. The water to be ozonized is less dynamic in composition and a detectable aqueous ozone concentration is present. Additionally, using the R_{ct} concept (see Section 2.2.3.4), both ozone and hydroxyl radical induced conversion of micropollutants is predictable. Unfortunately, the R_{ct} approach cannot be used for ozonation of secondary effluent as the $HO^{\bullet}$ concentration and scavenging capacity of the water matrix are highly variable in time (Buffle and von Gunten, 2006) (see also Chapter 7). An example of model predictive control of drinking water ozonation is described elsewhere by van der Helm (2007). The model is used to predict disinfection and the formation of bromate and assimilable organic carbon (AOC). On-line UV_{254} measurements are a major model input (van der Helm, 2007).

Costs

A detailed estimation of the costs associated with ozone systems designed for different treatment capacities and oxygen sources is given in Table 2.6. An ozone dose of 7.5 mg L^{-1} was assumed. The costs for the reaction system and housing for the ozone generator are not included in the table (Ried et al., 2009). In some cases, existing infrastructure can be used. Important to notice is that costs for liquid oxygen and energy and hence, the choice of oxygen supply, are highly dependent on the region where the plant is located.

In general, the combined capital and operational costs vary between 0.02 and 0.07 € m^{-3} water treated (Ried et al., 2009). Costs rapidly decline with increasing plant capacity following a power function (Haltmeier and Pazhepurackel, 2012). Total costs for plants having capacities >100,000 p.e. vary between 0.02 and 0.04 € m^{-3} while costs at plants treating wastewater of less than 10,000 p.e. can reach 0.10 € m^{-3} (Bolle and Pinnekamp, 2011).

Costs related to some of the full-scale applications given in Table 2.5 are presented in Table 2.7. Only the ozonation process is considered, except for the South Caboolture AWTP, where the cost of the entire advanced treatment train was included.

Table 2.6: Cost calculation for different ozone systems (Ried et al., 2009)

Parameters	Unit	Price	Price	Price	Price	Price
Feedgas:		LOX	AIR	LOX	AIR	PSA
Availability:						
Year	h/a	8,760	8,760	8,760	8,760	8,760
Availability	%	95%	95%	95%	95%	95%
Availability per year	h/a	8,322	8,322	8,322	8,322	8,322
Ozone production capacity:						
Ozone production	kg/h	5.0	5.0	50.0	50.0	50.0
Yearly ozone production capacity	kg/a	41,610	41,610	416,100	416,100	416,100
Capacity:						
Water flow rate per hour, design	m^3/h	750	750	7,500	7,500	7,500
Water flow rate per year, design	m^3/a	6,241,500	6,241,500	62,415,000	62,415,000	62,415,000
Capital costs:						
Investment costs	Euro	230,000	300,000	850,000	1,450,000	1,450,000
Depreciation time	a	10	10	10	10	10
Interest rate	%/a	6.0	6.0	6.0	6.0	6.0
Annuity	%	13.59%	13.59%	13.59%	13.59%	13.59%
Annual capital costs	Euro/a	31,250	40,760	115,488	197,009	197,009
Operating costs:						
Energy demand @ 100% O_3 production	kWh/h	58.7	130.2	590.2	1,280.9	953.2
Oxygen demand @ 100% O_3 production	Nm^3/h	34.9	0	349.3	0	0
Yearly energy demand	kWh/a	488,435	1,083,924	4,911,948	10,659,421	7,932,530
Yearly oxygen demand	Nm^3/a	290,708	0	2,907,077	0	0
Yearly energy costs (0.07 € / kWh)	Euro/a	34,190	75,875	343,836	746,159	555,277
Yearly oxygen costs (0.12 € / Nm^3)	Euro/a	34,885	0	348,849	0	0
Yearly maintenance costs (2.0%)	Euro/a	4,600	6,000	17,000	29,000	29,000
Annual operating costs	Euro/a	73,675.36	81,874.67	709,685.61	775,159.47	584,277.13
Annual costs (capital & operating)	Euro/a	104,924.99	122,635.06	825,173.38	972,168.01	781,285.67
Specific invest-operating costs for ozone production	€/kg O_3	2.52	2.95	1.98	2.34	1.88
Specific invest-operating costs of ozone plant	€ cent/m^3	1.68	1.96	1.32	1.56	1.25
Specific operating costs for ozone production	€/kg O_3	1.77	1.97	1.71	1.86	1.40
Specific operating costs of ozone plant	€ cent/m^3	1.18	1.31	1.14	1.24	0.94

Table 2.7: Costs related to advanced wastewater treatment in three different plants

AWTP	OPEX (€ m^{-3})	CAPEX (€ m^{-3})	Total cost (€ m^{-3})
WWTP Ranica, Italy[a]	0.012		
WWTP Wüeri, Switzerland[a]			0.07
South Caboolture AWTP, Australia[b]	0.13	0.17	0.3

[a]Ried et al., 2009; [b]Watertec Engineering, 2006

2.4 Discussion and future developments

Due to multiple factors, the need for advanced water treatment and water reuse is significantly increasing and hence, the interest in ozone and AOPs is expected to follow the same trend. The main advantage that these processes hold over others is that destructive, effective and less specific contaminant removal can be achieved.

Considering UV applications for disinfection only, the number is expected to increase significantly within the next decade. According to a prediction by Malley (2010) the number of new wastewater disinfection applications will be around 15,000 and for drinking water disinfection, the expected number is around 7,000. However, a much slower growth is expected for UV based AOPs with 50 to 100 new applications to be designed during the coming decade. Although the UV/H_2O_2 process is currently considered as the standard for water reuse, the technique is still in full development which implies that a lot of optimization of both process design and operation can (and must) be performed. Examples are a reduction of the power consumption (improved UV lamps), application of more efficient initiators (others than hydrogen peroxide) and optimization of hydrogen peroxide quenching (Malley, 2010).

At present, two other issues that are of vital importance for further development of both the UV/H_2O_2 and ozonation process still have to be addressed: (1) improved knowledge of the organic matrix is needed, including the ability to predict the scavenging capacity and transformation products formation and the development of suitable surrogates that are of value for process control and (2) a better understanding of the basis on which process design is performed. Although the design and operation of both processes is affected, these knowledge gaps are especially hindering a rapid development of ozone processes applied at WWTPs. This is because the process set-up and underlying chemical pathways of ozonation are much more complex than those of the UV/H_2O_2 process. Additionally, extensive treatment prior to UV/H_2O_2 (e.g. reverse osmosis) significantly lowers the bulk organic matter and trace pollutant concentrations which implies that both issues become less important.

The first issue is related to the need of suitable surrogates and mathematical models that are essential for effective process control based on real-time assessment of the matrix composition. In this way, the process response can be adjusted to the changes occurring (as explained in Sections 2.3.3.2 and 2.3.4.4). The second issue is associated with a design problem and will be explained in the next paragraphs

Despite significant evidence of occurrence, scientists, regulators and policy makers have not reached consensus regarding the actual toxicological implications of micropollutants in drinking water and aquatic ecosystems (Gerrity and Snyder, 2011). The main cause is a current lack of toxicological knowledge. Extrapolation from bioassay tests to more complex organisms like humans is a complex issue (Daughton and Ternes, 1999) that currently is an important subject in scientific research. The problem is that based on these extrapolations, future regulations have to be developed and consequently, the regulatory process regarding micropollutants is hindered (Gerrity and Snyder, 2011). Besides micropollutant toxicity, also the research regarding the toxicity of transformation products is not yet in that stage, that regulations are ready to be applied.

As a result of the lack of established threshold values with respect to the oxidation part, it is difficult for plant operators to identify the appropriate oxidant dose. Although the construction of (or upgrade to) an advanced wastewater treatment may be driven by the presence of micropollutants (e.g. due to public concern), the process design will be not necessarily based on their removal (Gerrity and Snyder, 2011).

The current knowledge gaps (both chemical and toxicological) and the lack of regulatory values that impede process design of an ozonation (oxidation) step in a WWTP are schematically presented in Figure 2.22. All elements are

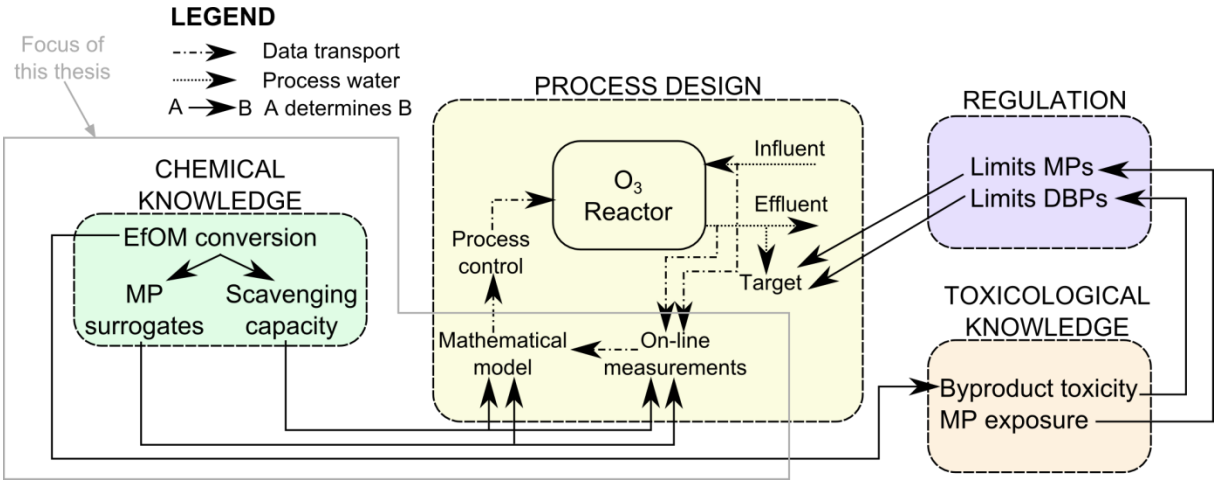

Figure 2.22: Knowledge and regulation that is needed for effective process design and control of ozone (or other oxidation) processes for advanced wastewater treatment

interconnected. The parts where this thesis will focus on are highlighted with the grey frame. These parts include experimental study of EfOM conversions, kinetic

modelling of ozonation and UV/H_2O_2 treatment in non-synthetic water and the assessment of multiple surrogates that can be measured on-line.

Although the combination of RO and UV/H_2O_2 is currently the state of the art technology for IPR, significant concerns over cost, energy consumption and brine disposal will stimulate the development of other alternatives (Gerrity and Snyder, 2011). As the knowledge and regulation depicted in Figure 2.22 will further develop, the worldwide application of ozone for municipal wastewater treatment is expected to grow at an aggressive rate (Loeb et al., 2012). This is because the efficacy of ozone to remove trace pollutants is to a large extent similar to that of UV/H_2O_2, but with the potential for reduced energy and chemical requirements (Gerrity and Snyder, 2011). In Europe, multiple research projects related to advanced wastewater treatment were recently finalized or were started up. Mainly Switzerland, Austria, Germany, the Netherlands and the UK were or are involved. (Mielcke and Ried, 2012). The most tested techniques, together with important evaluation criteria are given in Table 2.8. This complex evaluation has led to an overall European preference for ozone and activated carbon (Mielcke and Ried, 2012).

Table 2.8: Comparison of four advanced treatment processes for trace pollutant removal based on different criteria (Mielcke and Ried, 2012)

	ozone treatment	activated carbon (PAC/`GAC)	UV/H_2O_2 (Photo-oxidation)	membrane treatment
Effectiveness	high	high	limited	high
Disinfection	yes	no	yes	yes
Interferences	SS, high organic loads	SS, high organic loads	UV(T), SS, Fe/Mn, hardness high organic loads	SS, hardness, high organic loads
Operational cost	acceptable	acceptable	increased	high
Investment cost	acceptable	acceptable	lower	acceptable
Transformation, by-products	relevant	less relevant	relevant	not relevant
Environmental issues	degradation of POPs	adsorption and separation of POPs (recycling AC and/or disposal of sludge/AC)	degradation of POPs (residual H_2O_2!)	concentration and separation of POPs (disposal of concentrate)
Process handling	comfortable, reliable	AC handling, reliable	lamp replacement, quartz scaling/fouling	comfortable, membrane fouling
Process controlling design	available	undefined	not available	available
Full scale installation	yes	yes	no	yes
Comments	promising	promising	not efficient	too costly

Chapter 3

Simulation methods

3.1 Introduction

All simulations described in this work were performed using the WEST modelling platform and its backend Tornado. Different models were implemented and studied in detail using sensitivity analyses. In this chapter, the software and mathematical tools that were used will be shortly described.

3.2 WEST modelling platform

The modelling and simulation package WEST (distributed by DHI, mikebydhi.com) is especially designed for the modelling of wastewater treatment processes and provides a default set of wastewater treatment models that can be readily used for simulation. However, each model that consists of a set of differential and algebraic equations (DAEs) can be implemented in the software with a minimal programming effort (Vanhooren et al., 2003).

As the chemical models studied in this dissertation were not available in WEST by default, they were first implemented in the WEST *model editor*. Models are implemented in matrix format, as depicted in Figure 3.1, the so-called Gujer matrix. In a first step, all model components (e.g. ozone, hydrogen peroxide, …) are defined. For each component defined in the matrix a mass balance in a completely stirred tank reactor (CSTR) will be generated which results in an ordinary differential equation (ODE). Components included in the matrix are called the model's *derived state variables*. The second step is to implement the reactions (processes) that are taking place. For each reaction, a name and reaction rate is defined. Finally, the stoichiometric coefficients corresponding to the reactions between different components are introduced as central matrix elements. Parameters that are implemented in the matrix as a symbol must be defined in the parameter section. If needed, algebraic equations (e.g. acid-base equilibriums,

absorbance equations, …) can be implemented in a separate section. Once the model is implemented in the matrix, the new model is transformed into *MSL* (model specification language) and added to the *model base*. In this model base, all physical units, default parameter values, mass balances, etc. are declared (Vanhooren et al., 2003).

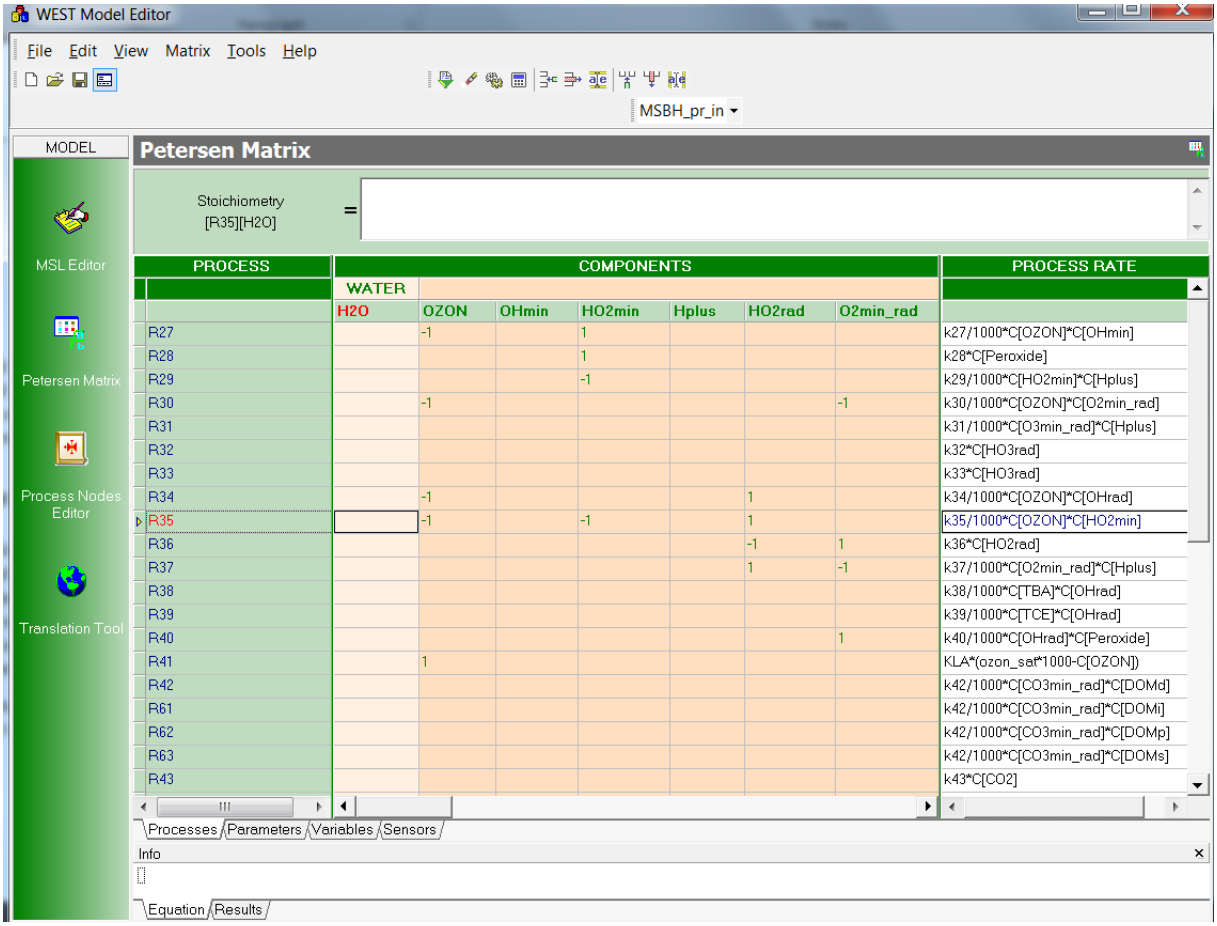

Figure 3.1: WEST model editor with model represented in matrix format

The software version used in this work (WEST 3.7.6) consists of a *modelling environment* and an *experimentation environment* (in the most recent version of WEST, i.e. WEST2011, these environments were merged).

When the modelling environment is launched, the model base is loaded. In the modelling environment, different graphical building blocks are available such as activated sludge units, settlers, controllers, … (Figure 3.2). These building blocks are related to one or more sub-models in the model base. The activated sludge unit of WEST represents a CSTR. One or more of these units were used to model the oxidation reactors studied in this work. With the help of a *hierarchical graphical editor* (HGE), complex model configurations can be constructed which represent a schematic layout of the system under study. If the configuration is built, the

building blocks and their associated models are coupled which results in a *coupled model*. Finally, the MSL code is converted into a low level C++ code which can be used in the experimentation environment after compilation into an executable model. The configuration is saved as a *.wco* file.

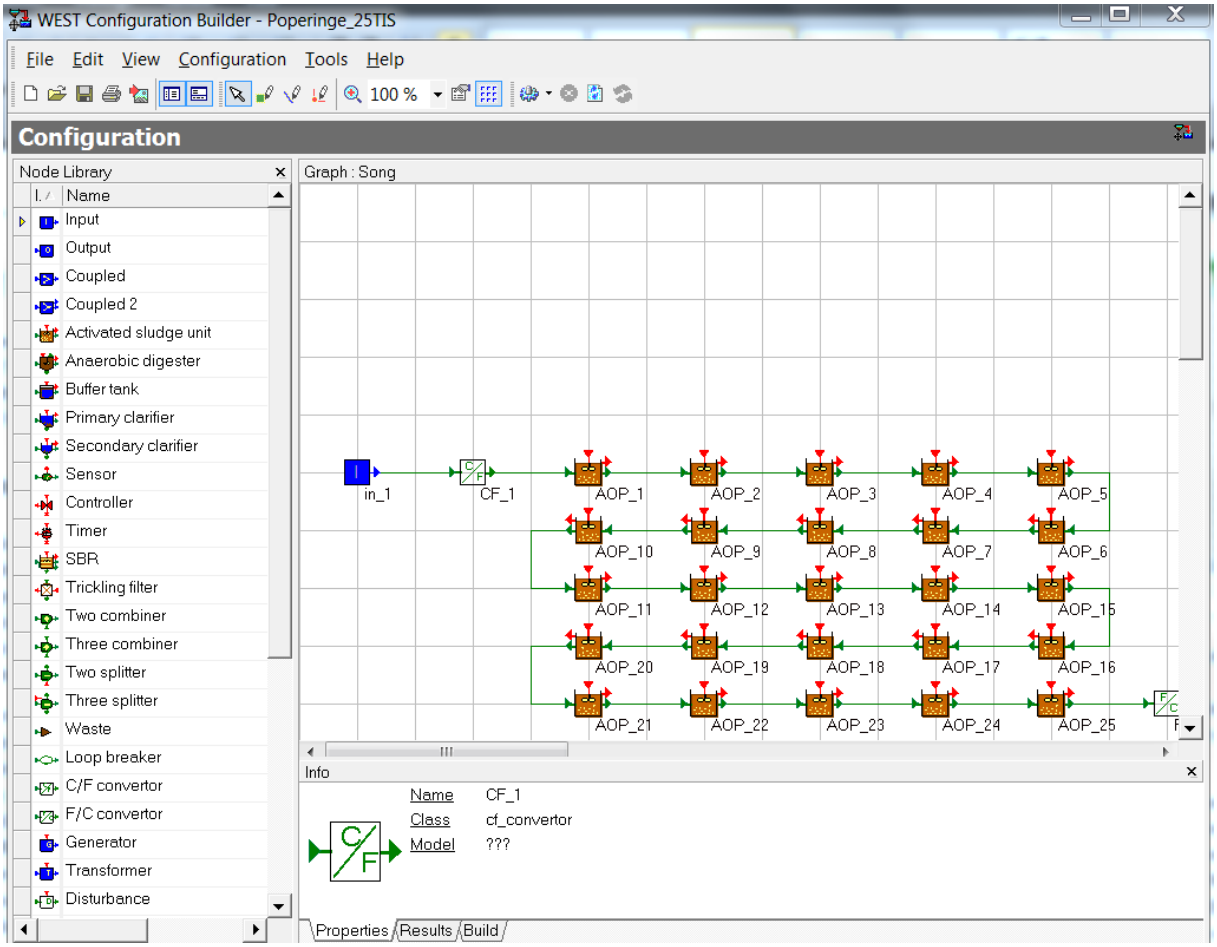

Figure 3.2: WEST modelling environment

The experimentation environment is used to perform the actual simulation experiments (Figure 3.3). Different numerical solvers are available to solve the DAEs. In this work, the stiff solver CVODE (Hindmarsh and Petzold, 1995) was used, as the chemical oxidation models typically behave as stiff systems (large differences of orders of magnitude between conversion rates of different components exist). The experimentation environment contains different automated functionalities such as data plotting, parameter optimization and sensitivity analysis. WEST experiments are saved as *.wxp* files.

If extensive configurations had to be simulated, Tornado, the backend of WEST2011 but not yet available in WEST 3.7.6, was used for its improved simulation performance in terms of speed and execution. After the .wco and .wxp

files are converted to a Tornado experiment, Tornado allows for rapid numerical simulation of the stiff systems of DAEs.

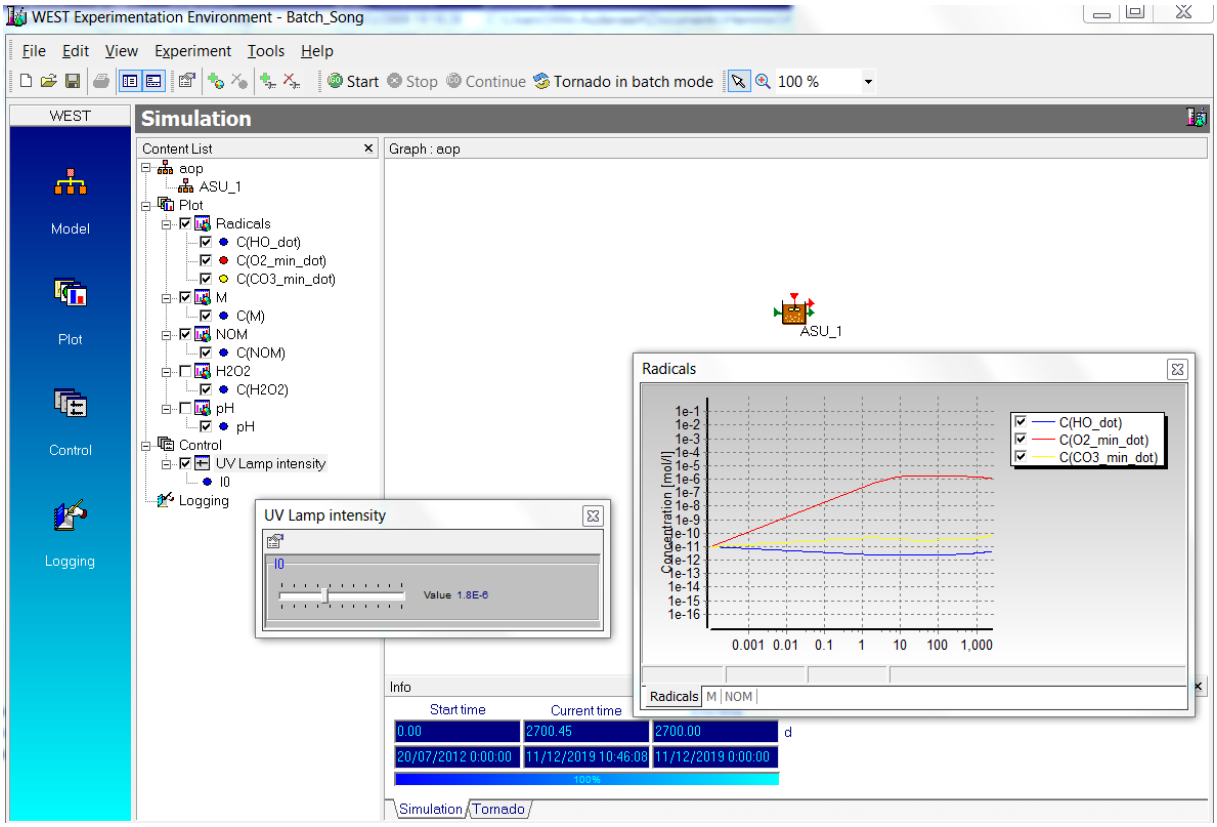

Figure 3.3: WEST experimentation environment

3.3 Local sensitivity analysis

A local sensitivity analysis (LSA) was used to help with determining the calibration parameters (if calibration was performed) and to investigate and quantify the influence each model parameter exerts on every variable calculated in the different systems studies. The latter could be described as a sort of robustness test. Additionally, in some cases, the LSA was used to get more insight into the reaction systems.

To allow comparison between sensitivity functions (SFs) of different variable-parameter combinations, relative sensitivity functions (RSFs) were used (Audenaert et al., 2010) rather than absolute SFs (ASFs). In this work, two different methods for calculating the ASFs were used.

Using the finite forward difference method, ASFs were calculated by perturbing the default parameter value (which acted as nominal value) with an amount equal to the

perturbation factor times the default value. For both parameter values (i.e. nominal and perturbed), the output variables were calculated:

$$\frac{\partial y_j}{\partial \theta_{k+}} = \frac{y_j(t,\theta_n+\zeta\theta_n)-y_j(t,\theta_n)}{\zeta\theta_n} \quad (3.1)$$

in which $y_j(t, \theta_n)$ represents the output variable, θ_n represents the nominal parameter value and ζ is the perturbation factor.

Using the finite central difference method, ASFs were calculated by (forward and backward) perturbing the default parameter value with an amount equal to the perturbation factor times the default value:

$$\frac{\partial y_j}{\partial \theta_j} = \frac{y_j(t,\theta_n+\zeta\theta_n)-y_j(t,\theta_n-\zeta\theta_n)}{2\zeta\theta_n} \quad (3.2)$$

Both finite forward and finite central difference methods were used in this work. RSFs were then calculated as follows:

$$RSF = \frac{ASF\times\theta_n}{y_j(t,\theta_n)} \quad (3.3)$$

A RSF less than 0.25 indicates that the parameter is not influential. Parameters are moderately influential when 0.25<RSF<1. When 1<RSF<2 and RSF>2, the parameter seems to be very and extremely influential, respectively (Audenaert et al., 2010) (and references therein). The sign of the RSF value specifies if raising the parameter impacts the variable in a positive (higher variable value) or negative (lower variable value) way.

RSF values are typically presented in tornado plots, in which parameters are sorted from most to least influential. The name of these plots was derived from their typical tornado shape.

3.4 Global sensitivity analysis

In contrast to a local sensitivity analysis, a global SA is performed by varying all parameters at the same time and over a broader user defined range. Consequently, the results of global SAs are multidimensional averages: the impact of a parameter variation on the process is assessed, while all other parameters are also varying (Saltelli et al., 2005; Neumann et al., 2009).

A schematic representation of global SA is given in Figure 3.4. Prior to a global SA, two important properties are assigned to each parameter of interest: a range in

which the parameter may vary and a shape of the probability density function (PDF) of the parameter in that range. Subsequently, by means of a sampling algorithm, a large number of independent samples are drawn from the parameter space, thereby accounting for the predefined parameter properties. Each sample represents a certain set of parameter values for which a separate simulation is run (Figure 3.4).

A uniform PDF was chosen which is characterized by a lower and upper bound and equal probability for the values in the interval to be chosen. Such PDFs are typically chosen when no specific information about the parameter is available. Latin Hypercube Sampling (LHS) was used as a sampling method to provide input for the Monte Carlo simulation. This is a commonly used and effective sampling technique (Saltelli et al., 2005) allowing to sample the space homogeneously with fewer shots compared to mere random sampling.

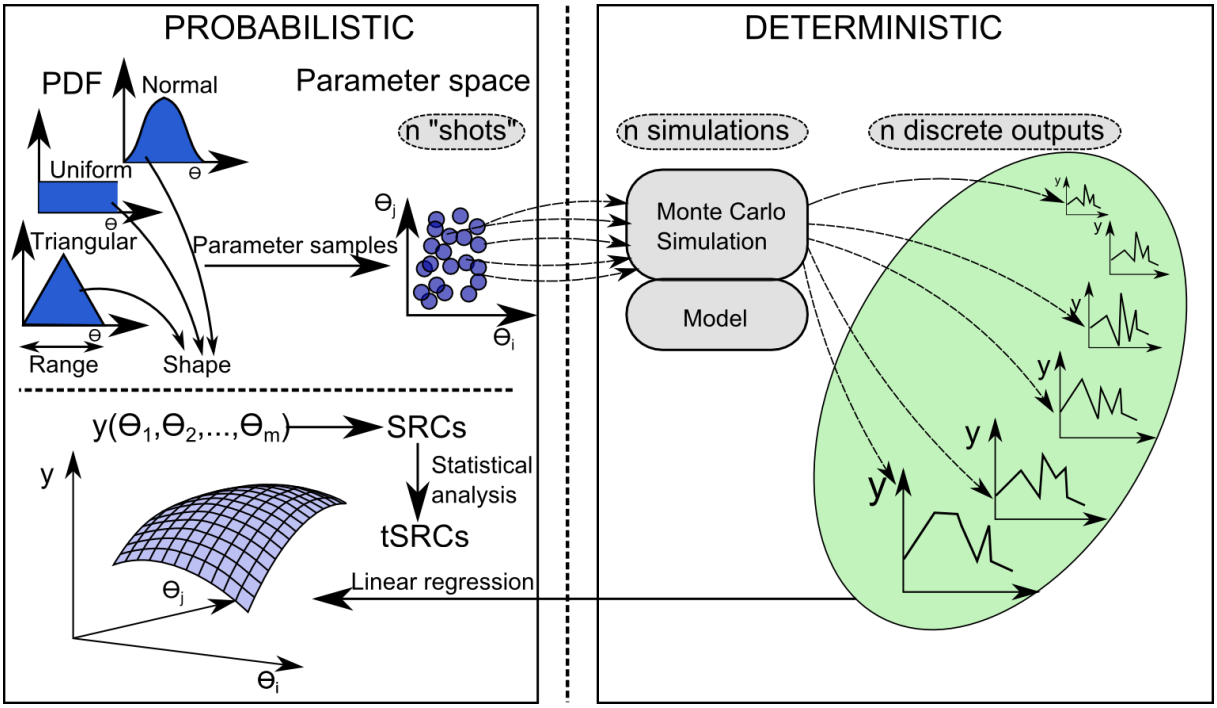

Figure 3.4: Schematic representation of global sensitivity analysis

Global sensitivities in this study were calculated by means of linear regression (Saltelli et al., 2005). A linear model that describes the relation between a certain variable y_j (e.g. aqueous ozone concentration) and a number of m studied parameters (θ_n) is derived from the output of the Monte Carlo simulation. The linear model $y_j(\theta_1, \theta_2,\ldots, \theta_m)$ contains the parameter values with their respective regression coefficients. The regression coefficients are a measurement for the linear dependency between the output variable and the respective parameters. After a

standardization of the regression coefficients (Saltelli et al., 2005), the t-statistic value of the standardized regression coefficients (SRCs) is calculated from the standard errors of the regression coefficients. The larger this tSRC value, the more influence a certain parameter has on the model output. If the t-statistic value is larger than 1.96 (the value corresponding to an infinite number of samples), then the parameter significantly impacts the variable at the 5% confidence level. The sensitivities (tSRC values) are presented using tornado plots.

A detailed description of performing global SAs and the statistical calculation can be found elsewhere (Saltelli et al., 2005).

3.5 Parameter estimation

Parameter estimation was performed by the minimization of an objective function using an optimization algorithm. The objective function calculation was based on a weighted sum of squared errors (WSSE) between the model predictions and measurements:

$$J(\theta) = \sum_{j}^{z} \sum_{i=1}^{N} w_j \left(\hat{y}_{ij} - y_{ij}(\theta)\right)^2 \quad (3.4)$$

in which J(θ) represents the objective function based on N data points and $\hat{y}_{ij}$ and $y_{ij}(\theta)$ represent the experimental data and model prediction of variable j, respectively, with i the index for data points, ranging from 1 to N. θ includes one or more parameters to be estimated, w_j is the weight factor applied to the variables and z is the number of variables used for the parameter estimation.

It can be derived from this equation that objective function calculation was performed for all variables simultaneously.

To optimize (minimize) the objective function, the Simplex algorithm (Nelder and Mead, 1965) was used.

3.6 Goodness-of-fit

When model calibration or validation was performed, the goodness-of-fit between measured and calculated values was quantified by calculating Theil's inequality coefficient (TIC) (Theil, 1961), which is expressed as follows:

$$TIC_j = \frac{\sqrt{\sum_{i=1}^{N}\left(\hat{y}_{ij} - y_{ij}(\hat{\theta})\right)^2}}{\sqrt{\sum_{i=1}^{N}\hat{y}_{ij}^2} + \sqrt{\sum_{i=1}^{N} y_{ij}^2(\hat{\theta})}} \quad (3.5)$$

in which $\hat{\theta}$ represent the optimized parameters. The remaining symbols are the same as in Equation 3.4.

A value of the TIC lower than 0.3 indicates a good agreement between experimental and calculated values (Theil, 1961). Noteworthy, however, is that the TIC is just one out of numerous existing tests to evaluate the quality of model predictions (Hauduc et al., 2011).

Chapter 4

Modelling of full-scale drinking water ozonation

Redrafted from: Audenaert, W.T.M., Callewaert, M., Nopens, I.,Cromphout, J., Vanhoucke, R., Dumoulin, A., Dejans, P. and Van Hulle, S.W.H., 2010. Full-scale modelling of an ozone reactor for drinking water treatment. Chemical Engineering Journal 157 (2-3), 551-557.

Abstract

In 2003, the Flemish Water Supply Company (VMW) extended its drinking water production site in Kluizen (near Ghent, Belgium) with a combined ozonation and biological granular activated carbon filtration (BGAC) process. Due to this upgrade, biostability increased, less chlorination was needed and drinking water quality improved significantly.

The aim of this study was to describe the full-scale reactor with a limited set of equations. In order to describe the ozonation process, a model including key processes such as ozone decomposition, organic carbon removal, disinfection and bromate formation was developed. Kinetics were implemented in WEST and simulation results were compared to real data. The predicting performance was verified with a goodness of fit test and key parameters were determined through a local sensitivity analysis.

Model parameters involving the DOM surrogate UV_{254} (both rate constants and stoichiometric coefficients) strongly affect model output Some parameters with respect to bromate and bacteria showed to be only, but to a large extent, sensitive to their associated concentrations. A scenario analysis was performed to study the system's behaviour at different operational conditions. It was demonstrated that the model is able to describe the operation of the full-scale ozone reactor, however, further data collection for model validation is necessary.

4.1 Introduction

In order to produce high quality drinking water from surface water resources, a combination of physical and chemical treatment steps is typically used. To achieve good bacteriological quality, chlorine is often used as disinfecting agent. However, it is well established that chlorine can lead to many problems in the aquatic environment due to the formation of potential toxic organochlorine compounds such as tetrachloroethene, trichloroethene and halo-acetic acids (Rook, 1974). Besides this, emerging pollutants became important contaminants in water systems during the last few decades (as discussed in Chapter 2). In order to minimize DBP formation and to remove harmful compounds, AOPs have already proven to be effective technologies (Boucherie et al., 2009; Werderitsch, 2009). Besides the potential benefits in drinking water production, AOPs have a large potential for the treatment of different types of water and waste streams originating from waste water, such as domestic and industrial effluent, sludge and membrane concentrates, swimming pool water and process water (see Chapter 2). Both low and high concentrated flows can be treated with AOPs (Parsons, 2004; Crittenden et al., 2005). Ozonation of water containing DOM can be regarded as an AOP as shown in Chapter 2. This technique is either used for (1) the complete or partial oxidation of the organic contamination, (2) the oxidation of a specific contaminant or (3) the removal of pathogens. However, it should be noted, that ozone also produces DBPs such as bromate which is formed out of naturally occuring bromide and considered to be a potential human carcinogen (von Gunten, 2003b). Ozone is used for removal of MIB in drinking water production installations as this component is responsible for T&O problems (Sagehashi et al., 2005). The stage 1 and stage 2 rules, promulgated by US EPA (Environmental Protection Agency), defined a MCL (maximum contaminant level) of 10 µg L^{-1} bromate for systems using ozone (EPA, 2006). In Europe a similar regulatory level is applied since 1998 (98/83/EC). If the incoming water contains high bromide levels, bromate formation can be restricted by e.g. adding hydrogen peroxide to the ozonation process (Werderitsch, 2009). In this case, $HO^{\bullet}$ becomes important in the reaction scheme.

Despite the many advantages and added value of the AOPs, there still exist several bottlenecks and research questions concerning these techniques. First, scale-up of lab-scale research reactors to full-scale industrial reactors is often failing. Second, further research on process control and optimization is necessary. Third, the removal mechanisms of organic components and micro-organisms are not yet completely unravelled. Modelling of AOPs offers an elegant and cost-effective tool to tackle these research questions.

Many different attempts have already been made to describe ozone decomposition with or without the presence of organic compounds (Beltrán, 2004; van der Helm, 2007). Two general accepted deterministic models for ozone decomposition in "pure water" have been developed in the early 80's, both based on the first model of Weiss (1935). The SHB model was experimentally developed at acidic to neutral pH's (Buhler et al., 1984; Staehelin et al., 1984) while TFG model was developed at high pH values (Tomiyasu et al., 1985). A comparison of both reaction schemes can be found elsewhere (Westerhoff et al., 1997). The SHB model is discussed in detail in Chapter 2 and simulations with it are described in Chapter 5.

On the other hand, numerous empirical and semi-empirical studies describing ozone decomposition (van der Helm et al., 2007; Lovato et al., 2009), reactions with organic compounds (Westerhoff et al., 1997; van der Helm et al., 2007), by-product formation (Sohn et al., 2004) and disinfection (Hunt and Mariñas, 1999) were conducted the last decades. Lovato and co-workers extended the SHB model with an empirical approach by relating one of the 18 kinetic constants to the solution pH (Lovato et al., 2009). Van der Helm et al. (2007) described ozone decomposition and organic compound removal by using UV_{254} as surrogate for NOM (the main content of DOM in natural water). Sohn et al. (2004) developed an empirical relation to predict bromate formation related to several operational and water quality parameters.

In this chapter a simplified model is presented for the simulation of the full-scale ozone reactor of the Flemish Water Supply Company (VMW) in Kluizen (Belgium). The aim of this study is to describe this process with a limited set of equations, to determine the key parameters and to perform different scenario analysis. The results will be used as a starting point for further model development, especially in terms of extending the mechanisms of organic compound removal and biodegradability enhancement. As such, the model might contribute to answering the research questions stated above.

The 60,000 m^3 day^{-1} WTP, subject of this study, is fed with raw water captured from lowlands. Until 2003, the treatment concept consisted of micro-sieving, enhanced coagulation followed by sludge blanket clarification, oxidation with chlorine, sand filtration and GAC filtration. A final disinfection with chlorine was applied (Cromphout et al., 2005; Cromphout and Vanhoucke, 2008). The intensive chlorination resulted in high trihalomethanes (THM) levels and prevented biofilm growth on the activated carbon granules. Due to the absence of biological activity and limited contact time in the GAC (15 minutes), NOM removal was mainly by adsorption, which is limited to the first 10,000 bed volumes (a unit that expresses

the volume of water that already passed through the filter as a multiple of the volume of the filter bed). In 2000 the earthy-musty T&O compound MIB appeared in the feed water with concentrations above the odour threshold value of 10 ng L^{-1}, caused by algal growth in the reservoirs. This, along with a lack of biostability of the water due to high DOC levels, forced the drinking water company to search for an effective oxidizing technique. An ozone production and mixing unit was introduced, together with BGAC filters. Ozone was implemented for both disinfection and oxidation. Due to the excellent disinfection capacities, a first chlorination step could be omitted. On the other hand, ozone was also implemented to enhance biodegradability in favour of the biofilm present in the BGAC to remove MIB and NOM. Only a final chlorination step remained (Cromphout et al., 2005; Cromphout and Vanhoucke, 2008).

4.2 Materials and methods

4.2.1 Reactor configuration

Ozone is produced from oxygen with two Wedeco EFFIZON® ozone generation units, each with a production capacity of 4000 g h^{-1} (180 g ozone per Nm^3 oxygen/ozone mixture). The ozone generating elements consist of discrete borosilicate glass tubes with a diameter less than 11 mm. A part of the main water stream is pumped up and pressured up with a high pressure booster pump. The water is brought into a venture injector where ozonated gas is introduced into the water. The side stream is then re-introduced to the main water-pipe prior to a static mixer. The normally applied ozone dose in the water is 2.5 mg L^{-1}. A schematic overview of the gas transfer process is given in Figure 4.1. A sampling point is located after the static mixer (before the activated carbon filters). After the mixing is completed, the water proceeds to the BGAC filters. Gas flow as well as ozone concentrations in the gas are continuously monitored in order to evaluate the ozone transfer efficiency. An off-gas ozone destruction system converts any residual or non-dissolved ozone to oxygen so that the ozone concentration in the treated off-gas is lower than 0.1 ppm (Cromphout et al., 2005; Cromphout and Vanhoucke, 2008).

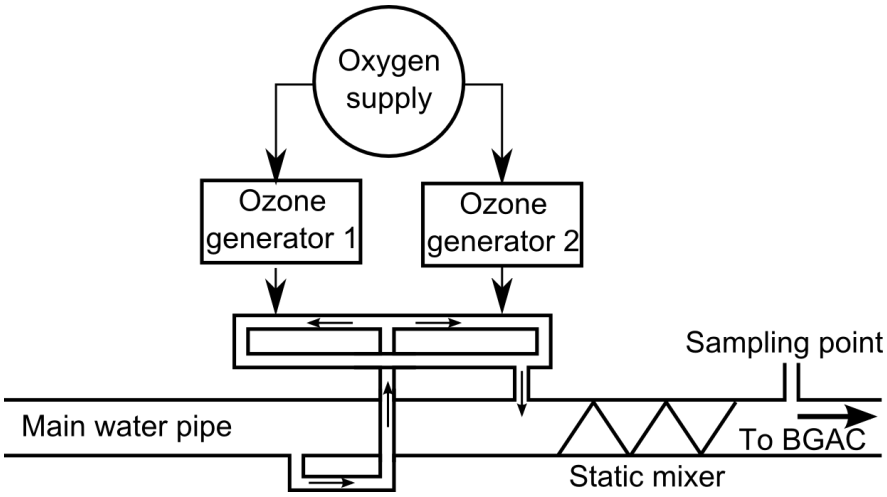

Figure 4.1: Schematic overview of the ozone production and mixing unit

4.2.2 Biological granular activated carbon filters

The BGAC consists of ten pressure filters with a diameter of 6 meter and operational pressure of 1,5 to 2 bar. GAC is operated as a two-stage filtration, the first filter stage operates between 25,000 and 50,000 bed volumes. After 50,000 bed volumes (two years) the carbon is reactivated and the filter is switched to the second stage position, which operates between 0 and 25,000 bed volumes. A contact time of 6 minutes is obtained in the filters, above the carbon bed. Non-dissolved gas is collected in an upward tee above each GAC filter and led away to the ozone destruction system (Cromphout et al., 2005; Cromphout and Vanhoucke, 2008).

4.2.3 Modelling approach

The ozone reactor of the Flemish Water Supply Company was implemented in the modelling and simulation platform WEST as two CSTR's in series. The simulation configuration as used in the software program is given in Figure 4.2.

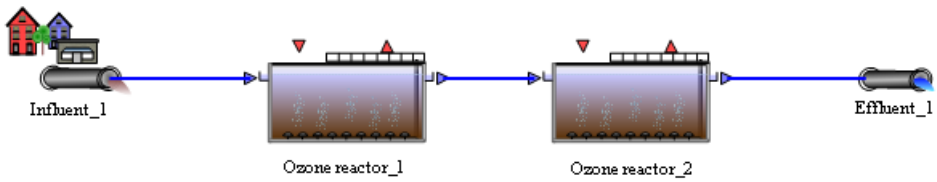

Figure 4.2: Implementation of the ozone reactor in the simulation platform WEST

In the first tank with a volume of 10.68 m³ the ozone is introduced. This tank represents the part of the main water pipe before and with the static mixer. A

second reactor represents the water on top of the activated carbon filters where a second reaction phase takes place.

Four ozone reactions were implemented in WEST (Hunt and Mariñas, 1999; von Gunten, 2003a; b; van der Helm, 2007):

- Ozone decomposition
- Reaction of UV_{254} with ozone (oxidation of NOM)
- Disinfection
- Bromide oxidation (bromate formation)

Ozone reactions in water can be classified as either direct or indirect (von Gunten, 2003a; Beltrán, 2004). Using Equation 2.23, the disinfection reaction rate can be described by the following equation, where molecular ozone as well as hydroxyl radicals contribute to the oxidizing capacity of the system:

$$\rho = (k_{O_3/X} + k_{HO^\bullet/X} R_{CT})[O_3][\mathrm{X_{bact}}] \quad \textit{with} \quad R_{CT} = \frac{[\mathrm{HO^\bullet}]}{[\mathrm{O_3}]} \approx 10^{-8} \sim 10^{-6} \tag{4.1}$$

with ρ the reaction rate (in this example the inactivation rate of bacteria), $k_{O_3/X}$ the second order rate constant for the direct reaction of molecular ozone with a specific compound (in this example micro-organisms) ($m^3\ g^{-1}\ s^{-1}$), $k_{HO^\bullet/X}$ the second order rate constant for the indirect ozone reaction pathway of hydroxyl radicals with micro-organisms ($m^3\ g^{-1}\ s^{-1}$), R_{CT} the ratio of the concentrations of hydroxyl radicals and ozone, $[O_3]$ the concentration of ozone in solution ($g\ m^{-3}$), $[X_{bact}]$ the density of viable micro-organisms ($CFU\ m^{-3}$).

When R_{CT} is assumed to be constant and very small (as discussed in chapter 2), both direct and indirect reactions can be lumped into one:

$$\rho = k_{O_3/X}[\mathrm{O_3}][\mathrm{X_{bact}}] \tag{4.2}$$

However, if the indirect mechanism plays an important role in the oxidation of some calculated species, predictive capabilities of the model will deteriorate because process efficiency in that case highly depends on other process conditions such as scavenger concentrations that are not included in the model. Probably radical reactions indeed occur in the waterworks because MIB was removed after ozonation, while rate constants with regard to the direct and indirect pathway are $<10\ M^{-1}\ s^{-1}$ and $3\times10^9\ M^{-1}\ s^{-1}$, respectively (von Gunten, 2003a).

Direct ozone decomposition is modelled assuming that ozone follows a first order decay with a rate constant of $0.000485\ s^{-1}$ (van der Helm, 2007). UV absorbance at

254 nm was used as a surrogate for the amount of DOM that reacts with ozone (van der Helm, 2007; Song et al., 2008). However, it has to be highlighted that this parameter represents a part of the DOM content as it specifically gives a measure of the amount of aromatic and unsaturated compounds in water (Westerhoff et al., 1999). On the other hand, this parameter offers great opportunities for modelling and control as it can be determined on-line and consequently a huge amount of real-time and accurate data are available. Accordingly, UV_{254} might be a useful parameter in model-based control of WTPs.

Model calibration was performed with historical data of the year 2008 over a period of 300 days. For $k_{O3/UV254}$, which is the rate constant for the reaction of UV_{254} with ozone, an initial value in the range of 0.1 $m^3.g^{-1}.s^{-1}$was used (van der Helm, 2007), while after calibration through parameter estimation a value of 0.0135 $m^3\ g^{-1}s^{-1}$ was found. The stoichiometry or yield (Y) of the reaction is represented by $Y_{O3/UV254}$, with a numerical value of 0.22 (van der Helm, 2007). This implies that one unit of UV_{254} (m^{-1}) consumes 0.22 grams of ozone.

Disinfection kinetics were adapted from the classic Chick-Watson model (Hunt and Mariñas, 1999) (and references therein):

$$\frac{d[X_{bact}]}{dt} = -k_{O_3/X}[O_3][X_{bact}] \qquad (4.3)$$

For $k_{O3/X}$, the inactivation rate constant for a particular microorganism ($m^3.g^{-1}\ s^{-1}$), a value of 0.6 $m^3\ g^{-1}\ s^{-1}$ was applied after calibration, while the initial value was 1.72 $m^3\ g^{-1}\ s^{-1}$ (van der Helm, 2007). The stoichiometry of the reaction is represented by $Y_{O3/X}$, with a numerical value of 1.29 10^{-14} (Hunt and Mariñas, 1999).

Bromide oxidation was incorporated as bromate is an important by-product of ozonation in bromide containing waters. Bromide was assumed to be directly oxidized to bromate, although in reality ozone first oxidizes bromide to form hypobromous acid and hypobromite. The latter is further oxidized to bromite which finally forms bromate (Haag and Hoigne, 1983; von Gunten and Hoigne, 1994; von Gunten, 2003a). As such, one rate constant for bromate formation was determined after calibration and the stoichiometric coefficients from this process were derived from a reaction where 1 mole of bromate is formed out of 1 mole of both ozone and bromide. The rate constant was found to be 0.00043 $m^3\ g^{-1}\ s^{-1}$.

The kinetics and stoichiometric coefficients used in the model are presented in Table 4.1 as a Gujer matrix. This matrix presentation offers a clear overview of the

chemical reaction mechanisms included in the model. Reaction rates are indicated in the right column. Matrix elements are stoichiometry parameters. More information on the Gujer matrix representation of models is provided in Appendix A.

Table 4.1: Gujer matrix representing the ozonation model used in this study

Process	Components					Reaction rate
	O_3 (g m^{-3})	UV_{254} (m^{-1})	X_{bact} (CFU m^{-3})	Br (g m^{-3})	BrO_3^- (g m^{-3})	
Ozone decomposition	-1[a]					$k'_{app}[O_3]$
Reaction of NOM with ozone	-$Y_{O3/UV254}$[b]	-1				$k_{O3/UV254}[O_3][UV_{254}]$
Disinfection	-$Y_{O3/X}$[c]		-1			$k_{O3/X}[O_3][X_{bact}]$
Bromide oxidation	-1			-1.66	-2.66	$k_{O3/Br}[O_3][Br^-]$

[a]von Gunten, 2003b; [b]van der Helm, 2007 [c]Hunt and Mariñas, 1999

The temperature and pH influence was not accounted for in this study as these parameters remain almost constant during the waterworks daily operation and to limit the level of model complexity. Throughout the year, only minor pH variations were observed while significant differences of temperature existed between winter and summer period. To some extent, temperature could have affected the systems' behaviour. For example the inactivation constant for bacteria, $k_{O3/X}$, is temperature dependent (Hunt and Mariñas, 1999). With respect to pH, this parameter has a slight effect on the ozone decomposition rate when lower than 7, but at higher values, the rate increases significantly (Beltrán, 2004). For instance, von Gunten and Hoigné showed that the half-life of ozone is 10 times higher at pH 10 than that at pH 11 (von Gunten and Hoigne, 1994). These researchers also reported that less bromate is formed when lowering the pH. Further, no gas transfer equations were included in the model. A dissolved ozone concentration in the influent of the first tank was defined at the beginning of each simulation run. Finally, the activated carbon present in the second compartment could have a catalytic effect on ozone decomposition. However, this was not considered.

4.2.4 Data interpretation

The goodness-of-fit between experimental and simulated values was quantified by calculating the TIC (Theil, 1961) as introduced in Chapter 3.

A LSA was performed to determine the most important model parameters (those parameters that have a major influence on the model output). The RSF was adopted to evaluate the sensitivity of the model output (concentration of ozone, UV_{254}, CFU and bromate) to a change of model parameters (Rate constants k'_{app}, $k_{O3/UV254}$, $k_{O3/X}$

and $k_{O3/Br}$ and the stoichiometric coefficients $Y_{O3/UV254}$ and $Y_{O3/X}$). A perturbation factor of $1x10^{-4}$ was used.

Detailed information on how the TIC and local sensitivity functions were calculated can be found in Chapter 3.

4.2.5 Analyses

Ozone was measured spectrophotometrically with the indigo reagent method at 600 nm (Bader and Hoigne, 1981). UV_{254} was constantly measured with a process integrated UV spectrometer at 254 nm. Bromide, bromate and total CFU were analysed according to Standard Methods (APHA, 1992). All analyses were performed by the Flemish Water Supply Company.

4.3 Results and discussion

4.3.1 Modelling results

Model calibration was performed with historical data of the year 2008 over a period of 300 days. The influent flow rate and UV_{254} are represented in Figure 4.3.

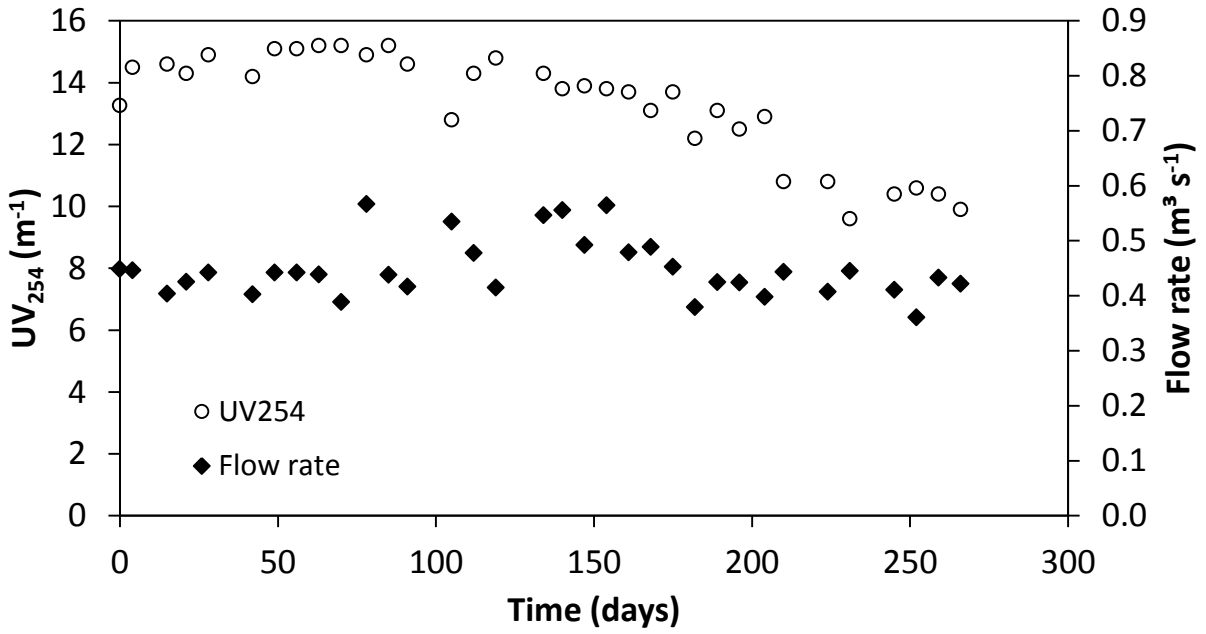

Figure 4.3: Influent flow rate and UV_{254}

The influent bacteria and bromide concentration were on average 183 CFU L^{-1} and 138 µg L^{-1}, respectively. The descending trend of the UV_{254} can be attributed to

improved settling and flotation performance in the pre-treatment steps during that period.

As mentioned earlier, all samples were withdrawn prior to the activated carbon bed (after the static mixer). Consequently, all simulation results are representing the effluent of the first reactor in Figure 4.2. Figure 4.4 shows the measured and calculated UV_{254} after the first reactor. A good agreement was obtained as the TIC for this parameter is calculated to be 0.044 (<0.3). The deviation of the applied rate constant for k_{UV254} in comparison with literature reported values can be explained by differences in organic carbon content of the water.

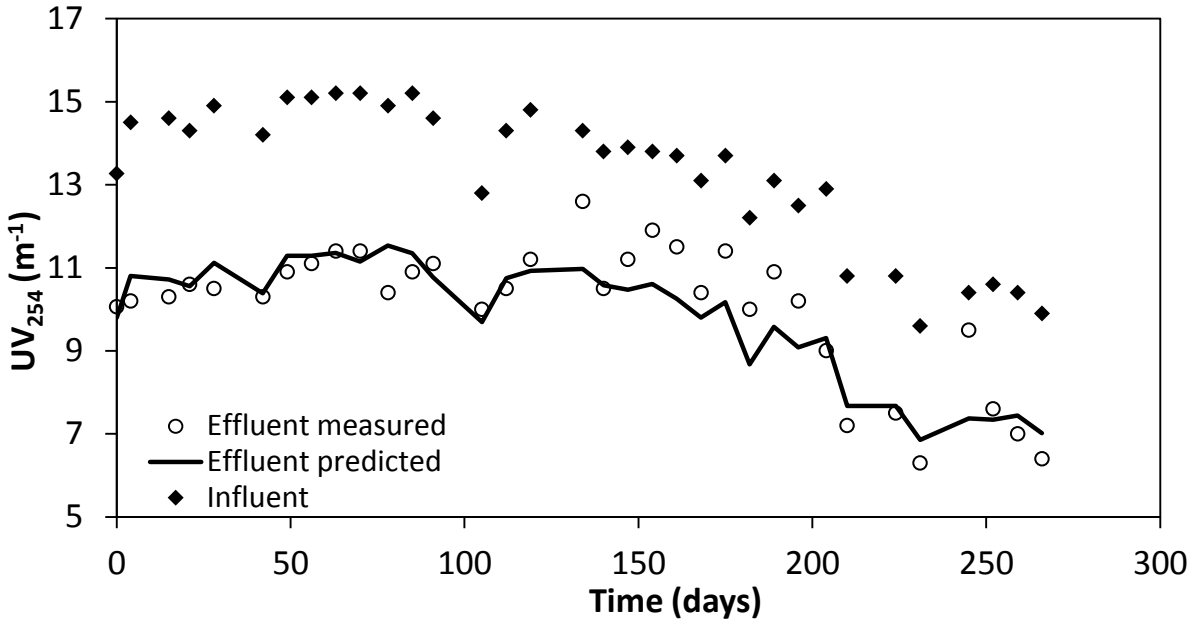

Figure 4.4: Comparison of measured and calculated UV_{254}

On average, 25% of the UV_{254} was removed for both calculated and modelled values. Concerning the number of CFU, an average log removal of 1.2 was calculated, which is in accordance with the measured removal (1.1 log). Measured influent bacteria concentrations vary between 80 and 200 CFU L^{-1} while those of the effluent are in the range of 10 CFU L^{-1}. Calculated and measured bacteria removals are compared in Figure 4.5. As can be seen, calculated values agree well with experimental ones. This is confirmed with a calculated TIC of 0.084, although it has to be highlighted that more data points have to be collected in future studies.

Only one data point for bromate was collected (4 µg L^{-1}). Therefore, the average calculated bromate concentration and the measured value are presented in Figure 4.6. Based on the measured value, it can be seen that model predictions are realistic. In future work, the validation process will be repeated, especially for

bromate formation. Measured and calculated values are far below the regulatory level of 10 µg L^{-1}.

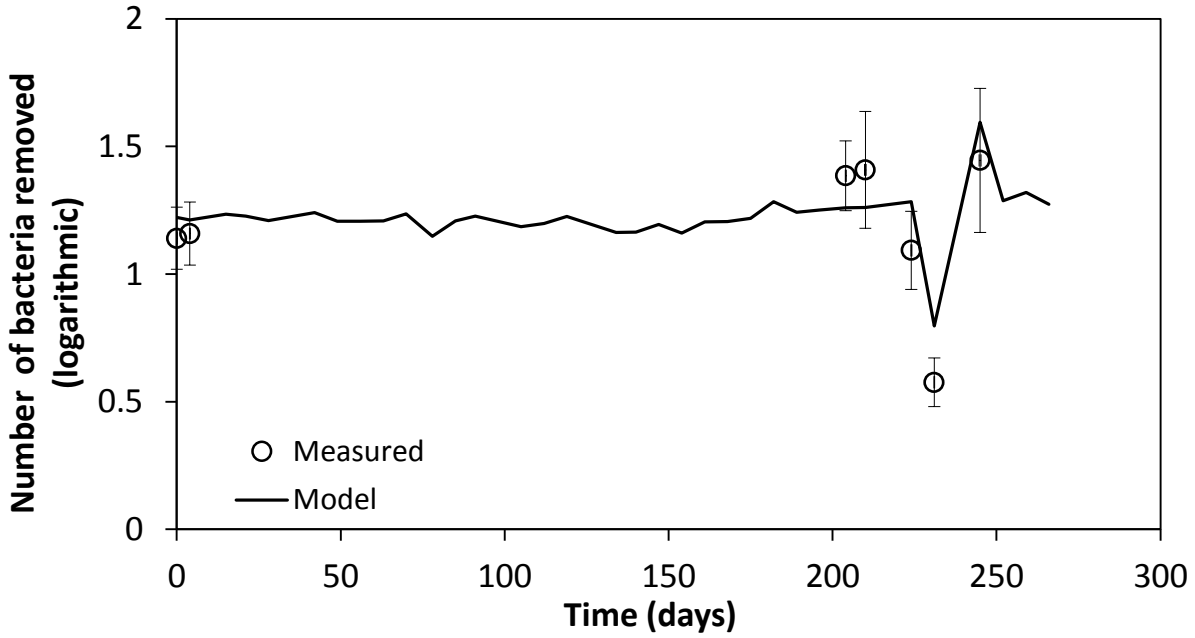

Figure 4.5: Comparison of measured and calculated logarithmic bacteria removal (error bar represents the standard deviation based on replicate measurements)

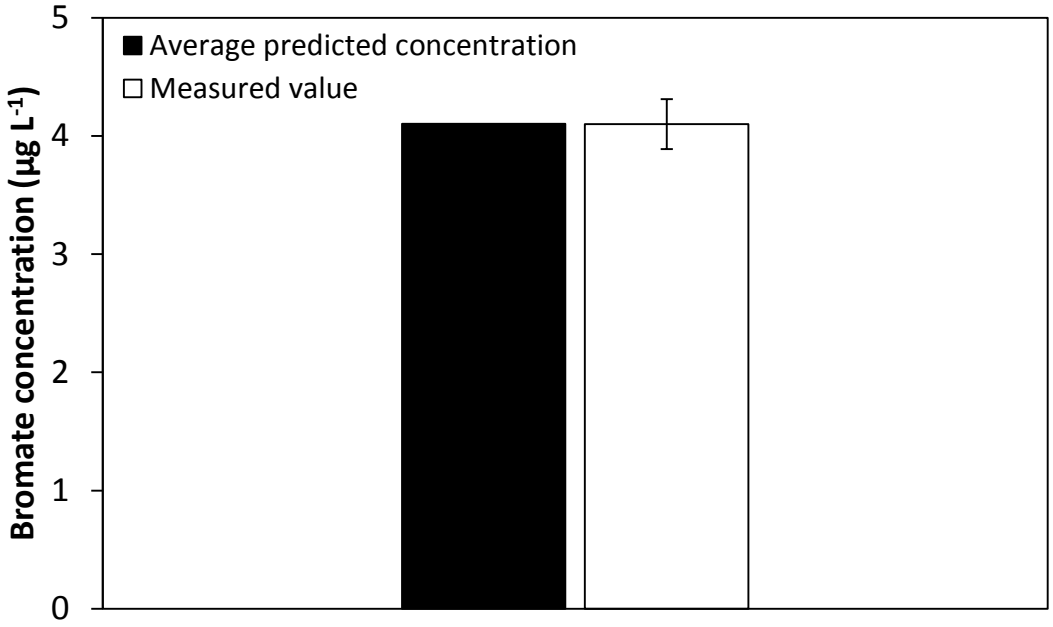

Figure 4.6: Predicted and measured bromate concentration in the effluent (error bar represents the standard deviation based on replicate measurements)

4.3.2 Sensitivity analysis

The initial parameter values used in the sensitivity analysis are shown in previous paragraphs. It can be clearly noticed that parameters involving UV_{254} ($k_{O3/UV254}$ and $Y_{O3/UV254}$) strongly affect model output compared to others (Table 4.2). $k_{O3/UV254}$ has a moderate effect on calculated ozone, bacteria and bromate concentrations. There's a smaller influence with respect to UV_{254} itself. The same conclusions can be made for $Y_{O3/UV254}$, although moderate effects are slightly higher. $k_{O3/X}$ and $k_{O3/Br}$ only influence their associated concentrations [X] and [BrO_3^-]. However, due to the very affecting character (RSF≈1), accurate estimation regarding these parameters will be necessary to obtain realistic predictions of bacteria and bromate levels. k'_{app} and $Y_{O3/X}$ do not exert an influence on simulation output. Bacteria (X) form part of ozone consuming substances, but they consume a negligible amount of ozone due to their extremely low concentrations (Huang et al., 2004). This explains that $Y_{O3/X}$ has no effect on the bacteria concentration as the ozone requirement for this reaction is met under normal operational conditions.

Comparable results are described in Chapter 6, where parameters involving the DOM surrogate UV_{310} were found to be very influential to the output of a mechanistic UV/H_2O_2 model.

Table 4.2: RSF values indicating the degree influence of model parameters on output variables

Parameter	RSF			
	[O_3]	[UV_{254}]	[X]	[BrO_3^-]
k'_{app}	0.07	0.02	0.07	0.07
$k_{O3/UV254}$	0.30	0.18	0.28	0.30
$k_{O3/X}$	0	0	0.94	0
$k_{O3/Br}$	0	0	0	0.98
$Y_{O3/UV254}$	0.4	0.11	0.38	0.4
$Y_{O3/X}$	0	0	0	0

4.3.3 Scenario analysis

The effect of applied ozone concentration and flow rate on certain key variables was evaluated. The normally operational ozone dose in the drinking water production centre is 2.5 mg L^{-1}. Scenarios were calculated for concentrations varying from 0 to 5 mg L^{-1}. Flow rate (and consequently hydraulic retention time) was varied within a range of 0 (batch reactor) to 1 m^3 s^{-1} while real influent flow rates are in the range of 0.4 to 0.5 m^3 s^{-1}.

Effects of ozone dose on effluent UV_{254} and bromate formation are shown in Figure 4.7. This figure reveals that a compromise has to be made regarding ozone dose and flow rate to comply with bromate levels without losing UV_{254} (and bacteria) removal goals. Figure 4.7 also shows that the normally applied flow rates in this case are in a beneficial range. A significant amount of UV_{254} is removed and the bromate level stays well below the standard of 10 µg L^{-1}. The influent UV_{254} was 11.3 m^{-1}.

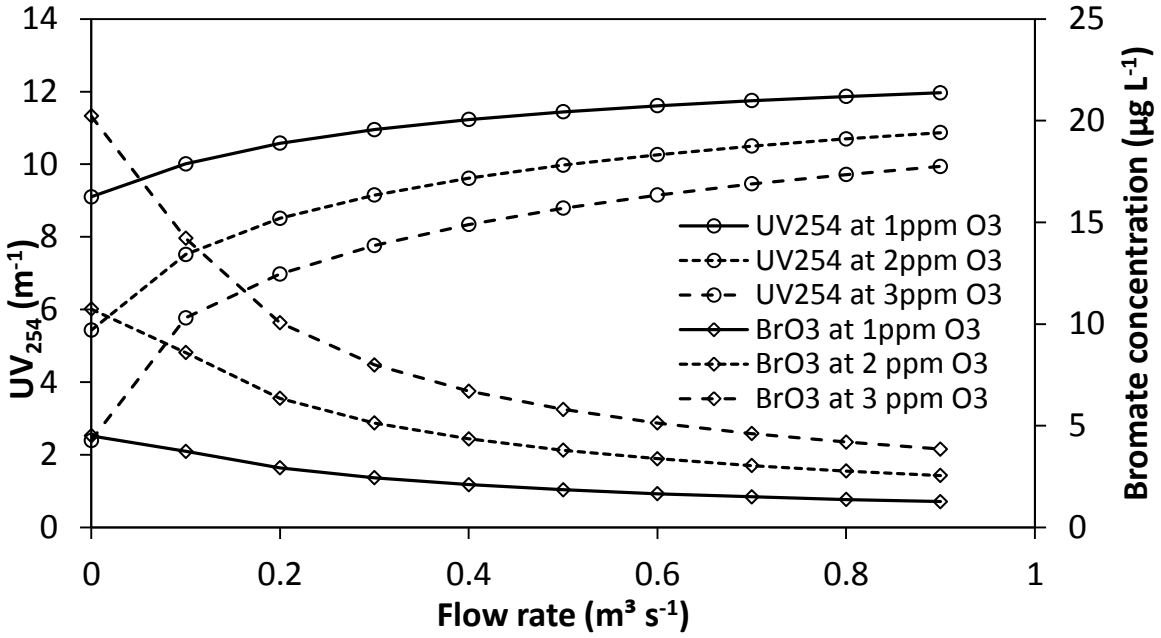

Figure 4.7: Scenario analysis, effect of flow rate on UV_{254} and bromate concentrations

As can be deduced from Figure 4.8, the operational ozone concentration of 2.5 mg L^{-1} is well chosen. Again, sufficient UV_{254} is removed and the bromate guideline is met without problems.

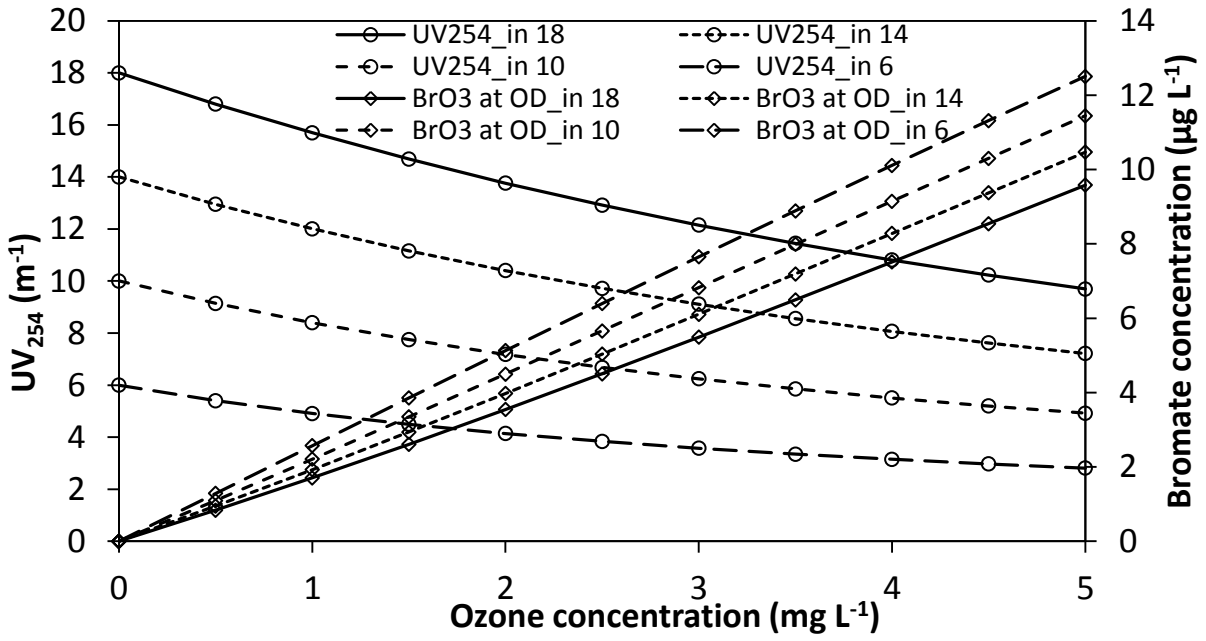

Figure 4.8: Scenario analysis, effect of ozone dose on UV_{254} and bromate concentrations

4.3.4 Bromate formation

Sohn and co-workers stated that most of the models for predicting residual ozone and bromate formation take empirical functional forms because the complexity of natural organic matter restricts developing complete theoretically based chemical kinetic models (Sohn et al., 2004). They developed a multiple regression model that was compared to experimental data from the VMW (Cromphout and Vanhoucke, 2008) (and references therein):

$$[BrO_3] = 1.55 \times 10^{-6} \times [TOC]^{-1.26}$$
$$\times [pH]^{5.82} \times [O_3]^{1.57} \times [Br^-]^{0.73} \times t^{0.28} \times (1.035)^{T-20} \qquad (4.4)$$

Figure 4.9 shows this comparison. The model developed in this study was added to the graph. The regression model seems to show a better prediction of the experimental data, as also indicated when comparing the TIC values of both, the regression and the kinetic model with values of 0.17 and 0.21, respectively. However, both models agree well with reality (TIC<0.3). The over-estimation of bromate by the kinetic model can be caused by inaccurate parameter estimation with insufficient data as $k_{O3/Br}$ has proven to be very influential to simulated bromate concentrations (see sensitivity analysis). The assumptions that were made regarding the bromate mechanism, together with not included temperature effects can contribute to less prediction accuracy, together with the fact that only 1 data point was available for calibration. Regression models are able to describe

experimental data very well and temperature or reactor correction factors can be easily added (Sohn et al., 2004). On the other hand, models based on well-defined mechanisms can give more substantiated insight in processes and are easier to apply.

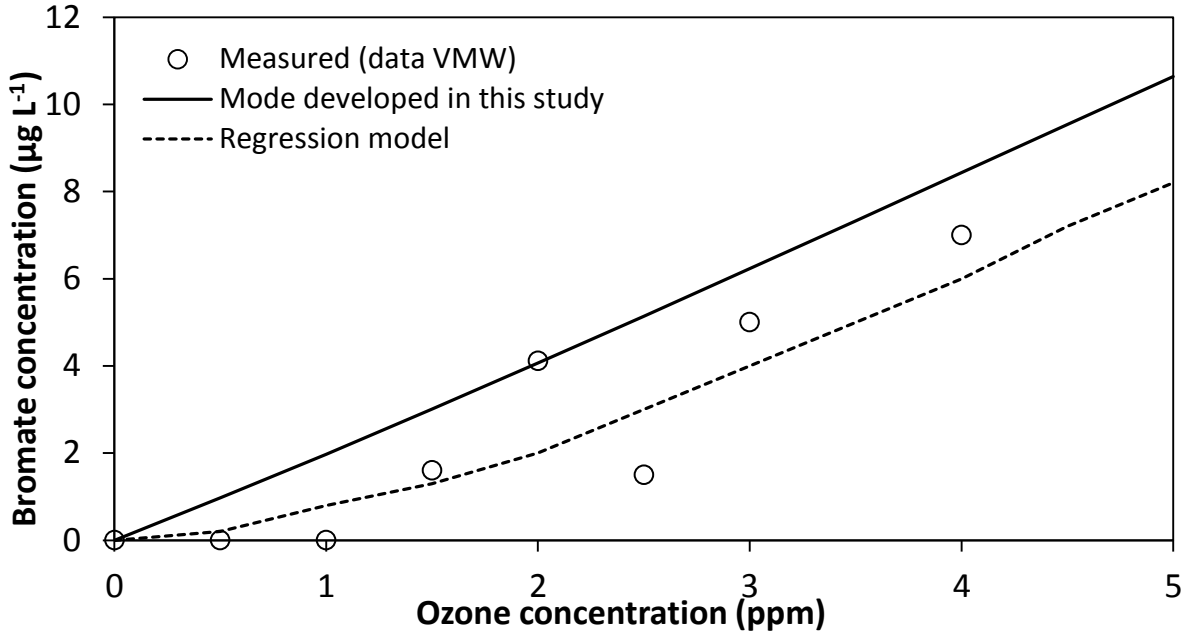

Figure 4.9: Comparison of predicting performance of a regression model and the kinetic model developed in this study.

4.4 Conclusions

In this study, a simplified kinetic model describing ozone decomposition, organic carbon removal, disinfection and bromate formation during ozonation applied in drinking water production was developed. Calibration and simulation runs were based on historical data from a full-scale ozonation system at the Flemish Water Supply Company waterworks in Kluizen, Belgium. It was demonstrated that the developed model is able to predict excess ozone concentration, UV_{254} removal, bacteria inactivation and bromate formation, although further data collection and batch experiments will be necessary to further validate the model. The latter was not performed in this PhD thesis. A sensitivity analysis revealed that parameters involving UV_{254} (both rate constants and stoichiometric coefficients) strongly affect model output. Some parameters with respect to bromate and bacteria showed to be only, but to a large extent, sensitive to their associated concentrations. UV_{254} seems to be a valuable measurement for the application of model-based control and optimization strategies as it can be determined on-line and consequently a huge amount of real-time and accurate data are available.

With drinking water standards becoming more stringent, models will become an important tool to assess drinking water plant performance (Van Hulle et al., 2006). The model will be used for further scenario analysis (particularly effect of ozone dosage on reactor performance). Further model extension may be required to guarantee satisfactory model predictions and to improve the applicability and optimization capacities.

Chapter 5

Influence of DOM concentration on parameter sensitivity of a mechanistic ozone decomposition model

Redrafted from:

Audenaert, W.T.M., Vandevelde, M., Van Hulle, S.W.H., Nopens, I. Influence of Dissolved Organic Matter (DOM) on Parameter Sensitivity of a Mechanistic Ozone Decomposition Model, Ozone: Science & Engineering, submitted.

Audenaert, W.T.M., Vandevelde, M., Van Hulle, S.W.H., Nopens, I. Influence of DOM Concentration on Parameter Sensitivity of a Mechanistic Ozone Decomposition Model, 4th IWA Specialist Conference on natural organic matter, July 27-29, 2011, Irvine, USA

Abstract

Aqueous ozone decomposition proceeds through a complex chain mechanism of radical reactions. When DOM is present, the system becomes even more complex and often (semi-)empirical modelling approaches are used to describe ozonation of water and wastewater systems. Mechanistic models, however, can be of great value to gain knowledge in the chemical pathways of ozonation and advanced oxidation processes in view of engineering applications. However, the numerous model parameters and model complexity often restrict their applicability. Model simplification is then an option to cure these drawbacks. In this study, SAs were used to determine the most important elementary reactions from the complex kinetic model. Additionally, SAs were used to understand the reaction mechanism. Only seven of the twenty-eight first and second order rate constants showed to impact ozone and $HO^{\bullet}$ concentrations. Processes involving $HO^{\bullet}$ scavenging by inorganic carbon were of minor importance. Mass-transfer related parameters k_La_{O3}

and ozone saturation concentration ($C_{O3\_L}^{*}$) were of major importance in all cases. Hence, it is of extreme importance that these parameters are experimentally determined with high accuracy. It was shown that the aqueous ozone concentration is extremely sensitive to parameters involving DOM at very low scavenger concentrations implying that impurities should always be considered in models, even in ultrapure water systems. Uncertainty analysis showed that both the ozone and $HO^{\bullet}$ concentrations are susceptible to variations in influent composition. The uncertainty regarding the oxidative species significantly reduced with increasing levels of scavengers and especially DOM. It was demonstrated that simplification of the elementary radical scheme should be considered. On the other hand, a model extension with regard to reactions involving DOM should be performed in order to improve the applicability of future wastewater ozonation models.

5.1 Introduction

Nowadays, a vast amount of research still focuses on mechanisms involving water and wastewater ozonation and (advanced) oxidation in general, and related to this, the role of DOM in these processes (Elovitz and von Gunten, 1999; Westerhoff et al., 1999, 2007; Buffle et al., 2006a; b; Van Geluwe et al., 2011). The complexity of the aqueous organic matrix and oxidant induced molecular conversions severely impede efforts to describe the oxidation processes in a mechanistic way. DOM present in natural waters and wastewaters is a complex heterogeneous mixture of organic compounds that can be divided into several classes of which in some cases the exact composition still remains unknown (Van Geluwe et al., 2011). The goal of the earlier mentioned studies is mainly to gain fundamental knowledge on the oxidation kinetics in order to provide detailed models that can have various applications. Adequate mathematical models can be used to engineer, optimize and control the treatment process. A key issue in all model applications is the assessment of oxidant exposures. This is an important process factor that determines disinfection and oxidation efficacy. Prediction of trace pollutant oxidation can be of great value as laboratory analysis is laborious and resource intensive and no on-line measurement methods exist (Neumann et al., 2009).

5.1.1 Modelling approaches for the ozonation process

Aqueous ozone decomposition proceeds through a complex chain mechanism of radical reactions. A general accepted reaction sequence for ozone decomposition in

ultrapure water at acidic to neutral pH is the SHB model (Buhler et al., 1984; Staehelin et al., 1984) as explained in Chapter 2. In natural water and wastewater where DOM is present, the system becomes much more complex and often empirical approaches are used to model the ozonation process. Often, this is due to a lack of detailed information on reaction pathways of DOM and the uncertainty associated with the use of detailed elementary mechanisms in real systems (these reaction schemes were initially defined at well-known and controlled conditions in ultrapure water). Empirical models can be of value for some cases but lack flexibility to be applied over a wide range of conditions (Westerhoff et al., 1997). Additionally, extensive experimental data collection is needed to construct these models. There are, however, some important semi-empirical relations that have already proven to be very useful to model natural water ozonation. The use of first (or sometimes higher) reaction orders to model ozone decay in the presence of slow reacting organic matter compounds is well known (Westerhoff et al., 1999). This approach was used in numerous studies to calculate the aqueous ozone concentration as function of time and hence, the disinfection or oxidation progress. As already indicated, aqueous ozone decomposition gives rise to radicals. $HO^{\bullet}$ is proven to significantly enhance micropollutant oxidation during conventional ozonation (Buffle et al., 2006b; Zimmermann et al., 2011). This implies that both ozone and $HO^{\bullet}$ exposures should be calculated in order to accurately model the oxidation process. A semi-empirical approach to determine hydroxyl radical exposure which is proven to be very useful in water treatment is the R_{CT} concept developed by Elovitz and von Gunten (1999). This concept (discussed in Chapter 2) is based on the assumption that the ratio of $HO^{\bullet}$ and ozone exposure remains constant throughout the ozonation process (Elovitz and von Gunten, 1999). Consequently, the $HO^{\bullet}$ concentration (and exposure) can be simply calculated based on the measured ozone concentration and R_{CT} value (the latter is source-dependent and known from a preliminary experiment) (Elovitz and von Gunten, 1999). The R_{CT} concept allows for the use of literature-established second order rate constants for ozone and $HO^{\bullet}$ based oxidation to predict micropollutant concentrations. Additionally, the relative importance of direct and indirect oxidation in the process can be studied (Elovitz and von Gunten, 1999; Buffle et al., 2006b). It was shown, however, that the use of the R_{CT} concept and a single first order ozone decay constant are less suited to describe wastewater ozonation because these parameters are likely to change as function of oxidation time (Buffle et al., 2006a; b). Furthermore, natural water and wastewater ozonation may differ mechanistically as DOM moieties and corresponding transformation products were proven to exhibit significantly different absorbance spectra (Westerhoff et al., 2007). Hence, the development of more complex mechanistic models is required.

5.1.2 Shortcomings of current mechanistic models

The well-established SHB sequence can be a starting point for the construction of wastewater ozonation models. Many earlier applications of this model, however, showed poor agreement between experimental determined and predicted ozone concentration profiles (Elovitz and von Gunten, 1999; Bezbarua and Reckhow, 2004; Fabian, 2006; Lovato et al., 2009). Often, the literature values of the elementary rate constants were questioned and proposed to be the main reason for the disagreement. Hence, often one or more elementary rate constants of the extensive mechanisms are re-evaluated in order to obtain better fits (Bezbarua and Reckhow, 2004; Fabian, 2006; Lovato et al., 2009). This recalibration, however, does not rely on chemical or kinetic knowledge and thus implies that the originally well-defined models shift to the empirical side. In these cases, a modification of elementary kinetic constants compensates for important mechanistic knowledge that is missing in the model structure. In order to balance the model complexity, a simplification of the radical scheme (SHB model) on the one hand and an extension of the DOM reaction scheme on the other hand is recommended.

5.1.3 The use of sensitivity analysis for evaluation of the model structure

Prior to simplification or modification of a complex kinetic model, it is useful to analytically determine the most important elementary reactions. A SA is suitable for this purpose (Saltelli et al., 2005). This mathematical tool allows quantifying the sensitivity of one or more variables towards certain parameters of interest. Despite the benefits, literature reported applications of SAs on kinetic oxidation models are scarce. Neumann et al. (2009) conducted a global SA on a drinking water ozonation model. To model ozone decay, a first order rate law was used and the $HO^{\bullet}$ exposure was calculated by means of the R_{CT} concept. It was shown that R_{CT} is an extremely influential parameter with respect to the concentration of pollutants that are susceptible to $HO^{\bullet}$ attack (Neumann et al., 2009). This again may indicate that the R_{CT} approach is not suitable for wastewater ozonation because the value of R_{CT} becomes even more uncertain. The first order ozone decay constant seemed to be less important. Audenaert et al. (2010) performed a LSA on a simple model that was used to predict residual ozone, bromate formation, DOM oxidation and disinfection (see chapter 4). In that study, parameters related to DOM were found to be of major importance. The first order ozone decay constant was again regarded as less important. Audenaert et al. (2011) used an extensive UV/hydrogen peroxide advanced oxidation model to describe a full-scale reactor (see chapter 6). The model consisted of a set of elementary radical reactions,

comparable to the SHB model. A local sensitivity analysis revealed that with respect to the $HO^{\bullet}$ concentration, scavenging by hydrogen peroxide and bicarbonate were most important. The kinetic constant describing $HO^{\bullet}$ scavenging by DOM just slightly affected the $HO^{\bullet}$ concentration because of the existence of two counteracting processes. An increase of this parameter enhanced the scavenging rate on the one hand, but gave rise to a better UV transmission on the other hand, leading to an increased $HO^{\bullet}$ production rate. Nine second order rate constants were found to exert no influence to the variables at all and trace pollutant concentrations were found to be very sensitive to many of the parameters (Audenaert et al., 2011). Lovato et al. (2009) used the SHB model as a starting point for their study. A poor fit between the experimental and modelled ozone concentration was the rationale for modifying the standard kinetic scheme. The model adaptation, however, was not based on a SA. The impact of the model parameters on the ozone concentration was determined by changing each parameter separately to a higher and lower value on an arbitrary basis. For every parameter change, a new simulation was run and the overall ozone decay rate was studied. By making one rate constant pH dependent, a good fit could be obtained (Lovato et al., 2009). In another study, these authors used a modified version of the SHB model (Lovato et al., 2011). The mechanism was reduced from 31 to 23 reaction steps based on a SA (Lovato et al., 2011). It was, however, not totally clear what these authors meant with SA, how it was performed and on which basis eight elementary reactions were removed. Fabian et al. (2006) questioned the validity of the original SHB model and highlighted the uncertainty associated with literature reported values of the kinetic parameters. The model was recalibrated by means of an optimization algorithm (Fabian, 2006). Additionally, four elementary reactions were discarded based on a sensitivity analysis. Again, it was not very clear how this SA was performed and how it was decided to simplify the model.

5.1.4 Objectives of this study

In contrast to some previous studies, the SA in this study was based on a structured approach. The SHB model as described by Bezbarua and Reckhow (2006) was used and the reaction scheme was extended with simple equations to describe reactions of DOM with ozone and $HO^{\bullet}$. Hence, the main focus here was to study the SHB scheme, rather than to construct a complicated model including complex mass balances of different DOM moieties. Local and global SAs were conducted over a wide range of DOM and bicarbonate concentrations. The goals of this study were to: (i) determine the most important elementary reactions of the sequence, (ii) get insight into the reaction mechanism by distinguishing different phases (switches

in local sensitivity functions) occurring during ozonation in the presence of DOM at different concentrations and (iii) compare the results and corresponding conclusions of the local and global approach to perform SAs.

5.2 Methods

5.2.1 Model conceptualization

A reactor continuously fed with gaseous ozone was simulated using the SHB model as described by Bezbarua and Reckhow (2006). The model was extended with simple second order equations describing the oxidation of DOM by both ozone and $HO^{\bullet}$. The total DOM content (DOM_T) was assumed to consist of four distinct groups: DOM_1 and DOM_2, only reacting with $HO^{\bullet}$ and DOM_3 and DOM_4, reacting with both ozone and $HO^{\bullet}$. DOM_1 and DOM_3 were assumed to promote and initiate the radical chain by producing superoxide ($O_2^{\bullet-}$) and ozonide ($O_3^{\bullet-}$) radicals, respectively. Examples of compounds that have the properties of DOM_1 and DOM_2 are formic acid and tertiary butanol, respectively (Westerhoff et al., 1997). Compounds that can be classified as DOM_3 and DOM_4 are tertiary amines and olefins, respectively. Examples of different DOM moieties and their reactions with ozone and $HO^{\bullet}$ are schematically presented in Figure 2.7. DOM was consumed by ozone and/or $HO^{\bullet}$ with a molar ratio of 1:1 and DOM_T consisted of 25% of each group (Westerhoff et al., 1997). Additionally, a gas-liquid mass transfer equation was added to account for the gaseous ozone inflow. A Gujer matrix presentation of the reaction system can be found in Table 5.1. More information about the parameters and their values can be found in Table 5.2. A detailed description of composing the mass balances from the Gujer matrix is given in Appendix A.

Table 5.1: Gujer matrix presentation of the ozone decomposition model

Reaction	Components																	Reaction rate
	O_3	HO_2^-	$HO_2^\bullet$	$O_2^{-\bullet}$	$O_3^{-\bullet}$	$HO_3^\bullet$	$HO^\bullet$	H_2O_2	$CO_3^{-\bullet}$	CO_3^{2-}	CO_2	HCO_3^-	$HCO_3^\bullet$	DOM_1	DOM_2	DOM_3	DOM_4	
Chain initiation																		
$O_3 + OH^- \rightarrow HO_2^- + O_2$	-1	1																$k_1 \times [O_3] \times [OH^-]$
$O_3 + HO_2^- \rightarrow HO_2^\bullet + O_3^{-\bullet}$	-1	-1	1		1													$k_2 \times [O_3] \times [HO_2^-]$
Chain propagation																		
$HO_2^\bullet \rightarrow O_2^{-\bullet} + H^+$			-1	1														$k_3 \times [HO_2^\bullet]$
$O_2^{-\bullet} + H^+ \rightarrow HO_2^\bullet$			1	-1														$k_4 \times [O_2^{-\bullet}] \times [H^+]$
$O_3 + O_2^{-\bullet} \rightarrow O_3^{-\bullet} + O_2$	-1			-1	1													$k_5 \times [O_3] \times [O_2^{-\bullet}]$
$O_3^{-\bullet} + H^+ \rightarrow HO_3^\bullet$					-1	1												$k_6 \times [O_3^{-\bullet}] \times [H^+]$
$HO_3^\bullet \rightarrow O_3^{-\bullet} + H^+$					1	-1												$k_7 \times [HO_3^\bullet]$
$HO_3^\bullet \rightarrow HO^\bullet + O_2$						-1	1											$k_8 \times [HO_3^\bullet]$
$O_3 + HO^\bullet \rightarrow HO_2^\bullet + O_2$	-1		1				-1											$k_9 \times [O_3] \times [HO^\bullet]$
$HO^\bullet + H_2O_2 \rightarrow HO_2^\bullet + H_2O$			1				-1	-1										$k_{10} \times [HO^\bullet] \times [H_2O_2]$
$H_2O_2 \rightarrow HO_2^- + H^+$		1						-1										$k_{11} \times [H_2O_2]$
$HO_2^- + H^+ \rightarrow H_2O_2$		-1						1										$k_{12} \times [HO_2^-] \times [H^+]$
Carbonate reactions																		
$CO_2 + H_2O \rightarrow HCO_3^- + H^+$										-1	1							$k_{13} \times [CO_2]$
$HCO_3^- + H^+ \rightarrow CO_2 + H_2O$										1	-1							$k_{14} \times [HCO_3^-] \times [H^+]$
$HCO_3^- \rightarrow CO_3^{2-} + H^+$									1		-1							$k_{15} \times [HCO_3^-]$
$CO_3^{2-} + H^+ \rightarrow HCO_3^-$									-1		1							$k_{16} \times [CO_3^{2-}] \times [H^+]$
$HO^\bullet + HCO_3^- \rightarrow HCO_3^\bullet + OH^-$							-1				-1	1						$k_{17} \times [HO^\bullet] \times [HCO_3^-]$
$HO^\bullet + CO_3^{2-} \rightarrow CO_3^{-\bullet} + OH^-$							-1		-1				1					$k_{18} \times [HO^\bullet] \times [CO_3^{2-}]$
$HCO_3^\bullet \rightarrow CO_3^{-\bullet} + H^+$												-1	1					$k_{19} \times [HCO_3^\bullet]$
$CO_3^{-\bullet} + H^+ \rightarrow HCO_3^\bullet$												1	-1					$k_{20} \times [CO_3^{-\bullet}] \times [H^+]$
$CO_3^{-\bullet} + CO_3^{-\bullet} \rightarrow 2CO_3^{2-}$									2				-2					$k_{21} \times [CO_3^{-\bullet}]^2$
$CO_3^{-\bullet} + O_2^{-\bullet} \rightarrow CO_3^{2-} + O_2$				-1					1				-1					$k_{22} \times [CO_3^{-\bullet}] \times [O_2^{-\bullet}]$
$CO_3^{-\bullet} + HO_2^- \rightarrow CO_3^{2-} + O_3$	1	-1							1				-1					$k_{23} \times [CO_3^{-\bullet}] \times [HO_2^-]$
$CO_3^{-\bullet} + O_3^{-\bullet} \rightarrow CO_3^{2-} + HO_2^\bullet$			1		-1				1				-1					$k_{24} \times [CO_3^{-\bullet}] \times [O_3^{-\bullet}]$
$CO_3^{-\bullet} + H_2O_2 \rightarrow HCO_3^- + HO_2^\bullet$			1					-1			1		-1					$k_{25} \times [CO_3^{-\bullet}] \times [H_2O_2]$
$CO_3^{-\bullet} + HO^\bullet \rightarrow CO_2 + HO_2^-$		1					-1			1			-1					$k_{26} \times [CO_3^{-\bullet}] \times [HO^\bullet]$

Table 5.1 (continued)

DOM reaction																		
$CO_3^{\bullet-}$ + DOM → CO_3^{2-} + products									1				-1					k_{27} x [$CO_3^{\bullet-}$] x [$DOM_{1,2,3,4}$]
$HO^{\bullet}$ + DOM_1 → products				1			-1							-1				k_{28} x [$HO^{\bullet}$] x [DOM_1]
$HO^{\bullet}$ + $DOM_{2,3,4}$ → products							-1								-1	-1	-1	k_{28} x [$HO^{\bullet}$] x [$DOM_{2,3,4}$]
O_3 + DOM_3 → products	-1				1											-1		k_{29} x [O_3] x [DOM_3]
O_3 + DOM_4 → products	-1																-1	k_{29} x [O_3] x [DOM_4]
Mass transfer	1																	k_La x ([O_3*] – [O_3])

Table 5.2: Parameters of the kinetic model and their values

Parameters	Value	Unit	Source
Rate constants			
k_1	70	$M^{-1}s^{-1}$	(Bezbarua and Reckhow, 2004)
k_2	2.8×10^6	$M^{-1}s^{-1}$	
k_3	3.2×10^5	s^{-1}	
k_4	2×10^{10}	$M^{-1}s^{-1}$	
k_5	1.6×10^9	$M^{-1}s^{-1}$	
k_6	5.2×10^{10}	$M^{-1}s^{-1}$	
k_7	3.3×10^2	s^{-1}	
k_8	1.1×10^5	s^{-1}	
k_9	2×10^9	$M^{-1}s^{-1}$	
k_{10}	2.7×10^7	$M^{-1}s^{-1}$	
k_{11}	4.5×10^2	s^{-1}	
k_{12}	2×10^{10}	$M^{-1}s^{-1}$	
k_{13}	2.1×10^4	s^{-1}	(Westerhoff et al., 1997)
k_{14}	5×10^{10}	$M^{-1}s^{-1}$	
k_{15}	2.8	s^{-1}	
k_{16}	5×10^{10}	$M^{-1}s^{-1}$	
k_{17}	8×10^6	$M^{-1}s^{-1}$	
k_{18}	3.7×10^8	$M^{-1}s^{-1}$	
k_{19}	13	s^{-1}	
k_{20}	5×10^{10}	$M^{-1}s^{-1}$	
k_{21}	2×10^7	$M^{-1}s^{-1}$	
k_{22}	4×10^8	$M^{-1}s^{-1}$	
k_{23}	5.6×10^7	$M^{-1}s^{-1}$	
k_{24}	6×10^7	$M^{-1}s^{-1}$	
k_{25}	8×10^5	$M^{-1}s^{-1}$	
k_{26}	3×10^9	$M^{-1}s^{-1}$	
k_{27}	1×10^7	$M^{-1}s^{-1}$	
k_{28}	2×10^8	$M^{-1}s^{-1}$	
k_{29}	1×10^3	$M^{-1}s^{-1}$	
Reactor parameters			
$k_L a_{O3}$	1.7×10^{-3}	s^{-1}	Experimental work[a]
$C_{O3\_L}^*$	6.25×10^{-5}	M	Experimental work[a]
V	1	L	This study
Q	4	$L\ h^{-1}$	This study

[a]These values were obtained from preliminary tests that preceded the experiments described in Chapter 7. Hence, these values deviate from the final ones reported in that chapter. The values, however, are in the same order of magnitude.

5.2.2 Software implementation and simulation

The system, consisting of 30 parameters and 14 ODEs, was implemented in WEST. Simulations were run in Tornado which allows to rapidly numerically simulate the stiff system of differential equations (see Chapter 3 for more information on the software). The stiff solver CVODE (Hindmarsh and Petzold, 1995) was used for all numerical integrations with an absolute and relative tolerance of 1 x 10^{-20} and 1 x 10^{-5}, respectively.

Two different single-reactor configurations were simulated: (i) a completely stirred semi-batch reactor (continuous gaseous ozone inflow, no water flow) and (ii) a CSTR fed in flow-through mode (continuous gaseous ozone inflow, continuous influent and effluent water flow). Initial DOM_T concentrations were varied between 0 and 12 mg L^{-1} (0-1 mM) in the different simulations, thus ranging from ultra-pure water concentrations to natural water levels. Concentrations of the individual DOM compounds (DOM_{1-4}) thus varied between 0 and 3 mg L^{-1}. Total carbonate concentrations (C_T) ranged between 0 and 3.6 mM. For the continuous flow reactor, influent concentrations were set equal to the initial conditions and a fixed flow rate (Q) of 4 L h^{-1} was applied. The initial conditions used for each simulation are presented in Table 5.3. Initial values for the radical species were derived from Bezbarua and Reckhow (2004). Each simulation in this chapter was based on the same scenario: at time t=0, the gaseous ozone flow was switched on, after which the aqueous ozone concentration started to build up ($[O_3]_{t=0}$=0). Every simulation was run for at least 5000 seconds. The pH was fixed at 7.5 by implementing fixed concentrations for H^+ and OH^- ions.

Table 5.3: Initial conditions used for each simulation

Component	Concentration (M)	Component	Concentration (M)
O_3	0	$CO_3^{-\bullet}$	0
HO_2^-	1 x 10^{-12}	DOM_T	0-1 x 10^{-3}
$HO_2^\bullet$	5 x 10^{-14}	H^+	3.16 x 10^{-8}
$O_2^{-\bullet}$	5 x 10^{-14}	OH^-	3.16 x 10^{-7}
$O_3^{-\bullet}$	4 x 10^{-12}	CO_3^{2-}	0
$HO_3^\bullet$	1 x 10^{-13}	CO_2	0
$HO^\bullet$	5 x 10^{-14}	HCO_3^-	0.4-3.6 x 10^{-3}
H_2O_2	5 x 10^{-9}	$HCO_3^\bullet$	0

5.2.3 Local and global sensitivity analysis

Local sensitivity analyses were used to investigate and quantify the influence each model parameter exerts on certain variables of interest. Additionally, LSAs were performed to get insight into the reaction mechanism by distinguishing different phases (switches in local sensitivity functions) occurring during ozonation in the presence of DOM at different concentrations. To allow comparison between SFs of different variable-parameter combinations, RSFs were used (Audenaert et al., 2010, 2011). More information on the calculation of RSFs can be found in Chapter 3. The automated SF functionality in WEST was used and the steady-state RSF values were calculated using the parameter values indicated in Table 5.2. The RSF was calculated from the ASF using the finite central difference method with a perturbation factor ξ of 5×10^{-2} (this perturbation factor was applicable for all variables of interest). The sensitivity of the ozone and $HO^{\bullet}$ concentrations to all model parameters was investigated. Since these concentrations never reach steady state in the semi-batch reactor, the sensitivity functions also do not reach stable values. For this reason, only the steady-state RSF values of the flow-through reactor were used. The sensitivity functions of the semi-batch reactor were used to study the dynamics of the reaction system.

Parameters that were found to be important during the LSA were adopted in the global SA. An additional parameter related to $HO^{\bullet}$ scavenging by bicarbonate (k_{17}) was also considered (to check if this scavenging reaction is also found to be of minor importance using the global approach). An interval was assigned to each of them, based on literature or laboratory experience. The parameters with their respective sampling intervals are given in Table 5.4. In total, 1500 simulations were run (i.e. 150 simulations per parameter). The flow-through reactor was used to perform the global SA. To study the effect of scavenger levels on output sensitivity and uncertainty, a dynamic influent with changing C_T and $[DOM_T]$ was used. The influent was characterized by four regions: (i) low C_T and low $[DOM_T]$ (4000-5000s), (ii) high C_T and low $[DOM_T]$ (5000-6000s), (iii) low C_T and high $[DOM_T]$ (6000-7000s) and (iv) high C_T and high $[DOM_T]$ (7000-8000s). The influent composition was tentatively chosen and is depicted in Figure 5.1 as function of time. Flow rate and all other concentrations were kept fixed. The first 4000s, the influent composition was kept constant in order to allow the reactor to reach steady state. More detailed information regarding global SA is provided in Chapter 3.

Besides as an input for the global SA, the data of the Monte Carlo simulation was used to perform uncertainty analysis on ozone and $HO^{\bullet}$ concentrations. The 50^{th}, 95^{th} and 5^{th} percentiles as function of time of these species were calculated.

Table 5.4: Model parameters and confidence intervals used in the global SA

Parameter	Lowerbound	Upperbound	Unit	Source of uncertainty interval
k_1	40	100	$M^{-1}s^{-1}$	(Bezbarua and Reckhow, 2004; Fabian, 2006)
k_2	2.2×10^6	5.5×10^6	$M^{-1}s^{-1}$	(Bezbarua and Reckhow, 2004; Fabian, 2006)
k_9	1×10^8	3×10^9	$M^{-1}s^{-1}$	(Fabian, 2006)
k_{11}	0.045	0.125	$M^{-1}s^{-1}$	(Bezbarua and Reckhow, 2004; Lovato et al., 2009)
k_{12}	2×10^{10}	5×10^{10}	$M^{-1}s^{-1}$	(Bezbarua and Reckhow, 2004; Westerhoff et al., 1997)
k_{17}	8×10^6	9×10^6	$M^{-1}s^{-1}$	(Westerhoff et al., 1997)
k_{28}	1×10^8	1×10^9	$M^{-1}s^{-1}$	(Westerhoff et al., 1997)
k_{29}	9×10^2	1.1×10^3	$M^{-1}s^{-1}$	Tentatively chosen
$C_{O3\_L}{}^*$	5.4×10^5	6.6×10^5	M	Laboratory experience[a]
k_La_{O3}	1.35×10^3	1.65×10^3	s^{-1}	Laboratory experience[a]

[a]These values were derived from preliminary tests that preceded the experiments described in Chapter 7.

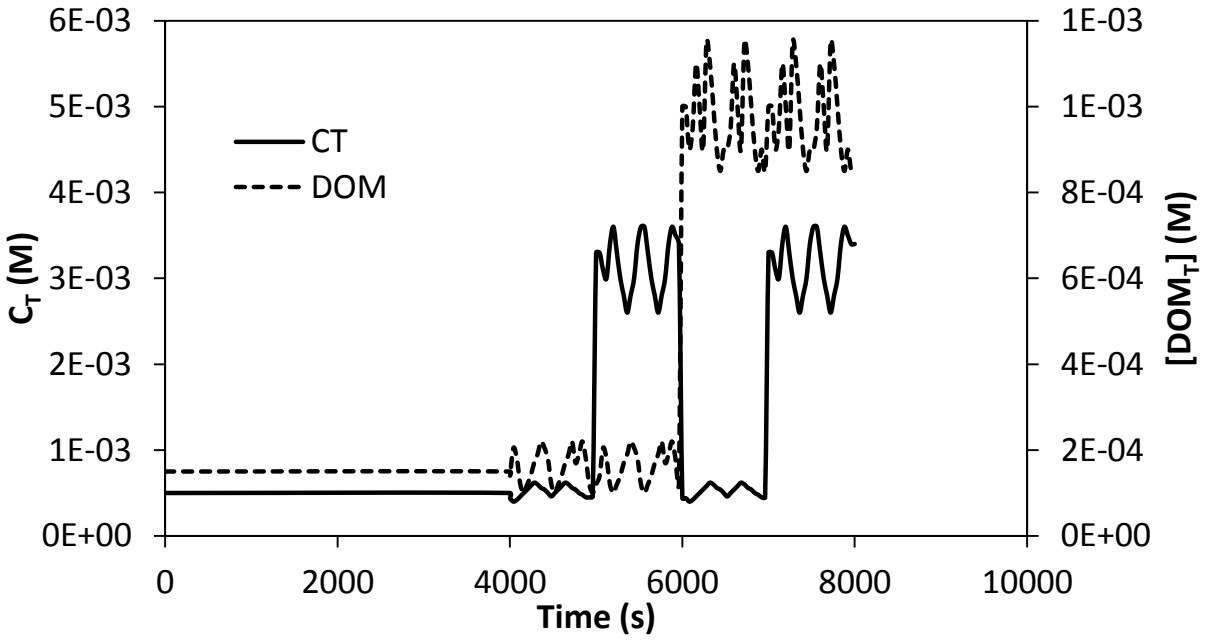

Figure 5.1: C_T and $[DOM_T]$ levels of the dynamic influent used in the global SA as function of time. DOM_T consists of 25% of each of the four individual compounds DOM_1, DOM_2, DOM_3 and DOM_4

5.3 Results and discussion

5.3.1 Local sensitivity analysis

5.3.1.1 Flow through reactor

Results of LSAs for a flow-through reactor are presented in Figure 5.2. The LSAs were performed at different concentrations of $HO^{\bullet}$ scavenging species (DOM and inorganic carbon). The parameters presented are the only parameters that were found to impact the ozone or $HO^{\bullet}$ concentration. Consequently, parameters involving reactions with inorganic carbon (characterized by rate constants k_{13}-k_{26}) have no impact on the process. Furthermore, it can be noticed that the sensitivity of the aqueous ozone concentration to parameter k_1 (related to the initiation reaction) is gradually decreasing with higher levels of DOM. At very low scavenger levels, radical-induced ozone decay is of major importance. An increase of the chain initiation will almost directly lead to higher ozone consumption as the major fate of the chain carriers is reaction with ozone. Higher DOM levels will lead to a shift of the fate of $HO^{\bullet}$ to reaction with DOM (or inorganic carbon). This shift is clearly illustrated by the decreasing importance of k_9 and increasing importance of k_{28} with an increasing scavenging rate (see Table 5.1 for reaction numbers). The positive influence of k_1 on the $HO^{\bullet}$ concentration rapidly decreases with increasing DOM concentrations. This is due to the indirect $HO^{\bullet}$ production of DOM_1 and DOM_3 via superoxide and ozone radicals, respectively. If sufficient DOM is present, its consumption becomes the major pathway of $HO^{\bullet}$ production. Figure 5.2 also shows that k_2 and the protonation constant of the hydroperoxyl ion (k_{12}) significantly impact the process at low scavenger concentrations. Again, this can be explained by the increased importance of the radical chain at low levels of scavengers. The second initiation step (reaction between ozone and the hydroperoxyl ion) is an important rate determining step. The protonation constant of the hydroperoxyl ion is four orders of magnitude higher than k_2 and hence, production of hydrogen peroxide will significantly slow down the chain initiation. It is already recognized that the addition of hydrogen peroxide to enhance chain initiation is only of value at high ozone and/or hydrogen peroxide concentrations, due to the slow dissociation and initiation reactions (Buffle et al., 2006a).

The mass-transfer related parameters $k_L a_{O3}$ and $C_{O3\_L}^{*}$ are of major importance in all cases (RSF>0.3), with the latter being the most influential parameter. Hence, it is of extreme importance that these parameters are determined with high accuracy.

However, these parameters are highly dependent on many physical and chemical

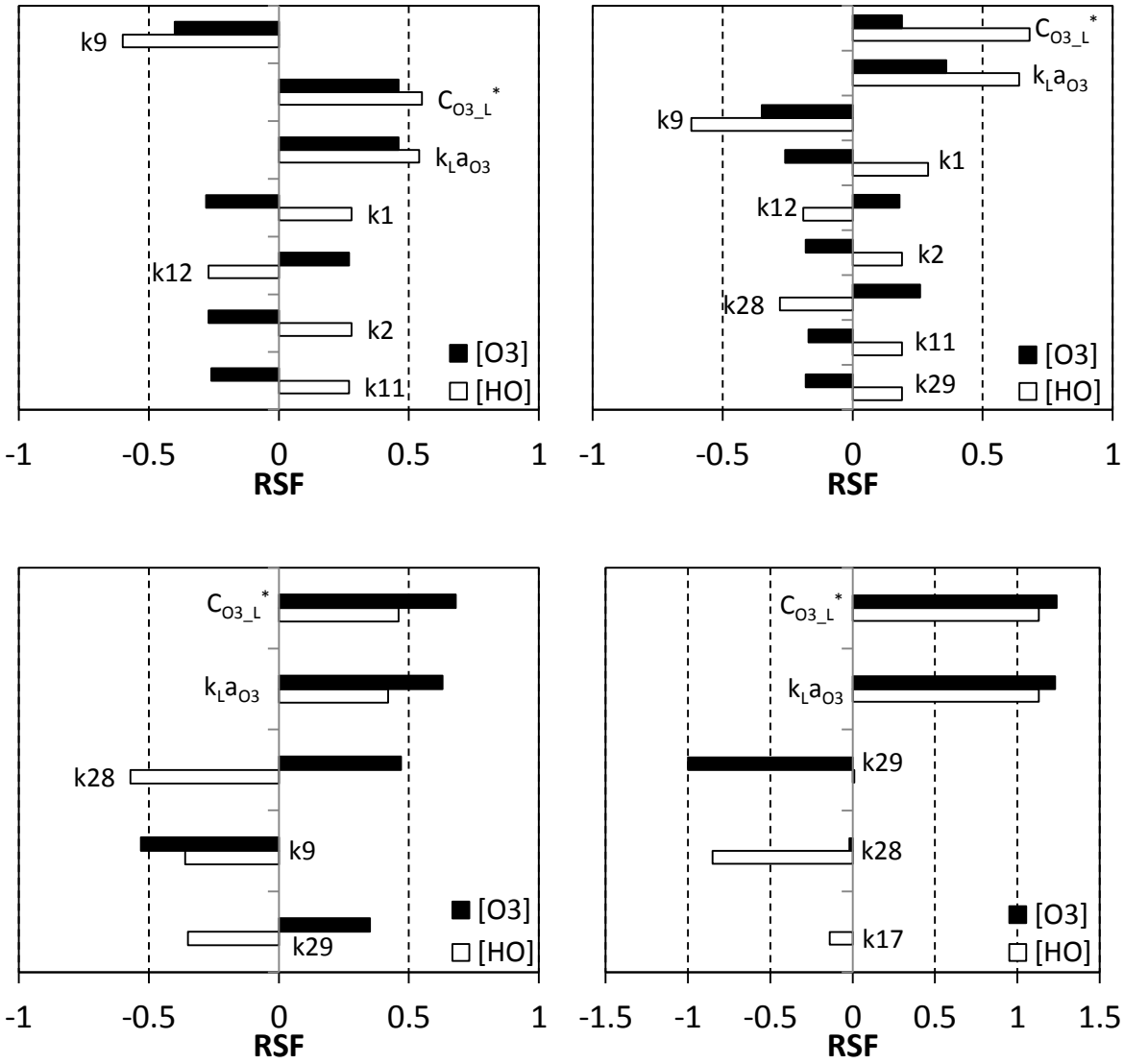

Figure 5.2: Results of LSA; sensitivity of O_3 and $HO^{\bullet}$ concentrations to most influential parameters in a flow-through reactor (Tornado plot). Parameters sorted from most to least influential. (a) $[DOM]_{T\_0}$= 0 mM and $[C_T]_0$= 0 mM, (b) $[DOM]_{T\_0}$= 0.2 x10^{-3} mM;[$C_T]_{T\_0}$= 0.2 x10^{-3} mM, (c) $[DOM]_{T\_0}$= 16.7 x10^{-3} mM and $[C_T]_0$= 10 x10^{-3} mM, (d) $[DOM]_0$= 1 mM and $[C_T]_0$= 3.3 mM

parameters (Beltrán, 2004; Kumar and Bose, 2004). Consequently, estimating these parameters at a high level of confidence will not be easily accomplished, especially at full-scale. Kumar and Bose (2004) in their study concluded that discrepancies between experimental and modelled ozone concentrations were almost totally due to uncertainties in k_La_{O3} and $C_{O3\_L}^*$ and not due to effects related to the mechanistic model under study.

5.3.1.2 Semi-batch reactor

The ozone concentration in a semi-batch reactor showed a dynamic behaviour. Figure 5.3 shows the relative sensitivity of ozone to parameters k_{28} and k_{29}. In Figure 5.4, the corresponding concentrations of DOM moieties and ozone are presented. Both figures show that four phases could be distinguished. During a first phase all DOM moieties were present and the aqueous ozone concentration increased steadily. Despite the presence of direct consumers, the $HO^{\bullet}$ scavenging rate was sufficiently high to allow the aqueous ozone concentration to increase.

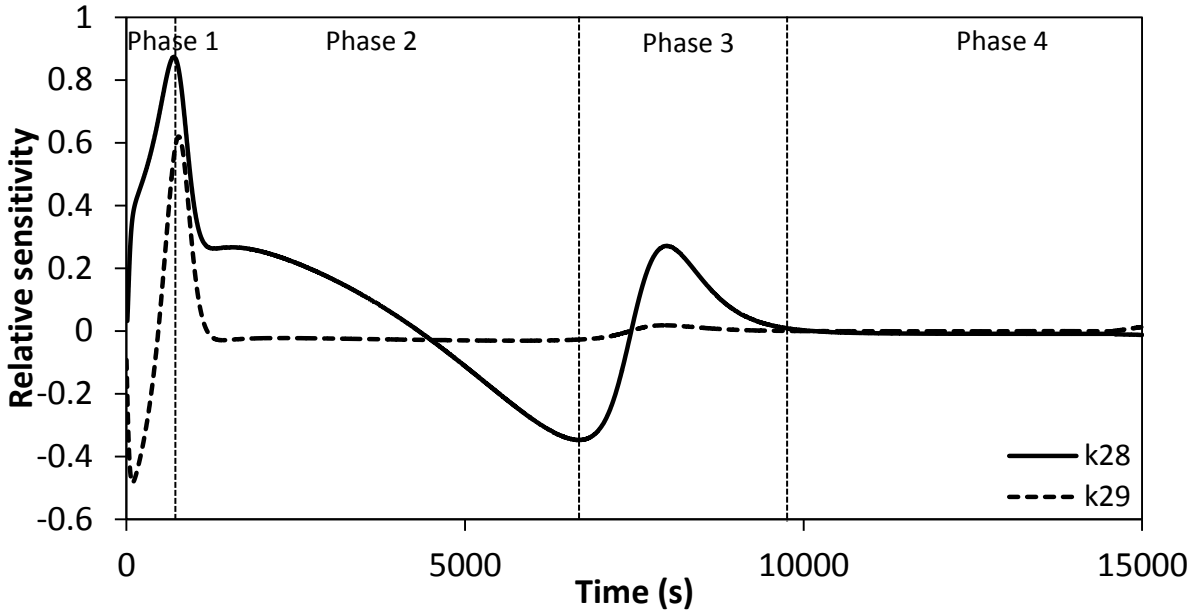

Figure 5.3: Local sensitivity function of k_{28} and k_{29} with respect to the aqueous ozone concentration; $[DOM]_{T\_0}$=16.7µM, C_T=10µM

The rate constant describing scavenging by DOM (k_{28}) positively influenced the ozone concentration, while parameter k_{29} (associated with direct ozone consumption) had a negative impact. At the end of phase 1, however, the RSF of k_{29} became positive and reached a maximum value of around 0.6. At that moment, DOM_3 and DOM_4 were limiting and hence, rising k_{29} led to a faster depletion of the direct consumers which resulted in a slower ozone consumption rate. As DOM_3 and DOM_4 were also attacked by $HO^{\bullet}$, the depletion of these species was also reflected in a maximum positive influence of k_{29} at the same moment. Reaching the second phase, the direct consumers were totally depleted and the influence of k_{28} and k_{29} decreased, with that of k_{28} approaching zero. In the course of phase 2, k_{29} became negatively influential. In analogy with the direct consumers during phase 1, DOM_1 and DOM_2 became limiting and raising this parameter implied those species to be depleted faster and hence, less radicals to be scavenged leading to a lower ozone concentration. In a third phase, the RSF of k_{28} switched back to positive values.

This was a result of a negative impact of k_{28} on the $HO^{\bullet}$ concentration. However, it remains unclear why this shift occurred. As of the moment where all DOM was depleted, the sensitivity functions reached zero (phase 4).

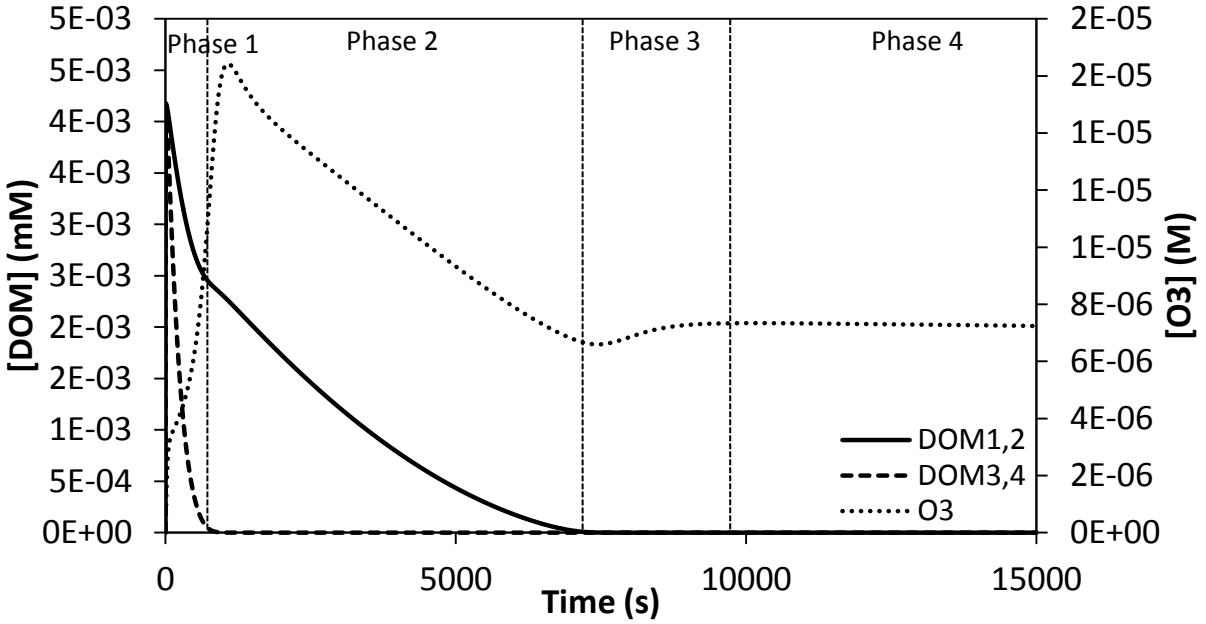

Figure 5.4: Evolution of the concentrations of DOM species and ozone in a semi-batch reactor; $[DOM]_{T\_0}$=16.7µM

5.3.1.3 Practical implications of parameter sensitivity

The fact that parameter sensitivities reach their maximum values at very low DOM concentrations has some important practical implications. Westerhoff et al. (1997) studied the SHB model using a batch reactor. Despite the fact that Milli-Q (ultrapure) water was used, the authors considered the presence of residual organic impurities with a concentration of 0.2 mg C L^{-1} (16.7 µM) (Westerhoff et al., 1997). The reaction sequence was therefore extended with a simple $HO^{\bullet}$ scavenging reaction with a second order rate constant of 2 x 10^8 M^{-1} s^{-1}. A satisfactory model prediction of the ozone decomposition profile could be obtained. Lovato et al. (2009) used the SHB model to describe ozone decomposition in a 11.5 L batch reactor at pH 4.8. The authors showed that the SHB model in its original form severely overestimated the ozone decay (Lovato et al., 2009). In order to obtain better fits, the model was modified. The reactor filled with ultrapure water was, however, assumed to be totally free of residual impurities and in contrast to the study of Westerhoff et al. (1997), the model did not account for these inhibiting substances. Figure 5.5 shows the measured ozone data adopted from Lovato et al. (2009). The dashed line represents a simulation in which the water was considered to be free of impurities (analogous to Lovato et al. (2009)). The solid line is

representing a simulation in which very low concentrations of impurities (tentatively chosen) were considered ($[DOM_2]_0$=0.1 µM, C_T=10 µM). It can be clearly observed from this figure that extremely low levels of impurities have a significant impact on model predictions. Consequently, impurities should always be considered in ultrapure water systems.

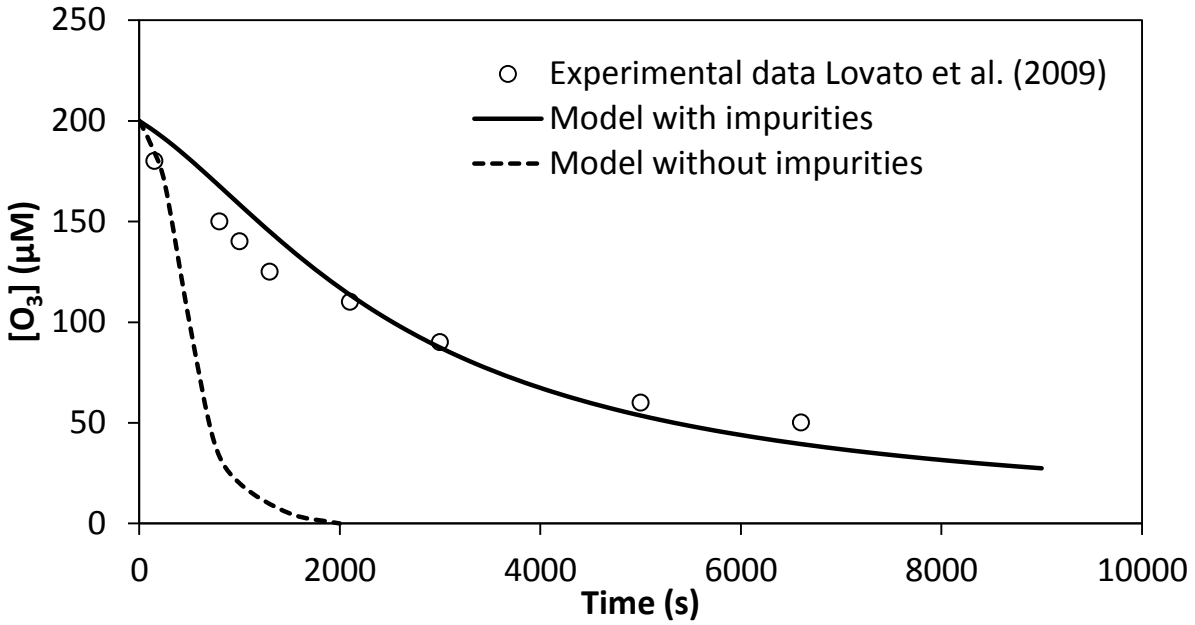

Figure 5.5: The effect of low levels of impurities on the modelled ozone concentration; experimental data points were adopted from Lovato et al. (2009)

5.3.2 Global sensitivity analysis

Results of the global SA for the ozone and $HO^{\bullet}$ concentration are presented in Figure 5.6. The tornado plots are comparable to those of the LSA conducted in the presence of scavengers (Figure 5.2). Therefore, only the most remarkable differences will be discussed in this section.

Similar to the results of the LSA, the sensitivity of the predicted ozone concentration to parameters $C_{O3\_L}^{*}$ and k_La_{O3} was found to be very significant (tSRC>1.96). In contrast, the impact of these parameters on the $HO^{\bullet}$ concentration is less visible but still significant. Rate constant k_1 is classified as an influential parameter with respect to the ozone concentration. Parameter k_{28} is the far most influential parameter with regard to the $HO^{\bullet}$ concentration. The importance of this parameter was also noticeable during local SAs, but to a lower extent. Probably the large interval that was defined for this parameter (Table 5.4) is the underlying reason for this observation. The parameter was allowed to uniformly vary over one order of magnitude. In other words, there are places in the parameter space where

the parameter becomes more important compared to the region studied in the LSA. This demonstrated the added value of a global SA. The rate constant for direct reaction with ozone (k_{29}) only had a significant impact on the ozone concentration. As expected, $HO^{\bullet}$ scavenging by bicarbonate was not found to significantly impact the output. Parameter k_{17} was of minor importance. Rate constant k_9 seemed to be important with respect to both concentrations although the LSA revealed that this parameter is only influential at low scavenger concentrations.

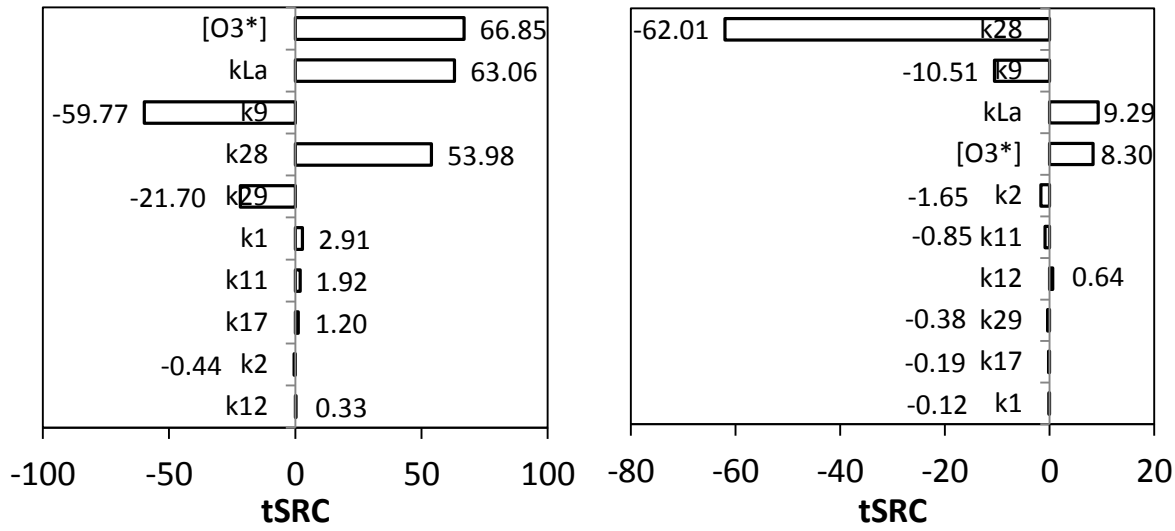

Figure 5.6: Results of global SA; sensitivity of O_3 (a) and $HO^{\bullet}$ concentrations (b) to most influential parameters in a flow-through reactor (Tornado plot). Parameters sorted from most to least influential.

5.3.3 Uncertainty analysis of output

The 50th percentile of ozone and $HO^{\bullet}$ concentrations and their respective 95% confidence intervals as function of time are presented in Figure 5.7 and Figure 5.8, respectively. Aqueous ozone and $HO^{\bullet}$ concentrations are clearly building up due to gas-liquid mass transfer. Fluctuations in the average concentrations were caused by dynamics in the influent. From both figures, the different phases shown in Figure 5.1 (varying concentrations of organic and inorganic carbon) can be clearly distinguished. Uncertainty significantly decreases from 6000s as more DOM is entering the reactor.

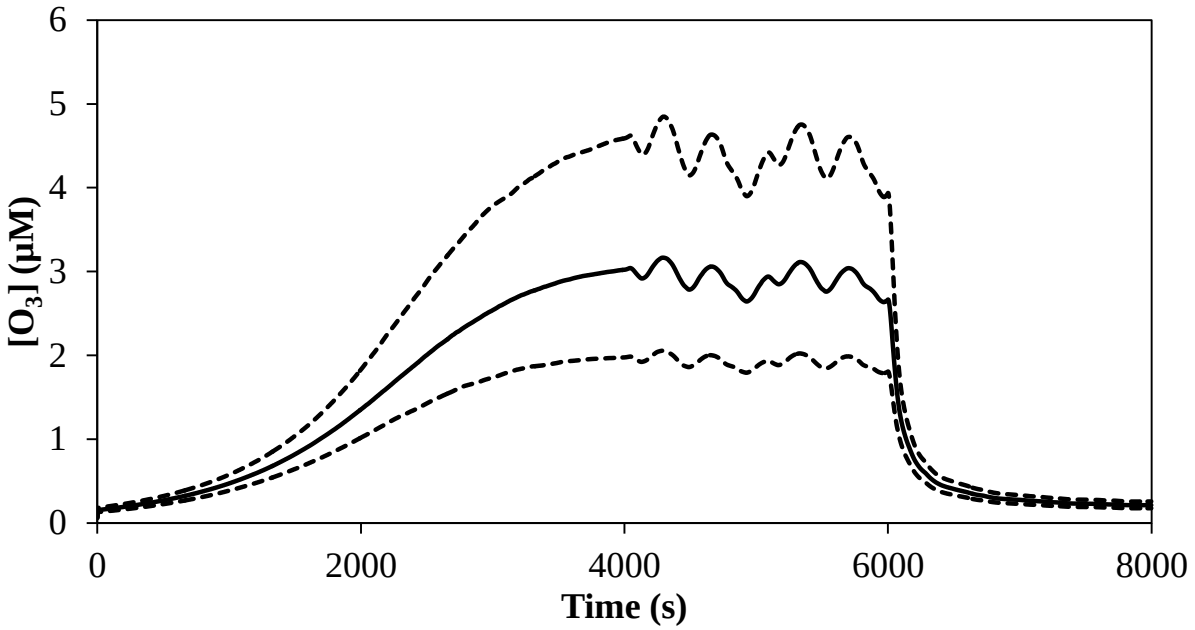

Figure 5.7: 50th percentile of predicted ozone concentration (solid line) with 95% confidence interval (dashed lines) as function of time; plot derived from 1500 Monte Carlo runs

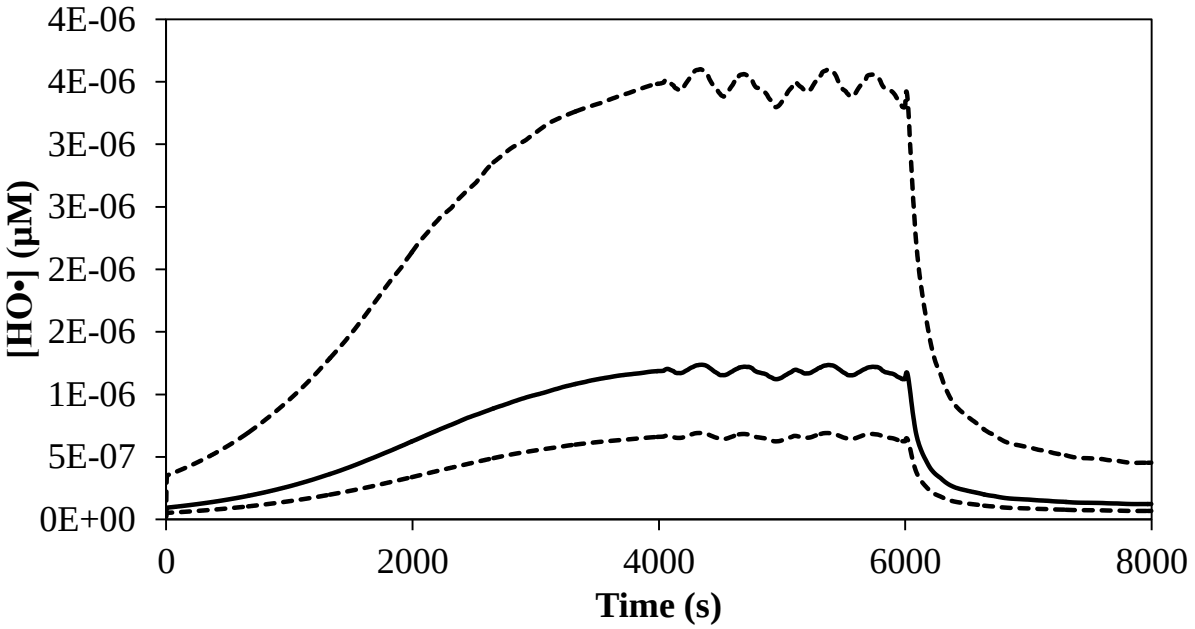

Figure 5.8: 50th percentile of predicted HO• concentration (solid line) with 95% confidence interval (dashed lines) as function of time; plot derived from 1500 Monte Carlo runs

Based on the global SA, most of the uncertainty in both concentrations is caused by a not well defined rate constant describing scavenging by DOM (k_{28}). This illustrates the importance of including more detailed DOM reaction sequences in

future models in order to reduce this uncertainty. A reliable estimation of $HO^{\bullet}$ exposure is of vital importance for DOM moieties that slowly react with ozone and hence, are primarily removed by $HO^{\bullet}$ induced oxidation (Neumann et al., 2009; Zimmermann et al., 2011).

5.4 Conclusions

In this chapter, the extensive SHB model consisting of a set of elementary reactions describing aqueous ozone decomposition was investigated in detail by means of SA. The model was extended with simple equations describing oxidation of DOM to study the effect of varying scavenger concentrations. LSAs revealed that only seven of the twenty-eight first and second order rate constants showed to impact ozone and $HO^{\bullet}$ concentrations. Processes involving $HO^{\bullet}$ scavenging by inorganic carbon were of minor importance. The effect of inorganic carbon only became clear when very low DOM concentrations were present and provided C_T was sufficiently high. Mass-transfer related parameters k_La_{O3} and $C_{O3\_L}^{*}$ were of major importance in all cases. Hence, it is of extreme importance that these parameters are determined with high accuracy, which is a rather difficult task given the many physical and chemical parameters affecting them. It was shown that the aqueous ozone concentration is extremely sensitive to parameters involving DOM at very low scavenger concentrations. Hence, impurities should always be considered in models, even in ultrapure water systems. It should, however, be highlighted that this was a theoretical study in which only simple reactions of four DOM classes were considered. Nevertheless, the study showed that the parameter sensitivity can vary significantly depending on the concentrations of reactive species.

Results of a global SA were to a high extent comparable to these of LSAs. The importance of the mass-transfer related parameters was even more pronounced. Furthermore, the global SA revealed that a detailed description of reactions involving DOM is of vital importance as their related parameters seem to be very important. Uncertainty analysis showed that the ozone and $HO^{\bullet}$ concentrations are susceptible to variations in influent composition. The uncertainty regarding these species significantly reduced with increasing levels of scavengers and especially DOM.

It was shown in this study that simplification of the elementary radical scheme should be considered. For example, it is questionable if inorganic reactions should be included when DOM levels are sufficiently high. Additionally, some dissociation reactions might be discarded if the model is used within a predefined

pH range. On the other hand, a model extension with regard to reactions involving DOM should be considered in order to improve the applicability of future wastewater ozonation models. This will be an important issue in future research.

Chapter 6

Modelling of a full-scale UV/H_2O_2 process for tertiary treatment

Redrafted from: Audenaert, W.T.M., Vermeersch, Y., Van Hulle, S.W.H., Dejans, P., Dumoulin, A., Nopens, I., 2011. Application of a mechanistic UV/hydrogen peroxide model at full-scale: Sensitivity analysis, calibration and performance evaluation. Chemical Engineering Journal 171 (1), 113-126.

Abstract

Numerous mechanistic models describing the UV/H_2O_2 process have been proposed in literature. In this study, one of them was used to predict the behaviour of a full-scale reactor. The model was calibrated and validated with non-synthetic influent using different operational conditions. A LSA was conducted to determine the most important operational and chemical model parameters. Based on the latter, the incident UV irradiation intensity and two kinetic rate constants were selected for model calibration. In order to investigate changes of the DOM content over time, some time delay was considered between calibration and validation data collection. Hydrogen peroxide concentration, the decadic absorption coefficient at 310 nm (UV_{310}, as a surrogate for DOM) and pH could be satisfactorily predicted during model validation using an independent data set. It was demonstrated that quick real-time calibration is an option at less controllable full-scale conditions. The reactivity of UV_{310} towards HO• did not show significant variations over time suggesting no need for frequent recalibration. Parameters that determine the initiation step, i.e. photolysis of hydrogen peroxide, have a large impact on most of the variables. Some reaction rate constants were also of importance, but nine kinetic constants did show absolutely no influence to any of the variables. Parameters related to UV shielding by DOM were of main importance. At the conditions used in this study, i.e. H_2O_2 concentrations between 0.5 and 4 mM, hydraulic residence times between 90 and 200 s and alkalinity concentrations

between 2.5 and 6 mM, competitive radiation absorption by DOM was more detrimental to the micropollutant removal efficiency than $HO^{\bullet}$ scavenging. Hydrogen peroxide concentration was classified as a non-sensitive variable, in contrast to the concentration of a micropollutant which showed to be very to extremely influential to many of the parameters. UV absorption as a DOM surrogate is a promising variable to be included in future models. Model extension by splitting up UV_{310} into a soluble and a particulate fraction seemed to be a good approach to model AOP treatment of real (waste)waters containing both dissolved and particulate (suspended) material.

6.1 Introduction

6.1.1 The UV/hydrogen peroxide process

The increasing pressure of emerging micropollutants on the aquatic environment and fresh water resources has resulted in an intensification of scientific research on the sources, fate, effects and removal of these products. AOPs have recently been proven to be very suitable in this context, which has already led to several full-scale applications (Kruithof et al., 2007; Swaim et al., 2008) (see Chapter 2). The driving force of AOPs is the formation of $HO^{\bullet}$ which can virtually oxidize any compound present in the water matrix because of its high oxidation potential (Parsons, 2004). Besides this oxidative power, AOPs often simultaneously achieve disinfection and can facilitate the removal of DOM, which perfectly fits into the multiple-barrier concept often applied at water treatment sites.

UV irradiation can effectively deactivate waterborne cysts and oocysts of Gardia and Cryptosporidium which are resistant to conventionally applied chlorine doses (Campbell et al., 1995; Bukhari et al., 1999; Clancy et al., 2000). This, along with their oxidizing performance and process flexibility makes that UV-initiated AOPs are appealing to be part of the water treatment train, in particular the UV/H_2O_2 process. This AOP is initiated by the UV photolysis of hydrogen peroxide resulting in a direct production of $HO^{\bullet}$, as shown in Chapter 2. Nowadays, research also focuses on the use of AOPs for wastewater treatment and especially the role they can play as integrated tertiary treatment (Chapter 2). The use of mathematical models in this context can be of great value for design and optimization purposes. Whereas different models describing the UV/H_2O_2 process were already developed, it is noteworthy that full-scale model studies and implementations are scarce. This can probably be attributed to two major causes: (i) often, research ends at lab-scale and experiments conducted in real natural water are limited, which restricts actual

implementation of models at full-scale AOP reactors; (ii) even when very detailed and generally accepted radical pathways are available, the complex reaction mechanism of DOM often impedes the modelling exercise severely which leads to black box approaches that severely limit model performance and applicability. Another important issue is the overparameterisation of models and the lack of sensitivity studies. The latter could shed light on the extent at which model parameters are influencing the model's output variables. Detailed studies regarding this question are scarce, but are very important when performing modelling studies, especially at full-scale.

6.1.2 Modelling the UV/H_2O_2 process

The structure and features of models describing the UV/H_2O_2 process are highly dependent on the goal of the modelling exercise. Consequently, comparing existing models is not straightforward, although some common features exist. In the following section, an overview of different types of models is given, based on differences in research goals and approaches.

Empirical models are not based on known physical and chemical laws and in this way try to avoid ending up with complex sets of equations. Artificial neural networks can be used to investigate the influence of parameters on the process without understanding the actual phenomena (Salari et al., 2005). To optimize costs or efficiency, response surface methodologies can be used (Drouiche et al., 2001; Novak et al., 2009). Although these models are relatively easy to build, their value regarding AOP process design is rather limited. In addition, these models are data driven and therefore require intensive experimental investigation.

Often, phenomenological approaches can offer an answer to the abovementioned drawbacks. Mineralization studies are lab-scale studies that attempt to unravel a degradation mechanism of typically one or a few model compounds whereby parent compound and intermediary metabolite concentrations can be calculated as function of time (Stefan et al., 1996; Wu and Linden, 2008; Kralik et al., 2010). Often, the focus is to improve the understanding of a mechanism of (micro) pollutant decay, rather than to build a model for engineering application.

A third category of models aims to include more water quality and process variables in order to provide a flexible tool to determine operational optima and to gain process insight. These mechanistic models are based on known chemical and photochemical principles and can help understanding the often complex chemical mechanisms. They can be of great value during the design and engineering process

(Glaze et al., 1992, 1995; Liao and Gurol, 1995; Hong et al., 1996; Crittenden et al., 1999; Sharpless and Linden, 2003; Rosenfeldt and Linden, 2004; Li et al., 2008; Song et al., 2008). For this reason, the model selected and discussed in this chapter belongs to this group. More recently, attempts to combine the typical stiff systems of kinetic relations describing the UV/H_2O_2 process with hydrodynamic reactor models have been reported (Alpert et al., 2010; Mohajerani et al., 2010). CFD models allow computing the fluid hydrodynamics and can be combined with kinetic equations to make more accurate predictions in both space and time and account for spatial heterogeneity. This is indeed a powerful tool for design and optimization of pilot and full-scale reactors. However, before this can actually yield useful results, the kinetic model validity should be proven at full-scale. Hence, a CFD model was not considered in this study.

6.1.3 Kinetic model applications

Glaze et al. (1995) combined the results of several fundamental studies to propose a kinetic model for the UV/H_2O_2 process. 1,2-Dibromo-3-chloropropane (DBCP) was used as a model compound to verify the model. All radical species were assumed to be at steady-state concentrations which allowed to analytically solve all mass balances. The model was evaluated by calculating pseudo-first-order rate constants of DBCP at different reactor conditions and comparing model predictions with experimental data. Model predictions agreed well with experimental data, however, the modelling exercise did not incorporate effects of DOM such as scavenging and UV shielding and was limited to studies in a well-known water matrix. Hong et al. (1996) modelled AOPs based on ozone, hydrogen peroxide and UV irradiation by invoking the steady-state assumption for all radical species. UV initiated AOPs showed to be more effective in producing hydroxyl radicals as compared to dark processes. Nevertheless, the model was not experimentally verified and the modelling results were limited to organic-free water systems which severely limits its application. Liao and Gurol (1995) successfully incorporated the influence of DOM by studying the concentrations of n-chlorobutane and hydrogen peroxide in the presence of a known humic acid. No steady-state assumptions were made and the experimental reactor operated in a continuous flow mode. Crittenden et al. (1999) significantly improved the earlier model of Glaze et al. (1995) by rejecting the pseudo-steady-state assumptions and including a pH change during the process as a result of acid formation. Further, the effects of DOM could be included although this was not verified as no new experiments were carried out. A useful application of this model was the optimization and dimensioning of a full-scale UV/H_2O_2 reactor (Li et al., 2008). Sharpless and Linden (2003) investigated

NDMA removal with LP- and MP-UV lamps. As NDMA is subject to direct photolysis, this study particularly stressed aspects related to UV reactor geometry. Nevertheless, the addition of hydrogen peroxide was tested and the effects of scavengers as DOM were included into a model that accurately predicted pseudo-first order rate constants. UV shielding by DOM was not considered. In the work of Rosenfeldt and Linden (2004), the model was used to predict the degradation of three endocrine disruptors. In this case, $HO^{\bullet}$ induced degradation was the dominating destruction mechanism and consequently, scavenging by DOM became more important. The model was verified in synthetic natural water, but also in real natural water, which cannot commonly be found in literature. These researchers highlighted the influencing role of DOM during UV/H_2O_2 treatment and the importance of its variability.

6.1.4 UV absorption as DOM surrogate

Total organic carbon (TOC) and DOC, expressed in mg (or mole) carbon L^{-1}, are frequently used surrogates for (natural) organic matter (Liao and Gurol, 1995; Sharpless and Linden, 2003; Li et al., 2008; Alpert et al., 2010). These variables can be easily determined and cover all organic compounds present in the water. However, it is known that using this surrogate has several disadvantages. First, lumping the whole organic carbon content into one variable implies the use of just one kinetic rate constant in the hydroxyl radical mass balance. It has been demonstrated that not all DOC can be classified as NOM and that some waters contain different DOM structures with varying reactivity towards $HO^{\bullet}$ (Westerhoff et al., 1997). Second, in cases where AOPs are integrated in a treatment train and DOM itself is also a target compound to (partially) oxidize (e.g. in drinking water production), models must be able to predict also the concentration and/or structural changes of the organic matter during the treatment. As in these cases the focus is merely to partially oxidize compounds at relatively short hydraulic retention times (HRTs), TOC or DOC do not give a good representation of the reaction progress as they only describe mineralization which mainly occurs at longer reaction times. Third, because of the lack of information provided at short term, the use of TOC or DOC in UV shielding equations is only valid at the beginning of simulations because the amount of shielding can decrease rapidly as the reaction proceeds. This is mainly due to $HO^{\bullet}$ attack at reactive double bond sites, which often occurs at a speed which is not proportional to the TOC or DOC reduction. For these reasons, Song et al. (2008) used UV_{310} as a DOM surrogate (the decadic absorption coefficient is defined as the absorbance divided by the optical path length of the solution (Braslavsky, 2007)). Indeed, only an insignificant TOC reduction during

the first 10 minutes of UV/H_2O_2 treatment at H_2O_2 concentrations ranging between 2 and 6 mM was demonstrated. Moreover, Beltrán et al. (1997) highlighted the disadvantages of TOC in kinetic AOP modelling and used the chemical oxygen demand (COD) instead. As such, the model of Crittenden et al. (1999) was modified with this new surrogate and additionally, a pH decrease as a result of TOC mineralization was included. However, it is important to note that the latter is just a rough and simplistic assumption as not all TOC is being mineralized during AOP treatment. Mostly, low MW fractions are produced such as aldehydes and carboxylic acids (Parsons, 2004), which is not equivalent to carbon dioxide formation. Additionally, the shape of the TOC mineralization curve shown by Song et al. (2008) was clearly not in accordance with that of a conventional second order reaction, while the model did assume this. Due to a current lack of knowledge, not many alternatives exist. As similar HRTs and H_2O_2 concentrations as in the study of Song et al. (2008) were applied, this model seemed suitable to use in the study described in this chapter. Moreover, the interest was to predict DOM concentrations and structural changes during the oxidation process, rather than to follow the concentration of a single organic pollutant in time. An important drawback of UV measurements however, is that they do not cover the whole organic carbon content, but focus on the olefinic structures containing carbon-carbon double bonds. As such, this surrogate is limited to describe the conversions of only the unsaturated part of DOM (Westerhoff et al., 1999).

The objectives of this contribution are to: (i) evaluate the performance of a kinetic UV/H_2O_2 model from literature calibrated at full-scale using a real water matrix, (ii) evaluate the usage of the DOM surrogate using non-synthetic influent for different operational conditions, (iii) determine the relative importance of each model parameter through a LSA and (iv) extend the model and discuss further improvements in order to broaden its applicability. Consequently, gaining mechanistic knowledge of the process was the main goal.

6.2 Materials and methods

6.2.1 Reactor configuration and operation

A full-scale UV reactor for water reuse at a horticultural industry was used for this study. To investigate the potential of additional water treatment with advanced oxidation to lower the overall TOC content, the reactor, originally only designed for disinfection, was extended with a hydrogen peroxide dosing system. Obviously, the purpose of this research was not to obtain an optimal AOP reactor, but to get

insight into the process at full-scale. A schematic representation of the installation is shown in Figure 6.1. A picture of the reactor is given in Figure 6.2. The AOP unit is part of a small wastewater treatment plant consisting of primary sedimentation, biological reed bed filtration, secondary sedimentation, sand filtration, UV/H_2O_2 treatment, granular activated carbon filtration and storage. Surplus crop irrigation water as well as grey and black domestic wastewater are treated by the system.

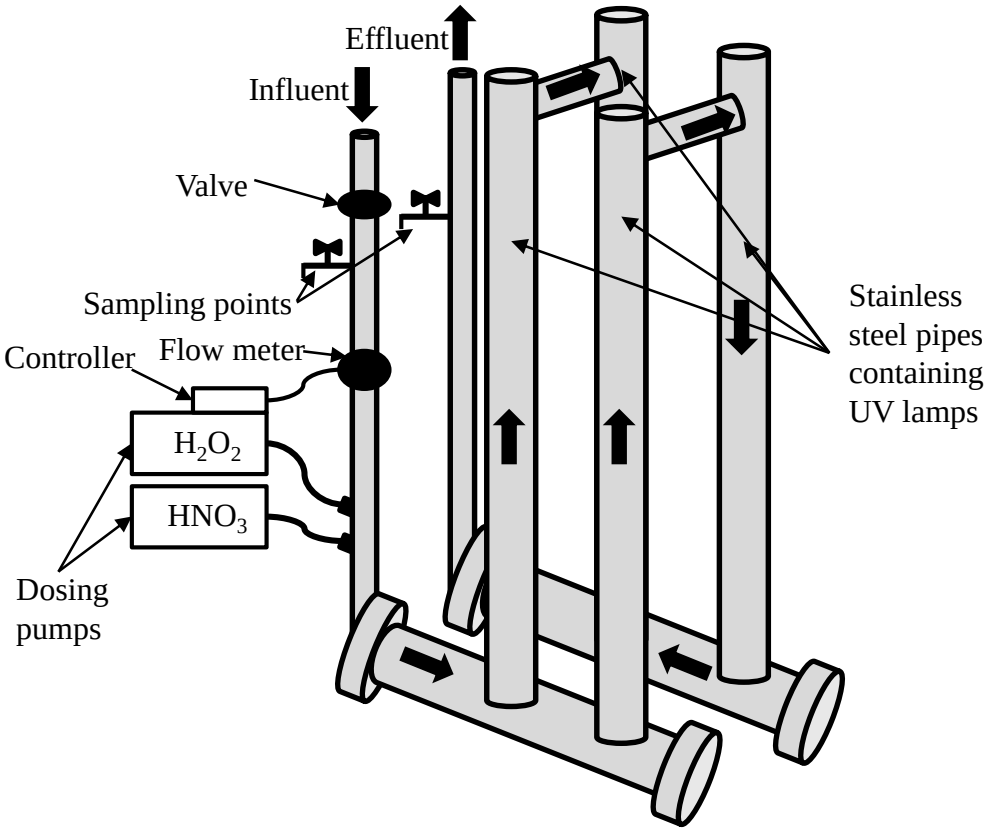

Figure 6.1: Schematic presentation of the process set-up

The typical influent composition of the UV/H_2O_2 reactor (already primary and secondary treated) is given in Table 6.1. The AOP reactor consisted of four stainless steel pipes each containing a 205 Watt low-pressure UV lamp that was 114.5 cm in length (Heraeus, No. NNI 201/107 XL, 480 µW/cm² irradiance at 1 m distance) and installed parallel to the water flow. Each lamp was enclosed by a quartz jacket. The total irradiated reactor volume of the four pipes approximated 7.3 L. The influent channel was split into two parts so that each water stream flowed along two lamps in series. The reactor, operating at a nominal flow rate of 2,000 L h^{-1}, was equipped with nitric acid and hydrogen peroxide dosing systems. Nitric acid was used prior to each measurement campaign to rinse the quartz jackets and to prevent scaling of carbonates. Hydrogen peroxide dosing was flow

controlled after setting a fixed value at the dosing pump. The HRT in the reactor was manually adjusted by controlling the incoming water flow with a valve. Flow rates between 120 and 300 L h^{-1} were applied to allow for a sufficient reaction time. Influent samples were taken at a point located just before the hydrogen peroxide dosing pipe. A tap located downstream of the reactor was used to sample the effluent. Influent and effluent samples were taken after a period of three times the HRT to allow the reactor reaching steady-state. Two operational settings were varied during different runs: flow rate (and thus HRT) and H_2O_2 concentration.

Figure 6.2: Front image of the UV/H_2O_2 reactor that was used

6.2.2 Tracer test

To mimic the mixing behaviour of the AOP reactor, a tanks-in-series (TIS) approach was used. A tracer test (Froment and Bischoff, 1990) was performed to determine the number of CSTRs to be used in the simulation software. A pulse of 10 ml sodium chloride (10 %) was rapidly injected into the hydrogen peroxide addition port. On-line conductivity measurements at the effluent sampling valve were used to record the salt concentration residence time distribution (as sodium chloride concentration is directly correlated to conductivity). A data-acquisition device based on voltage measurements (model No. FN-18200-00, Cole-Parmer) connected to a PC was used for data storage. The tracer test was performed at three

Table 6.1: Summary of water properties of the reactor influent

Variable (unit)	Value
pH	7.4-8.2
COD (mg L^{-1})	20-26
TOC (mg L^{-1})	20
UV_{310} (cm^{-1})	0.10-0.11
UV_{254} (cm^{-1})	0.20-0.21
Alkalinity (mM)	2.6-6.1
Total nitrogen (mg L^{-1})	0.55
Ortho-phosphate (mg L^{-1})	0.70

different flow-rates to study the effect of the liquid velocity on the mixing properties. The tested flow-rates were 1,000, 350 and 120 L h^{-1}. From the measured tracer response, the dimensionless hydraulic residence time distribution (E(t')) can be calculated (Froment and Bischoff, 1990):

$$E(t') = HRT \times \frac{y_{cond,m}(t)}{\int_0^\infty y_{cond,m}(t)dt} \quad (6.1)$$

where $y_{cond,m}(t)$ represents the measured conductivity, HRT represents the hydraulic residence time (s) and t is the time (s).

Subsequently, every time point is converted into a dimensionless hydraulic residence time t':

$$t' = \frac{t}{HRT} \quad (6.2)$$

E(t') can also be calculated theoretically as function of the number of tanks in series (n):

$$E(t') = HRT \times \frac{n^n}{(n-1)!} t'^{n-1} e^{-nt'} \quad (6.3)$$

By comparing the experimentally obtained E(t') curve to the theoretical obtained one, the optimal value of n was determined.

As mentioned in section 6.2.1, the irradiated reactor volume approximated 7.3 L. Nevertheless, this volume could not be used in the calculations, because the reactor volume between the point of tracer injection and conductivity measurement contained extra, non-active reactor parts (see Figure 6.1). The total volume measured with the tracer test was calculated to be 11 L, which was a realistic value.

6.2.3 Modelling approach

6.2.3.1 Conceptualization

The kinetic model of Crittenden et al. (1999), later modified by Song et al. (2008) was used in this study. However, it should be noted that the simulated data of Song et al. (2008) could not be reproduced. An investigation of the mass balances revealed that a stoichiometric conversion factor to deal with the dissimilarity between the units of UV absorption (expressed in cm^{-1}) and the $HO^{\bullet}$ concentration (expressed in M) was missing. After adding a factor Y with a numerical value around $1x10^4$ M^{-1} cm^{-1} to the mass balance of DOM, the same results could be obtained and the model was ready for use. According to previous models and due to the ease of implementation, the semi- empirical Lambert-Beer law was used to describe the direct photolysis conversion rate. This implied that a point source was assumed and that the photolysis rate of a given compound was calculated from the irradiance absorbed by that compound over the optical path length of the reactor. The irradiance (Einsteins s^{-1}) was volume-averaged.

Some adaptations to the model were made. First, Crittenden et al. (1999) stated that degradation of humic substances by direct photolysis could be ignored. This was experimentally verified and indeed, no significant UV_{310} reduction could be observed. Furthermore, a preliminary SA of the original model of Song et al. (2008) classified the parameters with respect to direct DOM photolysis as insignificant. Hence, this effect was discarded from the model. Second, as this study merely focuses on DOM conversion, no micropollutant concentrations were predicted, nor experimentally determined. However, during the SA, a fictive synthetic organic compound was included to compare the sensitiveness of its concentration to the other variables.

The original model was extended by splitting up the DOM surrogate, UV_{310}, into two different fractions. UV_{310} was found to consist of a soluble and a particulate (suspended) fraction, each contributing to UV shielding at 254 nm, but playing different roles in scavenging $HO^{\bullet}$. The current research revealed that the particulate fraction, UV_{310}^{X}, remained relatively constant during the treatment, and thus only the soluble part, denoted as UV_{310}^{S}, was assumed to participate in the radical chain. Consequently, for the extended model, two extinction coefficients for DOM at 254 nm, ε_{UV310S} and ε_{UV310X} (cm^{-1}/cm^{-1}), were used in absorption calculations and $HO^{\bullet}$ scavenging by soluble DOM was calculated using one reaction rate constant, k_{16}' ($(1/cm^{-1}).s^{-1}$). For describing UV shielding and radical scavenging with the original model, one molar extinction coefficient, ε_{UV310} (cm^{-1}/cm^{-1}), and a rate constant, k_{16} ($(1/cm^{-1}).s^{-1}$), were used, respectively. In both models, a stoichiometric conversion

factor Y (L mole^{-1} cm^{-1}) was introduced as discussed earlier. Simulation results of the original and the extended model were compared.

The Gujer matrix representation of the reaction system is given in Table 6.2. Reaction products such as oxygen or water that do not have a mass balance are therefore not included in the table. A detailed overview of all reaction products can be found elsewhere (Crittenden et al., 1999; Song et al., 2008). A detailed description of composing the mass balances from this matrix is given in Appendix A. This Gujer matrix notation is an elegant way to summarize a set of ODEs and gives a clear overview of all elementary reactions occurring during the process. More information about the parameters and their values can be found in Table 6.3.

The fractions of UV radiation absorbed by hydrogen peroxide and a model compound M, respectively, were calculated with the following equations (Song et al., 2008):

$$f_{H_2O_2} = \frac{b\times(\varepsilon_{H_2O_2}\times[H_2O_2]+\varepsilon_{HO_2^-}\times[HO_2^-])}{A} \tag{6.4}$$

$$f_M = \frac{b\times(\varepsilon_M\times[M])}{A} \tag{6.5}$$

For the original model, the absorbance of the solution at 254 nm (A_{254}) was calculated during each time step as follows:

$$A_{254} = b \times (\varepsilon_{H_2O_2} \times [H_2O_2] + \varepsilon_{HO_2^-} \times [HO_2^-] + \varepsilon_{UV_{310}} \times [UV_{310}]) \tag{6.6}$$

For the extended model, Equation 6.6 becomes:

$$A_{254} = b \times (\varepsilon_{H_2O_2} \times [H_2O_2] + \varepsilon_{HO_2^-} \times [HO_2^-] + \varepsilon_{UV_{310}^S} \times [UV_{310}^S] + \varepsilon_{UV_{310}^X} \times [UV_{310}^X]) \tag{6.7}$$

The dissociation equilibria of carbonates, hydrogen peroxide and hydroperoxyl radicals were described as follows:

$$K_{a_{H2CO3}} = \frac{[H^+]\times[HCO_3^-]}{[H_2CO_3]} \tag{6.8}$$

$$K_{a_{HCO_3^-}} = \frac{[H^+]\times[CO_3^{2-}]}{[HCO_3^-]} \tag{6.9}$$

$$K_{a_{H_2O_2}} = \frac{[H^+]\times[HO_2^-]}{[H_2O_2]} \tag{6.10}$$

$$K_{a_{HO_2^\bullet}} = \frac{[H^+]\times[O_2^{-\bullet}]}{[HO_2^\bullet]} \tag{6.11}$$

Table 6.2: Gujer matrix presentation of the UV/H_2O_2 system

Process		Components											Reaction Rate
		H_2O_2	$HO^{\bullet}$	$O_2^{-\bullet}$	$CO_3^{-\bullet}$	HCO_3^-	H_2CO_3	M	UV_{310}	UV_{310}^S	UV_{310}^X	TOC	
Photolysis	H_2O_2 (initiation)	-1	2										$\phi_{H2O2}*I_0*f_{H2O2}*(1-exp^{(-2,303*A)})$
	M							-1					$\phi_M*I_0*f_M*(1-exp^{(-2,303*A)})$
Propagation	$H_2O_2 + HO^{\bullet}$	-1	-1	1									$k_1*[HO^{\bullet}]*[H_2O_2]$
	$HO_2^- + HO^{\bullet}$	-1	-1	1									$k_2*[HO^{\bullet}]*[HO_2^-]$
	$H_2O_2 + O_2^{-\bullet}$	-1	1	-1									$k_3*[O_2^{-\bullet}]*[H_2O_2]$
	$H_2O_2 + HO_2^{\bullet}$	-1	1	-1									$k_4*[HO_2^{\bullet}]*[H_2O_2]$
	$H_2O_2 + CO_3^{-\bullet}$	-1		1	-1	1							$k_5*[H_2O_2]*[CO_3^{-\bullet}]$
	$HO_2^- + CO_3^{-\bullet}$	-1		1	-1	1							$k_6*[HO_2^-]*[CO_3^{-\bullet}]$
Termination	$HO^{\bullet} + HO_2^{\bullet}$		-1	-1									$k_7*[HO^{\bullet}]*[HO_2^{\bullet}]$
	$HO^{\bullet} + HO^{\bullet}$	1	-2										$k_8*[HO^{\bullet}]*[HO^{\bullet}]$
	$HO^{\bullet} + CO_3^{-\bullet}$		-1		-1								$k_9*[HO^{\bullet}]*[CO_3^{-\bullet}]$
	$HO^{\bullet} + O_2^{-\bullet}$		-1	-1									$k_{10}*[HO^{\bullet}]*[O_2^{-\bullet}]$
	$O_2^{-\bullet} + CO_3^{-\bullet}$		-1		-1	1							$k_{11}*[O_2^{-\bullet}]*[CO_3^{-\bullet}]$
	$O_2^{-\bullet} + HO_2^{\bullet}$	1		-2									$k_{12}*[O_2^{-\bullet}]*[HO_2^{\bullet}]$
	$HO_2^{\bullet} + HO_2^{\bullet}$	1		-2									$k_{13}*[HO_2^{\bullet}]*[HO_2^{\bullet}]$
	$CO_3^{-\bullet} + CO_3^{-\bullet}$				-2								$k_{14}*[CO_3^{-\bullet}]*[CO_3^{-\bullet}]$
Scavenging	$HO^{\bullet} + CO_3^{2-}$		-1		1	-1							$k_{15}*[HO^{\bullet}]*[CO_3^{2-}]$
	$HO^{\bullet} + UV_{310}^S$		-1							-Y	0		$k_{16}'*[HO^{\bullet}]*[UV_{310}^S]$
	$HO^{\bullet} + UV_{310}$		-1						-Y				$k_{16}*[HO^{\bullet}]*[UV_{310}]$
	$HCO_3^- + HO^{\bullet}$		-1		1	-1							$k_{17}*[HO^{\bullet}]*[HCO_3^-]$
Micropollutant destruction	$HO^{\bullet} + M$		-1					-1					$k_{18}*[HO^{\bullet}]*[M]$
Acid formation	$HO^{\bullet} + TOC$						1					-1	$k_{19}*[HO^{\bullet}]*[TOC]$

Table 6.3: Parameters of the kinetic UV/H_2O_2 model and their values

Parameters		Initial value	Reference
Incident light intensity	I_0[a]	6.9 x10^{-5} Eins L^{-1} s^{-1}	This work
Optical path length	b	1.2 cm	This work
Second order rate constants	k_1	2.7 x10^7 $M^{-1}s^{-1}$	(Buxton et al., 1988)
	k_2	7.5 x10^9 $M^{-1}s^{-1}$	(Christensen et al., 1982)
	k_3	0.13 $M^{-1}s^{-1}$	(Weinstein and Bielski, 1979)
	k_4	2.7 x10^7 $M^{-1}s^{-1}$	(Bielski et al., 1985)
	k_5	8 x10^5 $M^{-1}s^{-1}$	(Neta et al., 1988)
	k_6	3 x10^7 $M^{-1}s^{-1}$	(Neta et al., 1988)
	k_7	6.6 x10^9 $M^{-1}s^{-1}$	(Buxton et al., 1988)
	k_8	5.5 x10^9 $M^{-1}s^{-1}$	(Buxton et al., 1988)
	k_9	3 x10^9 $M^{-1}s^{-1}$	(Holeman et al., 1987 as cited in (Song et al., 2008)
	k_{10}	8 x10^9 $M^{-1}s^{-1}$	(Neta et al., 1988)
	k_{11}	6.5 x10^8 $M^{-1}s^{-1}$	(Eriksen et al., 1985)
	k_{12}	9.7 x10^7 $M^{-1}s^{-1}$	(Bielski et al., 1985)
	k_{13}	8.6 x10^5 $M^{-1}s^{-1}$	(Weinstein and Bielski, 1979)
	k_{14}	2 x10^7 $M^{-1}s^{-1}$	(Neta et al., 1988)
	k_{15}	3.9 x10^8 $M^{-1}s^{-1}$	(Buxton et al., 1988)
	k_{16}[a]	1.2 x10^4 $(1/cm^{-1})s^{-1}$	(Song et al., 2008)
	k_{16}'[a]	1.2 x10^4 $(1/cm^{-1})s^{-1}$	(Song et al., 2008)
	k_{17}	8.5 x10^6 $M^{-1}s^{-1}$	(Buxton et al., 1988)
	k_{18}	2.2 x10^9 $M^{-1}s^{-1}$	(Song et al., 2008)
	k_{19}[a]	4.5 x10^7 $M^{-1}s^{-1}$	(Song et al., 2008)
Primary quantum yields for photolysis	ϕ_{H2O2}	0.5 mole $Einstein^{-1}$[b]	(Baxendale and Wilson, 1957)
	ϕ_M	0.14 mole $Einstein^{-1}$[b]	(Song et al., 2008)
Molar extinction coefficients	ε_{UV310S}	2.58 cm^{-1}/cm^{-1}	This work
	ε_{UV310X}	1.39 cm^{-1}/cm^{-1}	This work
	ε_{UV310}	2.04 cm^{-1}/cm^{-1}	This work
	ε_M	466.7 $M^{-1}cm^{-1}$	(Song et al., 2008)
	ε_{H2O2}	19.6 $M^{-1}cm^{-1}$	(Baxendale and Wilson, 1957)
	ε_{HO2-}	228 $M^{-1}cm^{-1}$	(Baxendale and Wilson, 1957)
Equilibrium constants	K_{aH2CO3}	6.3	(Crittenden et al., 1999)
	K_{aHCO3-}	10.3	(Crittenden et al., 1999)
	K_{aH2O2}	11.6	(Crittenden et al., 1999)
	$K_{aHO2\cdot}$	4.8	(Crittenden et al., 1999)
Stoichiometric factors	Y	1 x10^4(M^{-1} cm^{-1})	This work

[a]these parameters are modified later in this study through parameter estimation
[b]one Einstein equals one mole of photons

6.2.3.2 Software implementation and numerical solution

The system consisting of 33 parameters, 10 ODEs and 8 algebraic equations was implemented in WEST (Chapter 3 provides more information on the software used). Simulations were run in Tornado. The stiff solver CVODE (Hindmarsh and Petzold, 1995) was used for all numerical integrations with an absolute and relative tolerance of 1 $x10^{-35}$ and 1 $x10^{-5}$, respectively.

To simulate the AOP reactor, 25 CSTRs in series were used, according to results of tracer tests (see further). The configuration as used in the software program is given in Figure 6.3. The reactors describe the transport of the water in the system (Froment and Bischoff, 1990). Each reactor contains the complete kinetic model as described above.

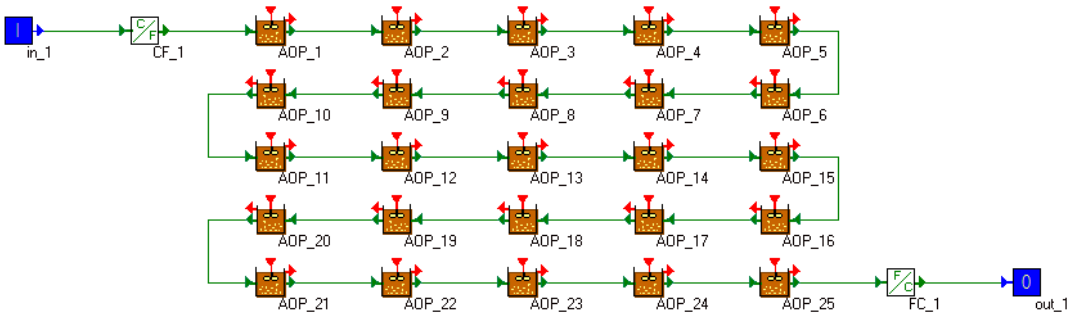

Figure 6.3: Implementation of the UV/H_2O_2 reactor in the simulation platform WEST

6.2.3.3 Model calibration and validation

Conventionally, the UV reactor modelling exercise starts with determining two important reactor properties by means of chemical actinometry: the optical path length and irradiation intensity (Parsons, 2004; Linden et al., 2005). In this case, performing these tests was not practically feasible. It was not allowed to stop the operation for a long period and to modify the water circuit. These conditions are needed to pump around pure water containing e.g. dissolved potassium ferrioxalate to perform the actinometer test. The irradiation intensity was mathematically estimated (see further), which is not commonly done. However, the most important of the three variables used for estimation of this parameter was the hydrogen peroxide concentration. This is a compound with a well-known extinction coefficient and quantum yield. The main difference with hydrogen peroxide actinometry was that the calibration was not performed in ultrapure water, but by using the real water matrix with a known absorbance. The initial value of I_0 was calculated according to the nominal power input of the lamps (data from the manufacturer), assuming that the LP-UV lamps have an efficiency of 33% (Sharpless and Linden, 2003). Using a factor U_{254} of 471,652 J Ein^{-1} at wavelength 254 nm (Parsons, 2004), a value of $6.9x10^{-5}$ Ein $L^{-1}s^{-1}$ was obtained as initial value.

The optical path length was assumed to be equal to the physical path length (1.2 cm) which is the distance between the quartz sleeve and the inner reactor wall and, hence, assumes that all transmitted UV radiation was instantly absorbed by the reactor wall. As mentioned earlier, optimizing the lamp configuration was not the main target of this study, because at this short path length, only around 35 % of the incident UV radiation gets absorbed by the hydrogen peroxide and the water matrix at standard experimental conditions (an intermediate H_2O_2 concentration of 1.8 mM and an average influent). UV radiation absorption by hydrogen peroxide ranges between 3.5 and 12 % of A_{254} (depending on the applied concentration) while the water matrix absorbs 88-97% of A_{254}). Also two chemical parameters related to DOM were mathematically estimated: rate constants k_{16} (k_{16}' in the extended model) and k_{19} (see Tables 6.2 and 6.3). The value of the stoichiometric parameter Y was kept constant for two reasons. First, this parameter is strongly correlated to k_{16} and as such, these two parameters are not practically identifiable (a unique value for the individual parameters cannot be found) and should not be estimated together. Only the product k_{16}xY is identifiable. Second, this allows a rough comparison of the estimated k_{16} with the value obtained by Song et al. (2008), assuming that still an equal amount UV_{310} reacts per mole $HO^{\bullet}$. The extinction coefficient of UV_{310} was determined by dividing the average influent UV_{254} by the average influent UV_{310}. For the extended model, the extinction coefficients of UV_{310}^{S} and UV_{310}^{X} were determined by dividing the average UV_{254}^{S} and UV_{254}^{X} values by the average UV_{310}^{S} and UV_{310}^{X} values, respectively. It was thus assumed that absorption coefficients at 310 nm were linearly related to absorption coefficients at 254 nm via the extinction coefficient, which was confirmed by the experimental results obtained.

The parameter estimation was performed by using the Simplex algorithm provided in Tornado and simulations were performed as discussed in section 6.2.3.2. The variables used to calculate the objective function were the effluent hydrogen peroxide concentration, UV_{310}^{S} and pH. The objective function calculation was based on a WSSE (Equation 3.5 in Chapter 3). Numerical values of pH and H_2O_2 concentrations (the latter expressed in mM) were of the same order of magnitude, while those of UV_{310} were about two orders of magnitude lower. Hence, a weighting factor of hundred was assigned to UV_{310} while factors of one were applied to pH and H_2O_2. Weighting factors for UV_{310} ranging between 50 and 150 were tested and yielded no significant differences in parameter estimates, confirming the location of the optimum is not affected by the definition of the objective function. Weighting factors were used to prevent discrimination of variables with low numerical values such as UV_{310}. To avoid finding local minima,

the parameter estimation was repeated with different starting values for the parameters.

Five experimental data points per variable were used in the calibration process. Each data point corresponded to an experimental run with specific operational conditions. Similarly, an independent dataset corresponding to five independent runs was used to validate the model. To investigate changes of the DOM content over time, several months were left between the collection of experimental data for validation and calibration. The dates of data collection together with the influent data and operational conditions that were used for calibration and validation are given in Table 6.4. Hydrogen peroxide concentrations were chosen according to literature (Glaze et al., 1995; Liao and Gurol, 1995; Hong et al., 1996; Crittenden et al., 1999; Sharpless and Linden, 2003; Rosenfeldt and Linden, 2004; Song et al., 2008; Wu and Linden, 2008) and practice.

6.2.4 Data interpretation and sensitivity analysis

During each simulation run, the system was allowed to stabilize and the corresponding steady state values were used to compare with the experimental data from the effluent. The goodness-of-fit between experimental and simulated values was quantified by calculating the TIC (Theil, 1961) which is explained in Chapter 3.

A LSA was used to help with determining the calibration parameters and to investigate and quantify the influence each model parameter exerts on every variable calculated in the system. The latter could be described as a sort of robustness test. To allow comparison between SFs of different variable-parameter combinations, RSFs were used (Audenaert et al., 2010) rather than ASFs. ASFs were calculated using the finite forward difference method with a perturbation factor (ξ) of $1x10^{-6}$. All simulations were run using the Tornado kernel and all RSF values were obtained using the optimized parameters. An additional organic compound (M) with known reactivity towards $HO^{\bullet}$ was included in this experiment to study the parameter sensitivity of micropollutants during model predictions. According to (Song et al., 2008), this compound was assumed to be completely mineralized. The synthetic organic compound alachlor was used for this purpose (Song et al., 2008). The extended model was used to perform the sensitivity analysis. Detailed information on how the TIC and local SFs were calculated can be found in Chapter 3.

Table 6.4: Influent and operational conditions used for calibration and validation data collection

		Operational condition		Influent variable							
Calibration run No.	**Date**	Flow rate ($L\ s^{-1}$)	HRT (s)	$[H_2O_2]$ (mM)	$[HCO_3^-]$ (mM)	$[UV_{310}]$ (cm^{-1})	$[UV_{310}^S]$ (cm^{-1})	$[UV_{310}^X]$ (cm^{-1})	[TOC] (mM)	SUVA ($cm^{-1}\ M^{-1}$)	pH
1	10/06/2010	0.077	95	0.7	4.46	0.108	0.056	0.052	1.7	0.0105	7.49
2	10/06/2010	0.077	95	1.1	4.46	0.109	0.059	0.050	1.7	0.0108	7.59
3	10/06/2010	0.077	95	1.8	4.41	0.108	0.060	0.048	1.7	0.0108	7.54
4	10/06/2010	0.077	95	2.7	4.41	0.108	0.060	0.048	1.7	0.0108	7.58
5	10/06/2010	0.077	95	4.0	4.41	0.107	0.059	0.048	1.7	0.0109	7.54
Validation run No.											
1	03/12/2009	0.086	85	1	2.59	0.112	0.051	0.061	1.9	0.0097	7.39
2	03/12/2009	0.086	85	3.8	2.59	0.101	0.046	0.055	1.9	0.0089	7.39
3	28/04/2010	0.035	212	0.48	6.172	0.127	0.070	0.057	2.0	0.0095	8.16
4	28/04/2010	0.035	212	1.65	5.987	0.118	0.061	0.057	2.9	0.0062	8.13
5	28/04/2010	0.035	212	2.34	6.099	0.118	0.058	0.060	2.4	0.0075	8.12

6.2.5 Analytical procedures

All samples were collected in glass bottles and immediately brought to 2°C using ice. Small aliquots of effluent samples for hydrogen peroxide analysis were adjusted to pH 4 using sulfuric acid. In this way, spontaneous hydrogen peroxide loss during transportation was prevented. The remainder of the effluent samples was stored as such for all other analysis. Although a relatively constant influent composition could be expected, an influent sample was taken at the beginning of each individual experimental run.

Hydrogen peroxide concentrations were determined using the iodide/iodate method of Klassen et al. (1994). Prior to all other analysis, hydrogen peroxide was removed by adding small amounts of freshly prepared sodium sulphite solution to the stirred samples at room temperature. At regular intervals, the method of Belhateche et al. (1991) was used to qualitatively verify hydrogen peroxide depletion. All hydrogen peroxide was assumed to be removed when the green cobalt-hydrogen peroxide complex could no longer be detected. Influent hydrogen peroxide was determined by switching off the UV lamps and determining the effluent concentration using the same procedure as outlined above.
UV absorption measurements were performed in 1 cm path-length quartz cuvettes using a Shimadzu UV-1601 spectrophotometer. UV-visible (UV-VIS) spectra between 200 and 700 nm with a resolution of 0.5 nm were measured. Of each influent and effluent sample, a part was filtered using a prewashed 0.45 µm PTFE filter to determine the soluble fraction of UV_{310} (UV_{310}^{S}). The particular fraction, UV_{310}^{X}, was determined by subtracting UV_{310}^{S} from the total UV_{310}.
A Shimadzu TOC-VCPN analyzer was used to measure the TOC. pH was monitored using an Ecoscan pH5 apparatus (Eutech Instruments). Alkalinity was determined according to Standard Methods (APHA, 1992).

6.3 Results and discussion

6.3.1 Tracer test

A typical curve obtained during the tracer tests is shown in Figure 6.4. This graph represents a tracer test at a flow rate of 1,000 L h^{-1}. It can be clearly observed that a perfect fit could not be reached. Apparently, a small fraction of the tracer load leaves the reactor later than would be expected. As a result, the measured curve has a shoulder at larger residence times. This effect becomes more pronounced as the flow-rate decreases, suggesting the occurrence of different hydrodynamical behaviour in the two parallel water streams. Indeed, Figure 6.1 shows that the first

set of two pipes in series at the beginning of the influent pipe is favoured due to a higher local water pressure. Consequently, the second parallel lane, which is located more downstream, receives a lower flow rate and thus has a longer residence time. However, as it was impossible to test each reactor tube separately with a tracer test, this effect was further neglected.

For all three flow rates tested, a value of 25 TIS was the final outcome, indicating not well-mixed conditions. As such, this number was used in the simulation configuration depicted in Figure 6.3 with each reactor having the same volume (V_n) of 0.44 L. Four non-irradiated tanks at the beginning and at the end represented the dark reactor parts, with the irradiance set to zero. Hence, the active reactor part was represented by 17 of the 25 tanks. The influent was found to be non-dynamical and hence, every effluent data point represents a steady-state situation of constant flow, influent concentration and H_2O_2 dosing. Consequently, drastic transitions of influent (and thus effluent) concentration-time profiles did not have to be predicted, but only the final steady-state values. Unfortunately, due to practical limitations, it was not possible to conduct tracer experiments for each irradiated pipe separately.

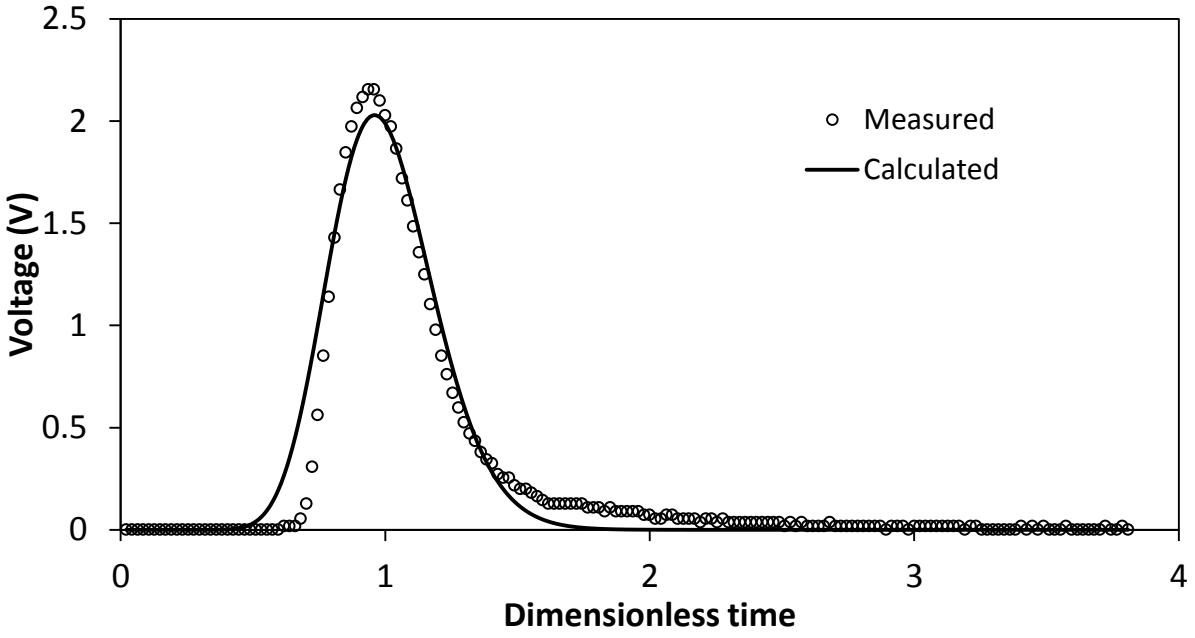

Figure 6.4: Measured and calculated E(t') curves at a flow rate of 1000 L h^{-1}; the best fit was obtained using a number of 25 TIS

The number of TIS for these pipes could be expected to be higher than 17 because these smooth and straight channels are optimal to create plug flow conditions. Apart from the shape of transient concentration profiles, the number of TIS also determines the level of the steady-state plateau, but preliminary experiments

revealed that increasing the number above 15 no longer significantly affects the output. This sensitivity check indicated that the number of 17 could be used without expecting significant errors. In the irradiated tanks, the estimated irradiance (see further) was used.

6.3.2 Model calibration

The rationale for extending the model can be explained using Figure 6.5. This figure shows that the particulate fraction of UV_{310} is not affected by AOP treatment and only the soluble part is oxidized and thus responsible for UV_{310} decrease.

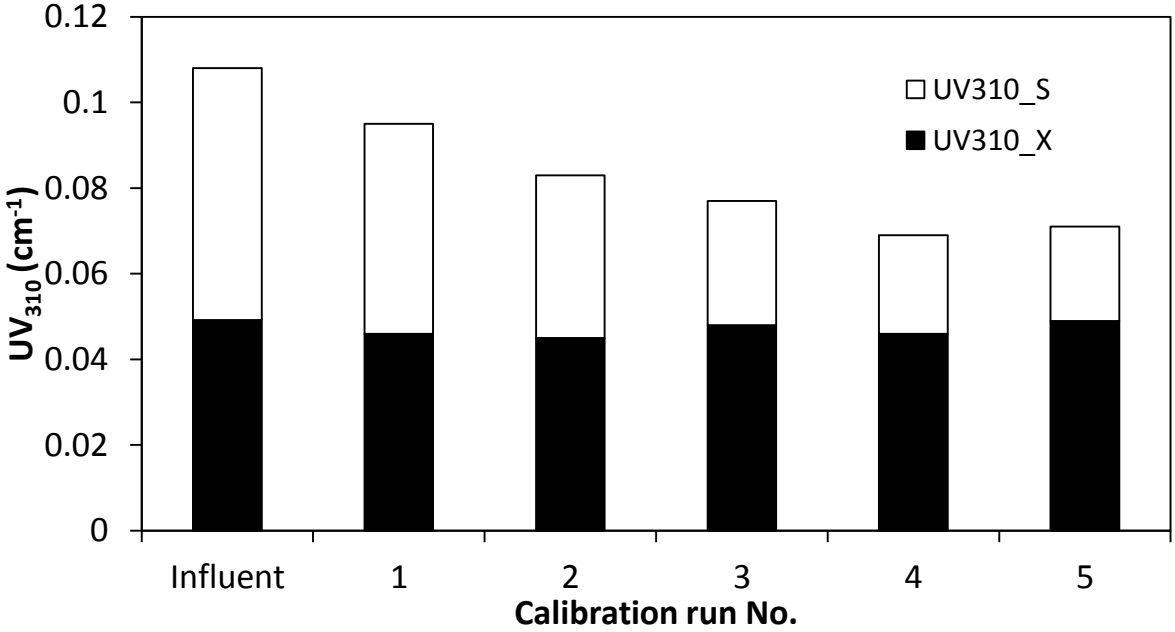

Figure 6.5: Changes of UV_{310} composition due to AOP treatment during the calibration runs

The influent bar was constructed by averaging the influent values of each calibration run, while the remaining bars represent the effluent concentrations corresponding to the respective runs. The influent UV_{310} was around 0.108 cm^{-1} and remained relatively constant during the different experimental runs. The conditions corresponding to each run number (indicated on the x-axis) are presented in Table 6.4. UV_{310} rapidly decreases as the applied hydrogen peroxide concentration is increased up to 2.7 mM (run No. 4). Beyond this concentration (run No. 5), the remaining UV_{310} remains unchanged at a value of 0.070 cm^{-1}. It is hypothesised that at this concentration hydrogen peroxide itself becomes an important scavenger for $HO^{\bullet}$. Song et al. (2008) in their studies used the synthetic organic chemical alachlor and showed a stabilization of the observed pseudo-first-order rate constant between 2 and 3 mM hydrogen peroxide.

Calibration results for UV_{310} are depicted in Figure 6.6. Low TIC values (0.009 for the original and 0.013 for the extended model) revealed that an excellent agreement was obtained between calculated and experimental data for both models. The value of k_{16}, the second order rate constant for reaction between $HO^{\bullet}$ and UV_{310} in the original model, was estimated to be 17,138 $(1/cm^{-1})$ s^{-1}. This value is in the same order of magnitude but significantly higher than the value of 12,000 $(1/cm^{-1})$ s^{-1} experimentally determined by Song et al. (2008). This illustrates the variable character and related reactivity of organic matter, even within the class of olefinic structures (associated with UV measurements). Westerhoff et al. (1999) highlighted the importance of MW and other characteristics with respect to $HO^{\bullet}$ attack. Rate constant k_{16}' related to $HO^{\bullet}$ scavenging of $UV_{310}{}^{S}$ in the extended model was estimated to be 34,498 $(1/cm^{-1})$ s^{-1}. It was expected that this value would be approximately twice the value of k_{16} of the original model since the influent total UV_{310} consists of about 50% $UV_{310}{}^{S}$ (see Figure 6.5).

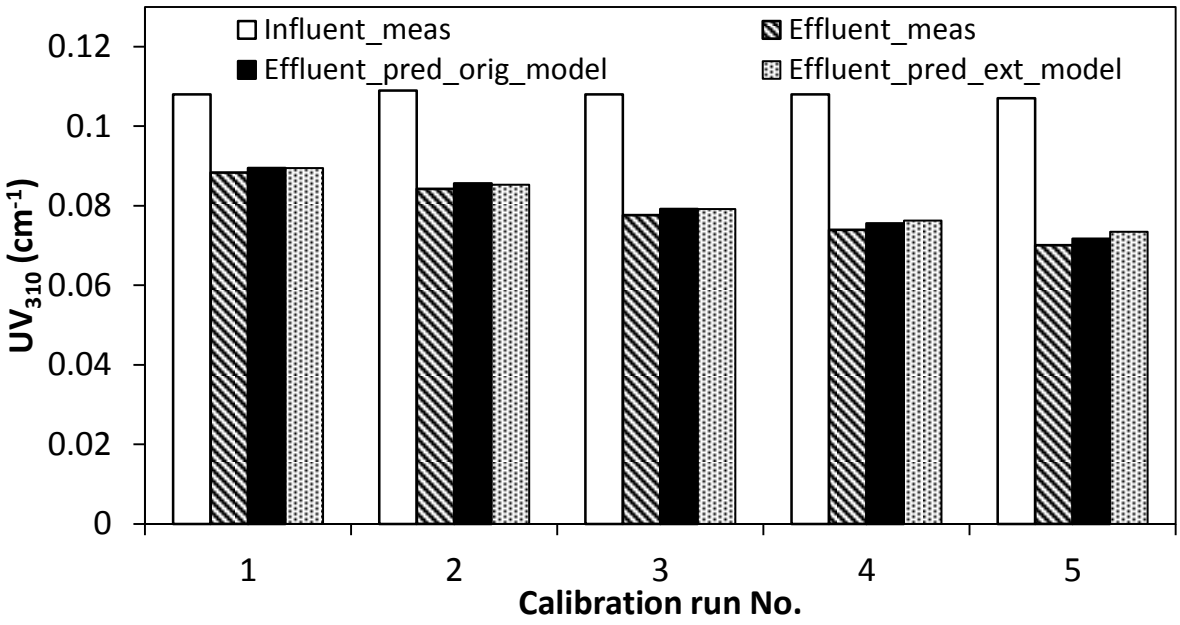

Figure 6.6: Measured (meas) and predicted (pred) UV_{310} after model calibration using the original (orig) and extended (ext) model

Measured and predicted hydrogen peroxide concentrations are presented in Figure 6.7. The error bars correspond to the 95% confidence interval of three replicate measurements. Simulation outputs of the two models were not presented separately as the results obtained were almost identical.

It can be clearly observed that the effluent hydrogen peroxide concentration could be accurately predicted, resulting in a very low TIC value (0.028). Based on the

sensitivity analysis (see further), I_0 was the most important fitting parameter with respect to this variable. I_0 was estimated to be 2.96 $x10^{-5}$ Einsteins L^{-1} s^{-1} for the original model and 2.92 $x10^{-5}$ Einsteins L^{-1} s^{-1} for the extended version. The slight difference between the two estimated values can be explained by taking into account the difference in model structure with respect to the DOM reaction mechanism. The extended model assumed that only the soluble part of UV_{310} was removed, while no different UV_{310} fractions were included in the original model. The extinction coefficient of UV_{310}^{S}, however, was approx. 25% higher than that of UV_{310} (see Table 6.3). Consequently, the final value of A_{254} calculated with the extended model was slightly lower than the value obtained with the original version, despite the lower overall UV_{310} removal (as shown in Figure 6.6).

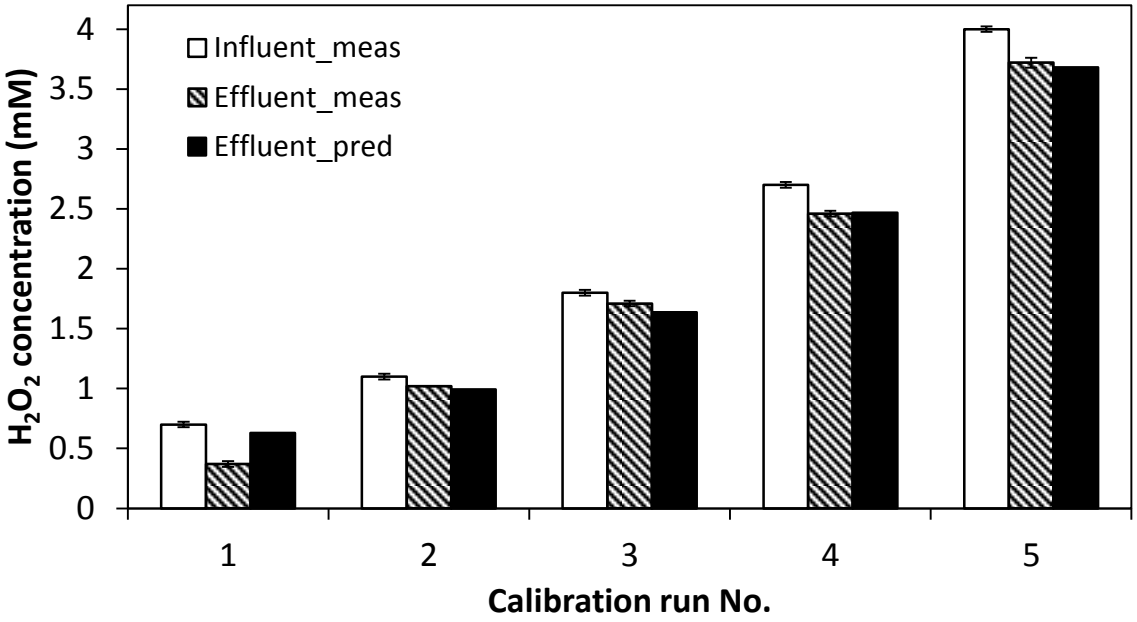

Figure 6.7: Measured (meas) and predicted (pred) H_2O_2 concentration after model calibration

Hence, to obtain the same level of H_2O_2 decay, I_0 was estimated a little lower using the extended model. These values are about 50% lower than the theoretical initial value. However, the initial value (calculated in section 6.2.3.3) assumed that all emitted radiation reached the solution. Most likely, effects such as lamp aging, scaling and sleeve absorption are the underlying reasons for this finding. Sharpless and Linden (2003) estimated the attenuation caused only by the quartz sleeve at 10%. Li et al. (2008) took into account a UV irradiation decrease of 30% caused by scaling and lamp aging. Probably, sleeve absorption, (irreversible) scaling and lamp aging all contributed to a lower incident UV irradiation.

The calibration results of the solution pH are given in Figure 6.8. DOM oxidation slightly affects the pH with a pH drop ranging between 0 and 0.11. Model predictions were very satisfactory with a calculated TIC of 0.002 (for both models). As stated earlier, pH was calculated via TOC mineralization resulting in carbonic acid formation, although the pH drop is probably a result of the formation of intermediate products such as carboxylic acids (Parsons, 2004). To get more insight into this discrepancy, the TOC mineralization rate constant (k_{19}) was investigated in more detail. The optimal values obtained by parameter estimation were 16,704 $M^{-1}s^{-1}$ for the original model and 15,289 $M^{-1}s^{-1}$ for the extended one, which are several orders of magnitude lower than the value of [21]. A higher contrast can be found when comparing with values reported by [27] and [40] which varied between 1 $x10^8$ and 1 $x10^9$ $M^{-1}s^{-1}$. Liao and Gurol (1995) used parameter estimation to determine the rate constant for the reaction of a known humic acid with $HO^{\bullet}$ and found a value of 1.9 $x10^8$ $M^{-1}s^{-1}$. The contradictory outcome of k_{19} probably has the following two explanations: (i) describing TOC mineralization (and carbonic acid formation) by a second order relationship is not valid, which can be substantiated by studying the shape of a typical TOC concentration-time profile and (ii) if this wrong assumption is used, the implementation of a stoichiometric conversion factor (S) is essential, as only a fraction of the $HO^{\bullet}$-TOC reaction events directly forms carbon dioxide. Consequently, an implementation in the form of Sxk_{19} in the mass balance of TOC has to be performed. E.g. if it is assumed that in this study k_{19} has a value of 2 $x10^8$, which is in the range of the reported values, the stoichiometric factor in this case would be around 7.6 $x10^{-5}$ mole carbon dioxide per mole $HO^{\bullet}$. The product of those values gives the estimated k_{19}. It is noteworthy that the calculated stoichiometric factor is merely a rough estimate to illustrate a possible kinetic implementation and needs further validation. However, the simplistic assumption apparently resulted in a good agreement between experimental determined and calculated pH values.

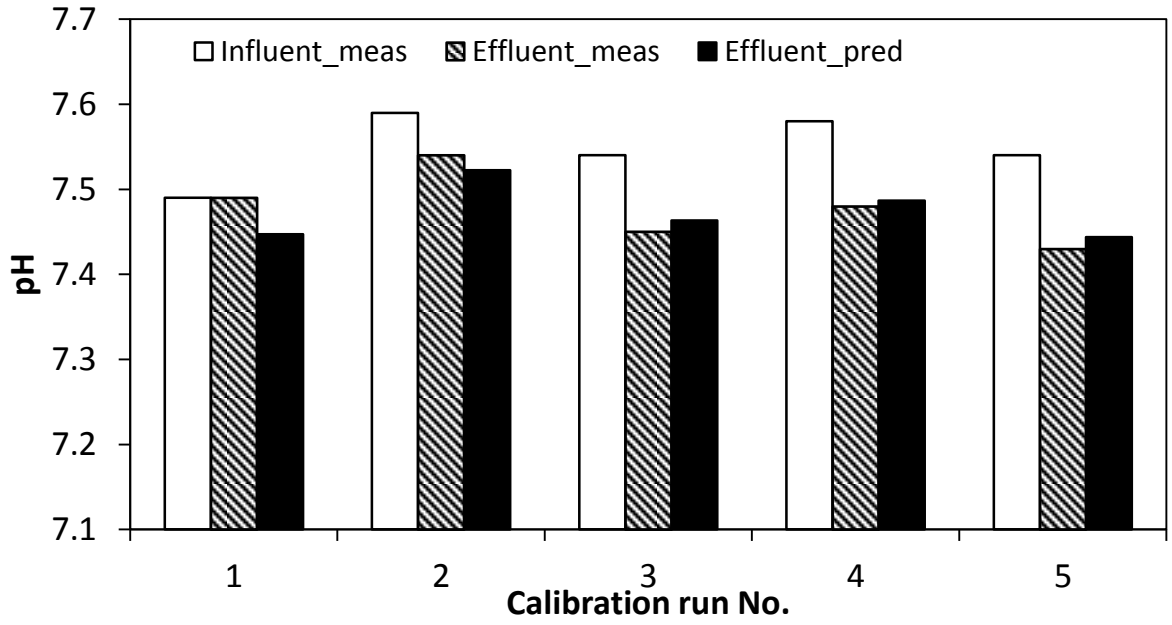

Figure 6.8: Measured (meas) and predicted (pred) pH after model calibration

6.3.3 Model validation

To check the model validity, an independent set of experimental data was used as input for the model. The same three variables were used to evaluate the model predictions. Validation results for the UV_{310} are shown in Figure 6.9. This graph indicates a successful validation. Very low TIC values of 0.056 and 0.052 for the original and extended model, respectively, confirmed the good agreement between experimental and calculated data. Based on TIC, the extended model thus gives a slightly better result which is, however, not statistically significant by using an F-test (Kletting and Glatting, 2009). The validation data were collected at least four months before the data for calibration (and data of run No's 1 and 2 with another two weeks difference). The deviations between experimental and predicted data are most likely a result of a changing DOM content and its complex reaction mechanism. The specific UV absorption coefficient at 254nm ($SUVA_{254}$, $(mg\ C\ L^{-1})^{-1}\ cm^{-1}$) which is calculated by dividing the UV_{254} by the TOC concentration (in $mg\ L^{-1}$) is often related to the reactivity of DOM (Westerhoff et al., 1999). The mean SUVA of the influent during the calibration experiments was around 0.0108 $(mg\ L^{-1})^{-1}\ cm^{-1}$ while that of the validation runs was approximately 20% less. SUVA values and dates of data collection are provided in Table 6.4.

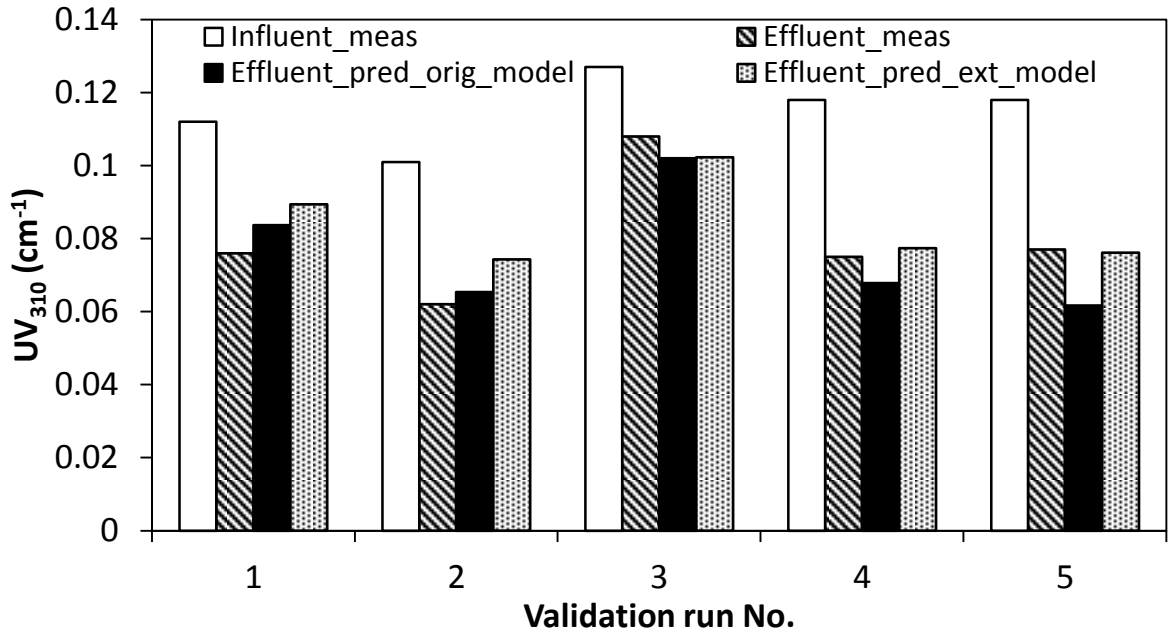

Figure 6.9: Measured (meas) and predicted (pred) UV_{310} during validation of the original (orig) and extended (ext) model

Rosenfeldt and Linden (2004) recognized the complexity of performing modelling studies in the presence of an unknown DOM matrix. Several factors that can influence the reaction rate are not included in the model. pH may affect the reactivity of the humic acid part of the DOC content. The reactivity of the deprotonated and thus negatively charged form is usually higher than that of the protonated form because of the decreased nucleophilicity (von Gunten, 2003a). However, this effect is probably of less importance as only minor changes in pH were observed during all experiments (see further). Moreover, a part of DOM acts as direct radical scavenger, while another fraction can act as a chain promoter (Westerhoff et al., 1997). Another issue that may affect the $UV_{310}{}^{S}$ concentration profile is the formation of oxidation by-products that have a higher extinction coefficient at 254 nm than the parent compound. Glaze et al. (1992) showed that during the oxidation of naphthalene naphthols and quinones are formed, which have higher absorptivities than naphthalene. Hence, a stabilization of UV absorption was observed during prolonged oxidation. These results suggest that UV_{310} is a promising variable to be part of future and more complex models but more studies are needed to further improve the predictions.

The validation results for hydrogen peroxide are depicted in Figure 6.10. Again, simulation outputs of both models were not presented separately as these results were almost identical.

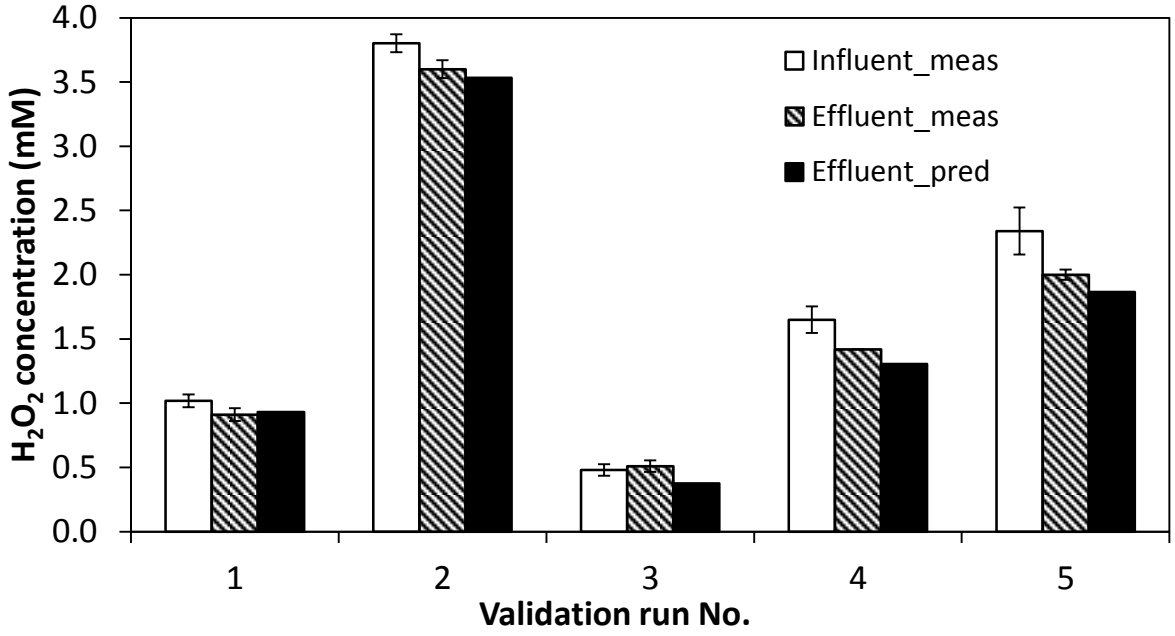

Figure 6.10: Measured (meas) and predicted (pred) H_2O_2 concentration in the validation process

Bearing in mind the excellent calibration results, the hydrogen peroxide concentration was expected to show good predictions during validation. Indeed, the residual hydrogen peroxide concentration was described very well by the model, with a resulting TIC value of 0.026. However, a slight underestimation of the H_2O_2 concentration can be observed. Although the UV_{310} extinction coefficients ε_{UV310} (for the original model) and ε_{UV310S} and ε_{UV310X} (for the extended model) showed some time-related variations, they are unlikely to significantly influence the hydrogen peroxide conversion as they can be classified as not influential with regard to this variable (see further in section 6.3.4). On the other hand, a process variable that is not included in the model and known to alter chemical rate constants is temperature. As mentioned before, the data collection for calibration and validation was separated by several months. The water temperature in the secondary sedimentation basin however, is to a large extent dependent on weather conditions. A comparison of the influent temperatures during calibration and validation experiments revealed a mean difference of 8°C. Performing the calibration procedure at significantly higher influent temperatures most likely resulted in a higher hydrogen peroxide decomposition rate. Hence, this leads to an overestimation of this rate when using the validation data which was collected at colder reactor temperatures. Possibly, some of the rate constants related to indirect hydrogen peroxide decomposition (k_1-k_6) are temperature dependent (Einschlag et al., 1997). However, this issue was not subject of this study and needs further investigation.

The validation results for pH are presented in Figure 6.11. For the same reason as mentioned above, simulation outputs of both models were presented by just one bar. A satisfactory model prediction was obtained (TIC=0.01). The shape of the

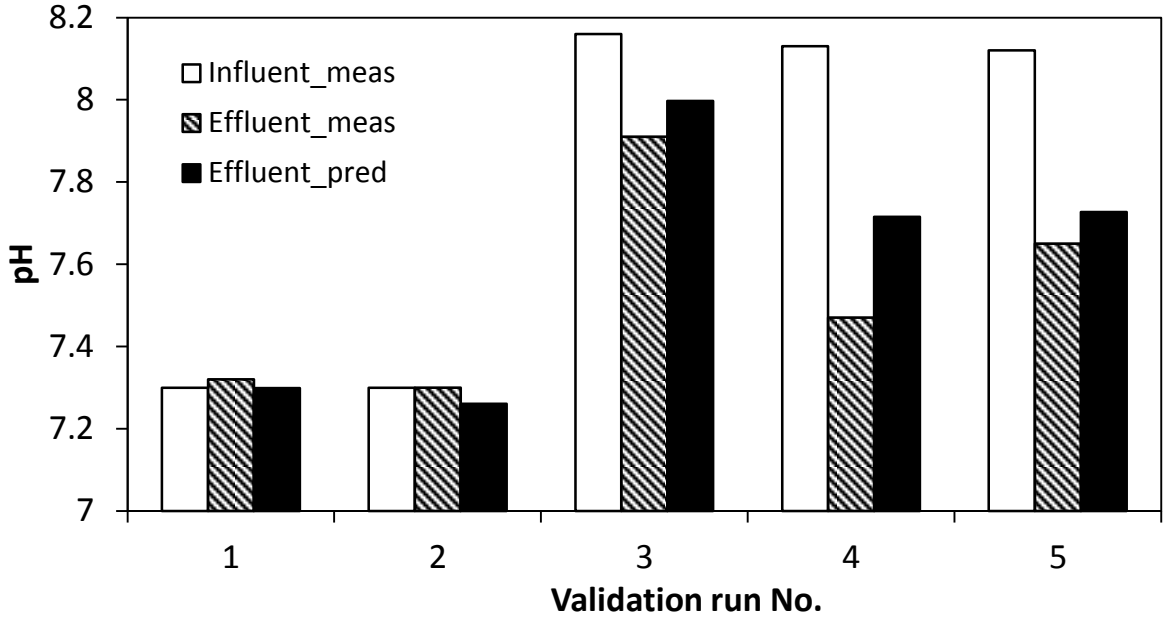

Figure 6.11: Measured (meas) and predicted (pred) pH in the validation process

calculated curve describes the general trend of the experimental data points very well. The influent pH of run Nos 3 to 5 is relatively high compared to all others, which explains the more drastic pH drops during AOP treatment (as pH is a logarithmic scale). However, the model significantly underestimates the acid formation of these runs. This can be a result of time-related changes of TOC characteristics with respect to reactivity (the variability of SUVA was discussed earlier).

6.3.4 Sensitivity analysis

An important goal of this study was to quantify the influence (i.e. importance) of each model parameter with respect to all output variables. As such an analysis results in a large amount of information, only the most remarkable outcomes were graphically presented and/or discussed. The influent characteristics of calibration run No. 3 (see Table 6.4) extended with an additional micropollutant (M) were used in this analysis. This run was chosen because of the intermediate applied hydrogen peroxide concentration. The concentration of M ([M]) was chosen to be 1 µM. The sensitivity of the key variables [UV_{310}^{S}], [$HO^{\bullet}$], A and [M] to four kinetic rate constants is presented in Figure 6.12. This figure illustrates to what extent hydroxyl

radical scavengers influence the UV/H_2O_2 process. Kinetic rate constants k_1 and k_{17}, describing scavenging by hydrogen peroxide and bicarbonate ions, respectively, are found to be very important. The same parameters are, however, only moderately influential to the $UV_{310}{}^S$ and the $HO^\bullet$ concentration. Contrarily, the effect of these parameters on micropollutant concentrations is even higher with RSF values indicating a major impact (RSF>1) (Audenaert et al., 2010) (and references therein). Also noteworthy is that in this case, increasing the hydrogen peroxide scavenging rate has a larger impact on the process performance compared to altering scavenging by bicarbonate. Scavenging by carbonate ions seems to be of less importance, at least in the pH range studied here, as k_{15} (not included in this graph) was classified as a non-influential parameter. Rate constant k_{16}' has a moderate impact on $UV_{310}{}^S$ and absorbance at 254 nm. This can be easily explained by the fact that this rate constant is directly related to UV_{310} reduction. Increasing this value results in a lower effluent UV absorption and hence, a lower absorbance. It is remarkable that k_{16}' also exerts a negative influence on the concentration of M (which means that with a higher value of k_{16}', a lower micropollutant concentration could be achieved), although this rate constant is related to a scavenging process. This reveals that competitive radiation absorption by DOM is more detrimental than its reaction with $HO^\bullet$ regarding micropollutant removal. Kinetic constant k_{10} is only moderately affecting [M] and has a minor impact on all other variables. The latter, however, may highlight the need for extension of future models with equations describing DOM as a chain promoter (producing superoxide radicals) in order to reliably predict micro-pollutants decay in a real water matrix. Additionally, this parameter has widespread reported literature values ranging between 7 $x10^9$ and 1 $x10^{10}$ (Glaze et al., 1995; Einschlag et al., 1997; Crittenden et al., 1999; Fabian, 2006; Song et al., 2008), indicating that the process description in the model is likely not adequate. This finding illustrates the importance of including uncertainty analysis in the modelling exercise in order to quantify the reliability level of future models. Furthermore, Figure 6.12 shows that the RSF pattern of the $HO^\bullet$ concentration is the opposite of that of organic pollutants (DOM and M). This is easy to understand as effluent pollutant concentrations are inversely correlated to the hydroxyl radical concentration. Similarly, Figure 6.13 describes the influence of other important operational and chemical parameters. Here, the importance of parameters related to hydrogen peroxide photolysis surfaces. ϕ_{H2O2}, ε_{H2O2} and I_0 have a very high impact on the hydroxyl radical concentration. This sensitivity is directly reflected in moderate impacts on the $UV_{310}{}^S$. Increasing the hydrogen peroxide extinction coefficient involves a higher $HO^\bullet$ production and hence, a lower final DOM concentration. Although the absorption of hydrogen peroxide increases, the absorbance at 254 nm is negatively influenced. This can be explained

by the important role DOM plays in Equation 6.7. Analogically, an increment of DOM extinction coefficients leads to the opposite effects and extreme impacts on the concentration of M (Figure 6.14). The extinction coefficients of DOM seem to be only influential to the concentration of M, and this to a moderate level.

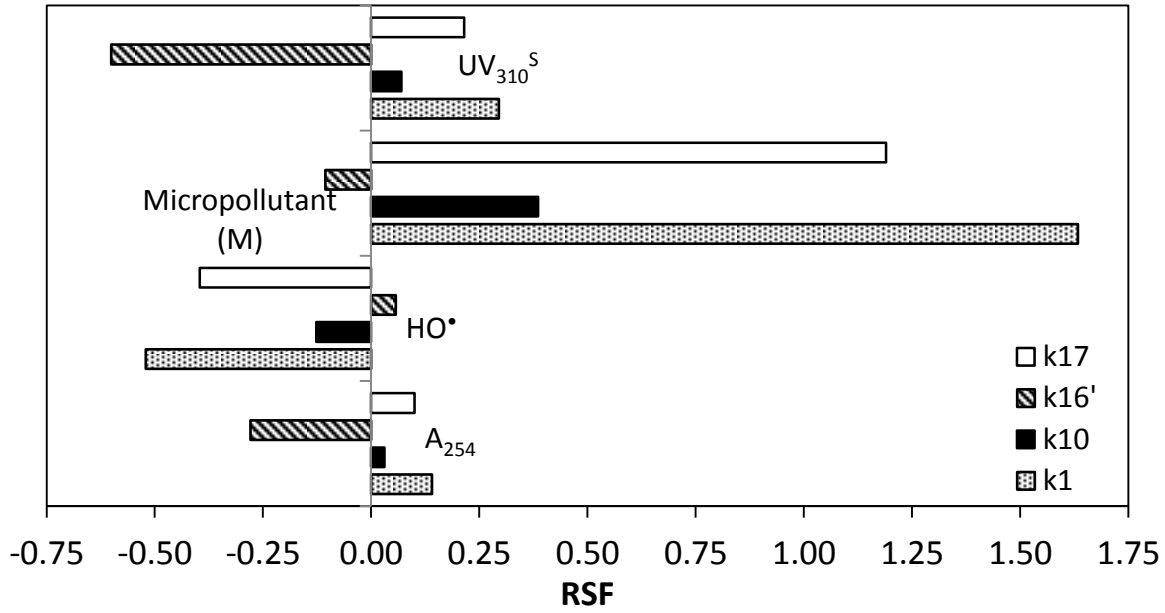

Figure 6.12: Sensitivity of [UV_{310}^S], [M], [$HO^•$] and A_{254} to influential rate constants

Although it was expected that these coefficients would also significantly affect the hydrogen peroxide concentration according to Equations 6.4, 6.6 and 6.7, only minor influences could be observed. Most likely, this is a result of the relative low difference between initial and effluent H_2O_2 concentrations at the HRTs applied. Additionally, direct photolysis of H_2O_2 seems to be a less sensitive process with respect to the DOM extinction coefficients as opposed to micropollutants removal facilitated by $HO^•$. As the initial H_2O_2 concentrations were lowered, the sensitivity regarding the extinction coefficients increased, but only marginally.

It becomes clear from Figure 6.14 that concentrations of micropollutants (in this case alachlor as example) are very sensitive to some of the rate constants and extremely sensitive to most of the process parameters. Regarding this sensitivity to the model parameters, one thus has to consider determination of parameters as an important and delicate issue, whether these parameters are being experimentally or mathematically determined, in order to predict these (low) concentrations in a reliable way. In contrast, hydrogen peroxide can be classified as an insensitive variable. Only the parameters associated to direct H_2O_2 photolysis such as I_0, b, ε_{H2O2} and ϕ_{H2O2} have a little (negative) effect on this variable with RSF values around -0.10.

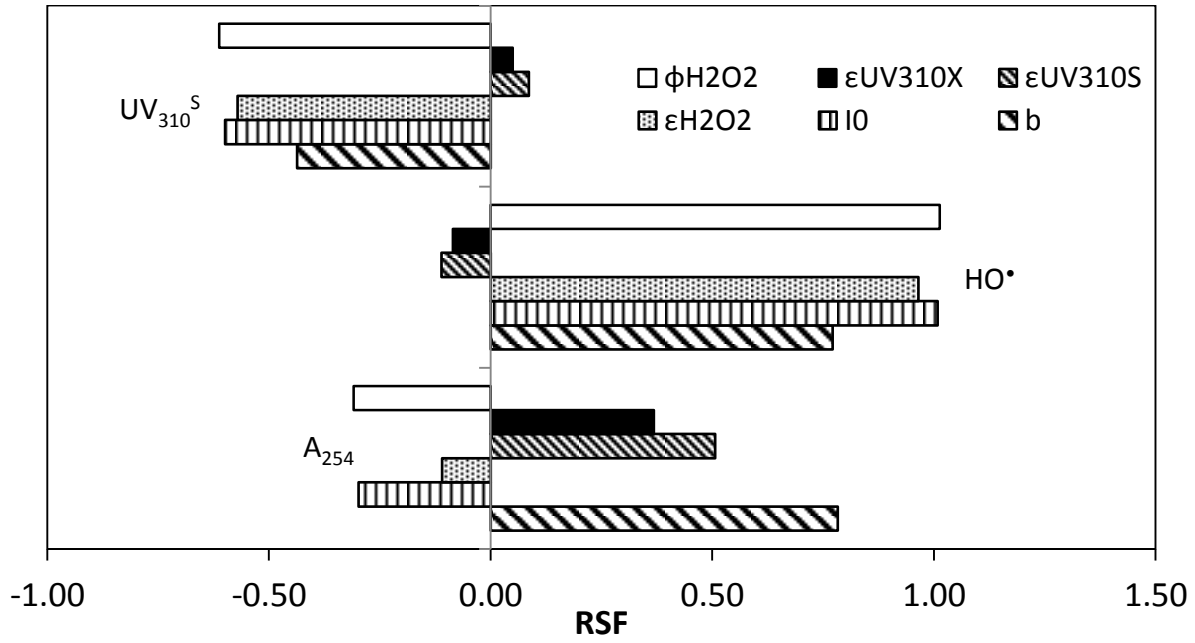

Figure 6.13: Sensitivity of [UV_{310}^{S}], [$HO^{\bullet}$] and A_{254} to influential physical and chemical parameters

The influence of the most important parameters regarding the concentrations of the intermediate radical species is given in Figure 6.15. Again, parameters related to hydrogen peroxide photolysis are moderately to very influential which can be easily understood as the initiation reaction is the driving force of the radical chain. In addition, the scavenging reaction of hydrogen peroxide producing the superoxide anion is of moderate importance. The dissociation constant of carbonic acid moderately affects the superoxide and hydroperoxyl concentrations. Raising Ka_{H2CO3} results in a stronger pH drop and, hence, in a shift from the superoxide to the protonated hydroperoxyl species.

Although only very little amounts of the protonated form are produced at the pH levels in this study ($pKa_{HO2\bullet.}$=4.8), the dissociation constant of carbonic acid (and thus pH) has a moderate impact on the superoxide anion concentration. This may indicate that the termination reaction from the protonated and deprotonated form to hydrogen peroxide is of major importance. This was confirmed by the RSF value of k_{12} indicating a moderate impact. The principal fate of the carbonate radical probably is its reaction with hydrogen peroxide (Glaze et al., 1995). A strong impact of the rate constant related to this reaction (k_5) supported this finding. Another but slightly less important termination step with respect to this radical is the reaction with the superoxide anion. The involvement of bicarbonate in carbonate radical production seemed to be negligible at the applied pH values.

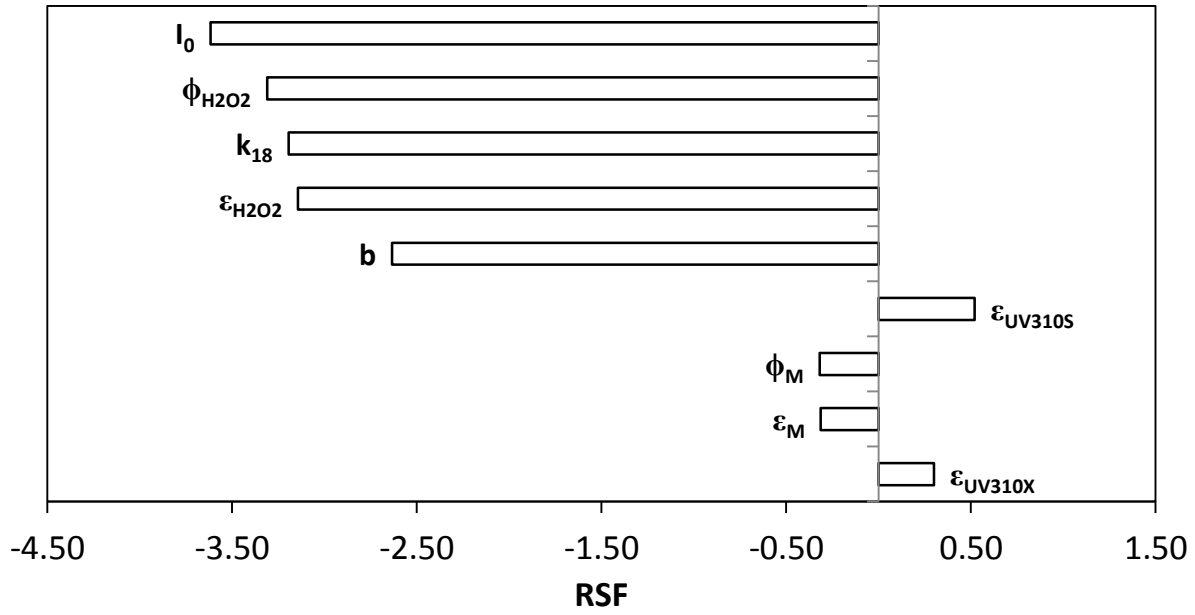

Figure 6.14: Influence of process and chemical parameters on the prediction of a micropollutants concentration [M]

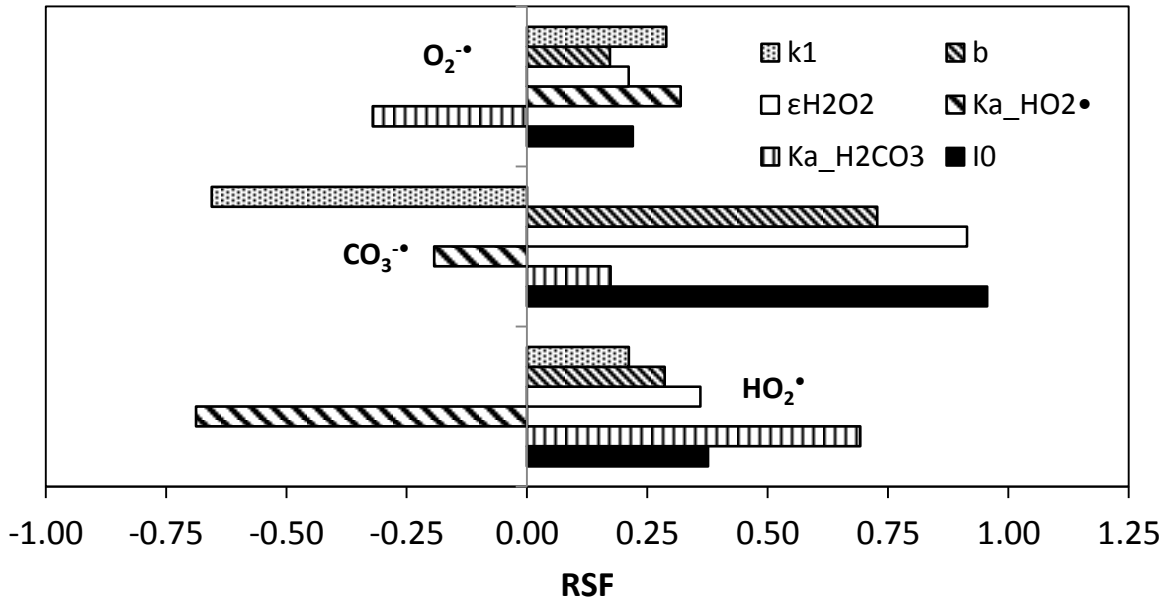

Figure 6.15: Sensitivities of the intermediate radical species to their most influential parameters

Nine rate constants showed to exert absolutely no influence to all of the variables: k_2-k_4, k_6-k_9 and k_{13} and k_{14}. Fábián (2006) mechanistically modelled ozone decomposition in the presence of hydrogen peroxide and removed some of these kinetic parameters. Also in this study, the reliability of the handful of literature

reported kinetic parameters was questioned. They were therefore determined by mathematical parameter estimation. Another parameter that was of negligible influence was ε_{HO2^-}, at least for the conditions used in this study. Despite the contrast with the value of ε_{H2O2}, the dissociation of hydrogen peroxide seems to be of minor importance.

6.4 Conclusions

Mechanistic modelling of organic matter conversions during AOP treatment is one of the current research challenges. Although these mechanisms are often very complex and highly time and case dependent, completing this exercise is essential in order to provide models that are widely applicable and can be used for system optimization and process control. In this study, an existing UV/H_2O_2 model containing a general accepted radical mechanism was calibrated and validated using data of a full-scale reactor treating non-synthetic influent. It was shown that using the decadic absorption coefficient at 310 nm is a useful variable to include in AOP models. Both the models were able to describe the residual hydrogen peroxide concentration, DOM conversions in terms of UV_{310} and acid formation resulting in pH drops. The models were successfully validated. Model extension by splitting up the UV_{310} into a soluble and a particulate fraction seemed to be a good approach to model AOP treatment of real (waste)waters containing both dissolved and particulate (suspended) material. Based on TIC, predictions of the extended model were slightly better than those of the original model but differences were not statistically significant. Hence, further model development, has to focus on understanding and effectively extending the concept of (natural) organic matter conversion. A small attempt to extend an existing model was made in this study. To build these more complex models, more advanced measurement techniques should be used that provide more detailed information about the characteristics of the organic matrix such as mass spectrometry and polarity measurements. On-line spectral measurements could be of great value in this context as they often supply a large amount of (reliable) data. Future AOP models should also incorporate parameter and input uncertainty to quantify their output uncertainty. This is a very important issue with respect to full-scale applications.

Making models more complex at one side might be performed in parallel with simplifying the models at the side of the radical mechanism in order to balance the model complexity. SAs can be of great value in this context as it indicates insensitive model parameters. Additionally, the sensitivity output provides information that can be valuable in process engineering as the most important

parameters are determined. Model simplification can be part of future research but was not performed during this PhD study.

This chapter showed that the UV/H_2O_2 process is highly affected by just a fraction of the operational and chemical parameters. Parameters that determine the initiation step, i.e. photolysis of hydrogen peroxide, are very influential to most of the variables. Some reaction rate constants, however, were also of importance. Residual hydrogen peroxide concentration could be classified as a non-sensitive variable. This is in contrast with the extreme sensitivity of micropollutant concentrations to most of the process parameters. In order to predict these in a reliable way, one thus has to consider determination of parameters as an important and delicate issue, whether these parameters are being experimentally or mathematically determined.

Chapter 7

Experimental study of effluent organic matter (EfOM) conversion during ozonation and UV/H_2O_2 treatment

Redrafted from: Audenaert, W.T.M., Vandierendonck, D., Van Hulle, S.W.H. and Nopens, I. Comparison of ozone and $HO^{\bullet}$ induced conversion of effluent organic matter (EfOM) using ozonation and UV/H_2O_2 treatment. Water Research, submitted.

Abstract

This study examined the impact of (advanced) oxidation on the properties of EfOM using two different oxidation techniques: ozonation and UV/H_2O_2 treatment. Multiple surrogates for EfOM related to its concentration, polarity, biodegradability, molecular size and spectral properties were used to study the oxidant induced conversions. Spectral calculations as differential absorbance spectra (DAS) and absorbance slope index (ASI) have proven to be useful to unravel mechanistic differences between ozone and $HO^{\bullet}$ induced transformation of EfOM. DAS and ASIs behaved totally different in the presence or absence of ozone. Effluent ozonation inherently led to significant $HO^{\bullet}$ production as a result of electron transfers between ozone and electron rich moieties of EfOM. As a result of changing EfOM properties, the $HO^{\bullet}$ production yield increased as function of ozone dose. During the UV based process, pseudo steady-state behaviour of the $HO^{\bullet}$ concentration was observed. The $HO^{\bullet}$ production during ozonation was strongly correlated with UV_{254}. The pH extremely impacted ozone decomposition. Most likely, the degree of dissociation of EfOM controlled its reactivity towards ozone. The ozone decomposition constant (k'_{app}) rapidly decreased as function of ozone dose following a power function. Both processes had similar effects on oxygen demand, DOC, polarity and biodegradability. COD decreased between 20 and 30% and biodegradability was enhanced by 15 to 20% after treatment. Some

mineralization took place as DOC reductions between 20 and 40% were observed after prolonged oxidation. Important shifts in EfOM polarity were observed: EfOM initially was mainly hydrophobic in nature (70% of DOC) but became highly hydrophilic after treatment.

7.1 Introduction

WWTPs are applied all over the world to remove solids, biodegradable organic carbon and nutrients. In most of the cases, wastewater originating from households and industry is treated by CAS systems that can include primary settling, nitrification, denitrification and secondary clarification. Sometimes, additional treatment steps such as coagulation, membrane filtration or final disinfection are applied (Mielcke and Ried, 2012). The secondary treated water (effluent) is released into the environment. Recent studies have proven that CAS systems poorly remove trace pollutants and as such, WWTPs become the major point sources of EDCs and PPCPs (Daughton and Ternes, 1999; Heberer, 2002; Kolpin et al., 2002). Furthermore, effluent disinfection by chlorine can lead to the formation of chlorinated DBPs (Krasner et al., 2009). These facts, together with the increasing interest in water reuse, recently initiated numerous studies on tertiary treatment of secondary effluent. Many of these studies are related to ozonation or AOPs.

7.1.1 Ozone and AOPs for tertiary wastewater treatment

AOPs (and especially ozonation) have already been applied in drinking water production (see Chapters 2 and 4) and industrial wastewater treatment and are promising tertiary treatment technologies because trace pollutant oxidation, DOM transformation and disinfection occur simultaneously. Hence, current research focuses on the removal of trace pollutants (Huber et al., 2005; Domenjoud et al., 2011a; Zimmermann et al., 2011; Reungoat et al., 2012), the role of bulk organic matter (Buffle and von Gunten, 2006; Gong et al., 2008; Rosario-Ortiz et al., 2008; Noethe et al., 2009; Ratpukdi et al., 2010; Domenjoud et al., 2011b; Gonzales et al., 2012; Sharif et al., 2012), the relation between bulk organic matter transformations and trace pollutant removal (Dickenson et al., 2009; Wert et al., 2009; Nanaboina and Korshin, 2010), formation of byproducts (Wert et al., 2007; Tripathi et al., 2011) and disinfection (Savoye et al., 2001; Xu et al., 2002; Zimmermann et al., 2011).

Ozone is a strong oxidant that is able to selectively oxidize electron rich moieties of water pollutants (von Gunten, 2003a). Additionally, ozonation involves the

production of the highly reactive $HO^{\bullet}$ which can virtually oxidize any compound, often at diffusion controlled reaction speeds. Especially during wastewater ozonation, $HO^{\bullet}$ plays a major role as reactions between ozone and DOM indirectly lead to enhanced $HO^{\bullet}$ production rates (Buffle and von Gunten, 2006; Noethe et al., 2009) (see also Chapter 2). If ozone resistant compounds have to be removed, combinations of ozone, (UV irradiation or hydrogen peroxide can be used to produce significantly more $HO^{\bullet}$, which transforms the process into an AOP (Parsons, 2004).

EfOM significantly impacts the oxidation process as it directly reacts with ozone and $HO^{\bullet}$ and competes for the available radiant energy in UV based applications. EfOM is a complex mixture of NOM originating from drinking water, SMPs originating from the activated sludge and recalcitrant organics with an industrial and residential origin (Shon et al., 2006). The composition of EfOM is site-specific and depends on weather conditions, seasonal variations and specific operational conditions of the WWTP. Additionally, the chemical properties of EfOM change drastically during oxidative treatment (Gong et al., 2008; Rosario-Ortiz et al., 2008; Nanaboina and Korshin, 2010; Ratpukdi et al., 2010; Gonzales et al., 2012; Sharif et al., 2012). The complex nature and variable composition and chemical properties of EfOM have a direct impact on the oxidation process itself and all downstream treatment steps. Hence, getting insight into the conversions taking place is essential for optimization of the tertiary treatment train and for model building. This profound knowledge is needed to successfully implement tertiary treatment processes at full-scale (Mielcke and Ried, 2012). For this reason, adequate surrogates for EfOM are needed that provide quantitative and/or qualitative information. Although much information on natural water oxidation is available, EfOM oxidation studies are still scarce and very recent. However, some valuable surrogates were already used in literature to study EfOM properties during (advanced) oxidation. Most of them were adapted from natural water studies focusing on NOM characterisation.

7.1.2 Surrogates for EfOM

The most widely used EfOM surrogate is UV_{254}. This variable is a measure for the unsaturated part of EfOM as aromatic moieties and double bonds strongly absorb at this wavelength (Wert et al., 2009). These electron rich sites are very reactive to both molecular ozone and $HO^{\bullet}$ and are responsible for very fast initial ozone consumption, often called IOD. A rapid UV_{254} decrease as function of reaction time is generally observed, which reflects the progress of oxidation (Gong et al., 2008; Wert et al., 2009; Nanaboina and Korshin, 2010; Ratpukdi et al., 2010; Tripathi et

al., 2011; Sharif et al., 2012). Measurement of UV_{254} is relatively fast, cheap and easy and can be performed on-line. Relating this parameter to other variables that are more difficult to measure can therefore be of added value. Wert et al. (2009) for example, correlated UV_{254} with ozone dose, $HO^{\bullet}$ exposure and the removal of six selected pharmaceuticals with varying reactivity towards ozone and $HO^{\bullet}$. Strong relations were established using effluent from four different WWTPs. The study revealed that measurement of UV_{254} before and after ozonation could provide real-time evaluation of pharmaceutical oxidation, even if no ozone could be measured (i.e. if the ozone dose did not exceed the IOD, which can be the case in wastewater ozonation). However, more research will be needed to validate the method in order to make it applicable. Nanaboina and Korshin (2010) developed a semi-empirical model that was able to predict the removal of selected PPCPs during ozonation based on UV_{254} removal. The EfOM surrogate was divided into two fractions, each having different reactivity towards ozone and $HO^{\bullet}$. Qualitative fits between experimental and calculated data were obtained using effluent of one WWTP. Validation of the model still has to be conducted. Apart from using the absorption coefficient at a single wavelength as a surrogate for EfOM, these authors also indicated the added value of using the whole UV-VIS absorbance spectrum to investigate ozone induced EfOM transformations. Absorbance spectra between 240 and 800 nm were studied and used to calculate DAS. The results showed that some wavelength regions (e.g. 260-280 nm) were more affected by oxidation than others. In this chapter, DAS will be used for the first time to compare EfOM transformations induced by ozone and UV/H_2O_2 treatment.

TOC an DOC are frequently used surrogates that express the EfOM concentration in terms of total and dissolved carbon content per unit of volume (mg C L^{-1}). DOC is a valuable surrogate that can offer an estimate of the $HO^{\bullet}$ scavenging propensity of EfOM by using a fixed second order rate constant for the reaction between EfOM and $HO^{\bullet}$ (Rosario-Ortiz et al., 2008). Additionally, ozone doses applied are often based on the DOC load of the water to be ozonized (Zimmermann et al., 2011). However, DOC provides no information on EfOM transformation as minimal mineralization occurs at the typical oxidant doses applied (only small reductions of DOC are generally observed) (Domenjoud et al., 2011a; Tripathi et al., 2011; Reungoat et al., 2012).

To offer an answer to this drawback, EfOM can be fractionated into several classes based on polarity and charge. The fractionation procedure generally includes sample filtration using a series of different macroporous resins (Chow et al., 2004; Ratpukdi et al., 2009). Although the DOC is almost not altered by oxidation, this method allows studying the conversions taking place as clear shifts between the

DOM fractions can occur. Usually, DOM is becoming less hydrophobic and more hydrophilic as the oxidation proceeds (Buchanan et al., 2005; Gong et al., 2008; Rosario-Ortiz et al., 2008; Ratpukdi et al., 2010). The oxidation of larger, hydrophobic molecules results in the production of smaller, more hydrophilic fragments such as carboxylic acids, aldehydes and ketones (Wert et al., 2007; Tripathi et al., 2011).

These gradual shifts from high MW to low MW classes can be studied into more detail using high performance size exclusion chromatography (HPSEC) (Chow et al., 2008). UV absorption at 254 or 260 nm is commonly used to record the HPSEC chromatogram. Organic carbon detection (OCD) is sometimes used in parallel which has the advantage that also non-aromatic moieties of EfOM can be detected. The UV signal on the other hand, provides information on reactivity towards ozone (see above). The apparent molecular weight (AMW) range of non-colloidal EfOM is typically between 100 and 10.000 Dalton (Da) (Ratpukdi et al., 2010; Gonzales et al., 2012; Sharif et al., 2012). Gonzales et al. (2012) correlated the pseudo-first order decay constant of ozone (k'_{app}) with the MW of EfOM originating from four different WWTPs. EfOM was divided into four AMW fractions using membranes with different pore sizes. An increase of k'_{app} was observed if the colloidal part of EfOM (>10 kDa) was absent, indicating that EfOM with AMW below 10 kDa was more reactive to ozone. This fact was explained by a lower aromaticity of the colloidal matter. Additionally, the second order reaction constant for the reaction between ozone and EfOM increased as AMW decreased. Sharif et al. (2012) studied EfOM conversion as function of ozone dose by means of size exlusion in combination with OCD. Samples were collected at eight different WWTPs. After ozonation, the colloidal response reduced dramatically, while more low MW organics were formed. Ratpukdi et al. (2010) found that AOPs were more effective in reducing higher MW ranges compared to ozonation. HPSEC chromatograms revealed that ozone especially reacted with lower MW molecules (<350 Da). This is in agreement with the earlier mentioned results of Gonzales et al. (2012). However, the effluent used in the aforementioned study was already coagulated and softened and thus high MW fractions were already removed. As previous studies showed, trends in HPSEC chromatograms are perfectly suited to illustrate the degree of EfOM oxidation. Nevertheless, the data behind these chromatograms is rarely processed in order to extract quantitative information that can be of scientific or practical value. Chow et al. (2008) and Korshin et al. (2009) applied two different data processing techniques on HPSEC spectra obtained from surface water coagulation experiments. Chow et al. (2008) resolved the HPSEC spectra using six separate Gaussian peaks. Each peak corresponded to a certain molecular weight

class and chemical group. This "peak fitting" method allowed for a prediction of NOM treatability by coagulation as a distinction could be made between easy removable, removable and non-removable NOM. On the other hand, Korshin et al. (2009) highlighted the limited information that fixed-wavelength HPSEC profiles provide with respect to NOM activity in reactions affecting water quality. These researchers introduced a multi-wavelength absorbance parameter that was used as an estimate for the activity of aromatic groups in reactions that are e.g. related to THM formation. The ASI can be defined as the ratio of the slope of the absorbance between 254 and 272 nm and the slope between 220 and 230 nm. In the first wavelength region, especially activated aromatic groups will absorb, while in the second one both carboxylic and aromatic groups are important. NOM reactivity increases with increasing ASI. The ASI was found to be strongly correlated with SUVA and the THM formation potential (THMFP) of NOM originating from three different natural waters. To the best of our knowledge, the use of the ASI has been limited to natural water studies only and has never been used to study EfOM oxidation. This could be interesting as besides a decreasing overall absorbance, also dynamical shifts between different AMW classes occur during (advanced) oxidation. This is not the case during e.g. a coagulation process, where high AMW classes are selectively removed (instead of being transformed) (Korshin et al., 2009).

7.1.3 Objectives of this study

In view of the above overview of the state-of-the-art, the objectives of the present study were to: (i) study ozone and $HO^{\bullet}$ induced EfOM conversions in terms of concentration, polarity, molecular size, spectral response and biodegradability using a set of different surrogates including DAS and ASI, (ii) compare two different oxidation processes (ozone and UV/H_2O_2 treatment) in terms of EfOM transformation and $HO^{\bullet}$ production and (iii) establish correlations between the different measurements performed which provide insight into the process and can be used as a starting base for mathematical modelling.

7.2 Materials and methods

7.2.1 Sample collection and treatment

Effluent samples were collected from the secondary clarifier of a municipal WWTP in Harelbeke, Belgium. This WWTP is operated by Aquafin (www.aquafin.be) and has a treatment capacity of 116,100 p.e. The wastewater is treated by a CAS

process (21d average sludge residence time) equipped with screen filtration, sand and oil trap, primary settling, nitrification and denitrification and secondary clarification. Samples were taken at two different times to account for changes in effluent composition (further in this publication referred to as "sample 1" and "sample 2"). Each time, 250 L of sample was collected, successively filtered through a rapid sand filter and 0.45µm filter (Porafil® CM, Macherey-Nagel) and stored at 4°C until use. Filtration was performed to enhance sample conservation and to remove solids as only the dissolved part was of interest in this study. Furthermore, full-scale application of the oxidation techniques for tertiary treatment mostly involves a pre-filtration step. The characteristics of the effluent samples are given in Table 7.1.

Table 7.1: Summary of water variables for the two samples

Variable (unit)	Sample 1 (October 2011)	Sample 2 (January 2012)
pH	7.95	8.54
DOC (mg L^{-1})	6.3[1]	7.0
Nitrate (mg L^{-1})	1.4[2]	3.7[2]
Ammonium (mg L^{-1})	0.45[2]	0.6[2]
Alkalinity (mg L^{-1} as $CaCO_3$)	124	274
UV_{254} (m^{-1})	13.5	12.7
SUVA (L mg^{-1} m^{-1})	2.13[1]	1.81
COD (mg L^{-1})	17.8	19.8
Biochemical Oxygen Demand (BOD) (mg L^{-1})	1.24	0.7

[1]Due to an erroneous DOC measurement for Sample 1, the DOC value was estimated based on the measured COD and the COD:DOC ratio of Sample 2.

[2]These values were obtained by averaging values of the week the samples were collected

The COD:DOC ratio for WWTP effluent is typically around 3 mg O_2 mg^{-1} C (Noethe et al., 2009). This is in close agreement with the effluent used in this study (the ratio was on average 2.8 mg O_2 mg C^{-1}). SUVA values of the effluent varied around 2 mg^{-1} L m^{-1}, which is a moderate value (Korshin et al., 2009).

7.2.2 Experimental set-up

Experiments were conducted in a 11 L cylindrical batch reactor made of glass and equipped with a water jacket (25 cm inner diameter, 58 cm height; Figure 7.1). Mixing of the aqueous phase was accomplished by a magnetic stirrer and a circulation pump. The circulation flow rate was maintained at 500 L h^{-1} and all fittings and tubings were made of Teflon®. Part of the circulation flow (60 L h^{-1}) was directed through a measuring cell (DEPOLOX® 5, Wallace and Tiernan) containing a pH, temperature and amperometric ozone sensor. The circulation circuit was configured as such that maximal mixing performance could be achieved

(see Appendix B for fluid mixing tests). The distance between the reactor outlet and measuring cell was kept minimal. Temperature was controlled at 25.0±0.1°C using a thermostatic bath and a cooling element. This temperature was chosen in order to allow comparison with literature, as most of the studies reported were performed at this temperature. pH was maintained at a constant value of 7.5±0.1 using a programmable logic controller (Siemens) with proportional-integral control. Pulse pumps were used to add a 5M solution of hydrochloric acid or sodium hydroxide in order to lower or increase the pH, respectively. Buffering the sample with phosphate was not applied as instantaneous precipitation of calcium phosphate occurred due to the presence of calcium ions in the effluent. At the start of each experimental run, the reactor was filled with 11 L of sample. The temperature was allowed to stabilize and the pH was brought to a value of 7.5. pCBA was used as a $HO^{\bullet}$ probe compound and was spiked into the water at a concentration of 5 µM (Rosenfeldt and Linden, 2007). Reactor conditions were identical for sample 1 and sample 2, except that the ozone and H_2O_2 doses were varied for the ozonation and UV/H_2O_2 experiments, respectively (see further). The wastewater was treated for 70 min and duplicate experiments were performed.

At regular time intervals, samples were taken and the remaining oxidant was quenched. For ozone, a 10 fold excess of sodium nitrite was added (Zimmermann et al., 2011), H_2O_2 was removed by adding 0.2 mg L^{-1} bovine liver catalase (Sigma) (Liu et al., 2003). The latter was freshly prepared and prior to its addition, samples were brought to room temperature (according to results of preliminary tests described in Appendix B). Temperature, pH and aqueous ozone concentrations were monitored and logged every second using a data acquisition device (model No. FN-18200-00, Cole-Parmer) connected to a computer. Prior to the oxidation experiments, some preliminary tests were conducted in order to determine some important reactor parameters such as the radiant power and volumetric mass transfer coefficient (k_La_{O3}) of the reactor. Furthermore, some tests on fluid mixing and quenching of hydrogen peroxide were performed. These experiments are explained in more detail in Appendix B.

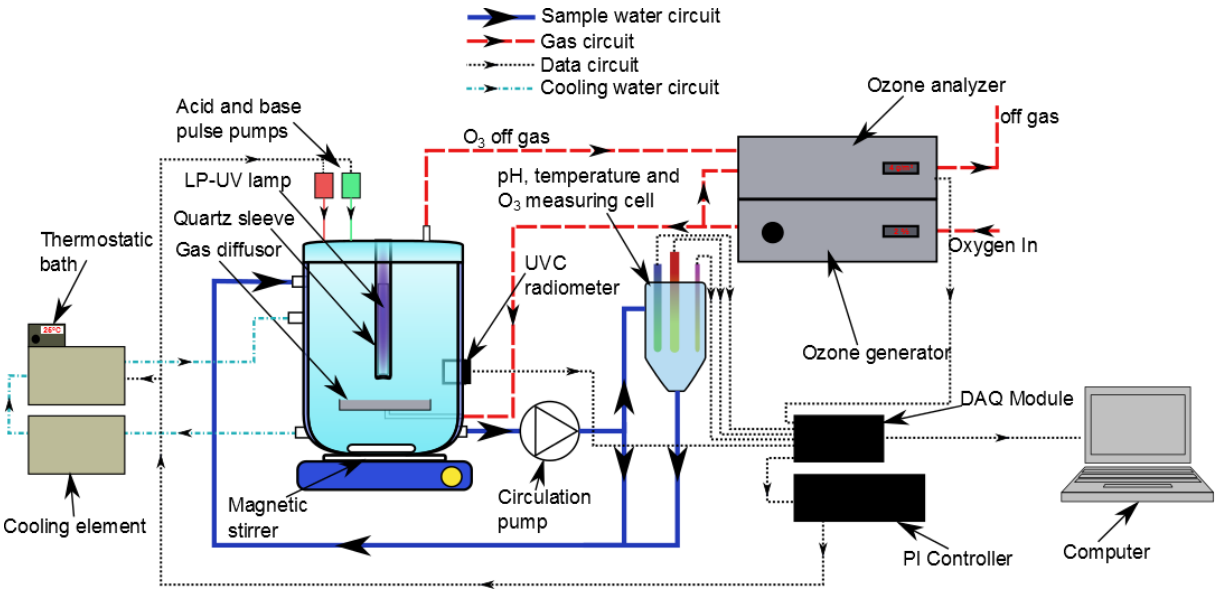

Figure 7.1: Scheme of the reactor used for ozone and UV/H_2O_2 experiments

Ozonation

For ozonation experiments, the reactor operated in semi-batch mode with a continuous inflow of an oxygen/ozone mixture. A semi-batch configuration was used rather than a batch system to allow for slow ozone addition in order to extend the time frame of the fast reactions related to EfOM. As such, in depth kinetic investigation is possible. Although alternative reactors such as stopped-flow and quench systems can be used to kinetically study rapid ozone consumption (as discussed in Chapter 2), their small volumes restrict post-experimental analyses that require more than several milliliters of sample. Hence, these reactors were not suitable for this study as most of the analyses related to EfOM require tens to hundreds of milliliters of sample.

Ozone was generated from high purity oxygen using a corona discharge ozone generator (Ozomat COM-AD-02, Anseros). The oxygen flow rate was set at 1000±15 mL min^{-1} with the help of a mass flow meter (model No. SN-32649-12, Cole-Parmer). The inlet gaseous ozone concentration was set at 4.0±0.2 or 7.7±0.2 mg L^{-1} for experiments performed with sample 1 and sample 2, respectively. Ozone was introduced via a porous glass diffusion plate. Gaseous ozone was determined with UV measurement using an ozone monitor (GM-OEM, Anseros). Prior to each run, the inlet gaseous ozone concentration was measured for 1 min. Afterwards, the gas circuit was modified as such, that the off gas was measured for the remaining period. The gaseous ozone concentration was logged every second.

7.2.2.2 UV/H_2O_2 treatment

For UV/H_2O_2 experiments, a 11 W LP-UV lamp (TUV, Philips) was used. The lamp was enclosed by a quartz jacket located at the centre of the reactor. A voltage regulator (PE1610, Philips) was used to account for fluctuations in the power supply to the lamp. The stability of the lamp output was checked using a UV radiometer (IL1772 device with XRD140/T254 detector, International Light Technologies). At the beginning of each run, 2 mM and 4 mM H_2O_2 were added to sample 1 and sample 2, respectively.

7.2.3 Analytical procedures

Samples were analysed for the following parameters: DOC, biodegradable fraction of DOC (bDOC), BOD and COD, UV-VIS spectrum, HPSEC, pCBA, H_2O_2, ozone and alkalinity. Additionally, DOC was fractionated into four fractions based on polarity. If sample volumes of more than 500 mL were desired (for BOD measurements and DOC fractionation), the experiment was stopped after sample collection and the reactor was refilled for a next run.

The DOC measurement was conducted with a Shimadzu TOC-VCPN analyser based on infrared detection. The method described by Khan et al. (1998) was used to determine the bDOC. Samples were inoculated with 1 mL fresh effluent per 100 mL sample and incubated for five days in 300 mL flasks. Simultaneously, the BOD analysis was performed by measuring the oxygen concentration before and after incubation using a self-stirring oxygen electrode (EC620SSP, Eutech) and a CyberScan PCD 6500 measurement device (Eutech). COD was measured using Hach-Lange cuvettes (LCK414) and a DR2800 spectrophotometer. UV-VIS absorption measurements were performed with a Shimadzu UV-1601 spectrophotometer. Absorption spectra between 200 and 800nm with a resolution of 0.5nm were recorded. 4-cm path-length quartz cuvettes were used to increase the sensitivity of the measurement (especially needed at higher wavelengths).

HPSEC was carried out with a HPLC (Agilent 1100 series) and a diode array detector (model G1315B) which acquired absorbance data in the wavelength range of 200-400 nm at a 1 nm resolution. A Shodex protein KW-802.5 silica packed column (Showa Denko, Japan) was used as stationary phase. A 0.02 M phosphate buffer solution (pH 6.8) adjusted to 0.1 M ionic strength with sodium chloride was sent through the column at a flow rate of 1 mL min^{-1}. Prior to injection, samples were buffered to have the same ionic strength and pH as the eluent. The injection volume was 250 µL. Retention times were converted into AMW using polystyrene sulfonate (PSS) standards of 32.9, 14.9, 6.5, 4.2 and 0.2 kDa (Fluka). pCBA

analysis was performed using the same HPLC device as for HPSEC. The stationary phase consisted of a C-18 reverse phase column (Alltima, Alltech), with 1 mL min^{-1} of eluent consisting of acetonitrile:water (50:50) adjusted to pH 2 with phosphoric acid (Rosenfeldt and Linden, 2007).

The hydrogen peroxide concentration during UV/H_2O_2 runs was determined by the iodate method (Klassen et al., 1994). Aqueous ozone was determined by the indigo method (Bader and Hoigne, 1981). This method was used to calibrate the ozone electrode prior to the experiments. At a regular base, manually determined ozone concentrations were compared to the sensor reading. Alkalinity was determined according to Standard Methods (APHA, 1992).

EfOM was fractionated into four fractions: very hydrophobic acids (VHA), slightly hydrophobic acids (SHA), charged hydrophilics (CHA) and neutral hydrophilics (NEU) according to the method developed by Chow et al. (2004). Supelite DAX-8, Amberlite XAD-4 and Amberlite IRA-958 resins (all purchased from Sigma-Aldrich) were conditioned by means of successive soxhlet extraction with HPLC grade methanol and acetonitrile (Aiken et al., 1992). The filtration columns contained 15 mL of resin and samples were passed through at a flow rate of 3 mL min^{-1}. As shown in Figure 7.2, the raw sample (sample 1 in the figure) was acidified to pH 2 with hydrochloric acid and successively delivered through the DAX-8 and XAD-4 resins. The effluent from the XAD-4 column was adjusted to pH 8 with sodium hydroxide after it was passed through the IRA-958 column.

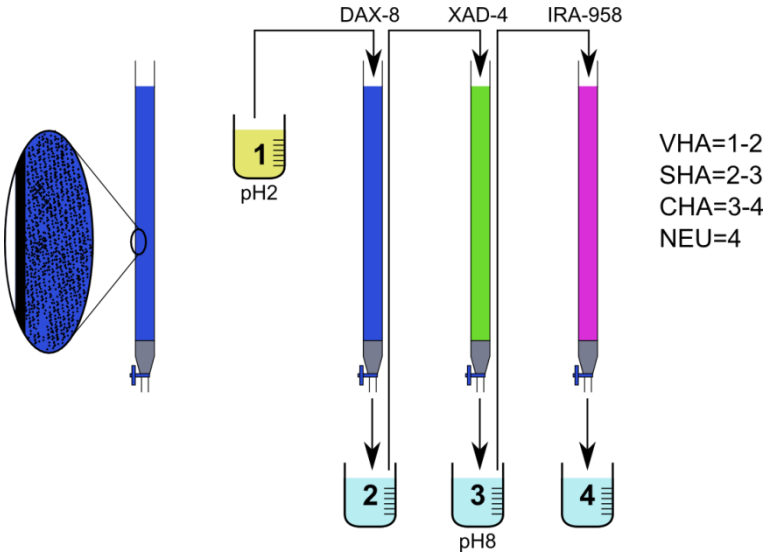

Figure 7.2: Schematic presentation of the DOC fractionation technique

The first two bed volumes of effluent (30 mL) of each column were discarded and 100 mL of sample was kept for DOC and COD analyses (samples 2-4 in Figure 7.2). The calculation of the fractions was performed by subtracting DOC or COD values of samples 1-4 (Chow et al., 2004) as shown in Figure 7.2.

7.2.4 Spectral calculations

DAS were obtained by calculating the difference between the initial absorbance spectrum and that at a specific reaction time, according to Nanaboina and Korshin (2010). The absorption values (cm^{-1}) of a spectrum obtained after a certain reaction time were thus subtracted from those of the initial spectrum for each wavelength separately and as such yielded differential absorption values (cm^{-1}). Subsequently, DAS were normalized relative to the differential absorbance at 270 nm.

The following expression was used to calculate the ASI (Korshin et al., 2009):

$$ASI = 0.56\left(\frac{A_{254}-A_{272}}{A_{220}-A_{230}}\right) \quad (7.1)$$

in which A_i represents the absorbance at wavelength i.

7.3 Results and discussion

7.3.1 Effect of pH on ozone decomposition

A typical image of the aqueous ozone concentration and pH during ozonation is given in Figure 7.3. It was shown that a suitable pH control was applied as the measured values closely varied around the setpoint of 7.5. Each sharp pH decrease was due to the addition of acid. Base was scarcely used, as most of the time carbon dioxide stripping caused the pH to increase. The IOD was very similar for both samples with a value around 6 mg O_3 L^{-1}. The IOD is highly dependent on water source and can easily vary between 1 and 7 mg O_3 L^{-1} (Wert et al., 2009). Noteworthy, however, is that IOD also depends on reactor configuration (batch/semi-batch) and experimental set-up. The time that is needed for a sample to be measured can impact the value of IOD, especially when fast reactions are taking place. After the TOD exceeded the IOD, the aqueous ozone concentration increased with time. Interestingly, the slight (but drastic) variations in pH had a visible impact on the ozone concentration. An increase of pH directly resulted in a decrease of dissolved ozone. At first sight, this outcome was not surprizing, given the initiation reactions of the autocatalytic ozone decomposition chain (Beltrán, 2004):

$$O_3 + OH^- \rightarrow HO_2^- + O_2 \qquad k=70\ M^{-1}\ s^{-1} \qquad (7.2)$$

$$O_3 + HO_2^- \rightarrow HO_2^{\cdot} + HO_2^- \qquad k=2.2x10^6\ M^{-1}\ s^{-1} \qquad (7.3)$$

However, at a pH value of 7.5 the half-life of ozone derived from reaction 7.2 is 8.7 h, thus the behaviour of the aqueous ozone concentration could not be attributed to autocatalytic ozone decomposition. Most likely, the pH indirectly affected the reaction rate between ozone and certain moieties of EfOM. It is well established that deprotonated (charged) species react several orders of magnitude faster with ozone than protonated (neutral) species (Buffle and von Gunten, 2006).

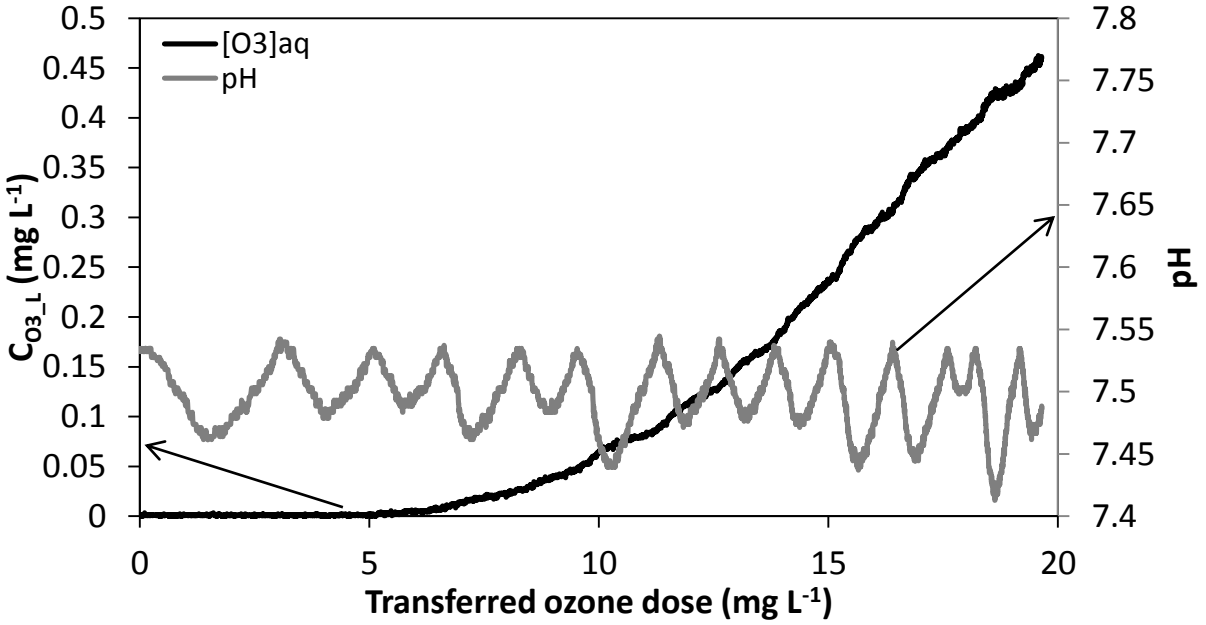

Figure 7.3: Aqueous ozone and pH profile during ozonation of sample 2.

Amine and phenolic-like compounds represent an important part of EfOM and their degree of protonation could have affected direct ozone decomposition significantly (see Chapter 2 for more information on reactions of ozone in the presence of organic matter). E.g. phenol will react six orders of magnitude slower with ozone than its deprotonated form phenolate. Consequently, ozone will react almost exclusively with the charged form, even though the pKa value is significantly higher than the pH (Mvula and von Sonntag, 2003). The importance of phenolic compounds can even increase as function of reaction time as they can be produced upon reactions between poly-aromatic compounds and ozone (Mvula and von Sonntag, 2003; Noethe et al., 2009). Reactions of phenolic compounds and amines

were expected to affect ozone decomposition also indirectly due to direct formation of the superoxide radical, an intermediate that accelerates ozone decomposition (Buffle and von Gunten, 2006).

To get an estimate of the ozone decomposition rate as function of time, the following simple mass balance was used (Beltrán, 2004):

$$\frac{dC_{O3\_L}}{dt} = k_L a_{O3}\left(C^*_{O3\_L} - C_{O3\_L}\right) - k'_{app} C_{O3\_L} \quad (7.4)$$

in which k_La represents the volumetric mass-transfer coefficient (s^{-1}), $C_{O3\_L}{}^*$ is the equilibrium concentration of O_3 in the liquid phase (mg L^{-1}) and k'_{app} is the apparent first order decay constant of O_3 (s^{-1}). For k_La and $C_{O3\_L}{}^*$ values of 3.9×10^{-3} s^{-1} and 1.59 mg L^{-1} were found, respectively (details on how these values were obtained are given in Appendix B).

By assuming a linear increase of the ozone concentration with time, the slope of the profile ($\frac{dC_{O3\_L}}{dt}$) can be calculated for each separate time interval in which the pH is increasing or decreasing. Hence, k'_{app} becomes:

$$k'_{app} \approx \frac{k_L a\left(C^*_{O3\_L} - C_{O3\_L}\right) - \frac{dC_{O3\_L}}{dt}}{C_{O3\_L}} \quad (7.5)$$

As shown in Figure 7.4a. k'_{app} drastically decreased with reaction time (or ozone dose) and could be accurately described with a power function. This result is consistent with earlier findings of Buffle et al. (2006a) and Nöthe et al. (2009), despite the fact that these researchers used a totally different approach (ozone was dosed in dissolved state). The value of k'_{app} varied over more than two orders of magnitude during the experiments. Worth mentioning, however, is that the delay with which ozone was measured could have affected the calculated values of k'_{app}, especially at high ozone decomposition rates. Nevertheless, this could not have affected the observed trend.

After prolonged ozonation, ozone decay became pseudo-first order with k'_{app} approaching values that are commonly found in drinking water ozonation (0.005-0.01 s^{-1}). This is consistent with earlier findings where k'_{app} after prolonged ozone exposure was found to be 10-100 times smaller than at the start of oxidation (Buffle et al., 2006b). By visualizing the residuals (deviation of data points from the power function in Figure 7.4a), the net effect of pH becomes clear. It became clear from Figure 7.4b that if the pH moved from one extreme to another, the corresponding change of k'_{app} was between 5 and 15%. As such, the influence of pH on the reaction kinetics can be demonstrated.

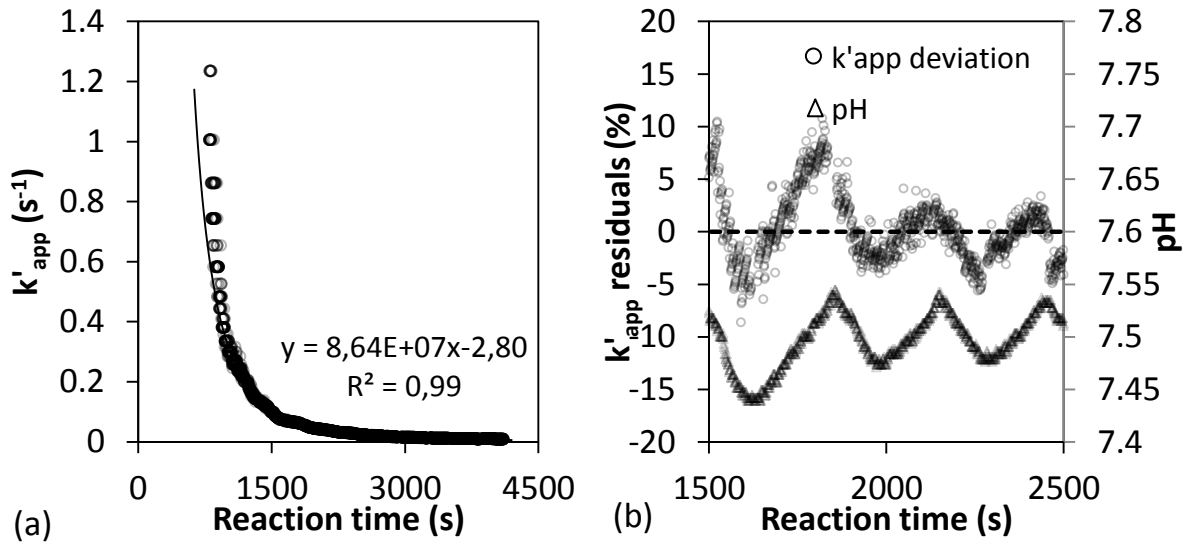

Figure 7.4: (a) Apparent first order rate constant (k'_{app}) for ozone decay during ozonation of Sample 2. (b) residuals of k'_{app}: deviation from the base line (dashed line) are due to fluctuation of pH

7.3.2 Oxygen demand and DOM

7.3.2.1 Carbon content and biodegradability

Because both processes had similar effects on COD, BOD, DOC and bDOC, the results will be briefly discussed together. The evolution of COD and DOC is depicted in Figure 7.5. A DOC reduction between 20 and 40% was observed at highest oxidant doses, indicating that some mineralization took place. COD reductions were very similar with values between 20 and 30% after 70 minutes of treatment. COD decreased following a linear trend (Figure 7.5). Oxidation led to an enhancement of the biodegradability of EfOM. bDOC values increased significantly which led to an increase of the bDOC/DOC ratio up to 15%. Also BOD/COD ratios increased with 15 to 20% after treatment. A good correlation was obtained between bDOC and BOD with an average BOD/bDOC ratio of 2. Results for BOD are presented in Figure 7.6. A rapid initial increase of BOD was generally observed after which the values leveled off. Noteworthy, however, is that due to the biological nature of the BOD test, a relatively large variation of the measurements was observed.

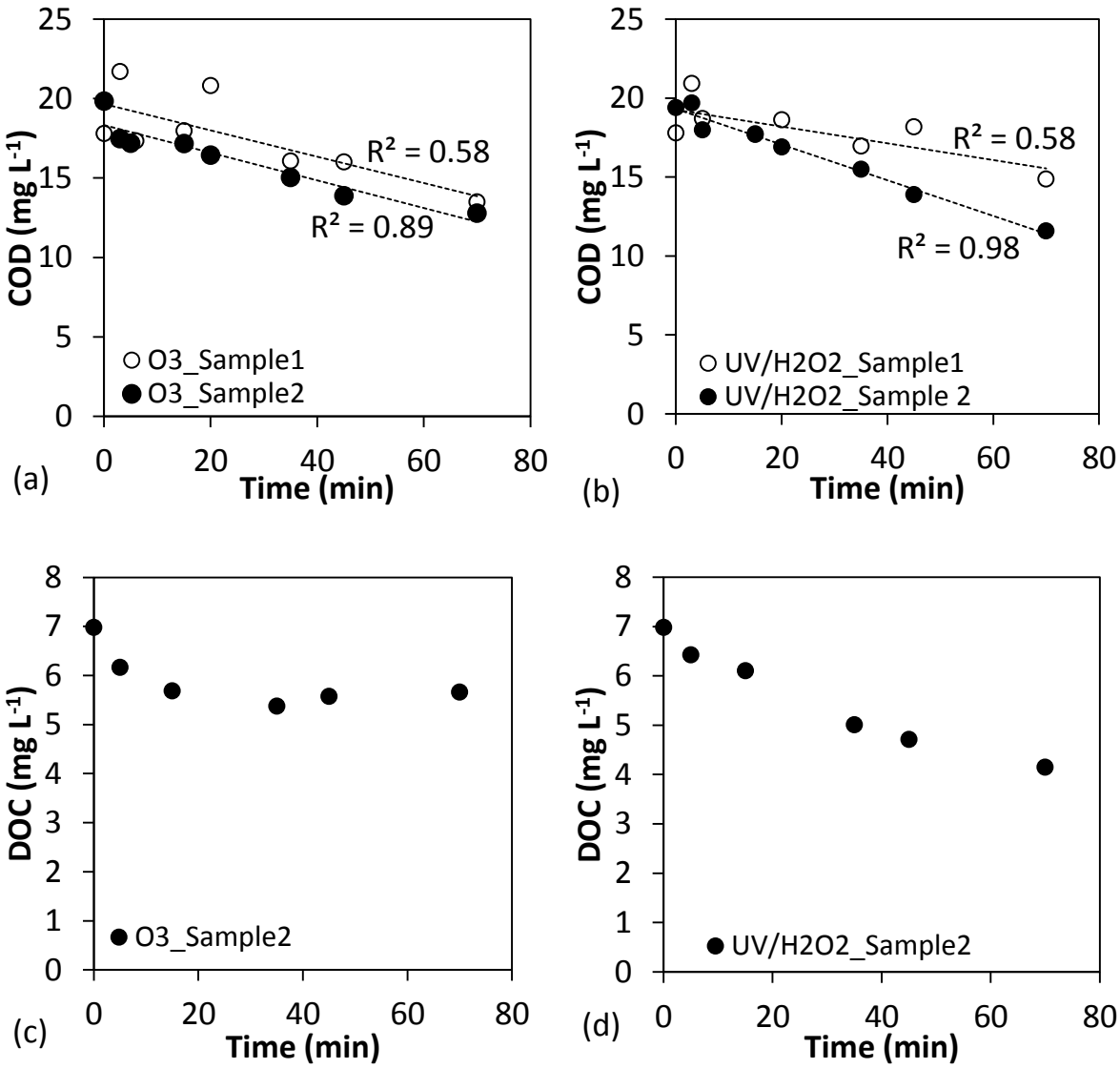

Figure 7.5: Evolution of COD (a and b) and DOC (c and d) during ozone (a and c) and UV/H_2O_2 (b and d) treatment of sample 1 and 2

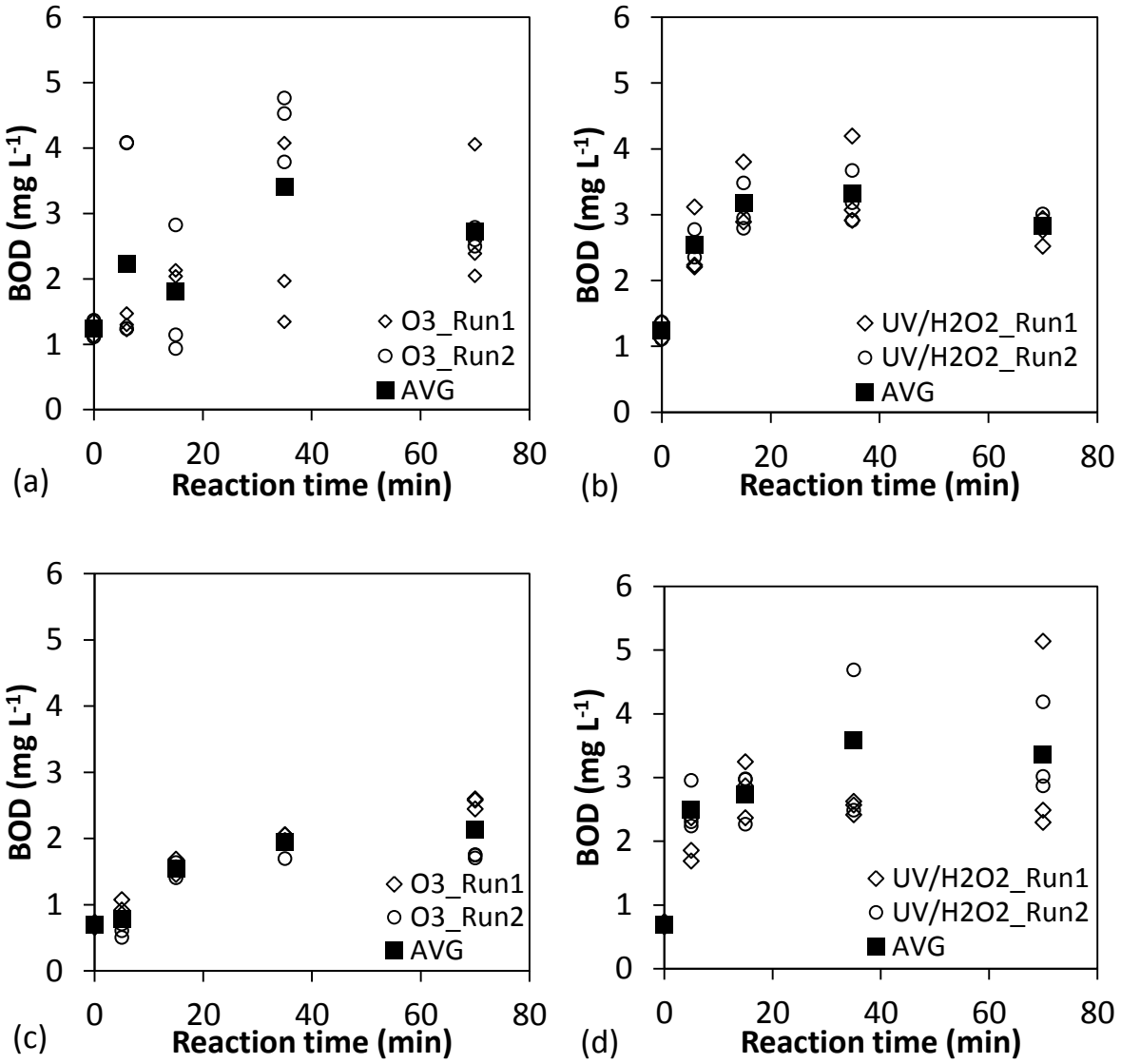

Figure 7.6: Evolution of BOD during ozone (a and c) and UV/H_2O_2 (b and d) treatment of sample 1 (a and b) and sample 2 (c and d). Squares represent the average of two duplicate experimental runs.

7.3.2.2 DOC fractionation

DOC fractionation revealed that EfOM was mainly hydrophobic in nature (Figure 7.7). Although EfOM composition is highly site dependent, these results were consistent with earlier findings of Gong et al. (2008). Very and slightly hydrophobic acids represented 46 and 23% of the initial DOC, respectively. Both ozonation and UV/H_2O_2 treatment drastically changed the polarity of EfOM. At the end of the experiments, most of the DOC was hydrophilic in nature and very hydrophobic acids were almost completely removed. Similar trends were described by other researchers (Gong et al., 2008; Rosario-Ortiz et al., 2008; Ratpukdi et al., 2010).

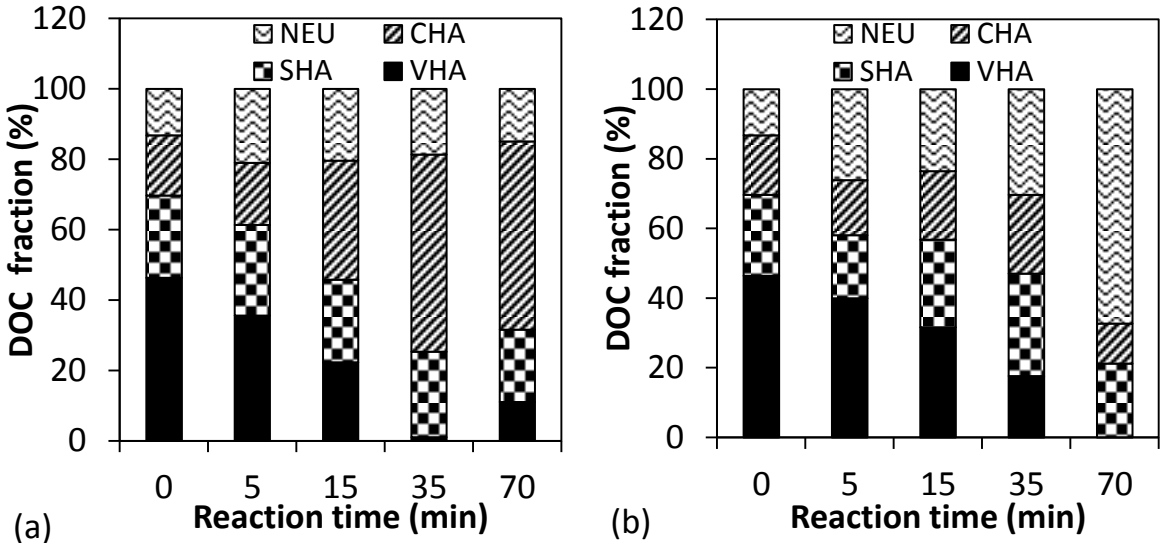

Figure 7.7: Polarity of EfOM during (a) ozone and (b) UV/H_2O_2 treatment of sample 2

7.3.3 UV-visible spectroscopic measurements

Transformations of UV-VIS spectra as function of treatment time are illustrated in Figure 7.8. The initial absorbance spectrum contained a shoulder with a maximum at around 270 nm. During both ozonation and UV/H_2O_2 treatment, a general decrease in absorbance was observed as a result of the partial oxidation of chromophoric moieties of EfOM. These observations are in agreement with earlier findings (Liu et al., 2010; Nanaboina and Korshin, 2010). Nanaboina and Korshin (2010) found that ozone especially attacked EfOM moieties that absorbed in the 260-280 nm UV region. This preferential reaction was also the case in this study and resulted in a total disappearance of the shoulder after treatment. Contrarily, the shoulder was still visible after UV/H_2O_2 treatment. Differences in spectral changes during the two oxidation processes were further investigated using the normalized DAS depicted in Figures 7.9 (sample 1) and 7.10 (sample 2).

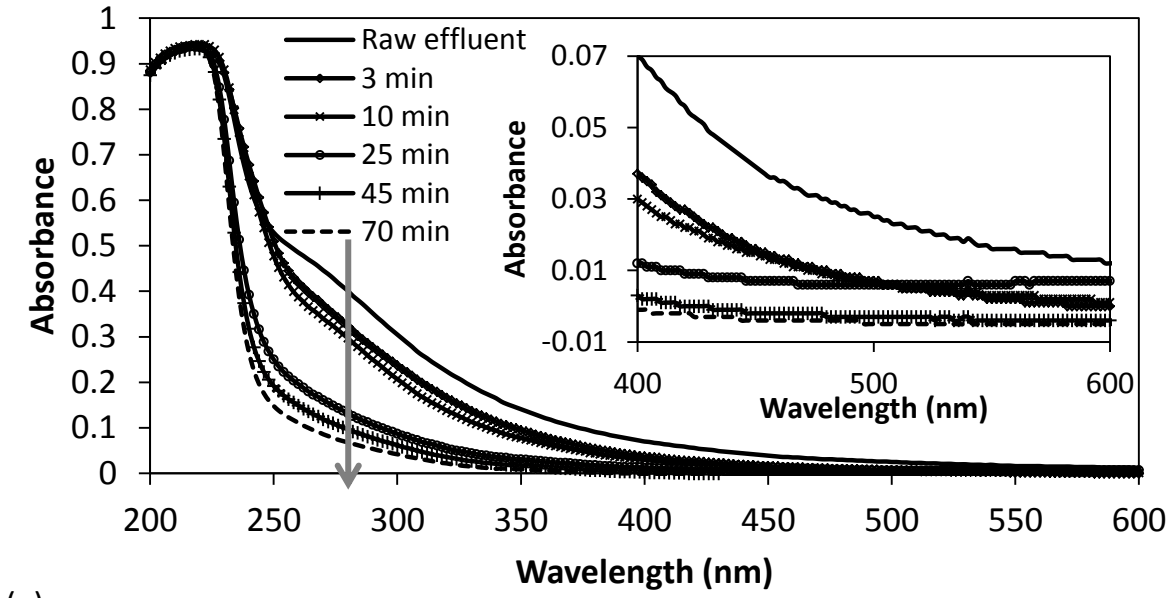

(a)

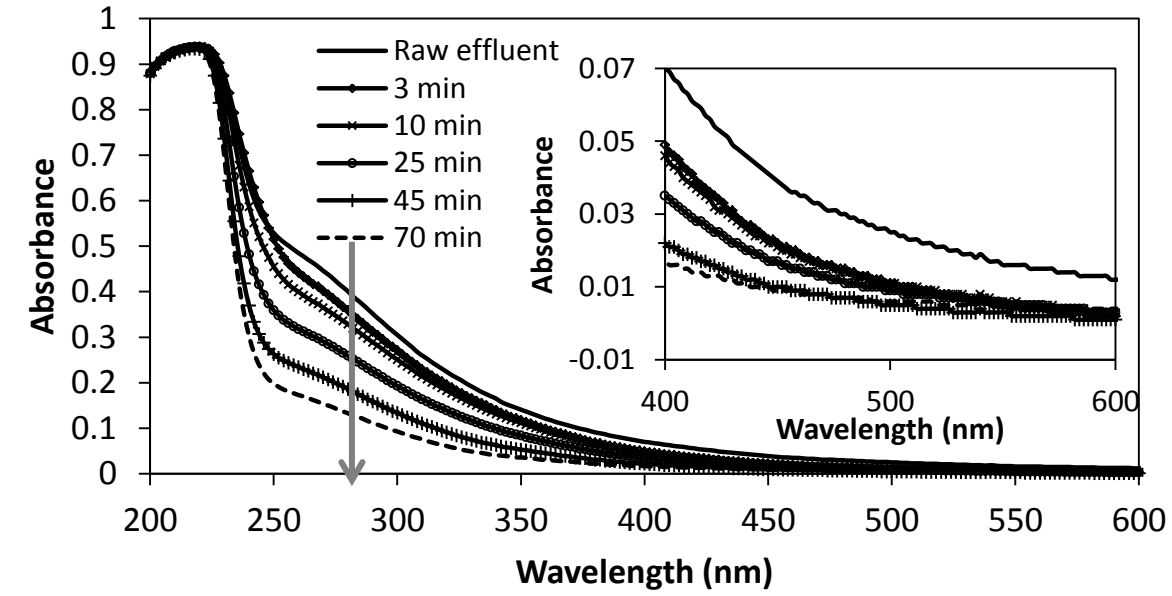

(b)

Figure 7.8: Evolution of absorbance spectra during (a) ozone and (b) UV/H_2O_2 treatment (sample 2). Insets show the removal of colour in the visible light region. 4 cm optical path length.

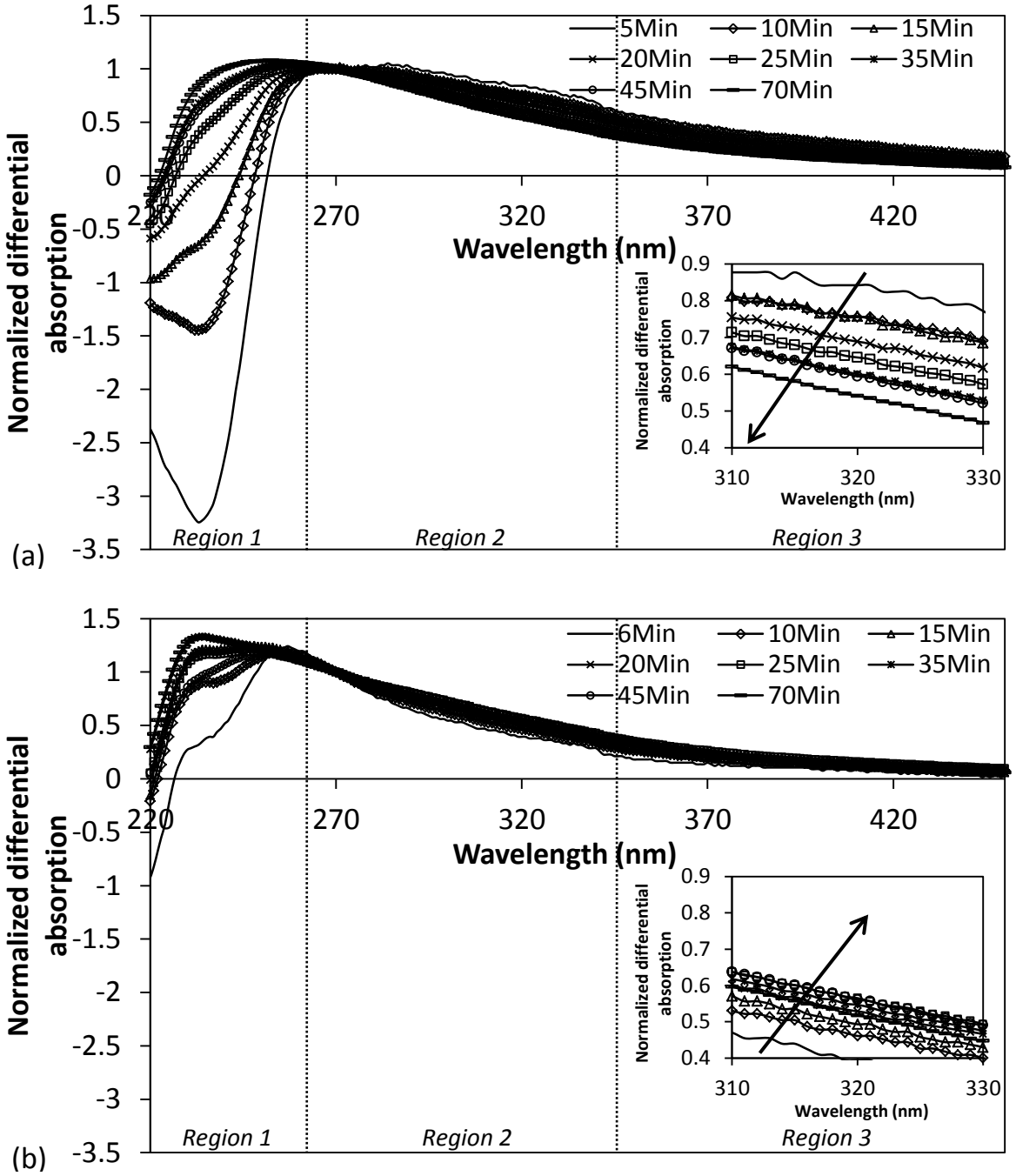

Figure 7.9: Normalized differential absorbance spectra during (a) ozone and (b) UV/H_2O_2 treatment of sample 1. Insets are a magnification of the 310-330 nm wavelength region; arrows indicate the increasing treatment time.

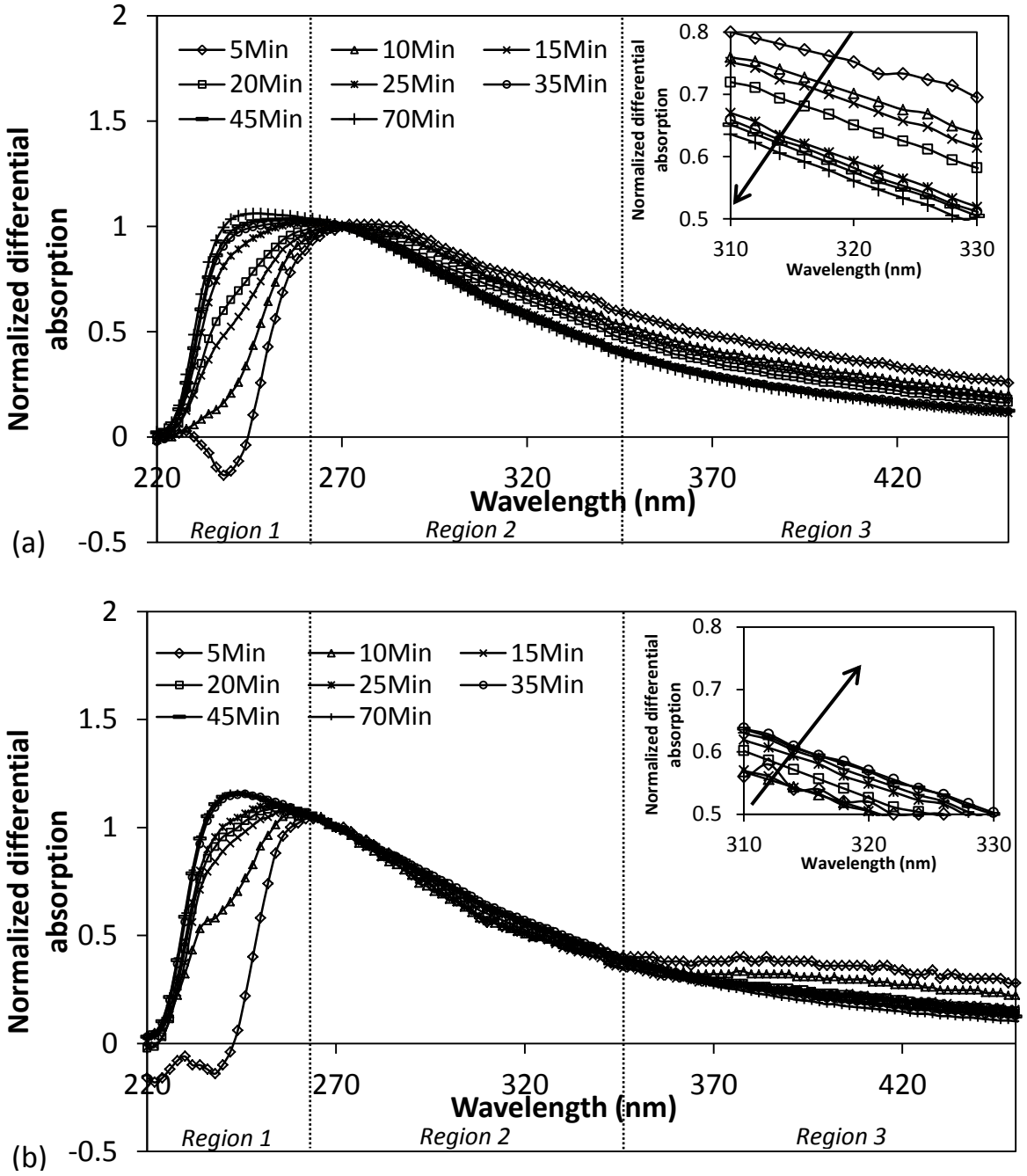

Figure 7.10: Normalized differential absorbance spectra during (a) ozone and (b) UV/H_2O_2 treatment of sample 2. Insets are a magnification of the 310-330 nm wavelength region; arrows indicate the increasing treatment time.

The curves for ozone and UV/H_2O_2 treatment have some similarities but also reveal that fundamental differences exist between ozone and $HO^{\bullet}$ attack. To facilitate the discussion, Figures 7.9 and 7.10 were divided into three wavelength regions: region 1 (220-270 nm), region 2 (270-350 nm) and region 3 (350-450 nm). An initial increase of absorbance in the lower UV region (region 1) occurred during both processes, leading to a depression in the normalized DAS. Even at later treatment

times, the depression was still visible. A minimum value was obtained at a wavelength of around 240 nm. Additionally, the vertical arrangement of the curves in region 3 (higher wavelengths) was the opposite than that in region 1. Most likely, transformation products were formed that absorbed at lower wavelengths. Liu et al. (2010) reported an initial absorbance increase during photocatalytic oxidation of NOM and suggested that new products were formed. However, this increase was only visible at lower wavelengths (<230 nm). Nöthe et al. (2009) hypothesized that highly conjugated material (such as aromatic compounds) that strongly absorbs at higher wavelengths (e.g. 436 nm) can be transformed into compounds that still exhibit absorption at lower wavelengths (e.g. 254 nm) after ozonation. Most interestingly is that during UV/H_2O_2 treatment, as opposed to ozonation, also the vertical arrangement of the curves in region 2 was the opposite of that in region 3 (part of region 2 is depicted in the insets of Figures 7.9 and 7.10). This might indicate that some of the transformation products formed also absorbed in the higher UV region. Most likely, these transformation products were also formed during ozonation, but their rate of degradation exceeded their rate of formation due to their high reactivity towards ozone (compounds that absorb in region 2 are still electron rich). The selectivity of ozone was also exemplified in the fact that the shape of normalized DAS changed visibly as function of time. In analogy with the results of Nanaboina and Korshin (2010), normalized DAS values at higher wavelengths were higher at the beginning and gradually decreased with the ozone dose (see regions 1 and 2 of Figures 7.9a and 7.10a). Contrastingly, the curves during UV/H_2O_2 treatment almost completely coincide (especially in region 2). This means that during the $HO^{\bullet}$ driven process DAS curves changed more or less uniformly, and hence, the absorbance removal efficiency at a certain wavelength was almost independent of oxidant exposure. To conclude, it was hypothesized that transformation products of compounds that initially absorbed in region 3 contributed to formation of products absorbing in region 1 and/or 2. Compounds absorbing in region 2 served as a pool for products absorbing in region 1. After 25 minutes of ozonation, normalized DAS became more overlapping as moieties that were preferentially attacked by ozone were almost completely oxidized.

7.3.4 Hydroxyl radical production

7.3.4.1 First order approximation

In Figure 7.11 $HO^{\bullet}$ induced pCBA oxidation for both ozonation and UV/H_2O_2 treatment is illustrated. The corresponding $HO^{\bullet}$ exposures ($\int[HO^{\bullet}]dt$) are shown in Figure 7.12. Substantial $HO^{\bullet}$ production occurred during ozonation of both samples

and the highest HO• production rate was observed during treatment of Sample 2. This difference could be expected as this sample was oxidized using a higher gaseous ozone inlet concentration (higher mass transfer rate). If pCBA degradations for both samples were compared using TOD instead of time scale, similar trends were obtained, with Sample 1 having a slightly higher

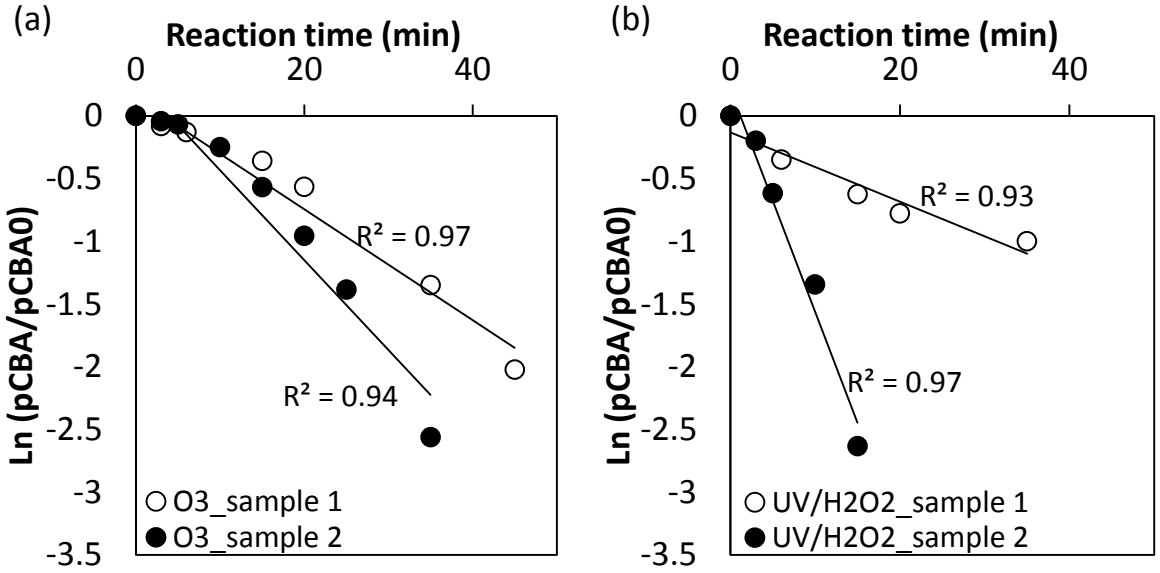

Figure 7.11: HO• induced pCBA (a) oxidation during ozonation and (b) UV/H_2O_2 treatment of two different effluent samples.

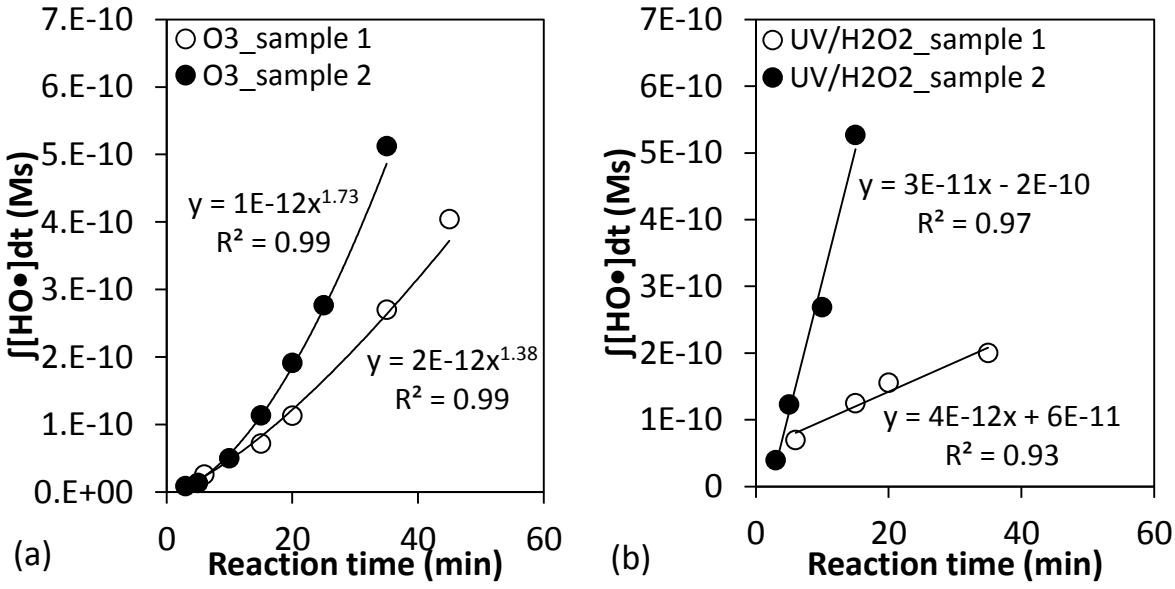

Figure 7.12: HO• exposure (∫[HO•]dt) during (a) ozonation and (b) UV/H_2O_2 treatment of two different effluent samples.

$HO^{\bullet}$ production rate. Most likely, this could be explained by the higher alkalinity and thus higher $HO^{\bullet}$ scavenging propensity of Sample 2 (see Table 7.1). During UV/H_2O_2 treatment, pCBA removal differed significantly for both samples.

There are two explanations for this: (1) for Sample 2, the H_2O_2 concentration that was spiked was the double of the amount added to Sample 1, implying that H_2O_2 was less limiting, and (2) the higher H_2O_2 concentration in Sample 2 may have led to a higher absorption of UV light with less UV being absorbed by the reactor wall (in this case, the reactor path length was limiting). pCBA degradation profiles during UV/H_2O_2 treatment followed more or less pseudo-first order trends, as indicated by the linear relationships shown in Figures 7.11b and 7.12b (the averaging of replicate runs caused the curves to slightly deviate from linearity). This could be expected as during this UV driven process the $HO^{\bullet}$ production rate is only dependent on lamp intensity and H_2O_2 concentration; two properties that have more or less constant behaviour (Audenaert et al., 2011). In contrast, during ozonation $HO^{\bullet}$ production relies on a more complex mechanism and is significantly affected by oxidant induced changes of DOM properties (and thus is time dependent) (Buffle and von Gunten, 2006). This is visible in Figure 7.11a as the slopes of the pCBA degradation profiles change. $HO^{\bullet}$ exposure increased with time following a power law (Figure 7.12a).

7.3.4.2 Relation between pCBA reduction and UV_{254}

The reductions in pCBA concentration and UV_{254} during ozonation correlated very well (Figure 7.13a). A single linear relationship was able to describe the data corresponding to the two different samples that were treated. The trend line crossed the x-axis at about 4% UV_{254} reduction, which means that a slight absorbance reduction was visible prior to any pCBA degradation. Wert et al. (2009) established the same relationship with a comparable slope and found that UV_{254} decreased 15% before any pCBA was oxidized. This relation was valid for effluent originating from three different WWTPs. Given the ease and low cost related to absorbance measurements together with the fact that this relation seems to be valid for different effluent samples, this finding can be of significant value for follow-up and modelling of effluent ozonation. The $HO^{\bullet}$ exposure cannot be easily determined at full-scale and the assessment of micropollutant removal is time, cost and labour intensive.

The same relation, but with data from UV/H_2O_2 experiments is given in Figure 7.13b. It becomes clear that in this case only a weak correlation exists. Probably, this can be explained considering the mechanistic difference between ozonation and UV/H_2O_2 treatment. During ozonation, reactions between ozone and electron rich

moieties of EfOM such as poly-aromatic compounds can inherently give rise to $HO^{\bullet}$ production. This is the main pathway of $HO^{\bullet}$ generation during wastewater ozonation and implies that the process in that case is an ozone based AOP (Buffle et al., 2006a; Noethe et al., 2009). Consequently, as UV_{254} is a measure for the unsaturated part of EfOM, its removal can be expected to be directly correlated with pCBA removal (i.e. $HO^{\bullet}$ generation) and will be mainly based on ozone attack. This is in contrast with the UV/H_2O_2 process, where $HO^{\bullet}$ production only relies on hydrogen peroxide photolysis. As expected, UV_{254} removal during ozonation was mainly due to ozone attack, while $HO^{\bullet}$ was the main oxidant during the UV based process (at similar $HO^{\bullet}$ exposures, the corresponding removals of UV_{254} during ozonation were always significantly higher than during UV/H_2O_2 treatment).

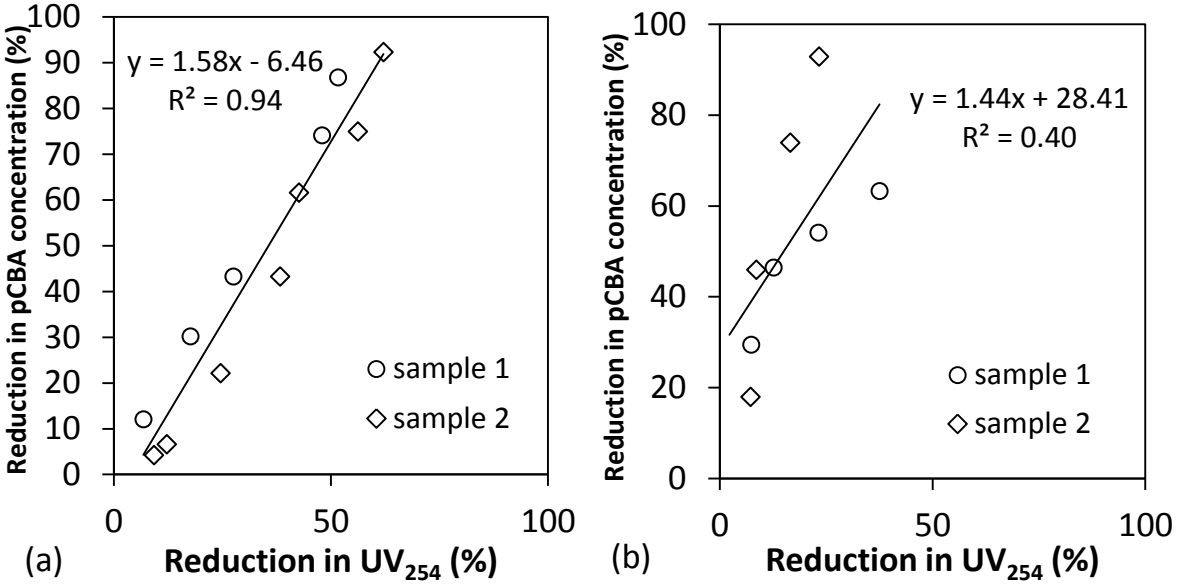

Figure 7.13: Relation between reduction of pCBA and UV_{254} absorbance obtained after (a) ozonation and (b) UV/H_2O_2 treatment. Trend line was constructed using the combined dataset of samples 1 and 2.

The reactions between EfOM and ozone could also be used to explain the increasing $HO^{\bullet}$ production rate that is observed in Figures 7.11a and 7.12a. It was hypothesized that some of the reactions between EfOM and ozone gave rise to transformation products with high reactivity towards ozone and possibly even higher $HO^{\bullet}$ production yields than the parent compounds. It is known that as the ozonation proceeds, the degree of hydroxylation can increase and new phenolic compounds can be formed which in their turn can lead to $HO^{\bullet}$ production (Noethe et al., 2009).

7.3.5 High performance size exclusion chromatography

Based on HPSEC chromatograms obtained at a wavelength of 254 nm, the EfOM samples used in this study consisted of molecules with AMWs ranging between 0.1 and 4 kDa. The majority of chromophoric organic matter could be found in the 1.5 and 3.5 kDa range for sample 1 and between 1 and 3 kDa for sample 2. The HPSEC chromatograms of both samples were similar in shape with some variations in signal strength. Biopolymers or colloidal matter could not be detected. Typically, these molecules have AMWs exceeding 10kDa (Gonzales et al., 2012). Both oxidation processes resulted in a rapid decrease of absorbance values over the entire AMW range, as reported by several authors (Buchanan et al., 2005; Liu et al., 2010; Ratpukdi et al., 2010; Lamsal et al., 2011; Gonzales et al., 2012). Hence, as depicted in Figure 7.14, the area under the chromatogram followed the same trend for different AMW classes. However, this figure also reveals that the relative

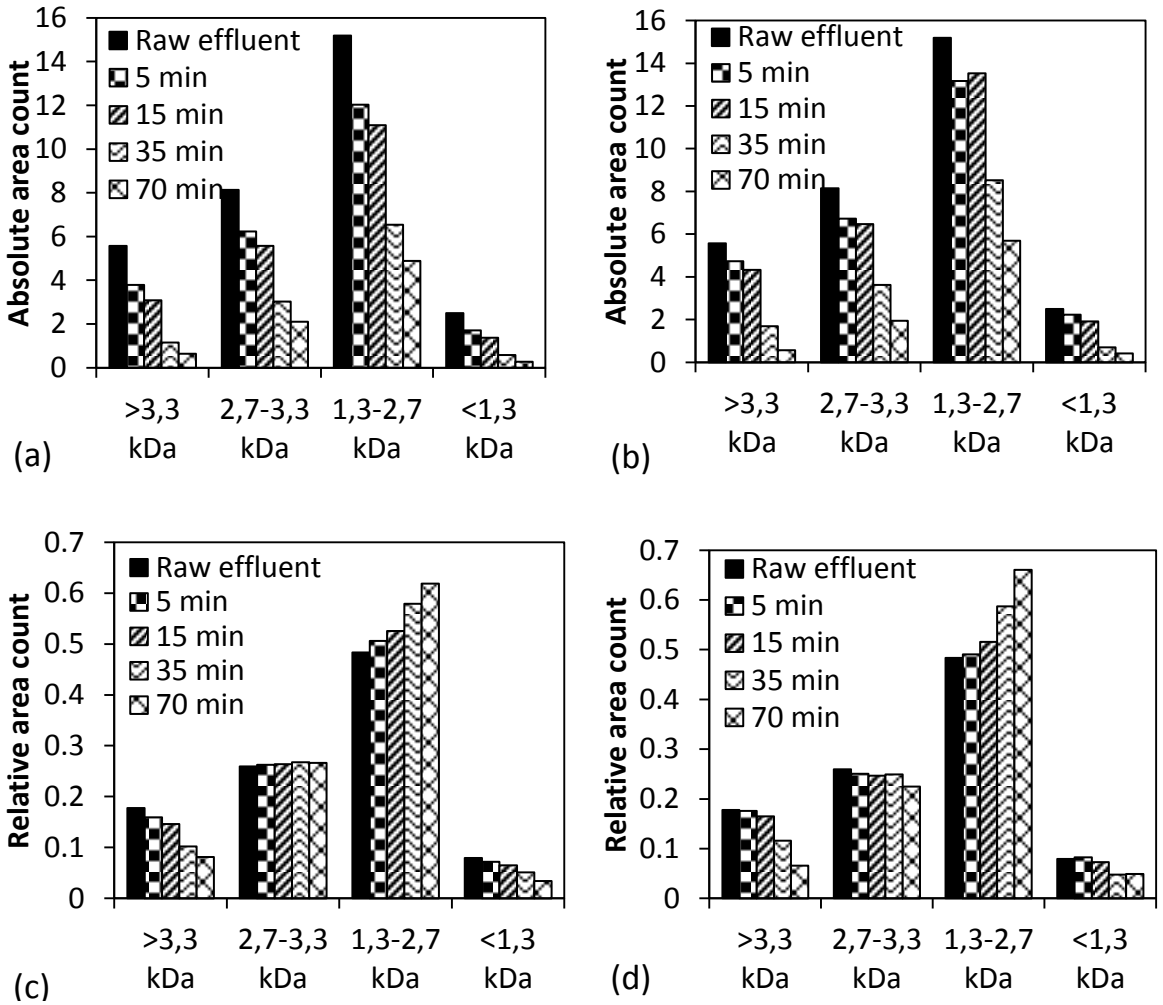

Figure 7.14: Evolution of absolute and relative area count during ozone (a and c) and UV/H_2O_2 treatment (b and d) of sample 2

proportion of smaller molecules increased with treatment time for both oxidation processes. It was shown that the AMW fraction between 1.3 and 2.7 kDa becomes even more dominant at the expense of larger AMW classes. This could be attributed to oxidant induced transformation of large molecules into smaller ones (Rosario-Ortiz et al., 2008). Similar results were obtained during oxidation of sample 1.

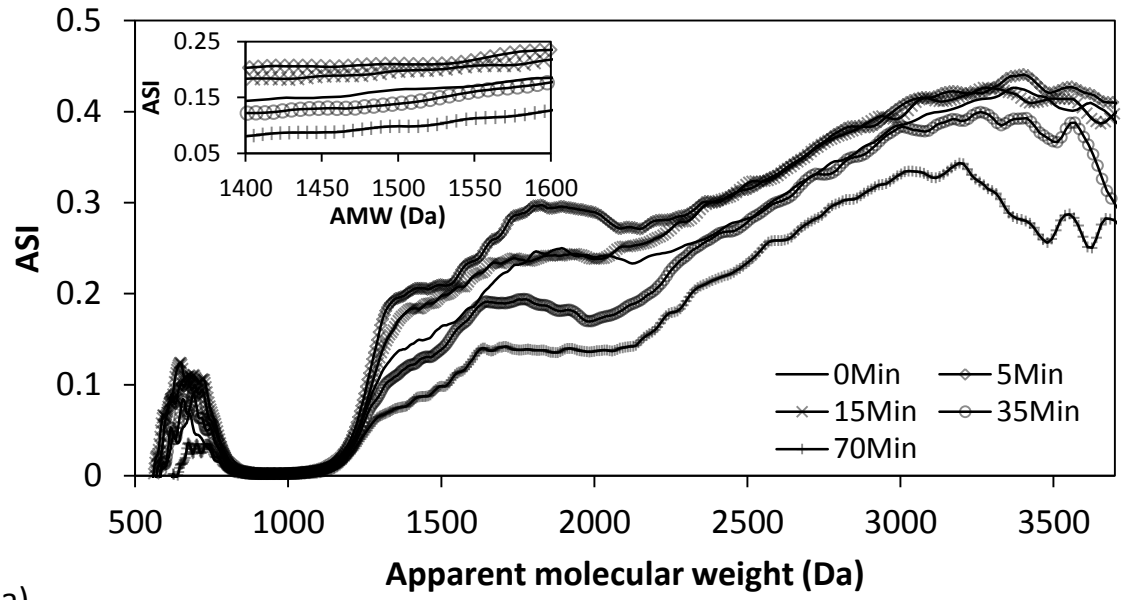

(a)

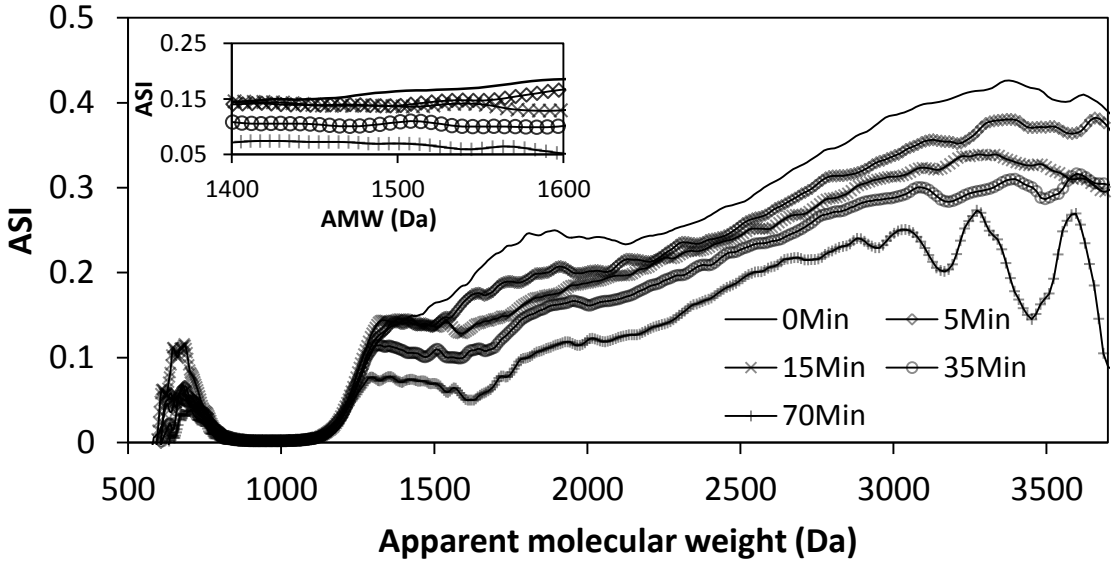

(b)

Figure 7.15: Evolution of the absorbance slope index during (a) ozone and (b) UV/H_2O_2 treatment. Insets: magnification of 1400-1600 Da range.

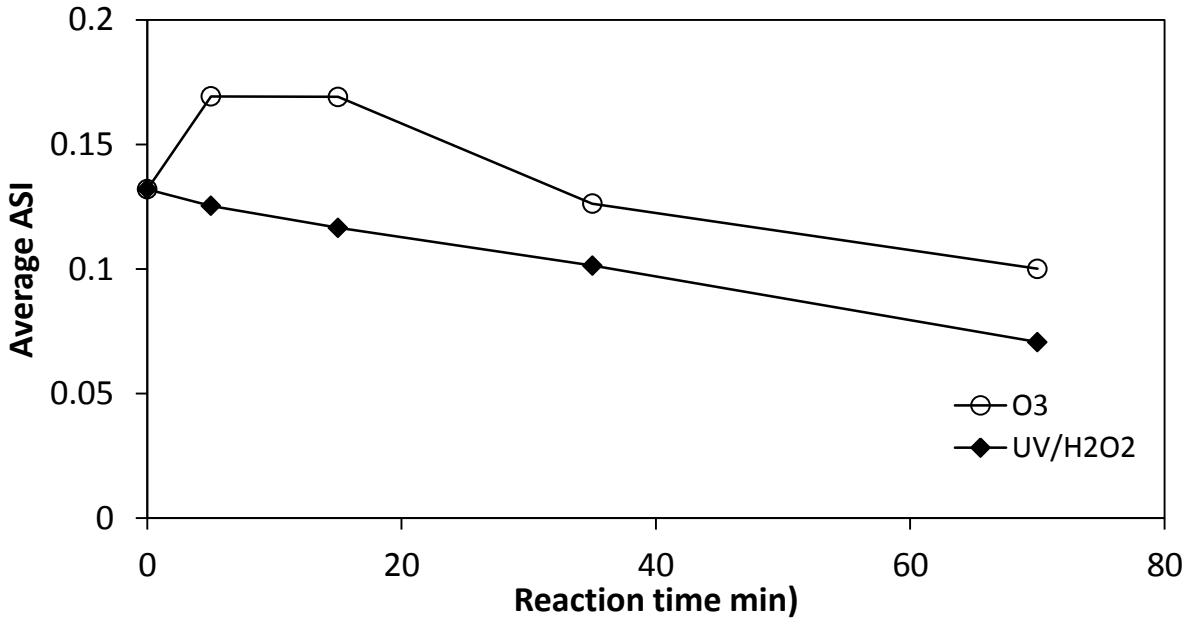

Figure 7.16: Evolution of absorbance slope index during ozone and UV/H_2O_2 treatment; average values of 500-3700 Da range

The first 15 minutes of ozonation (TOD between 0 and 0.5 mg O_3 mg C^{-1}), the ASI tended to increase (inset of Figure 7.15). This was rather unexpected, as ozone is known to especially attack the activated aromatic moieties of DOM (Buffle and von Gunten, 2006) of which their presence has a direct positive impact on the ASI (Korshin et al., 2009). This initial increase of ASI was also observed when the slope index was calculated using the UV-VIS spectra as shown in Figure 7.17. Only a small increase was observed during UV/H_2O_2 treatment (first 5 minutes).

Probably, some unknown transformations of EfOM occurred which led to this result. Liu et al. (2010) reported an initial increase in THMFP during the first minutes of photocatalytic oxidation of NOM and hypothesized that more reactive sites for chlorine attack were available during the initial stage of oxidation. As discussed earlier, some of the transformation products still absorb at lower wavelengths. It might be possible that during the early stage of ozonation some new products were formed that absorbed at 254 nm. This may have led to a temporal increase of the slope of the absorbance between 254 and 272 nm. Further investigation of the slopes indeed revealed that an increase of the numerator (and not a decrease of the denominator) of Equation 7.1 was responsible for the increase in ASI, which confirmed this hypothesis. The aforementioned slope increased up to 51% during the first phase of ozonation and exceeded the initial value for about 25 min. Only a maximum increase of 15% was observed during UV/H_2O_2 treatment and after less than 10 minutes, the value was back below the initial one. As was

shown with the DAS before, also transformation products absorbing at higher wavelengths (e.g. 272 nm) could be detected during UV/H_2O_2 measurement. This could explain why an initial increase in ASI was much less pronounced during UV/H_2O_2 treatment.

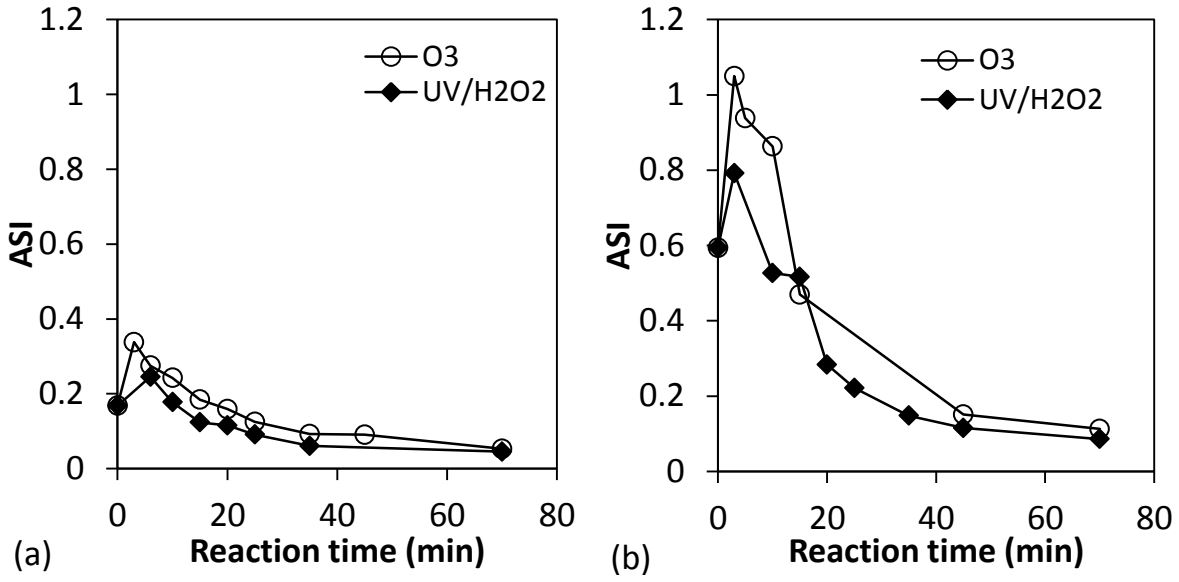

Figure 7.17: Evolution of absorbance slope index during ozone and UV/H_2O_2 treatment of sample 1 (a) and sample 2 (b); values obtained from UV-VIS spectra

The increasing ASI at lower AMWs during both oxidation processes was most likely the result of production of smaller transformation products with a residual aromaticity (still detectable at 254 nm). Furthermore, ASIs were correlated to AMW as was hypothesized by Korshin et al. (2009).

7.4 Conclusions

This study examined the impact of (advanced) oxidation on the properties of EfOM using two different oxidation techniques: ozonation and UV/H_2O_2 treatment. Both processes rely on totally different mechanisms of $HO^{\bullet}$ production and during ozonation, ozone itself is of major importance. Results of this study can be outlined as follows:

- pH extremely impacted ozone decomposition. pH variations between 7.4 and 7.6 resulted in variations of the 1st order ozone decomposition constant of 10 to 15%. It was hypothesized that the degree of dissociation of EfOM controlled the reactivity towards ozone. k'_{app} rapidly decreased as function of ozone dose and could be described with a power function.

- Both processes had similar effects on oxygen demand, DOC, polarity and biodegradability: more oxygen rich, less hydrophobic and more biodegradable transformation products were formed.
- DAS and ASIs have proven to be useful to unravel mechanistic differences between ozone and $HO^{\bullet}$ induced transformation of EfOM.
- DAS and ASIs behaved totally different in the presence or absence of ozone. Ozone preferentially reacted with compounds absorbing at higher wavelengths, while during the $HO^{\bullet}$ based technique spectral changes were more uniformly. Additionally, the absorption of transformation products impacted the spectral results for both oxidation techniques differently.
- Effluent ozonation inherently led to significant $HO^{\bullet}$ production a result of electron transfers between ozone and electron rich moieties of EfOM. $HO^{\bullet}$ production increased as function of ozone dose as most likely, an increased degree of hydroxylation positively impacted the $HO^{\bullet}$ yield of EfOM. During the UV based process, pseudo steady-state behaviour of the $HO^{\bullet}$ concentration was observed.
- Reduction in UV_{254} was strongly correlated to $HO^{\bullet}$ production during ozonation. This relation was not valid for the other process. The differences could be mechanistically explained.

Chapter 8

Modelling of the UV/H_2O_2 process for tertiary treatment: prediction of EfOM conversion and $HO^{\bullet}$ concentration

Abstract
A lab-scale UV/H_2O_2 system for secondary effluent oxidation was modelled. Two slightly different kinetic UV/H_2O_2 models were successfully calibrated. Only poor predictions of effluent organic matter conversion and $HO^{\bullet}$ exposure could be obtained during model validation. This was not the case for hydrogen peroxide decay, which could be satisfactorily predicted. The modelling exercise was severely impeded by the complex and variable character of EfOM. Model-based description of secondary effluent treatment was found to be much more difficult compared to the modelling of natural water oxidation (the latter was performed in Chapters 4 and 6). More research should be conducted to extend the model in order to predict UV/H_2O_2 treatment of secondary treated municipal effluent. Alternatively, possible extensions of semi-empirical concepts should be investigated.

8.1 Introduction

To predict the conversion of trace pollutants, kinetic AOP models must be able to predict the $HO^{\bullet}$ concentration. This means that both $HO^{\bullet}$ production and scavenging rates must be included in the model structure. As opposed to ozonation, the $HO^{\bullet}$ production rate during UV/H_2O_2 treatment can be mechanistically modelled provided that the hydrogen peroxide concentration and UV-C intensity are known (Audenaert et al., 2011). In contrast, phenomenological description of the $HO^{\bullet}$ scavenging rate is much more difficult due to assumptions that have to be made with respect to the different scavengers, their concentrations and reaction rates (Rosenfeldt and Linden, 2007). As shown in Chapter 7, complex conversions of EfOM take place and hence, the scavenging rate of EfOM may vary during the oxidation process. The development of mechanistic models, however, is of major

importance for design and operation of full-scale reactors as these models can cope with a broad range of operational and water quality conditions (Audenaert et al., 2011). With the help of kinetic models, the process operation can be optimized in order to save operational costs (Hofman-Caris et al., 2012).

This chapter investigated the modelling of the lab-scale UV/H_2O_2 experiments conducted and described in Chapter 7. The mechanistic UV/H_2O_2 model used in Chapter 6 was applied to the lab-scale data. As such 2 major parts of this PhD (experimental investigation of EfOM transformation and model development and testing) are combined.

8.2 Methods

The experimental data of the UV/H_2O_2 experiments described in Chapter 7 were used as input for the model presented in Chapter 6. The extended model was not used as no particulate fraction (UV_{310}^{X}) was assumed to be present (the secondary effluent was filtered prior to oxidation).

8.2.1 Model parameters

In contrast to the full-scale reactor described in Chapter 6, the UV-C irradiance (I_0) could be analytically determined and hence, it was not needed to optimize this parameter during model calibration. The UV-C irradiance was determined using ferrioxalate actinometry, as described in Appendix B. The optical path length corresponded to the physical distance between the quartz sleeve and the inner reactor wall. In analogy with the method applied in Chapter 6, the extinction coefficient of UV_{310} was determined by dividing the average UV_{254} value of Samples 1 and 2 (see Table 7.1) by their average UV_{310} values. To measure the $HO^{\bullet}$ concentration, pCBA was spiked to the reactor. As such, compound M and parameter k_{18} included in Table 6.2 corresponded to pCBA and the second order rate constant for reaction with $HO^{\bullet}$, respectively. Parameters related to reactions between EfOM and $HO^{\bullet}$ were obtained through parameter estimation (see further).

In addition to the modelling approach used in Chapter 6 (scavenging by UV_{310}, according to the scavenging reactions presented in Table 6.2), the experiments were modelled by assuming scavenging by DOC (denoted as TOC in Table 6.2). The models respectively assuming scavenging by UV_{310} and DOC will be further referred to as model 1 (scavenging rate $k_{16}[HO^{\bullet}][UV_{310}]$) and model 2 (scavenging rate $k_{19}[HO^{\bullet}][DOC]$). Hence, two slightly different model structures were tested with each of them including two parameters related to EfOM scavenging: k_{16} and

Y_{UV310} for model 1 and k_{19} and Y_{DOC} for model 2. The parameters as used in the model are presented in Table 8.1. Acid formation was discarded as the pH was controlled at a constant value. Direct photolysis of pCBA was not included as this compound has a very low quantum yield (Rosenfeldt and Linden, 2007).

Table 8.1: Parameter values used to model the lab-scale UV/H_2O_2 experiments

Parameter	Value (unit)
Volume (V)	11 L
Irradiance (I_0)	$6.74x10^{-7}$ Einsteins L^{-1} s^{-1}
Optical path length (b)	10 cm
Molar extinction coefficient for EfOM at 254 nm (ε_{UV310})	1.96 cm cm^{-1}
k_{18}	$5x10^9$ M^{-1} s^{-1}[a]
Model 1	
k_{16}	Selected for parameter estimation
Y_{UV310}	Selected for parameter estimation
Model 2	
k_{19}	Selected for parameter estimation
Y_{DOC}	Selected for parameter estimation

[a]Elovitz and von Gunten (1999)

8.2.2 Model calibration and validation

A CSTR in batch mode was implemented in WEST. Sample 2 was used for model calibration as DOC data were available for this case. Model validation was subsequently performed using the data of Sample 1. Parameter optimization was conducted as described in Chapter 3. The objective function calculation was based on a WSSE between the model predictions and measurements, according to Equation 3.4. The variables used for objective function calculation were the pCBA concentration and UV_{310} for model 1, while UV_{310} was replaced by DOC for calibration of model 2. To prevent discrimination of the pCBA concentration (which has low numerical values), a weighing factor of 10,000 was assigned to this variable. To the remaining variables, a factor of 1 was applied. Weighing factors were not expected to affect the optimization result, as the parameters that were estimated were practically identifiable and a unique solution existed. Two parameters were estimated for each model (see Table 8.1). Model 1 was calibrated first, after which the optimized parameter values of k_{16} and Y_{UV310} were used in Model 2 (the latter still included a conversion term of UV_{310}). The initial concentrations of the scavenging species and hydrogen peroxide used for calibration and validation are presented in Table 8.2.

Table 8.2: Initial conditions of important variables used for calibration and validation

	Initial value (unit)	
Variable	**Calibration**	**Validation**
UV_{310}	0.65 m^{-1}	0.65 m^{-1}
HCO_3^-	4.39 mM	2.48mM
DOC	6.98 mg L^{-1}	6.98 mg L^{-1}
H_2O_2	4.37 mM	2.14 mM

8.3 Results and discussion

8.3.1 Calibration

The goodness-of-fit between experimental and simulated values after calibration of models 1 and 2 is presented in Figure 8.1a. For all three variables, an excellent fit was obtained (TIC<0.3). Calibration results for UV_{310} are depicted in Figure 8.2.

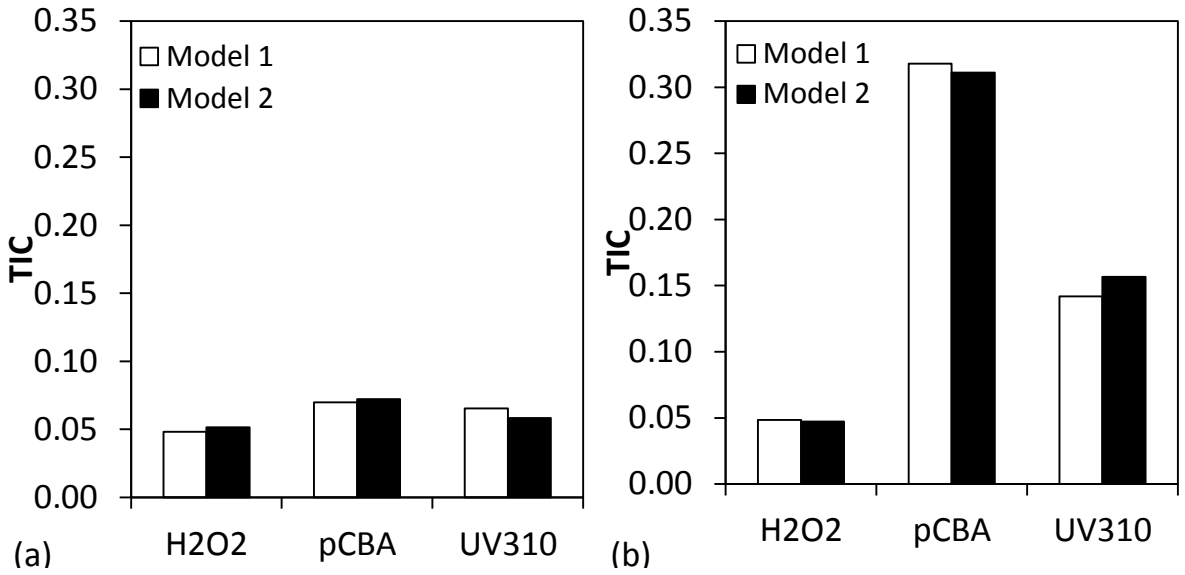

Figure 8.1: Goodness-of-fit after calibration (a) and validation (b)

Although model 1 has the lowest TIC value, model 2 was able to capture the trend of the data better. The increasing deviation between both models with time is a result of the difference in model structure. It was expected that the EfOM scavenging rate of model 1 would decrease more rapidly compared to that of model 2 due to a more rapid decrease of UV_{310} compared to DOC (shown in Figure 8.3). A value of 0.07 M^{-1} cm^{-1} was obtained for the stoichiometric factor Y_{UV310}. The value of k_{16}, the second order rate constant for reaction between $HO^{\bullet}$ and UV_{310} was estimated to be 8.03×10^6 cm s^{-1}. As opposed to the calibration performed in

Chapter 6, in this case both parameters were practically identifiable as data for a $HO^{\bullet}$ probe compound (pCBA) were available.

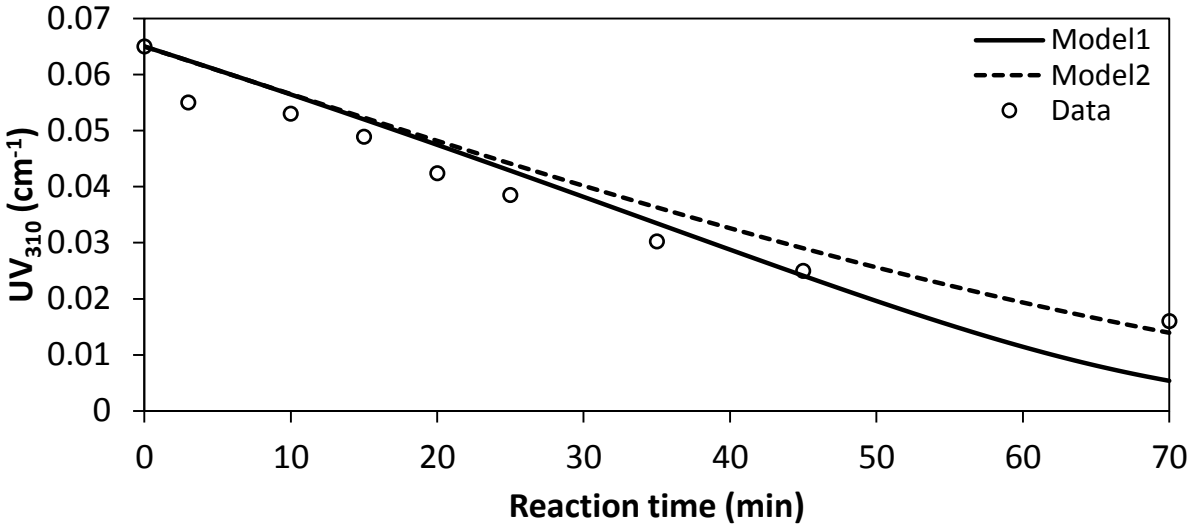

Figure 8.2: Measured and predicted UV_{310} after calibration of models 1 and 2

Simulated and experimental values for pCBA during calibration are presented in Figure 8.4. Results for both models were almost identical as all pCBA was depleted after 30 minutes of treatment. As shown in Figures 8.2 and 8.3, the model predictions of UV_{310} and DOC (and hence, the $HO^{\bullet}$ scavenging rate) start to diverge later.

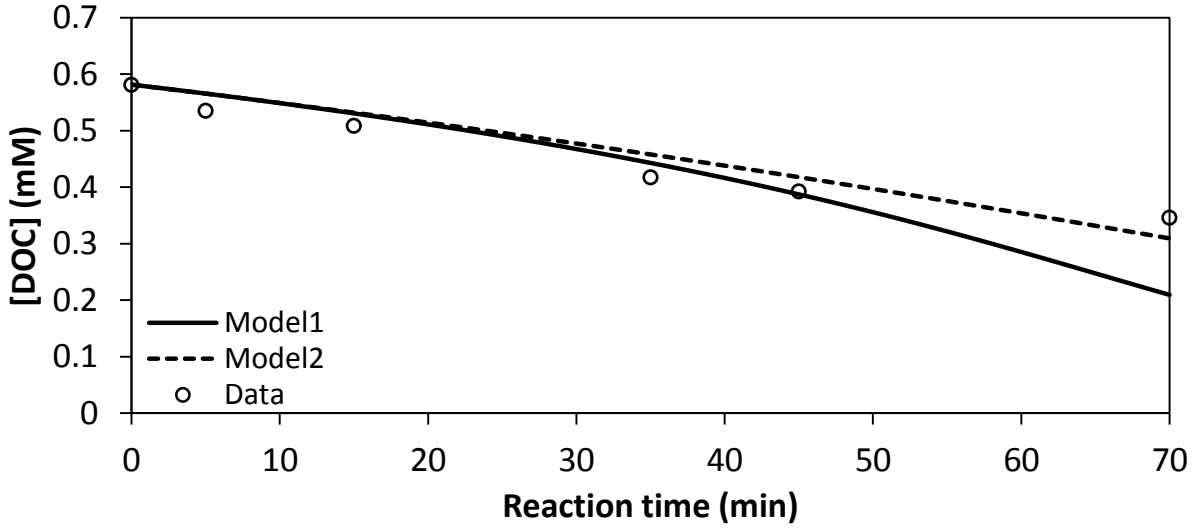

Figure 8.3: Measured and predicted DOC after calibration of models 1 and 2

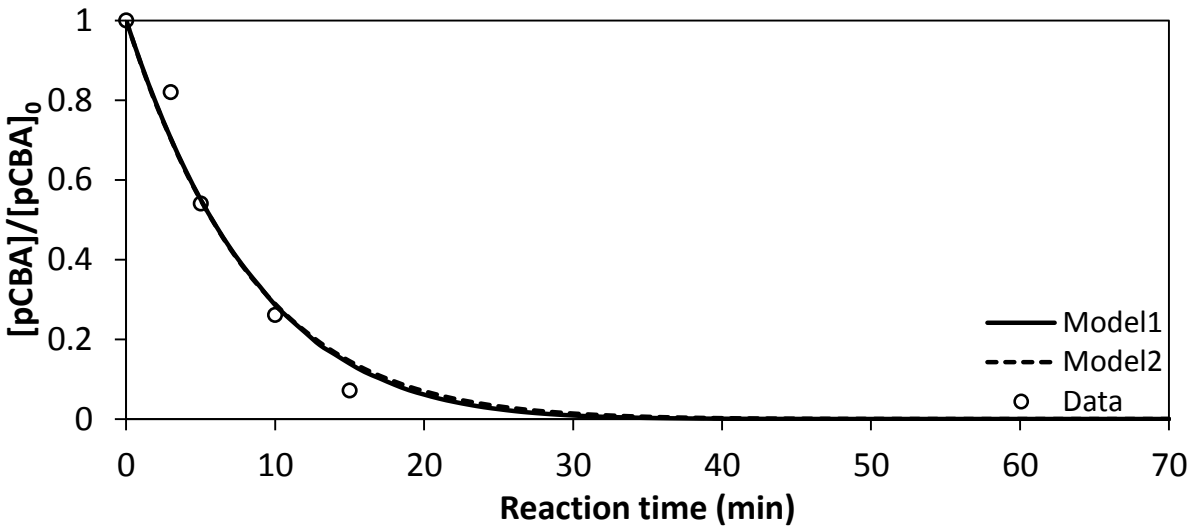

Figure 8.4: Measured and predicted pCBA removal after calibration of models 1 and 2

For model 2, k_{19} and Y_{DOC} were estimated to be 8.73×10^5 M^{-1} s^{-1} and 0.26 M M^{-1}, respectively. The value found for k_{19} is two orders of magnitude lower than conventional values for EfOM. Values in the order of $2\text{-}12 \times 10^8$ M^{-1} s^{-1} have been reported (Rosario-Ortiz et al., 2008). Possibly, side reactions or compounds that were not included in the model structure were the underlying reason for this discrepancy. It is well established that a fraction of the organic content acts as a promotor of the chain by producing superoxide radicals upon reaction with $HO^{\bullet}$, as shown in Figure 2.7. However, the importance of superoxide radicals for the production of $HO^{\bullet}$ during the UV/H_2O_2 process is much less important than during ozonation. A sensitivity analysis revealed that parameters involving superoxide radical reactions do not significantly impact the $HO^{\bullet}$ concentration (Audenaert et al., 2011). The reason of the unexpected result remains unclear.

As shown in Figure 1.5, satisfactory predictions of the hydrogen peroxide concentration were obtained. Hence, the measured irradiance and optical path length were determined correctly.

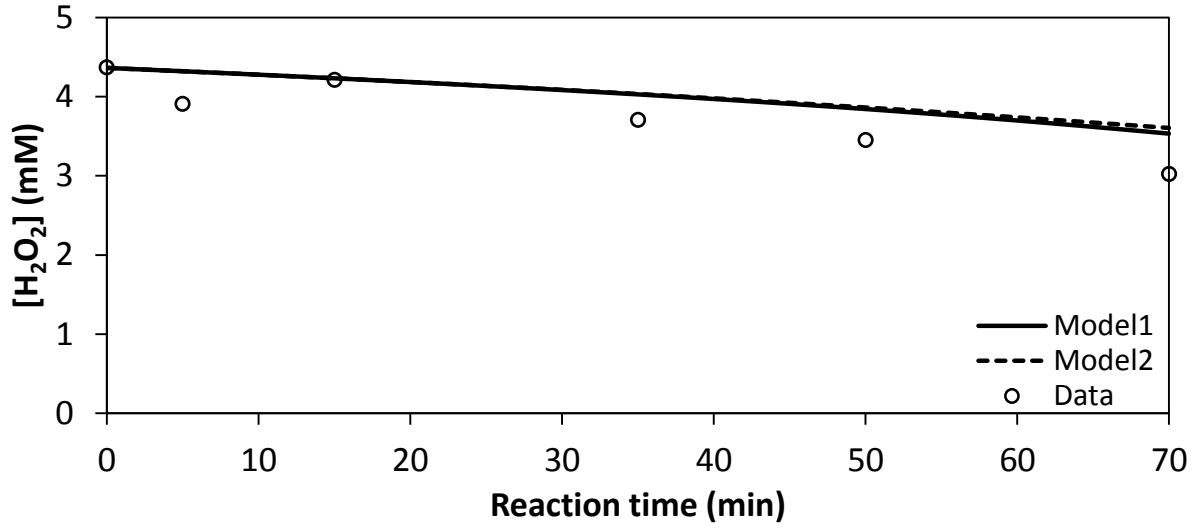

Figure 8.5: Measured and predicted H_2O_2 concentration after calibration of models 1 and 2

8.3.2 Validation

As shown in Figure 8.1b, validation results for pCBA and UV_{310} were less satisfactory. Results for UV_{310} and pCBA are shown in Figures 8.6 and 8.7, respectively. A severe over prediction of the pCBA decay rate for both models occurred. In contrast, UV_{310} removal was under predicted. Apparently, the estimated rate constants for $HO^{\bullet}$ scavenging were too low to allow a satisfactory prediction. As mentioned in Section 8.3.1, the estimated value of k_{19} was lower than expected, but the reason remained unclear. Most likely, the poor fits were caused by dynamics in EfOM properties that were not included in the model. Recalibration of model 1 significantly improved the agreement between experimental and predicted data (Figures 8.6 and 8.7). Values of respectively 0.09 M^{-1} cm^{-1} and 2.64 $x10^7$ cm s^{-1} were obtained for the stoichiometric factor Y_{UV310} and for k_{16} after recalibration. Especially the value of k_{16} significantly differed from that obtained after calibration using Sample 2 (as described earlier). Paradoxically, the modelling of the full-scale UV/H_2O_2 reactor as described in Chapter 6 was more successful than this modelling exercise although the latter was performed at well-defined lab-scale conditions. The waters that were used in both studies, however, differed significantly. In the full-scale case, the treated water was surface water-like, rather than having the properties of secondary effluent. Hence, the dynamics of the organic content were expected to be less severe compared to the secondary effluent studies here.

As opposed to the other concentrations, the hydrogen peroxide concentration could be satisfactorily predicted as shown in Figure 8.8. This species, however, is

predicted using a well-established photochemical rate law and its concentration is almost not affected by the other compounds.

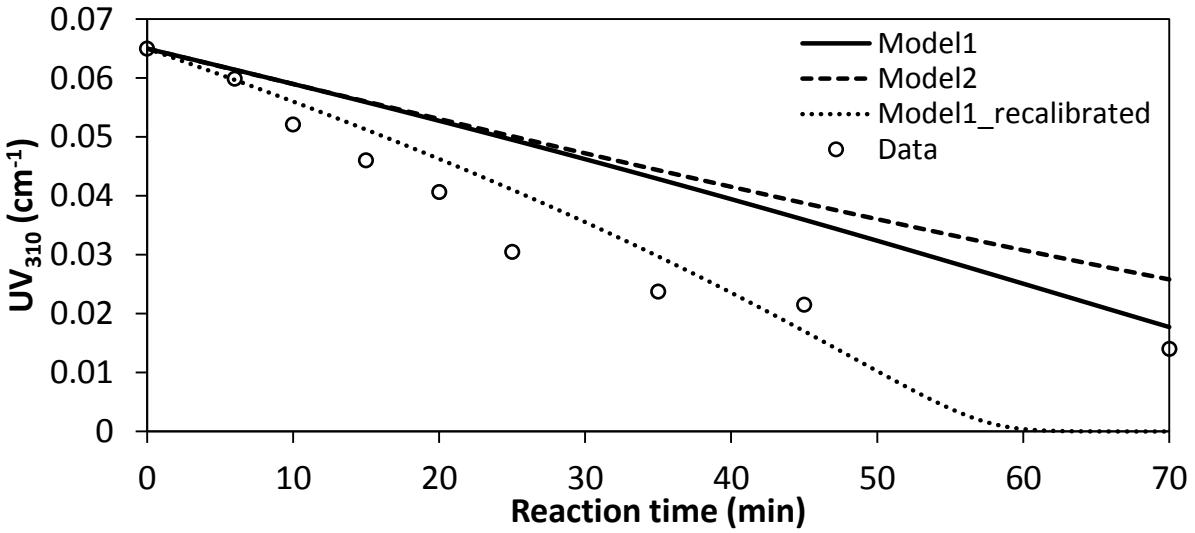

Figure 8.6: Measured and predicted UV_{310} during validation of models 1 and 2; dotted line was obtained after recalibration of model 1

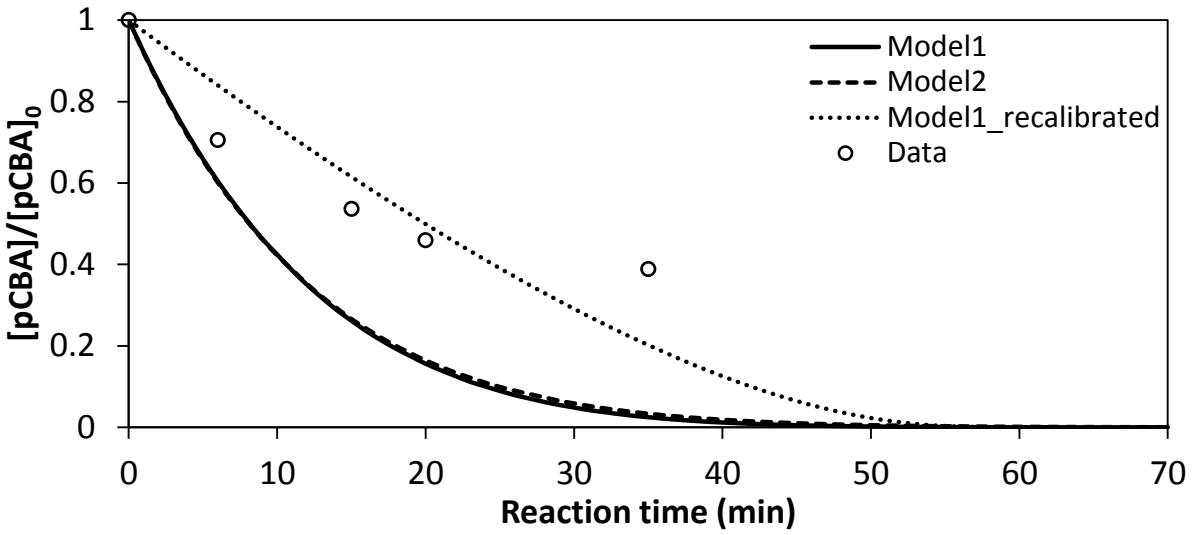

Figure 8.7: Measured and predicted pCBA removal during validation of models 1 and 2; dotted line was obtained after recalibration of model 1

Concentrations of the intermediate radical species during the validation run are depicted in Figure 8.9. The $HO^{\bullet}$ concentration initially varied around $3x10^{-13}$ M and slightly increased with a decreasing EfOM scavenging rate. The final concentrations were around $1x10^{-12}$ and $5x10^{-13}$ M for model 1 and 2, respectively. The concentrations of the radical species were in the same order of magnitude than those found in another simulation study (Song et al., 2008).

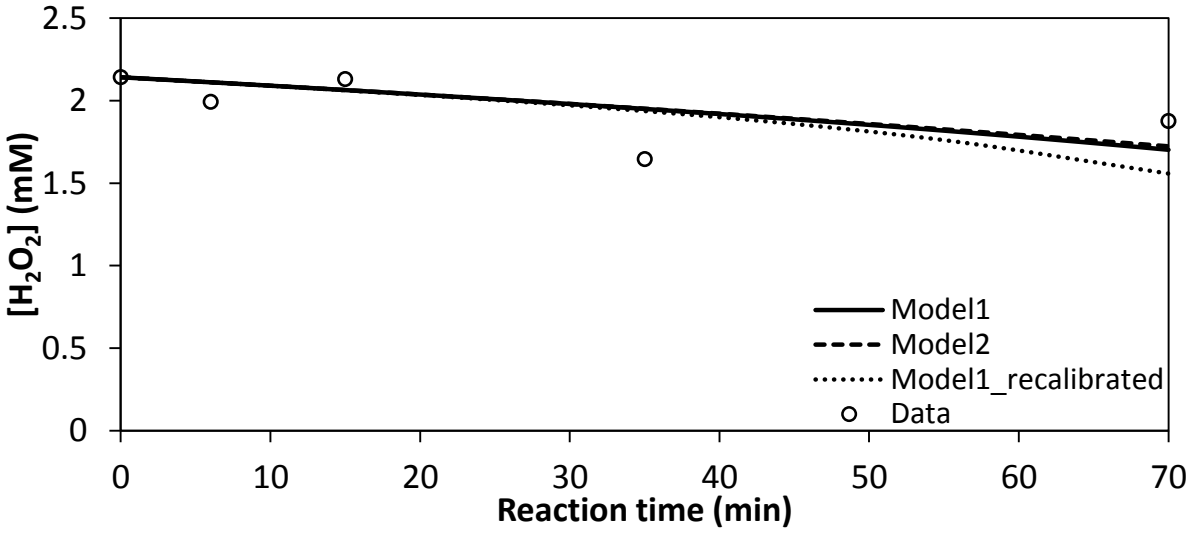

Figure 8.8: Measured and predicted H_2O_2 concentration during validation of models 1 and 2; dotted line was obtained after recalibration of model 1

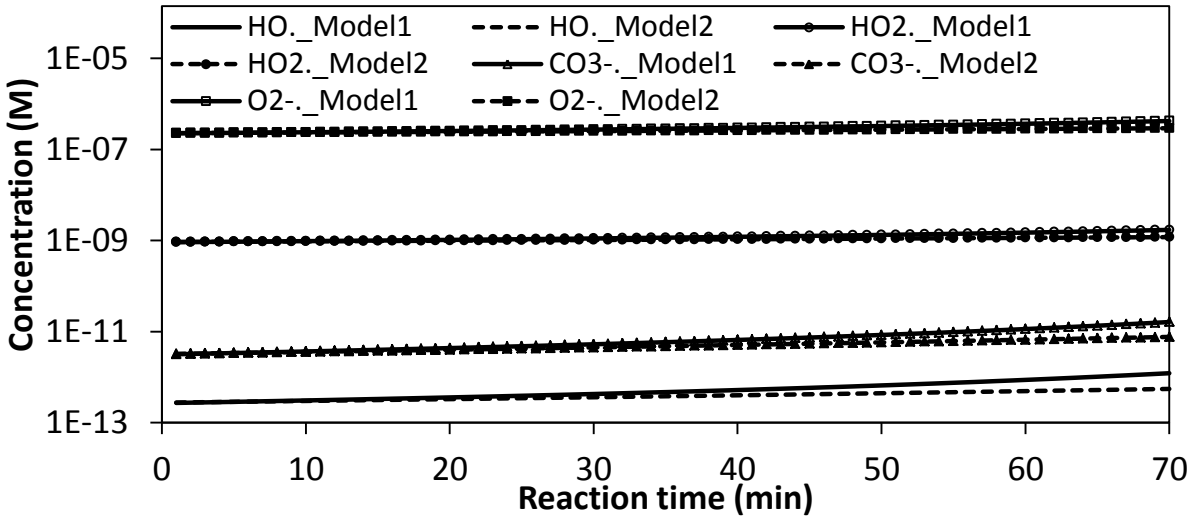

Figure 8.9: Calculated concentrations of the intermediate radical species for both models; y-axis with logarithmic scale

8.4 Conclusions

Two slightly different kinetic UV/H_2O_2 models were successfully calibrated. However, only poor fits were obtained between experimental and simulated values of UV_{310} and pCBA during model validation. This was not the case for hydrogen peroxide decay, which could be satisfactorily predicted. Most likely, the variable character of EfOM severely impeded the modelling exercise. Model-based description of secondary effluent treatment was found to be much more difficult

compared to the modelling of natural water oxidation. The current model structure did not allow for reliable prediction of the $HO^{\bullet}$ exposure. More research should be conducted to extend the model in order to predict UV/H_2O_2 treatment of secondary treated municipal effluent. Alternatively, possible extensions of the $R_{OH,UV}$ concept (described in Chapter 2) should be investigated.

Chapter 9

Conclusions and perspectives

In this PhD dissertation, ozonation and UV/H_2O_2 treatment were studied at various process conditions by a combination of practical experimentation and mathematical modelling. Different mechanistic models were analysed, extended, calibrated and validated using data that was collected both at full-scale and lab-scale. This chapter contains the main conclusions from this work and highlights some opportunities and perspectives for future research.

9.1 General conclusions

9.1.1 Mechanistic modelling of ozonation and UV/H_2O_2 treatment of non-synthetic water

Kinetic models for ozonation and UV/H_2O_2 treatment were applied to systems treating water with various characteristics. A relatively simple kinetic model for drinking water ozonation was developed and successfully calibrated using a full-scale ozone reactor (Chapter 3). Although the available dataset did not allow for extensive validation, the model showed to have the potential for prediction of ozone decomposition, disinfection, bromate formation and oxidation of the unsaturated part of DOM. By means of a scenario analysis, the effect of the applied ozone concentration and flow rate on certain key variables was evaluated.

An extensive UV/H_2O_2 model was calibrated and validated using two significantly different waters. In a first case (Chapter 6), the model was applied to a full-scale UV/H_2O_2 reactor for horticultural water reuse. Although primary and secondary treatment steps preceded the AOP, the water to be oxidized exhibited the properties of surface water, rather than those of secondary effluent. The model was successfully calibrated and validated at different operational conditions and was able to describe the residual hydrogen peroxide concentration, DOM conversions in terms of UV_{310} and acid formation resulting in pH drops. A sensitivity analysis

revealed that the UV/H_2O_2 process was highly affected by just a fraction of the operational and chemical parameters. In the second case (Chapter 8), the model was used to describe tertiary treatment of secondary effluent originating from a WWTP. In addition, a slightly modified model structure was tested incorporating $HO^{\bullet}$ scavenging by DOC. Despite the fact that model calibration and validation were performed at well-controlled lab-scale conditions, model validation was not satisfactory for both models due to a high deviation between the measured and calculated $HO^{\bullet}$ concentration. Only for the hydrogen peroxide concentration (which was calculated using a well-established photochemical rate law) good agreements between experimental and calculated values were obtained.

9.1.2 How DOM impacts the modelling exercise

During the application of the ozonation and UV/H_2O_2 models at full-scale (Chapters 4 and 6), sensitivity analyses revealed that parameters related to DOM were of main importance. Both the UV absorption and $HO^{\bullet}$ scavenging by DOM significantly impacted the UV/H_2O_2 process whereas direct ozone consumption severely affected the process of natural water ozonation. Additionally, a theoretical study of an ozone decomposition model extended with elementary reactions of DOM (Chapter 5) showed that ozone and $HO^{\bullet}$ concentrations were very sensitive to the parameters associated with those reactions. The degree of sensitivity was highly dependent on the level of DOM that was present.

The sensitivity of the model output to properties of DOM has some important implications. If the part of the model structure that contains the pathways of DOM is not well defined and/or contains parameters with uncertain values, slight variations in the water composition can lead to a drastic deterioration of the model performance, even though an extensive inorganic reaction scheme is included. As such, model-based description of secondary effluent treatment was found to be much more difficult compared to the modelling of natural water oxidation. The composition of EfOM is highly variable and depends on the dynamics of the influent entering the WWTP. Additionally, typical DOC values of secondary effluent are higher than those of natural water which implies that EfOM will affect the process to a larger extent. Although the $HO^{\bullet}$ production rate was known, the structure of the UV/H_2O_2 model used in Chapter 8 was not able to capture the changes in $HO^{\bullet}$ scavenging rate and hence, only poor predictions were obtained during validation. Model based description of secondary effluent ozonation would become even more difficult as besides the scavenging rate, the $HO^{\bullet}$ production rate varies as well (as shown in Chapter 7).

Hence, the DOM reaction scheme of future mechanistic models should be extended in order to acquire models that are widely applicable. On the other hand, to balance the model complexity, a simplification of the inorganic reaction scheme should be considered. As shown in Chapter 5, it is questionable if reactions involving inorganic carbon should be included when DOM levels are sufficiently high. Additionally, some dissociation reactions might be discarded if the model is used within a predefined pH range. Sensitivity analysis can be of great value in this context as it indicates insensitive model parameters. Additionally, the sensitivity output provides information that can be valuable in process engineering as the most important parameters are determined (Chapters 4 to 6).

9.1.3 The use of DOM surrogates in mathematical models

Models to be practically applied must include one or more surrogates for DOM that (1) allow for accurate prediction of the oxidant exposure and (2) can be readily measured (preferably on-line). Absorbance measurements (UV and/or visible range) have shown to meet these requirements very well. All models in this study that were applied to real water matrices included the absorption coefficient at a fixed UV wavelength (UV_{254} or UV_{310}). As stated in Chapters 4 and 6, the UV absorption coefficient is a promising variable for the application of model-based control and optimization strategies as it can be determined on-line and consequently a huge amount of real-time and accurate data are available. In contrast to e.g. DOC, spectral measurements clearly reflect the progress of oxidation as visible changes occur even at limited oxidant doses. During ozonation of secondary effluent, UV_{254} was found to be strongly correlated to $HO^{\bullet}$ production (Chapter 7). A disadvantage of these fixed-wavelength measurements however, is the limited information they provide regarding the reactivity and/or concentration of DOM as mainly chromophoric moieties of DOM are detected. The use of multi-wavelength spectral measurements can be an answer to this shortcoming. Although more research has to be conducted, the application of differential absorbance spectra can be regarded as promising for the model-based description of ozonation or UV/H_2O_2 treatment of complex matrices such as secondary effluent (Chapter 7).

9.1.4 Comparison of ozone and $HO^{\bullet}$ induced conversion of EfOM

In Chapter 7, the impact of ozonation and UV/H_2O_2 treatment on the properties of EfOM was experimentally examined. During both processes, more oxygen rich, less hydrophobic and more biodegradable transformation products were formed. However, differential absorbance spectra and absorbance slope indexes could be used to unravel some mechanistic differences between ozone and $HO^{\bullet}$ induced

transformation of EfOM. Ozone preferentially reacted with compounds absorbing at higher wavelengths, while during the UV/H_2O_2 process more uniform spectral changes were observed. Additionally, the absorption of transformation products impacted the spectral results for both oxidation techniques differently.

Ozonation of secondary effluent inherently led to significant $HO^{\bullet}$ production as a result of electron transfers between ozone and electron rich moieties of EfOM. $HO^{\bullet}$ production increased as function of ozone dose as most likely, an increased degree of hydroxylation positively impacted the $HO^{\bullet}$ yield of EfOM. During the UV based process, pseudo steady-state behaviour of the $HO^{\bullet}$ concentration was observed.

9.2 Perspectives and opportunities for future research

This PhD thesis provided insight on the mechanisms and modelling of ozonation and UV/H_2O_2 treatment of real and hence, complex water matrices. Especially in the case of secondary effluent oxidation, the system complexity restricts model development severely. Hence, future research should aim to broaden the knowledge in order to facilitate and optimize full-scale application of these advanced treatment techniques. Some issues that were found valuable to be covered by future research can be defined as follows:

- At present, no suitable mechanistic models exist to describe ozone or UV/H_2O_2 treatment of secondary effluent. With the number of full-scale applications expected to grow at a fast rate, research should focus on the development of models that can be of help to optimize process design, control and operation. Especially predictions with respect to oxidant production and consumption rates should be improved. In parallel, possible extensions of semi-empirical concepts developed for natural water oxidation should be investigated. Examples are the R_{CT} and $R_{OH,UV}$ concepts for ozonation and UV/H_2O_2 processes, respectively.
  Besides an improvement of the model structure, future models should also include cost calculation to allow for cost-optimization.

- Further experimental and modelling studies at full-scale plants will provide information that is not available at lab-scale. Data collection and sampling at existing full-scale plants can be of great value in this context. Parallel lab-scale studies with samples collected at the plants under study will provide detailed kinetic information.

- The conversion of trace pollutants from various classes and with diverse properties should be further assessed. Appropriate analytical methods will allow for accurate and sensitive determination of the concentrations of these compounds. These data are of vital importance for calibration and validation of both mechanistic and empirical models in future.

- The search for surrogate variables that allow for real-time prediction of trace pollutant conversion should continue. At present, on-line absorbance (UV or color) and fluorescence measurements are regarded as most promising candidates. The use of multi-wavelength data in combination with data reduction techniques such as principal components analysis may be of value to cope with the complexity of the systems. Only if proper surrogates are available, effective control strategies can be developed.

- Literature includes numerous "single-component" studies that provide detailed information on decay mechanisms of target compounds during oxidative treatment. However, the number of studies in which real (multicomponent) water matrices were treated is still very scarce. More of such studies are needed in order to increase the knowledge on the complex mechanisms that are occurring. Experiments with samples collected at different locations, times, weather conditions, operational settings,… should be included.

- AOPs are seldom used as stand-alone techniques and hence, are mostly part of a treatment train consisting of multiple unit processes. As each treatment step impacts the downstream processes, it is essential to gather knowledge on the relation between the individual steps. As such, studies should be conducted in which the whole treatment train is considered, rather than one separate unit. This will provide more knowledge on the interactions taking place and might allow the development of an integrated modelling framework that accounts for each individual step. Eventually, this can also open perspectives for control at the treatment train level.

- Currently, a clear knowledge gap in literature is related to the transformation products that are formed during oxidation. Especially information on their precursors, formation pathways, toxicity and potential degradation by downstream processes (e.g. BGAC) is limiting. In order to get oxidation techniques generally accepted, this issue should be properly addressed by

future research. Additionally, the development of monitoring techniques by rapid (or on-line) toxicity assays is a valuable research topic.

- Researchers and plant operators must be encouraged to exchange their experiences in the field and especially those related to full-scale applications. Currently, no clear framework exists for the design of full-scale plants and information related to the existing facilities is not readily available. A more dense cooperation between science and practice will contribute to improved process design.

Bibliography

APHA, 1992. Standard Methods for the Examination of Water and Wastewater. APHA, New York.

Aiken, G.R., McKnight, D.M., Thorn, K.A., Thurman, E.M., 1992. Isolation of Hydrophilic Organic Acids from Water Using Nonionic Macroporous Resins. Organic Geochemistry 18, 567–573.

Alpert, S.M., Knappe, D.R.U., Ducoste, J.J., 2010. Modeling the UV/hydrogen peroxide advanced oxidation process using computational fluid dynamics. Water Research 44, 1797–1808.

Audenaert, W.T.M., Callewaert, M., Nopens, I., Cromphout, J., Vanhoucke, R., Dumoulin, A., Dejans, P., Van Hulle, S.W.H., 2010. Full-scale modelling of an ozone reactor for drinking water treatment. Chemical Engineering Journal 157, 551–557.

Audenaert, W.T.M., Vermeersch, Y., Van Hulle, S.W.H., Dejans, P., Dumoulin, A., Nopens, I., 2011. Application of a mechanistic UV/hydrogen peroxide model at full-scale: Sensitivity analysis, calibration and performance evaluation. Chemical Engineering Journal 171, 113–126.

Bader, H., Hoigne, J., 1981. Determination of Ozone in Water by the Indigo Method. Water Research 15, 449–456.

Baxendale, J.H., Wilson, J.A., 1957. The Photolysis of Hydrogen Peroxide at High Light Intensities. Transactions of the Faraday Society 53, 344–356.

Belhateche, D., Symons, J.M., 1991. Using Cobalt Ultraviolet Spectrophotometry to Measure Hydrogen Peroxide Concentration in Organically Laden Groundwaters. Journal American Water Works Association 83, 70–73.

Beltrán, F.J., Gonzalez, M., Gonzalez, J.F., 1997. Industrial wastewater advanced oxidation. 1. UV radiation in the presence and absence of hydrogen peroxide. Water Research 31, 2405–2414.

Beltrán, F.J., 2004. Ozone Reaction Kinetics for Water and Wastewater Systems. CRC Press, Florida, USA.

Bezbarua, B.K., Reckhow, D.A., 2004. Modification of the standard neutral ozone decomposition model. Ozone-Science & Engineering 26, 345–357.

Bielski, B.H.J., Cabelli, D.E., Arudi, R.L., Ross, A.B., 1985. Reactivity of HO2/O-2 Radicals in Aqueous Solution. Journal of Physical and Chemical Reference Data 14, 1041–1100.

Bolle, F.W., Pinnekamp, J., 2011. Final report ENVELOS Project: Energiebedarf von Verfahren zur Elimination von organischen Spurenstoffen - Phase I, Report to the Ministry of Environment North-Rhine Westphalia. RWTH Aachen, Germany.

Bolton, J.R., Linden, K.G., 2003. Standardization of Methods for Fluence (UV Dose) Determination in Bench-Scale UV Experiments. Journal of Environmental Engineering 129, 209–215.

Boucherie, C., Lecarpentier, C., Fauchon, N., Djaferand, M., Heim, V., 2009. "Ozone" and "GAC Filtration" synergy for emerging micropollutants removal on Drinking Water Treatment Plant? In: Sievers, M., Geissen, S., Schäfer, S., Kragert, B., Niedermeiser, M. (Ed.), Proc. 5th IWA International Conference/10th IOA-EA3G Conference on Oxidation Technologies for Water and Wastewater Treatment, March 30-April 2, 2009. CUTEC, Berlin, Germany.

Braslavsky, S.E., 2007. Glossary of terms used in Photochemistry 3rd Edition (IUPAC Recommendations 2006). Pure and Applied Chemistry 79, 293–465.

Buchanan, W., Roddick, F., Porter, N., Drikas, M., 2005. Fractionation of UV and VUV pretreated natural organic matter from drinking water. Environmental Science & Technology 39, 4647–4654.

Buffle, M.O., von Gunten, U., 2006. Phenols and amine induced HO center dot generation during the initial phase of natural water ozonation. Environmental Science & Technology 40, 3057–3063.

Buffle, M.O., Schumacher, J., Meylan, S., Jekel, M., von Gunten, U., 2006a. Ozonation and advanced oxidation of wastewater: Effect of O-3 dose, pH, DOM and HO center dot-scavengers on ozone decomposition and HO center dot generation. Ozone-Science & Engineering 28, 247–259.

Buffle, M.O., Schumacher, J., Salhi, E., Jekel, M., von Gunten, U., 2006b. Measurement of the initial phase of ozone decomposition in water and wastewater by means of a continuous quench-flow system: Application to disinfection and pharmaceutical oxidation. Water Research 40, 1884–1894.

Buhler, R., Staehelin, J., Hoigne, J., 1984. Ozone Decomposition In Water Studied by Pulse-Radiolysis. 1. HO2/O2- and HO3/O3- as Intermediates. Journal of Physical Chemistry 88, 2560–2564.

Bukhari, Z., Hargy, T.M., Bolton, J.R., Dussert, B., Clancy, J.L., 1999. Medium-pressure UV for oocyst inactivation. Journal American Water Works Association 91, 86–94.

Buxton, G.V., Greenstock, C.L., Helman, W.P., Ross, A.B., 1988. Critical Review of Rate Constants for Reactions of Hydrated Electrons, Hydrogen Atoms and Hydroxyl Radicals (.OH/.O-) in Aqueous Solution. Journal of Physical and Chemical Reference Data 17, 513–886.

Böhme, A., 1999. Ozone Technology of German Industrial Enterprises. Ozone: Science & Engineering 21, 163–176.

CRMWD, 2009. Colorado River Municipal Water District Water Conservation and Drought Contingency Plan, http://www.crmwd.org/final_wcdc_8.24.09.pdf, website accessed: July 2012.

Campbell, A.T., Robertson, L.J., Snowball, M.R., Smith, H.V., 1995. Inactivation of Oocysts of Cryptosporidium Parvum by Ultraviolet Irradiation. Water Research 29, 2583–2586.

Chow, C.W.K., Fabris, R., Drikas, M., 2004. A rapid fractionation technique to characterise natural organic matter for the optimisation of water treatment processes. Journal of Water Supply Research and Technology-Aqua 53, 85–92.

Chow, C.W.K., Fabris, R., van Leeuwen, J., Wang, D.S., Drikas, M., 2008. Assessing natural organic matter treatability using high performance size exclusion chromatography. Environmental Science & Technology 42, 6683–6689.

Christensen, H., Sehested, K., Corfitzen, H., 1982. Reactions of Hydroxyl Radicals with Hydrogen Peroxide at Ambient and Elevated Temperatures. Journal of Physical Chemistry 86, 1588–1590.

Clancy, J.L., Bukhari, Z., Hargy, T.M., Bolton, J.R., Dussert, B.W., Marshall, M.M., 2000. Using UV to inactivate Cryptosporidium. Journal American Water Works Association 92, 97–104.

Comninellis, C., Kapalka, A., Malato, S., Parsons, S.A., Poulios, I., Mantzavinos, D., 2008. Advanced oxidation processes for water treatment: advances and trends for R&D. Journal of Chemical Technology & Biotechnology 83, 769–776.

Couriermail, 2008. Courier Mail on-line news, http://www.couriermail.com.au/news/features/bligh-d, website accessed: July 2012.

Crittenden, J.C., Hu, S.M., Hand, D.W., Green, S.A., 1999. A kinetic model for the H2O2/UV process in a completely mixed batch reactor. Water Research 33, 2315–2328.

Crittenden, J.C., Trussell, R.R., Hand, D.W., Howe, K.J., Tchobanoglous, G., 2005. Water Treatment Principles and Design. John Wiley and Sons, Hoboken, USA.

Cromphout, J., Vanhoucke, R., 2008. Reduction of exploitation costs and improvement of water quality by the implementation of Ozonization at the Waterworks in Kluizen. In: Proc. IOA-EA3G-VIVAQUA International Conference on Ozone and related oxidants in advanced treatment of water for human health and environmental protection - Disinfection, elimination of persistant pollutants and control of by-products, May 15-16, 2008. Brussels, Belgium.

Cromphout, J., Walraevens, E., Vanhoucke, R., 2005. Improvement of Water Quality in the Drinking Water Plant of Kluizen by the use of Ozone in Combination with GAC. Tribune de L'Eau 58, 15–18.

Daughton, C.G., Ternes, T.A., 1999. Pharmaceuticals and personal care products in the environment: Agents of subtle change? Environmental Health Perspectives 107, 907–938.

Dickenson, E.R.V., Drewes, J.E., Sedlak, D.L., Wert, E.C., Snyder, S.A., 2009. Applying Surrogates and Indicators to Assess Removal Efficiency of Trace Organic Chemicals during Chemical Oxidation of Wastewaters. Environmental Science & Technology 43, 6242–6247.

Domenjoud, B., Cortes-Francisco, N., Guastalli, A.R., Caixach, J., Esplugas, S., Baig, S., 2011a. Ozonation of Municipal Secondary Effluent; Removal of Hazardous Micropollutants and Related Changes of Organic Matter Composition. Journal of Advanced Oxidation Technologies 14, 138–146.

Domenjoud, B., Tatari, C., Esplugas, S., Baig, S., 2011b. Ozone-Based Processes Applied to Municipal Secondary Effluents. Ozone-Science & Engineering 33, 243–249.

Drewes, J.E., Reinhard, M., Fox, P., 2003. Comparing microfiltration-reverse osmosis and soil-aquifer treatment for indirect potable reuse of water. Water Research 37, 3612–3621.

Drouiche, M., Lounici, H., Mameri, N., Piron, D.L., Kharroune, M., 2001. Utilisation of factorial experiments for the UV/H2O2 process in a batch reactor. Water SA 27, 551–557.

Drury, D.D., Snyder, S.A., 2007. Use of Ozone for Disinfection and EDC Removal at CCWRD, http://www.acecindiana.org/content/Presentations/EBC07-O, website accessed: July 2012.

EPA, 2006. National Primary Drinking Water Regulations: Stage 2 Disinfectants and Disinfection Byproducts Rule. Federal Register 71.

EPA, 2011. United States Environmental Protection Agency, http://www.epa.gov/superfund/accomp/success/sangabriel.htm, website accessed: July 2012.

Einschlag, F.G., Feliz, M.R., Capparelli, A.L., 1997. Effect of temperature on hydrogen peroxide photolysis in aqueous solutions. Journal of Photochemistry and Photobiology A: Chemistry 110, 235–242.

Elovitz, M.S., von Gunten, U., 1999. Hydroxyl radical ozone ratios during ozonation processes. I-The R-ct concept. Ozone-Science & Engineering 21, 239–260.

Eriksen, T.E., Lind, J., Merenyi, G., 1985. On the Acid-Base Equilibrium of the Carbonate Radical. Radiation Physics and Chemistry 26, 197–199.

Fabian, I., 2006. Reactive intermediates in aqueous ozone decomposition: A mechanistic approach. Pure and Applied Chemistry 78, 1559–1570.

Froment, G.F., Bischoff, K.B., 1990. Chemical Reactor Analysis and Design. John Wiley & Sons, New York.

Geering, F., 1999. Ozone Applications: The State-of-the-Art in Switzerland. Ozone: Science & Engineering 21, 187–200.

Van Geluwe, S., Braeken, L., Van der Bruggen, B., 2011. Ozone oxidation for the alleviation of membrane fouling by natural organic matter: A review. Water Research 45, 3551–3570.

Gerrity, D., Snyder, S., 2011. Review of Ozone for Water Reuse Applications: Toxicity, Regulations, and Trace Organic Contaminant Oxidation. Ozone: Science & Engineering 33, 253–266.

Glaze, W.H., Beltran, F., Tuhkanen, T., Kang, J.-W., 1992. Chemical Models of Advanced Oxidation Processes. Water Pollution Research Journal of Canada 27, 23–42.

Glaze, W.H., Lay, Y., Kang, J.W., 1995. Advanced Oxidation Processes - A Kinetic Model for the Oxidation of 1,2-Dibromo-3-Chloropropane in Water by the Combination of Hydrogen Peroxide and UV-Radiation. Industrial & Engineering Chemistry Research 34, 2314–2323.

Gong, J.L., Liu, Y.D., Sun, X.B., 2008. O-3 and UV/O-3 oxidation of organic constituents of biotreated municipal wastewater. Water Research 42, 1238–1244.

Gonzales, S., Pena, A., Rosario-Ortiz, F.L., 2012. Examining the Role of Effluent Organic Matter Components on the Decomposition of Ozone and Formation of Hydroxyl Radicals in Wastewater. Ozone-Science & Engineering 34, 42–48.

Grünebaum, T., 2011. Elimination von Arzneimitteln und organischen Spurenstoffen: Entwicklung von Konzeptionen und innovativen, kostengünstigen Reinigungsverfahren, Schlussbericht Phase 1: Elimination von Arzneimittelrückständen in kommunalen Kläranlagen, Report to the Ministry of Environment North-Rhine Westphalia. Ruhrverband Essen, Germany.

von Gunten, U., 2003a. Ozonation of drinking water: Part I. Oxidation kinetics and product formation. Water Research 37, 1443–1467.

von Gunten, U., 2003b. Ozonation of drinking water: Part II. Disinfection and by-product formation in presence of bromide, iodide or chlorine. Water Research 37, 1469–1487.

von Gunten, U., Hoigne, J., 1994. Bromate Formation during Ozonization of Bromide-Containing Waters: Interaction of Ozone and Hydroxyl Radical Reactions. Environmental Science & Technology 28, 1234–42.

Haag, W.R., Hoigne, J., 1983. Ozonation of bromide-containing waters: kinetics of formation of hypobromous acid and bromate. Environmental Science & Technology 17, 261–267.

Haltmeier, T., Pazhepurackel, V., 2012. BAFU Studie: Kosten der Elimination von Mikroverunreinigungen im Abwasser, Report to the Swiss Ministry of Environment. BG Consulting Engineers Bern, Switzerland.

Hatchard, C.G., Parker, C.A., 1956. A new sensitive chemical actinometer. 2. Potassium ferrioxalate as a standard chemical actinometer. Proceedings of the Royal Society A 235, 518–538.

Hauduc, H., Neumann, M.B., Muschalla, D., Gamerith, V., Gillot, S., Vanrolleghem, P.A., 2011. Towards quantitative quality criteria to evaluate simulation results in wastewater treatment – A critical review. In: Proc. 8th IWA Symposium on Systems Analysis and Integrated Assessment, WATERMATEX 2011. San Sebastian, Spain.

Heberer, T., 2002. Occurrence, fate, and removal of pharmaceutical residues in the aquatic environment: a review of recent research data. Toxicology Letters 131, 5–17.

van der Helm, A.W.C., 2007. Integrated modeling of ozonation for optimization of drinking water treatment. PhD thesis, Delft University of Technology.

van der Helm, A.W.C., Smeets, P.W.M.H., Baars, E.T., Rietveld, L.C., van Dijk, J.C., 2007. Modeling of Ozonation for Dissolved Ozone Dosing. Ozone: Science & Engineering 29, 379–389.

Hindmarsh, A.C., Petzold, L.R., 1995. Algorithms and software for ordinary differential equations and differential-algebraic equations. Computers in Physics 9, 148–155.

Hofman-Caris, C.H.M.R., Harmsen, D.J.H., Beerendonk, E.F., Knol, A.H., Metz, D.H., Wols, B.A., 2012. Prediction of Advanced Oxidation Performance in Pilot UV/H2O2 Reactor Systems with MP- and LP-UV Lamps. Ozone: Science & Engineering 34, 120–124.

Hong, A., Zappi, M.E., Kuo, C.H., Hill, D., 1996. Modeling kinetics of illuminated and dark advanced oxidation processes. Journal of Environmental Engineering-ASCE 122, 58–62.

Huang, T., Brouckaert, C., Pryor, M., 2004. Application of computational fluid dynamics modelling to an ozone contactor. Water SA 30, 51–56.

Huber, M.M., Gobel, A., Joss, A., Hermann, N., Loffler, D., McArdell, C.S., Ried, A., Siegrist, H., Ternes, T.A., von Gunten, U., 2005. Oxidation of pharmaceuticals during ozonation of municipal wastewater effluents: A pilot study. Environmental Science & Technology 39, 4290–4299.

Hunt, N.K., Mariñas, B.J., 1999. Inactivation of Escherichia coli with ozone: chemical and inactivation kinetics. Water Research 33, 2633–2641.

Ikehata, K., Jodeiri Naghashkar, N., Gamal El-Din, M., 2006. Degradation of Aqueous Pharmaceuticals by Ozonation and Advanced Oxidation Processes: A Review. Ozone: Science & Engineering 28, 353–414.

Jiménez, B., Cisneros, B.E.J., Asano, T., 2008. Water Reuse: An International Survey of Current Practice, Issues and Needs. IWA Scientific and Technical Report No. 20. IWA Publishing, London, UK.

KMI, 2012. Karakteristieken van Belgisch klimaat, http://www.meteo.be/meteo/view/nl/360361-Parameters.html#ppt_505710, website accessed: August 2012.

Klassen, N.V., Marchington, D., McGowan, H.C.E., 1994. H2O2 Determination by the I-3(-) Method and by KMNO4 Titration. Analytical Chemistry 66, 2921–2925.

Kletting, P., Glatting, G., 2009. Model selection for time-activity curves: the corrected Akaike information criterion and the F-test. Zeitschrift für Medizinische Physik 19, 200–206.

Kolpin, D.W., Furlong, E.T., Meyer, M.T., Thurman, E.M., Zaugg, S.D., Barber, L.B., Buxton, H.T., 2002. Pharmaceuticals, hormones, and other organic wastewater contaminants in US streams, 1999-2000: A national reconnaissance. Environmental Science & Technology 36, 1202–1211.

Korshin, G., Chow, C.W.X., Fabris, R., Drikas, M., 2009. Absorbance spectroscopy-based examination of effects of coagulation on the reactivity of fractions of natural organic matter with varying apparent molecular weights. Water Research 43, 1541–1548.

Kralik, P., Kusic, H., Koprivanac, N., Bozic, A.L., 2010. Degradation of chlorinated hydrocarbons by UV/H2O2: The application of experimental design and kinetic modeling approach. Chemical Engineering Journal 158, 154–166.

Krasner, S.W., Westerhoff, P., Chen, B., Rittmann, B.E., Amy, G., 2009. Occurrence of Disinfection Byproducts in United States Wastewater Treatment Plant Effluents. Environmental Science & Technology 43, 8320–8325.

Kruithof, J.C., Kamp, P.C., Martijn, B.J., 2007. UV/H2O2 treatment: A practical solution for organic contaminant control and primary disinfection. Ozone-Science & Engineering 29, 273–280.

Kruithof, J.C., Masschelein, W.J., 1999. State-of-the-Art of the Application of Ozonation in BENELUX Drinking Water Treatment. Ozone: Science & Engineering 21, 139–152.

Kumar, R., Bose, P., 2004. Development and experimental validation of the model of a continuous-flow countercurrent ozone contactor. Industrial & Engineering Chemistry Research 43, 1418–1429.

Lamsal, R., Walsh, M.E., Gagnon, G.A., 2011. Comparison of advanced oxidation processes for the removal of natural organic matter. Water Research 45, 3263–3269.

Larocque, R.L., 1999. Ozone Applications In Canada A State of the Art Review. Ozone: Science & Engineering 21, 119–125.

Leach, M., Festger, A., Royce, A., Williamson, C., 2006. UV-Oxidation: Municipal Case Studies and New Applications. IUVA News 8, 11–16.

Li, K., Hokanson, D.R., Crittenden, J.C., Trussell, R.R., Minakata, D., 2008. Evaluating UV/H2O2 processes for methyl tert-butyl ether and tertiary butyl alcohol removal: Effect of pretreatment options and light sources. Water Research 42, 5045–5053.

Liao, C.H., Gurol, M.D., 1995. Chemical Oxidation by Photolytic Decomposition of Hydrogen Peroxide. Environmental Science & Technology 29, 3007–3014.

Linden, K.G., Sharpless, C.M., Andrews, S., Atasi, K., Korategere, V., Stefan, M., Suffet, I.H.M., 2005. Innovative UV Technologies to Oxidize Organic and Organoleptic Chemicals. IWA Publishing, London, UK.

Liu, W.J., Andrews, S.A., Stefan, M.I., Bolton, J.R., 2003. Optimal methods for quenching H2O2 residuals prior to UFC testing. Water Research 37, 3697–3703.

Liu, S., Lim, M., Fabris, R., Chow, C.W.K., Drikas, M., Korshin, G., Amal, R., 2010. Multi-wavelength spectroscopic and chromatography study on the photocatalytic oxidation of natural organic matter. Water Research 44, 2525–2532.

Loeb, B.L., Thompson, C.M., Drago, J., Takahara, H., Baig, S., 2012. Worldwide Ozone Capacity for Treatment of Drinking Water and Wastewater: A Review. Ozone: Science & Engineering 34, 64–77.

Lovato, M.E., Martin, C.A., Cassano, A.E., 2009. A reaction kinetic model for ozone decomposition in aqueous media valid for neutral and acidic pH. Chemical Engineering Journal 146, 486–497.

Lovato, M.E., Martín, C.A., Cassano, A.E., 2011. A reaction–reactor model for O3 and UVC radiation degradation of dichloroacetic acid: The kinetics of three parallel reactions. Chemical Engineering Journal 171, 474–489.

Lowndes, R., 1999. State of the Art for Ozone U.K. Experience. Ozone: Science & Engineering 21, 201–205.

Lucas, M.S., Peres, J.A., Li Puma, G., 2010. Treatment of winery wastewater by ozone-based advanced oxidation processes (O3, O3/UV and O3/UV/H2O2) in a pilot-scale bubble column reactor and process economics. Separation and Purification Technology 72, 235–241.

Malley, J.P., 2010. UV In Water Treatment: Issues for the Next Decade. IUVA News 12, 18–25.

Martijn, B.J., Kamp, P.C., Kruithof, J.C., 2008. UV/H2O2 Treatment: An Essential Barrier in a Multi Barrier Approach for Organic Contaminant Control. IUVA News 10, 12–19.

Masschelein, W.J., 2002. Ultraviolet Light in Water and Wastewater Sanitation. CRC Press, Boca Raton, Florida, USA.

Matsumoto, N., Watanabe, K., 1999. Foot Prints and Future Steps of Ozone Applications in Japan. Ozone: Science & Engineering 21, 127–138.

Mielcke, J., Ried, A., 2012. Removal of micro pollutants from municipal waste water – already “State of the art”? (A review on Europe’s activities). In: International Conference on Ozone and Related Oxidants to Meet Essential Human Needs - Uses for Agri-Food, Industry, Water and Health. International Ozone Association, Toulouse, France, 289–296.

MKULNV.NRW, 2012. Ozonierung und Aktivkohleadsorption in der Kläranlage Schwerte, project of Kompetenzzentrum Mikroschadstoffe.NRW, http://www.masterplan-wasser.nrw.de/data/files/588/20120425_Steckbrief_Schwerte.pdf, website accessed: July 2012.

Mohajerani, M., Mehrvar, M., Ein-Mozaffari, F., 2010. CFD Modeling of Metronidazole Degradation in Water by the UV/H2O2 Process in Single and Multilamp Photoreactors. Industrial & Engineering Chemistry Research 49, 5367–5382.

Mvula, E., von Sonntag, C., 2003. Ozonolysis of phenols in aqueous solution. Organic & Biomolecular Chemistry 1, 1749–1756.

Nanaboina, V., Korshin, G.V., 2010. Evolution of Absorbance Spectra of Ozonated Wastewater and Its Relationship with the Degradation of Trace-Level Organic Species. Environmental Science & Technology 44, 6130–6137.

Nelder, J.A., Mead, R., 1965. A Simplex Method for Function Minimization. The Computer Journal 7, 308–313.

Neta, P., Huie, R.E., Ross, A.B., 1988. Rate Constants for Reactions of Inorganic Radicals in Aqueous Solution. Journal of Physical and Chemical Reference Data 17, 1027–1284.

Neumann, M.B., Gujer, W., von Gunten, U., 2009. Global sensitivity analysis for model-based prediction of oxidative micropollutant transformation during drinking water treatment. Water Research 43, 997–1004.

Neyens, E., Baeyens, J., 2003. A review of classic Fenton's peroxidation as an advanced oxidation technique. Journal of Hazardous Materials 98, 33–50.

Noethe, T., Fahlenkamp, H., von Sonntag, C., 2009. Ozonation of Wastewater: Rate of Ozone Consumption and Hydroxyl Radical Yield. Environmental Science & Technology 43, 5990–5995.

Novak, N., Le Marechal, A.M., Bogataj, M., 2009. Determination of cost optimal operating conditions for decoloration and mineralization of C. I. Reactive Blue 268 by UV/H2O2 process. Chemical Engineering Journal 151, 209–219.

Oller, I., Malato, S., Sánchez-Pérez, J.A., 2011. Combination of Advanced Oxidation Processes and biological treatments for wastewater decontamination-a review. The Science of the total environment 409, 4141–4166.

Oneby, M.A., Bromley, C.O., Borchardt, J.H., Harrison, D.S., 2010. Ozone Treatment of Secondary Effluent at U.S. Municipal Wastewater Treatment Plants. Ozone: Science & Engineering 32, 43–55.

PWN, 2012. PWN Water Supply Company North Holland, http://www.mijnalbum.nl/Album=KVBQQDBI, website accessed: July 2012.

Parsons, S.A., 2004. Advanced Oxidation Processes for Water and Wastewater Treatment. IWA Publishing, London, UK.

Le Paulouë, J., Langlais, B., 1999. State-of-the-Art of Ozonation in France. Ozone: Science & Engineering 21, 153–162.

Pichat, P., 2012. A short overview of the state of the art and perspectives on the main basic factors hindering the development of photocatalytic treatments of water, In: 6th IWA Specialist Conference on oxidation technologies for water and wastewater treatment, Goslar, Germany.

Pignatello, J.J., Oliveros, E., MacKay, A., 2006. Advanced Oxidation Processes for Organic Contaminant Destruction Based on the Fenton Reaction and Related Chemistry. Critical Reviews in Environmental Science and Technology 36, 1–84.

Porter, R., 2010. Activities at the Gwinnett County F. Wayne Hill WRC to Utilize Less External Energy and Preserve a Watershed's Integriity, POTW workshop, Indiana, USA.

La Puente Valley County WD, 2010. La Puente Valley County Water District, http://www.lapuentewater.com/water-quality/water-treatment, website accessed: July 2012.

Ratpukdi, T., Rice, J.A., Chilom, G., Bezbaruah, A., Khan, E., 2009. Rapid Fractionation of Natural Organic Matter in Water Using a Novel Solid-Phase Extraction Technique. Water Environment Research 81, 2299–2308.

Ratpukdi, T., Siripattanakul, S., Khan, E., 2010. Mineralization and biodegradability enhancement of natural organic matter by ozone-VUV in comparison with ozone, VUV, ozone-UV, and UV: Effects of pH and ozone dose. Water Research 44, 3531–3543.

Reungoat, J., Escher, B.I., Macova, M., Argaud, F.X., Gernjak, W., Keller, J., 2012. Ozonation and biological activated carbon filtration of wastewater treatment plant effluents. Water Research 46, 863–872.

Rice, R.G., 1999. Ozone in the United States of America: State-Of-The-Art. Ozone: Science & Engineering 21, 99–118.

Ried, A., 2012. Ozone and its applications. In: International Conference on Ozone and Related Oxidants to Meet Essential Human Needs - Uses for Agri-Food, Industry, Water and Health. International Ozone Association, Toulouse, France, 19–20.

Ried, A., Mielcke, J., Wieland, A., 2009. The Potential Use of Ozone in Municipal Wastewater. Ozone: Science & Engineering 31, 415–421.

Rook, J.J., 1974. Formation of haloforms during chlorination of natural waters. J. Water Treatment Examination 23, 234–243.

Rosario-Ortiz, F.L., Mezyk, S.P., Wert, E.C., Doud, D.F.R., Singh, M.K., Xin, M., Baik, S., Snyder, S.A., 2008. Effect of ozone oxidation on the molecular and kinetic properties of effluent organic matter. Journal of Advanced Oxidation Technologies 11, 529–535.

Rosenfeldt, E.J., Linden, K.G., 2004. Degradation of endocrine disrupting chemicals bisphenol A, ethinyl estradiol, and estradiol during UV photolysis and advanced oxidation processes. Environmental Science & Technology 38, 5476–5483.

Rosenfeldt, E.J., Linden, K.G., 2007. The R-OH,R-UV concept to characterize and the model UV/H2O2 process in natural waters. Environmental Science & Technology 41, 2548–2553.

Roth, J.A., Sullivan, D.E., 1981. Solubility of ozone in water. Industrial & Engineering Chemistry Fundamentals 20, 137–140.

Rowe, L., 2009. A major project complete. Water Engineering Australia February, 18–25.

SERR/RESOC, 2007. RESOC-SERR Middle-West-Flanders, Region Pact 2007-2012.

SGVWater, 2010. San Gabriel Valley Water Company, http://www.sgvwater.com, website accessed: July 2012.

Sagehashi, M., Shiraishi, K., Fujita, H., Fujii, T., Sakoda, A., 2005. Ozone decomposition of 2-methylisoborneol (MIB) in adsorption phase on high silica zeolites with preventing bromate formation. Water Research 39, 2926–34.

Salari, D., Daneshvar, N., Aghazadeh, F., Khataee, A.R., 2005. Application of artificial neural networks for modeling of the treatment of wastewater contaminated with methyl tert-butyl ether (MTBE) by UV/H2O2 process. Journal of Hazardous Materials 125, 205–210.

Saltelli, A., Ratto, M., Tarantola, S., Campolongo, F., 2005. Sensitivity analysis for chemical models. Chemical Reviews 105, 2811–2827.

Sander, R., 1999. Compilation of Henry's Law Constants for Inorganic and Organic Species of Potential Importance in Environmental Chemistry.

Sarathy, S.R., Mohseni, M., 2006. An Overview of UV-based Advanced Oxidation Processes for Drinking Water Treatment. IUVA News 7, 16–27.

Savoye, P., Janex, M.L., Lazarova, V., 2001. Wastewater disinfection by low-pressure UV and ozone: a design approach based on water quality. Water Science and Technology 43, 163–171.

Schaar, H., Clara, M., Gans, O., Kreuzinger, N., 2010. Micropollutant removal during biological wastewater treatment and a subsequent ozonation step. Environmental pollution 158, 1399–404.

Sharif, F., Wang, J., Westerhoff, P., 2012. Transformation in Bulk and Trace Organics during Ozonation of Wastewater. Ozone-Science & Engineering 34, 26–31.

Sharpless, C.M., Linden, K.G., 2003. Experimental and model comparisons of low- and medium-pressure Hg lamps for the direct and H2O2 assisted UV photodegradation of N-nitrosodimethylamine in simulated drinking water. Environmental Science & Technology 37, 1933–1940.

Shon, H.K., Vigneswaran, S., Snyder, S.A., 2006. Effluent organic matter (EfOM) in wastewater: Constituents, effects, and treatment. Critical Reviews in Environmental Science and Technology 36, 327–374.

Sohn, J., Amy, G., Cho, J., Lee, Y., Yoon, Y., 2004. Disinfectant decay and disinfection by-products formation model development: chlorination and ozonation by-products. Water Research 38, 2461–2478.

Song, W., Ravindran, V., Pirbazari, M., 2008. Process optimization using a kinetic model for the ultraviolet radiation-hydrogen peroxide decomposition of natural and synthetic organic compounds in groundwater. Chemical Engineering Science 63, 3249–3270.

Staehelin, J., Buhler, R.E., Hoigne, J., 1984. Ozone Decomposition in Water Studied by Pulse-Radiolysis .2. OH and HO4 as Chain Intermediates. Journal of Physical Chemistry 88, 2560–2564.

Stefan, M.I., Hoy, A.R., Bolton, J.R., 1996. Kinetics and mechanism of the degradation and mineralization of acetone in dilute aqueous solution sensitized by the UV photolysis of hydrogen peroxide. Environmental Science & Technology 30, 2382–2390.

Swaim, P., Myers, A., Elliott, T., Voytko, L., Jacobs, B., Malley, J., 2011. UV: Not Just for Cryptosporidium Anymore. IUVA News 13, 18–24.

Swaim, P., Royce, A., Smith, T., Maloney, T., Ehlen, D., Carter, B., 2008. Effectiveness of UV advanced oxidation for destruction of micro-pollutants. Ozone-Science & Engineering 30, 34–42.

Theil, H., 1961. Economic Forecasts and Policy. North Holland Publishing Co, Amsterdam.

Tomiyasu, H., Fukutomi, H., Gordon, G., 1985. Kinetics and mechanism of ozone decomposition in basic aqueous solution. Inorganic Chemistry 24, 2962–2966.

Tripathi, S., Pathak, V., Tripathi, D.M., Tripathi, B.D., 2011. Application of ozone based treatments of secondary effluents. Bioresource Technology 102, 2481–2486.

TrojanUV, 2012. Trojan Technologies inc., http://www.trojanuv.com/solutions/municipal/ect, website accessed: July 2012.

Vanhooren, H., Meirlaen, J., Amerlinck, Y., Claeys, F., Vangheluwe, H., Vanrolleghem, P., 2003. WEST: Modelling biological wastewater treatment. Journal of Hydroinformatics 5, 27–50.

Van Hulle, S.W.H., Verstraete, J., Hogie, J., 2006. Modelling and simulation of a nitrification biofilter for drinking water purification. Water SA 32, 257–264.

VCWD, 2007. Valley County Water District, http://vcwd.org/water_comes_from.html, website accessed: July 2012.

WaterSecure, 2012. Queensland Manufactured Water Authority, http://www. watersecure.com.au/pub/what-we-do/water-purification, website accessed: July 2012.

WatertecEngineering, 2006. Ozone In The Water Reclamation Process At South Caboolture, Queensland, Australia, http://www.watertecengineering.com/Caboolture%20report%20-%20Watertec.pdf, website accessed: July 2012.

water-technology.net, 2011. water-technology.net. News, views and contacts from the global Water industry, http://www.water-technology.net/projects/bundamba-treatment/, website accessed: July 2012.

Weinstein, J., Bielski, B.H.J., 1979. Kinetics of the Interaction of HO2 and O2- Radicals with Hydrogen Peroxide - Haber-Weiss Reaction. Journal of the American Chemical Society 101, 58–62.

Weiss, J., 1935. Investigations on the radical HO2 in solution. Transactions of the Faraday Society 31, 668–681.

Werderitsch, M., 2009. Full Scale Advanced Oxidation Treatment Plant for Groundwater. In: Sievers, M., Geissen, S., Schäfer, S., Kragert, B., Niedermeiser, M. (Ed.), Proc. 5th IWA International Conference/10th IOA-EA3G Conference on Oxidation Technologies for Water and Wastewater Treatment, March 30-April 2 2009. CUTEC, Berlin, Germany.

Wert, E.C., Rosario-Ortiz, F.L., Drury, D.D., Snyder, S.A., 2007. Formation of oxidation byproducts from ozonation of wastewater. Water Research 41, 1481–1490.

Wert, E.C., Rosario-Ortiz, F.L., Snyder, S.A., 2009. Using Ultraviolet Absorbance and Color To Assess Pharmaceutical Oxidation during Ozonation of Wastewater. Environmental Science & Technology 43, 4858–4863.

West Basin MWD, 2011. West Basin Municipal Water District, http://www.westbasin.org/water-reliability-2020/recycled-water /current-projects, website accessed: July 2012.

Westerhoff, P., Aiken, G., Amy, G., Debroux, J., 1999. Relationships between the structure of natural organic matter and its reactivity towards molecular ozone and hydroxyl radicals. Water Research 33, 2265–2276.

Westerhoff, P., Mezyk, S.P., Cooper, W.J., Minakata, D., 2007. Electron pulse radiolysis determination of hydroxyl radical rate constants with Suwannee river fulvic acid and other dissolved organic matter isolates. Environmental Science & Technology 41, 4640–4646.

Westerhoff, P., Song, R., Amy, G., Minear, R., 1997. Applications of ozone decomposition models. Ozone-Science & Engineering 19, 55–73.

Wilke, C.R., Chang, P., 1955. Correlation of diffusion coefficients in dilute solutions. AIChE Journal 1, 264–270.

Wols, B.A., Hofman, J.A.M.H., Beerendonk, E.F., Uijttewaal, W.S.J., van Dijk, J.C., 2011. A systematic approach for the design of UV reactors using computational fluid dynamics. AIChE Journal 57, 193–207.

Wols, B.A., Hofman-Caris, C.H.M., 2012. Review of photochemical reaction constants of organic micropollutants required for UV advanced oxidation processes in water. Water Research 46, 2815–2827.

Wu, C.L., Linden, K.G., 2008. Degradation and byproduct formation of parathion in aqueous solutions by UV and UV/H2O2 treatment. Water Research 42, 4780–4790.

Xu, P., Janex, M.L., Savoye, P., Cockx, A., Lazarova, V., 2002. Wastewater disinfection by ozone: main parameters for process design. Water Research 36, 1043–1055.

Yamashita, H., Kaya, T., 2009. Outline and Problem of Reclaimed Water Supply Business in Tokyo. In: WEFTEC, the Water Environment Federation's Annual Technical Exhibition and Conference, Orlando, Florida, USA.

Zimmermann, S.G., Wittenwiler, M., Hollender, J., Krauss, M., Ort, C., Siegrist, H., von Gunten, U., 2011. Kinetic assessment and modeling of an ozonation step for full-scale municipal wastewater treatment: Micropollutant oxidation, by-product formation and disinfection. Water Research 45, 605–617.

Summary

Multiple factors impose severe stress on the global water system and urban water supplies. These factors include worldwide population growth in general and in water scarce areas in particular, depletion of groundwater resources, uneven geographical spread of water resources and increasing water consumption per capita. Additionally, the occurrence of emerging contaminants such as endocrine disruptors (EDCs), pharmaceuticals and personal care products (PPCPs) is a potential risk for both the environment and human health.

Hence, the interest in advanced water and wastewater treatment systems in view of water reuse and the removal of these harmful compounds is significantly increasing. Oxidation processes, and especially ozonation and ultraviolet (UV) irradiation in combination with hydrogen peroxide (H_2O_2) have found to be effective in this context. The UV/H_2O_2 process is generally called an advanced oxidation process (AOP) as it relies on the production of the reactive hydroxyl radical ($HO^{\bullet}$). The main advantage that these processes hold over other techniques is that target pollutants are (partially) destroyed, rather than transferred to another phase which is the case during e.g. adsorption or membrane filtration processes.

Despite the current interest and rapidly growing number of applications, the design and operation of ozone and UV/H_2O_2 processes for advanced water and wastewater treatment still have to be optimized. In this context, mathematical models can be of great value as they allow for prediction of process efficiency at different operational and water quality conditions and, hence, allow for virtually testing a multitude of scenarios before actual implementation in practice. However, despite extensive research on the reactions taking place during oxidation, the chemical complexity of the processes currently impedes modelling efforts. The presence of dissolved organic matter (DOM) is the main reason for the system complexity associated with “real water” oxidation. This knowledge gap has to be filled in order to enable optimal process design and operation and hence, cost effective advanced water treatment.

In this PhD dissertation, ozonation and UV/H_2O_2 treatment of surface water and secondary treated municipal wastewater were studied. Lab-scale or full-scale

reactors were used for experimenting and to calibrate and validate mechanistic models with an emphasis on conversion of DOM. As such, a combination of practical experimentation and mathematical modelling at various operational and water quality conditions was the major scientific contribution of the work performed during this study. Research was performed at both lab- and full-scale.

A full-scale ozone reactor for drinking water treatment (60,000 m^3 d^{-1} treatment capacity) was modelled using a kinetic model consisting of a limited set of equations. The model including key processes such as ozone decomposition, organic carbon removal, disinfection and bromate formation was implemented in the modelling platform WEST and calibrated using historical data collected over a period of 300 d. The absorption coefficient at 254 nm (UV_{254}) was used as a surrogate for DOM. The predicting performance was verified with a goodness-of-fit test and key parameters were determined through a local sensitivity analysis. Furthermore, different scenario analyses were conducted to study the system's behaviour at different operational conditions. Model parameters involving UV_{254} (both rate constants and stoichiometric coefficients) strongly affected model output. Some parameters with respect to bromate and bacteria showed to be only, but to a large extent, sensitive to their associated concentrations. The model was able to describe the operation of the full-scale ozone reactor, although further data collection for extensive model validation is necessary.

A more complex kinetic ozone decomposition model was used to study the impact of DOM on ozone and $HO^{\bullet}$ concentrations. Local and global sensitivity analyses were used to determine the most important elementary reactions and to understand the reaction mechanism. Only seven of the twenty-eight first and second order rate constants showed to impact ozone and $HO^{\bullet}$ concentrations. Processes involving $HO^{\bullet}$ scavenging by inorganic carbon were of minor importance. Mass-transfer related parameters k_La and ozone saturation concentration ($[O_3^*]$) were of major importance in all cases. Hence, it is of extreme importance that these parameters are determined with high accuracy. It was shown that the aqueous ozone concentration is extremely sensitive to parameters involving DOM at very low scavenger concentrations implying that impurities should always be considered in models, even in ultrapure water systems. Due to the limited importance of many of the parameters, simplification of the elementary radical scheme should be considered. On the other hand, a model extension with regard to reactions involving DOM should be performed in order to improve the applicability of mechanistic ozonation models.

Multiple mechanistic models describing the UV/H_2O_2 process have been proposed in literature. One of them was used to predict the behaviour of a full-scale reactor treating secondary treated wastewater. The model was calibrated and validated with non-synthetic influent using different operational conditions. A local sensitivity analysis was conducted to determine the most important operational and chemical model parameters. The hydrogen peroxide concentration, absorption coefficient at 310 nm (UV_{310}, as a surrogate for natural organic matter) and pH could be satisfactorily predicted during model validation using an independent data set. It was demonstrated that real-time calibration is an option at less controllable full-scale conditions. The reactivity of UV_{310} towards hydroxyl radicals did not show significant variations over time suggesting no need for frequent recalibration. Parameters that determine the initiation step, i.e. photolysis of hydrogen peroxide, exerted a large impact on most of the variables. Some reaction rate constants were also of importance, but nine kinetic constants did show absolutely no influence to one of the variables. Parameters related to UV shielding by DOM were of main importance. Hydrogen peroxide concentration was classified as a non-sensitive variable, in contrast to the concentration of a micropollutant which showed to be very to extremely influential to many of the parameters. UV absorption proved to be a valuable DOM surrogate to be included in models.

Based on the above findings, research was conducted to assess the impact of (advanced) oxidation on the properties of DOM. Conversions of effluent organic matter (EfOM) were experimentally examined using two different oxidation techniques: ozonation and UV/H_2O_2 treatment. Multiple surrogates for EfOM related to its concentration, polarity, biodegradability, molecular size and spectral properties were used to study the oxidant induced conversions. Spectral calculations as differential absorbance spectra (DAS) and absorbance slope indexes (ASIs) proved to be useful to unravel mechanistic differences between ozone and $HO^{\bullet}$ induced transformation of EfOM. DAS and ASIs behaved totally different in the presence or absence of ozone. Effluent ozonation inherently led to significant $HO^{\bullet}$ production and as a result of changing EfOM properties, the $HO^{\bullet}$ production yield increased as function of ozone dose. During the UV based process, pseudo steady-state behaviour of the $HO^{\bullet}$ concentration was observed. The $HO^{\bullet}$ production during ozonation was strongly correlated to UV_{254}. Further, the pH extremely impacted ozone decomposition. Most likely, the degree of dissociation of EfOM controlled its reactivity towards ozone. The ozone decomposition constant (k'_{app}) rapidly decreased as function of ozone dose following a power function. Both processes had similar effects on oxygen demand, dissolved organic carbon (DOC),

polarity and biodegradability. EfOM was converted to compounds with an increased oxidation state, decreased hydrophobicity and higher biodegradability.

Finally, the above mentioned lab-scale UV/H_2O_2 system for secondary effluent oxidation was modelled using two slightly different kinetic UV/H_2O_2 models. The models were successfully calibrated but only poor predictions of effluent organic matter conversion and $HO^{\bullet}$ exposure could be obtained during model validation. This was not the case for hydrogen peroxide decay, which could be satisfactorily predicted. The modelling exercise was severely impeded by complex and variable the character of EfOM. Model-based description of secondary effluent treatment was found to be much more difficult compared to the modelling of natural water oxidation. More research should be conducted to extend the model in order to predict UV/H_2O_2 treatment of secondary treated municipal effluent. Alternatively, possible extensions of semi-empirical concepts should be investigated.

Throughout this PhD thesis, several issues that were found valuable to be covered by future research could be defined. First, model structures should be extended in order to achieve more accurate predictions of oxidant production and consumption rates. In this context, the use of suitable surrogates for DOM is of vital importance. Second, more studies on oxidation of real, multicomponent water matrixes building upon those described in this work are needed to increase the level of understanding on the complex mechanisms that are occurring. These studies should be conducted using lab-, pilot- and full-scale reactors. Third, more information is needed on the integration of oxidation processes in a treatment train consisting of multiple unit processes. In this way, the interactions between each step can be assessed.

Samenvatting

Verscheidene factoren oefenen een druk uit op het globale watersysteem en wereldwijde publieke watervoorzieningen. Tot deze factoren behoren bevolkingsgroei in het algemeen en in waterschaarse gebieden in het bijzonder, uitputting van grondwaterbronnen, ongelijke globale spreiding van watervoorraden en een stijgende waterconsumptie per persoon. Daarnaast vormt de stijgende aanwezigheid van microverontreinigingen in het aquatische milieu een potentiële bedreiging voor mens en natuur. Tot deze componenten behoren endocriene disruptoren (hormoonverstorende stoffen; EDCs), geneesmiddelen en persoonlijke verzorgingsproducten (Pharmaceuticals and Personal Care Products, PPCPs).

Bijgevolg is er een stijgende interesse in geavanceerde technieken voor water- en afvalwaterbehandeling die waterhergebruik en de verwijdering van deze schadelijke componenten mogelijk maken. In deze context hebben oxidatieprocessen, en in het specifiek ozonering en ultraviolet (UV) straling gecombineerd met waterstofperoxide (H_2O_2) hun potentiëel al bewezen. Het UV/H_2O_2 proces is een geavanceerd oxidatieproces (advanced oxidation process, AOP) omdat zijn werking volledig berust op de productie van het zeer reactieve hydroxyl radicaal ($HO^{\bullet}$). Het belangrijkste voordeel dat deze processen hebben t.o.v. andere is dat doelcomponenten (gedeeltelijk) worden afgebroken in plaats van te worden getransporteerd naar een andere fase. Dit is bijvoorbeeld wel het geval bij adsorptieprocessen of membraanfiltratie.

Ondanks de sterke interesse in deze processen en snelle toename van het aantal toepassingen voor geavanceerde (afval)waterbehandeling en waterhergebruik, is er nog veel mogelijkheid tot optimalisatie van het procesontwerp en de procesvoering. Hierbij kunnen wiskundige modellen van groot belang zijn omdat ze in staat zijn de procesefficiëntie te voorspellen bij variërende operationele instellingen en watersamenstelling. Aan de hand van deze modellen kunnen talrijke scenario's worden doorgerekend alvorens het proces op volle schaal wordt toegepast. Ondanks intensief wetenschappelijk onderzoek omtrent de oxidatieve reacties die optreden, wordt de modellering echter bemoeilijkt door de chemische complexiteit van de processen. De voornaamste oorzaak van deze complexiteit is de aanwezigheid van opgelost organisch materiaal (Dissolved Organic Matter, DOM).

De kennis hieromtrent dient te worden uitgebreid om te komen tot geoptimaliseerde processen en tenslotte tot economisch interessante geavanceerde waterbehandeling.

In dit doctoraat werden ozonering en UV/H_2O_2 behandeling van oppervlakte water en secundair behandeld huishoudelijk afvalwater bestudeerd. Labo- en volle schaal reactoren werden gebruikt voor het uitvoeren van experimenten en voor calibratie en validatie van mechanistische modellen. Hierbij speelde DOM een belangrijke rol. De belangrijkste wetenschappelijke bijdrage van dit proefschrift is dus een combinatie van praktische experimenten met wiskundige modellering en dit bij verschillende operationele condities en watersamenstelling. Het onderzoek gebeurde op labo-schaal én op volle schaal.

Een volle schaal ozonreactor voor drinkwaterproductie (60.000 m^3 d^{-1}) werd gemodelleerd aan de hand van een kinetisch model dat bestond uit slechts enkele vergelijkingen. De modelstructuur bevatte belangrijke processen zoals ozonafbraak, oxidatie van organisch material, desinfectie en bromaatvorming. Het model werd geïmplementeerd in het modelleringsplatform WEST en gecalibreerd met meetdata die werd verzameld over een periode van 300 dagen. De absorptiecoefficiënt op 254 nm (UV_{254}) werd gebruikt als een surrogaatparameter voor DOM. De voorspelling van het model werd geëvalueerd en de belangrijkste parameters werden bepaald d.m.v. een lokale gevoeligheidsanalyse. Daarnaast werden ook verschillende scenario analyses uitgevoerd om de respons van het systeem te testen bij verschillende operationele condities. De modelparameters die gerelateerd waren aan UV_{254} (snelheidsconstanten en stoichiometrische coefficiënten) beïnvloedden het model zeer sterk. Sommige parameters gerelateerd aan bromaat en bacteriën waren ook invloedrijk, maar enkel t.o.v. hun respectievelijke concentraties. Het model werd capabel bevonden voor het beschrijven van de volle schaal ozonreactor, hoewel nog nieuwe data zijn vereist voor verdere validatie.

Een complexer model voor ozonafbraak werd gebruikt om de impact van DOM op de concentraties van ozon en $HO^{\bullet}$ te bestuderen. Lokale en globale gevoeligheidsanalyses werden toegepast voor het bepalen van de belangrijkste parameters en om meer inzicht te krijgen in het reactiemechanisme. Slechts zeven van de achtentwintig eerste en tweede orde snelheidsconstanten bleken een invloed uit te oefenen op de concentraties van beide oxidantia. De consumptie van $HO^{\bullet}$ door anorganische koolstof bleek van ondergeschikt belang te zijn. De belangrijkste parameters waren deze gerelateerd aan massatransfer van ozon: k_La en de ozon verzadigingsconcentratie ($[O_3^*]$). Bijgevolg is een nauwkeurige bepaling van deze parameters vereist om betrouwbare modelpredicties te verkrijgen. Verder werd aangetoond dat de ozonconcentratie extreem gevoelig is aan parameters gerelateerd

aan DOM, en zeker bij lage concentraties van radicaalvangers. Dit houdt o.m. in dat steeds rekening dient te worden gehouden met onzuiverheden, zelfs in systemen die worden beschouwd als zijnde "ultrapuur". Door de beperkte invloed van vele van de parameters, dient modelvereenvoudiging te worden overwogen. Anderzijds dienen reacties m.b.t. DOM te worden uitgebreid om zo de toepasbaarheid van mechanistische modellen te verhogen.

In de literatuur werden al meerdere modellen voor het UV/H_2O_2 proces beschreven. Een van deze modellen werd gebruikt voor het beschrijven van een volle-schaal reactor ter behandeling van secundair gezuiverd afvalwater. Het model werd gecalibreerd en gevalideerd met reëel influent bij verschillende operationele condities. De belangrijkste chemische en operationele parameters werden bepaald d.m.v. een lokale gevoeligheidsanalyse. De waterstofperoxide concentratie, absorptiecoefficiënt op 310 nm (UV_{310}; een surrogaat voor DOM) en de pH konden accuraat worden voorspeld gedurende de validatie. Hierbij werd gebruik gemaakt van een nieuwe, onafhankelijke dataset. De studie toonde aan dat on-line calibratie mogelijk is bij minder controleerbare volle schaal condities. De reactiviteit van UV_{310} t.o.v. $HO^{\bullet}$ vertoonde echter geen sterke schommelingen in de tijd, wat er op wees dat geen frequente hercalibratie nodig zou zijn. De parameters die gerelateerd waren aan de initiatiestap (directe fotolyse van H_2O_2) oefenden een sterke invloed uit op de meeste variabelen. Daarnaast werden ook enkele reactieconstanten invloedrijk bevonden, maar negen snelheidsconstanten vertoonden helemaal geen invloed. Parameters gerelateerd aan competitieve UV absorptie door DOM waren zeer belangrijk. De waterstofperoxide concentratie was relatief ongevoelig voor veranderingen in parameterwaarden. Dit stond in schril contrast met de concentratie van een micro verontreiniging, die extreem werd beïnvloed door meerdere parameters. De UV absorptiecoefficiënt bleek een zeer waardevolle surrogaat voor DOM te zijn voor toekomstige modelontwikkeling.

Op basis van bovenstaande bevindingen werd beslist om specifiek onderzoek te verrichten rond de impact van (geavanceerde) oxidatie op de eigenschappen van DOM. Omzettingen van organisch materiaal in secundair effluent (EfOM) werden experimenteel nagegaan gebruik makende van twee verschillende oxidatietechnieken: ozonering en UV/H_2O_2 behandeling. Verschillende surrogaten voor EfOM werden gebruikt om veranderingen in concentratie, polariteit, biodegradeerbaarheid, moleculaire grootte en spectrale eigenschappen van het organisch materiaal na te gaan. Spectrale berekeningen zoals differentiële absorptiespectra (DAS) en absorbantie helling indices (absorbance slope indexes, ASIs) bleken zeer nuttig te zijn om verschillen in de werkingsmechanismen van ozon en $HO^{\bullet}$ bloot te leggen. De vorm van de ASIs werd sterk beïnvloed door het al

dan niet aanwezig zijn van ozon. Ozonering van secundair effluent gaf aanleiding tot significante productie van $HO^{\bullet}$. Naarmate de eigenschappen van het EfOM veranderden (bij hogere ozondosissen), steeg de productiesnelheid van deze radicalen. Gedurende het UV geïnduceerde proces werd pseudo steady-state (constant) gedrag van de $HO^{\bullet}$ radicaal concentratie geobserveerd. De productie van $HO^{\bullet}$ was sterk gecorreleerd met de verandering van UV_{254} gedurende ozonering. Verder werd aangetoond dat ozonafbraak extreem werd beïnvloed door de pH. Vermoedelijk werd de reactiviteit van het EfOM sterk bepaald door de graad van dissociatie. De snelheidsconstante voor ozonafbraak (k'_{app}) verminderde snel als functie van de ozondosis en dit verloop kon worden beschreven met een machtsfunctie. Beide processen hadden gelijkaardige effecten op de zuurstofvraag, opgeloste organische koolstof (DOC), polariteit en biodegradeerbaarheid. EfOM werd omgezet naar hydrofobere en meer biodegradeerbare componenten met een hogere oxidatiegraad.

Als laatste werd het voorgenoemde laboschaal UV/H_2O_2 systeem voor oxidatie van secundair effluent gemodelleerd aan de hand van twee licht verschillende UV/H_2O_2 modellen. De modellen werden succesvol gecalibreerd, maar tijdens validatie werden slechts matige voorspellingen van de EfOM omzetting en blootstelling aan $HO^{\bullet}$ verkregen. De concentratie van waterstofperoxide kon echter wel goed worden voorspeld. Het modelleren werd erg bemoeilijkt door het complexe en variabele karakter van EfOM. Modelgebaseerde beschrijving van oxidatie van secundair effluent bleek moeilijker te zijn dan van natuurlijk water. Meer onderzoek met het oog op de uitbreiding van het model is vereist om goede voorspellingen te verkrijgen. Als alternatief zouden uitbreidingen van bestaande semi-empirische concepten kunnen worden onderzocht.

Doorheen dit proefschrift konden verschillende waardevolle pistes voor toekomstig onderzoek worden gedefiniëerd. Ten eerste zouden bestaande modelstructuren moeten worden uitgebreid teneinde te komen tot een betere voorspelling van de productie- en afbraaksnelheden van de oxidantia. Ten tweede zijn verdere studies omtrent oxidatie van reële, complexe watermatrices nodig verder bouwende op deze beschreven in dit doctoraat. Zo kan een diepgaander inzicht verworven worden inzake de mechanismen die optreden. Deze studies zouden moeten worden uitgevoerd op labo-, piloot- en volle schaal. Ten laatste dient meer informatie te worden verzameld omtrent de integratie van oxidatieprocessen in een behandelingstrein die bestaat uit verschillende eenheidsprocessen. Op deze manier kunnen de interacties tussen de verschillende stappen worden nagegaan.

Appendix A

Composing mass balances from the Gujer matrix

The complete mass balance of a species concentration (e.g. HCO_3^-) consists of transportation and conversion terms:

$$r_{HCO_3^-} = \frac{d[HCO_3^-]}{dt} = transport + conversion \quad \text{(B.1)}$$

To describe the bicarbonate concentration in the ith reactor of n completely stirred tank reactors (CSTRs) in series operating in a continuous flow mode, transportation terms must be added as follows:

$$transport = \frac{Q}{V_n}([HCO_3^-]_{out,i-1} - [HCO_3^-]_{out,i}) \quad \text{(B.2)}$$

Where Q represents the flow rate (L s^{-1}) and V_n is representing the volume of each single tank (L).

As an example, the mass balance of HCO_3^- is derived from the Gujer matrix presented in Table 6.1. The mass balance is built up by first multiplying each matrix element of the column of HCO_3^- by the reaction rate at the same row of the element. A summation of these products yields the conversion terms of the mass balance. Using the Gujer matrix, the conversion terms are composed:

$$conversion =$$

$$+k_5 \times [H_2O_2]_i \times [CO_3^{-\bullet}]_i + k_6 \times [HO_2^-]_i \times [CO_3^{-\bullet}]_i + k_{11} \times [O_2^{-\bullet}]_i \times [CO_3^{-\bullet}]_i$$

$$-k_{15} \times [HO^\bullet]_i \times [CO_3^{2-}]_i - k_{17} \times [HO^\bullet]_i \times [HCO_3^-]_i \quad \text{(B.3)}$$

The complete mass balance is as follows:

$$\frac{d[HCO_3^-]_i}{dt} = \frac{Q}{V_n}([HCO_3^-]_{out,i-1} - [HCO_3^-]_{out,i})$$

$$+k_5 \times [H_2O_2]_i \times [CO_3^{-\bullet}]_i + k_6 \times [HO_2^-]_i \times [CO_3^{-\bullet}]_i + k_{11} \times [O_2^{-\bullet}]_i \times [CO_3^{-\bullet}]_i$$

$$-k_{15} \times [HO^\bullet]_i \times [CO_3^{2-}]_i - k_{17} \times [HO^\bullet]_i \times [HCO_3^-]_i \quad \text{(B.4)}$$

Appendix B

Preliminary tests prior to oxidation experiments

B.1. Actinometry

B.1.1. Method

To determine the actual UV-C output of the lamp, chemical actinometry was used. Different approaches can be used, but due to its ease and accuracy, the method of Hatchard and Parker (1956) was used. For this method, potassium ferrioxalate ($K_3Fe(C_2O_4)_3.3H_2O$) is used as a chemical actinometer. The method relies on the photo reduction of ferric iron to ferrous iron at wavelengths shorter than 500 nm:

$$Fe^{3+} + {C_2O_4}^{2-} \xrightarrow{h\nu} Fe^{2+} + {C_2O_4}^{-} \quad \text{(B.1)}$$

By measuring the production rate of the ferrous iron, the photon flux can be calculated.

The synthesis of potassium ferrioxalate and the preparation of the calibration curve were all performed following the procedures of Hatchard and Parker (1956).

B.1.1.1. Preparation of potassium ferrioxalate

Potassium ferrioxalate was prepared with a mixture of 1:3 (mol:mol) ferric chloride ($FeCl_3$) and potassium oxalate ($K_2C_2O_4$). 204 g of $FeCl_3$ was dissolved in 200 ml water at a temperature of ±40°C. 410 g of $K_2C_2O_4$ was dissolved in 800 ml water at ±90°C. After compounds were completely dissolved, both solutions were mixed. $K_3Fe(C_2O_4)_3.3H_2O$ was produced according to the following reaction:

$$FeCl_3 + K_2\,C_2O_4 \rightarrow K_3\,Fe(C_2O_4)_3 + 3KCl \quad \text{(B.2)}$$

To prevent any interference of visible light, the synthesis was performed in almost complete dark using an infrared lamp. The precipitated potassium ferrioxalate was recrystallized three times to obtain a pure product (Hatchard and Parker, 1956).

B.1.1.2. Measurement of ferrous iron

To allow for spectrophotometric determination of Fe^{2+}, a calibration graph was prepared. For that, a dilution series of ferrous sulphate ($FeSO_4$) was used. The exact concentration of Fe^{2+} was determined with potassium manganate ($KMnO_4$) titration. For spectrophotometric determination of Fe^{2+}, phenanthroline monohydrate was used as an indicator. The absorbance of the phenantroline-ferrous iron complex at 510 nm was correlated with the Fe^{2+} concentration of the different dilutions. The detailed procedure can be found elsewhere (Hatchard and Parker, 1956).

B.1.1.3. Actinometric experiment

The reactor was filled with a 5 µM solution of potassium ferrioxalate in 0.05 M sulfuric acid. Subsequently, the lamp was switched on and on regular base, 2 ml samples were taken and analyzed for ferrous iron. During the actinometry experiment, temperature was controlled at 25°C and nitrogen gas was continuously bubbled through the reactor to purge all oxygen. From the slope of the Fe^{2+} concentration-time profile, the photon flux was determined.

B.1.2 Results

The ferrous iron concentration as function of time during the actinometry experiment is given in Figure B.1.

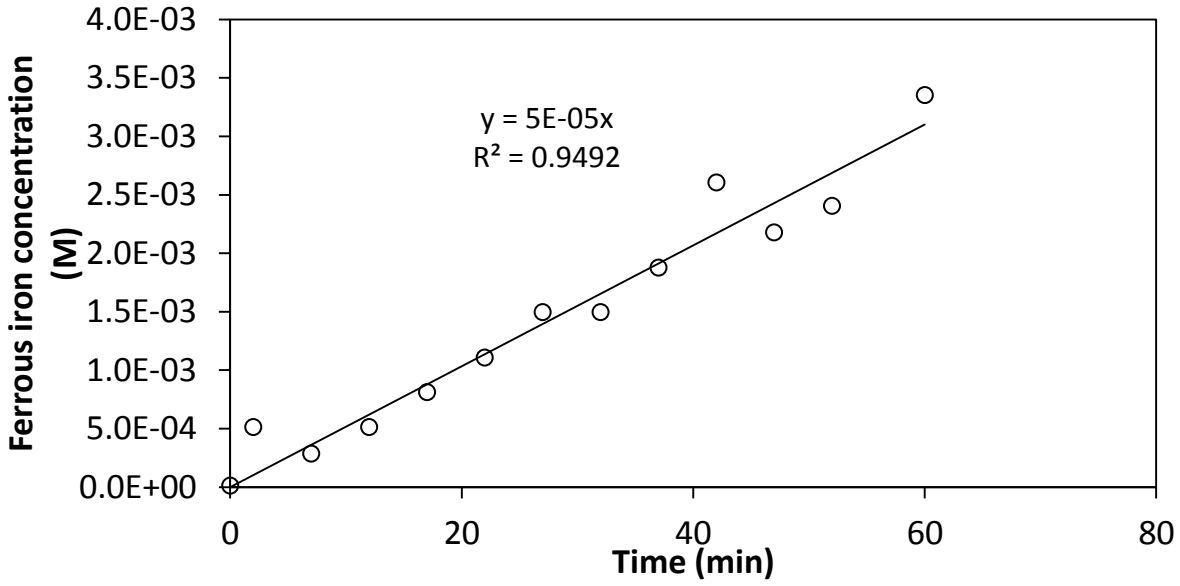

Figure B.1: Ferrous iron concentration profile during actinometry experiment

Using a quantum yield of 1.25 mole Einsteins^{-1} at 254 nm for ferrioxalate (Hatchard and Parker, 1956) and the slope obtained from Figure B.1 (i.e. the iron production rate; mole L^{-1} s^{-1}), the actual UV-C output was $6.74x10^{-7}$ Einsteins L^{-1} s^{-1} (3.5 W).

B.2 Ozone mass transfer

B.2.1 Methods

To allow kinetic investigation of secondary effluent ozonation, the mass balance of the ozone concentration in the liquid phase (C_{O3_L}) is needed. The following rate law can usually be applied, provided that liquid film reactions are negligible and that ozone decay follows a pseudo-first order kinetic regime (Beltrán, 2004):

$$\frac{dC_{O3\_L}}{dt} = k_L a_{O3}\left(C^*_{O3\_L} - C_{O3\_L}\right) - k'_{app} C_{O3\_L} \quad \text{(B.3)}$$

in which $k_L a_{O3}$ represents the volumetric mass-transfer coefficient of O_3 (s^{-1}), $C_{O3\_L}^*$ is the equilibrium concentration of O_3 in the liquid phase (mg L^{-1}) and k'_{app} is the apparent first order decay constant of O_3 (s^{-1}).

To determine $k_L a_{O3}$, a preliminary experiment on mass transfer from the gaseous phase to the liquid phase was conducted. $k_L a$ is a lumped parameter that consists of the individual liquid phase mass transfer coefficient (k_L, expressed in m s^{-1}) and the specific interfacial area of the gas bubbles (a, expressed in m^2 m^{-3}). According to the film theory (a theory that assumes that resistance to mass transfer is located in a stationary layer of a certain thickness and close to the gas-liquid interface: the film layer), k_L is related to the diffusion coefficient as follows (Beltrán, 2004):

$$k_L = \frac{D_a}{\delta_L} \quad \text{(B.4)}$$

where D_a and δ_L are the diffusion coefficient of the gas and the thickness of the film layer in m^2 s^{-1} and m, respectively.

The diffusion coefficient of a gas and hence, $k_L a$, are highly dependent on temperature and water composition. Therefore, $k_L a_{O3}$ should be determined using the same conditions as during the ozonation experiments. In dilute solutions where k'_{app} is constant and known from a preliminary homogeneous ozone decomposition experiment, $k_L a_{O3}$ can be easily determined from an ozone absorption experiment. Gaseous ozone is sent through the solution and the aqueous ozone concentration is recorded as function of time. From the ozone concentration profile, both $k_L a_{O3}$ and

the $C_{O3\_L}^{*}$ can be determined using Equation B.3 (Beltrán, 2004): However, as significant ozone consumption occurs in secondary effluent and k_{O3} is unknown and not constant in time, this approach could not be used. This problem was solved by first determining the k_La of oxygen (k_La_{O2}). Pure oxygen gas was sent through the effluent sample at the same flow rate as was used during the experiments. In addition, the aeration experiment was conducted at the same water temperature (25°C) and pH (7.5). The aqueous oxygen concentration was measured with a dissolved oxygen probe (WTW oxi 340-A/SET). If chemical reaction of oxygen was neglected (which is a reasonable assumption) and Equation B.3 was solved for oxygen, the following equation was obtained:

$$Ln\left(\frac{C_{O2\_L}^{*}-C_{O2\_L}}{C_{O2\_L}^{*}-C_{O2\_L0}}\right)=-k_La_{O2}t \tag{B.5}$$

in which k_La_{O2} represents the volumetric mass-transfer coefficient of O_2 (s^{-1}), $C_{O2\_L}^{*}$ is the equilibrium concentration of O_2 in the liquid phase (mg L^{-1}) and C_{O2_L0} is the dissolved oxygen concentration at the start of the aeration experiment (t=0).

Following the assumption that was made regarding chemical reaction of oxygen, $C_{O2\_L}^{*}$ could be directly determined from the oxygen concentration profile (i.e. the stable oxygen value after equilibrium was reached). k_La_{O2} was determined from the slope of the straight line that was obtained after applying equation (B.5).

After considering the difference in diffusivities of oxygen (D_{O2}) and ozone (D_{O3}), k_La_{O3} could be determined as follows (Beltrán, 2004):

$$k_La_{O3}=k_La_{O2}\sqrt{\frac{D_{O2}}{D_{O3}}} \tag{B.6}$$

The diffusion coefficients of oxygen and ozone were determined according to Wilke and Chang (1955):

$$D_a=7.4\times10^{-8}\frac{\sqrt{xM}T}{\eta V^{0.6}} \tag{B.7}$$

with x the solvent association parameter (2.6 for water), M the molecular weight of the solvent (g mol^{-1}), T the temperature (K), η the dynamic viscosity of the solution (centipoise) and V the molal volume of the gas (mL g^{-1} mol^{-1}).

$C_{O3\_L}^{*}$ was calculated using Henry's law (Beltrán, 2004):

$$P_{O3}=C_{O3\_G}RT=H_eC_{O3\_L}^{*} \tag{B.8}$$

with P_{O3} the partial pressure of ozone in the gas phase (atm), C_{O3_G} the ozone concentration in the gas phase (mol L^{-1}), R the ideal gas constant (L atm K^{-1} mol^{-1}) and H_e Henry's constant (L atm mol^{-1}).

H_e was determined according to the empirical law by Roth and Sullivan (1981):

$$H_e = 3.84 \times 10^7 [HO^-]^{0.035} e^{\frac{-2428}{T}} \quad \text{(B.9)}$$

where $[HO^-]$ is the concentration of hydroxyl ions in the liquid phase (mol L^{-1}). It should be noted that H_e in equation (B.9) is expressed in atm instead of in L atm K^{-1} mol^{-1}. A value of 6560 atm was obtained for H_e, which is a realistic value (Sander, 1999). Finally, $C_{O3\_L}^*$ was calculated as follows:

$$C_{O3\_L}^* = C_{O3\_G} \frac{RT}{H_e} \frac{\rho_{H_2O}}{M_{H_2O}} \quad \text{(B.10)}$$

where ρ_{H2O} (g L^{-1}) and M_{H2O} are the density and molecular weight of water, respectively and H_e is expressed in atm.

B.2.2 Results

The dissolved oxygen profile is depicted in Figure B.2. As pure oxygen gas was

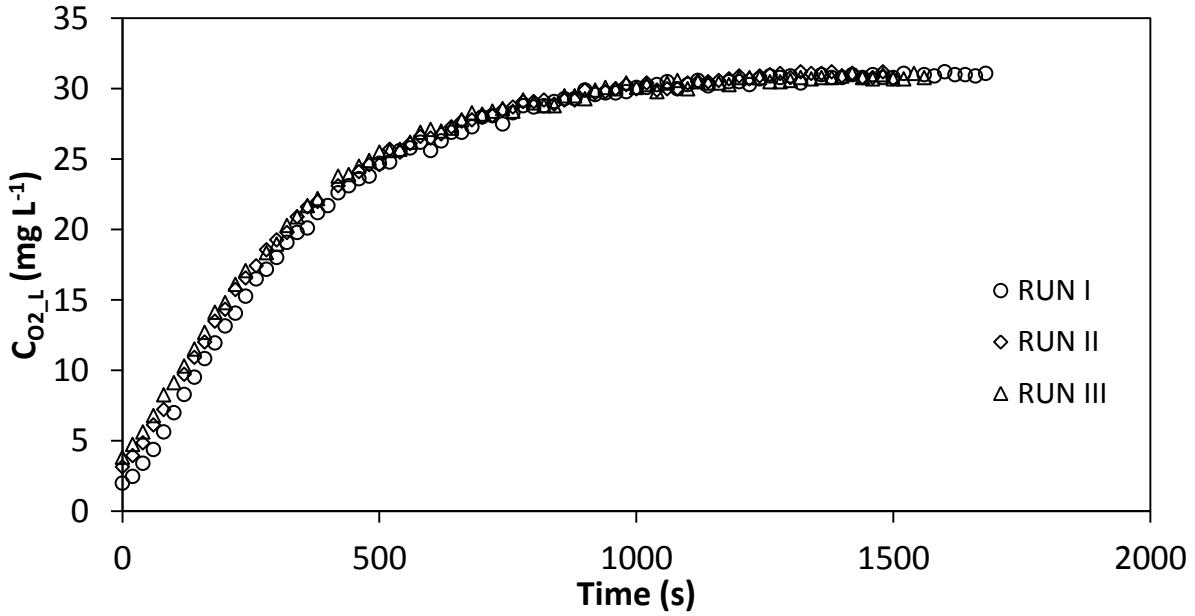

Figure B.2: Dissolved oxygen profile during aeration experiment (three identical runs)

used during the aeration experiment, the saturation concentration could reach 31 mg L^{-1}. Identical results were obtained for three replicate runs.

After applying Equation B.5, Figure B.3 was obtained. From the slope of the profiles, k_La_{O2} was found to be 0.0035 s^{-1}. Using Equation B.6, a value of 0.0040 s^{-1} was found for k_La_{O3}. Values for $C_{O3\_L}^*$ for ozonation of sample 1 and sample 2 after applying Equation B.10 are given in Table B.1.

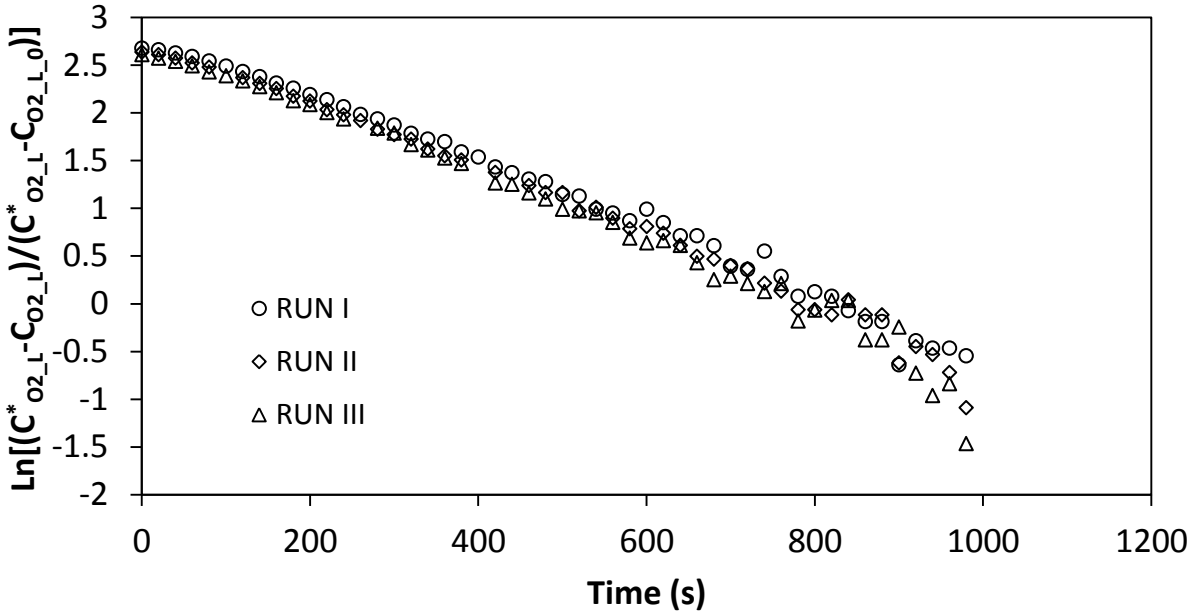

Figure B.3: Dissolved oxygen profile after applying Equation B.5.

Table B.1: Inlet gaseous ozone concentrations and corresponding liquid equilibrium concentrations for sample 1 and sample 2.

	C_{O3_g} (mg L^{-1})	$C_{O3\_L}^*$ (mg L^{-1})
Sample 1	4.07	0.85
Sample 2	7.67	1.59

B.3. Fluid mixing

B.3.1. Methods

A relatively large reactor volume was chosen for two reasons: (1) for some of the analyses, large sample volumes were needed and (2) a large reactor volume allowed neglecting the volume loss caused by small sample withdrawals. However, a large reactor volume impedes complete mixing. A tracer experiment was performed to get an estimate of the time that was needed to get complete mixing in the lab-scale reactor. Additionally, this experiment was used to optimize the configuration of the external circulation loop and to investigate the impact of gaseous inflow on the fluid mixing.

As shown in Figure B.4, two different configurations of the circulation loop were tested. In a first configuration, the water that was recirculated entered the reactor at the top. In a second configuration, the water entered the reactor at the centre. In both cases, the water was directed downward using a glass pipe at the end of the inlet tube. The position of the water outlet remained unchanged.

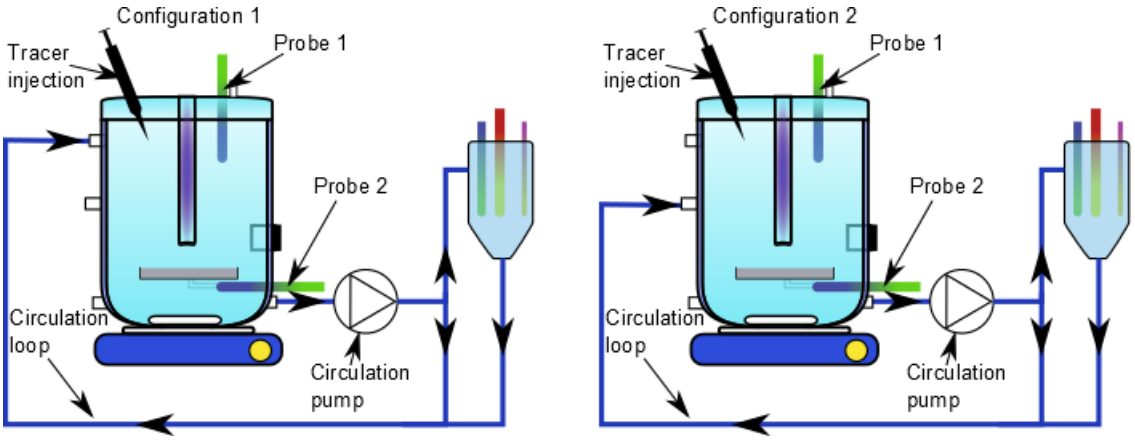

Figure B.4: Configurations used during fluid mixing tests

Sodium chloride was used as a tracer compound. 2.5 ml of a 10% salt solution was injected at the water surface. To measure the tracer response, two conductivity meters were used. A data-acquisition device based on voltage measurements (model No. FN-18200-00, Cole-Parmer) connected to a PC was used for data storage. The positions of the two probes and the location of tracer injection are indicated on Figure B.4. The probes were allowed to stabilize for 30 s prior to tracer injection.

Five different experiments were performed: configurations 1 and 2 were both tested without a gas flow, configuration 1 with a gas flow of 30 L h^{-1} and two different gas flow rates were tested for configuration 2 (30 L h^{-1} and 50 L h^{-1})

It has to be mentioned that, as these were preliminary experiments, the water volume (13 L) and the gas flow rates tested differed from the final settings that were applied during the experiments. Additionally, two different conductivity probes were used and hence, the voltage value after a stable signal was reached could be expected to be different. For this reason, conductivity values were normalized to the stable values found at the end of the runs.

B.3.2. Results

The tracer response curves for the different set-ups are given in Figures B.5-B.9. For configuration 1, the presence of a gas flow did not visibly affect the time that

was needed to obtain a stable signal at the two probes. This was not the case for configuration 2, where the raising gas bubbles improved mixing. For both configurations, maximal deviations from the end value were significantly lower if a gas flow was present. Figures B.5 and B.6 show that for configuration 1 during the first 10 s the tracer held up in the upper reactor part, the zone where the tracer was injected. This led to an immediate response of Probe 1 (at the surface and close to the tracer injection) and a delayed response of Probe 2. A slight delay (3 s) was observed for configuration 2 for both signals, but after that, both probes reacted simultaneously (Figures B.7-B.9). It became clear that mixing was significantly better using configuration 2 and best results were obtained using the highest gas flow rate. A stable system was reached after approximately 20 s (gas flow 50 L h^{-1}), while 45 s were needed for configuration 1 (gas flow 30 L h^{-1}).

As such, configuration 2 was chosen for all experiments. In order to improve the mixing behaviour, the active reactor volume was lowered to 11 L (instead of 13 L), and a gas flow rate of 60 L h^{-1} was used for all ozonation experiments.

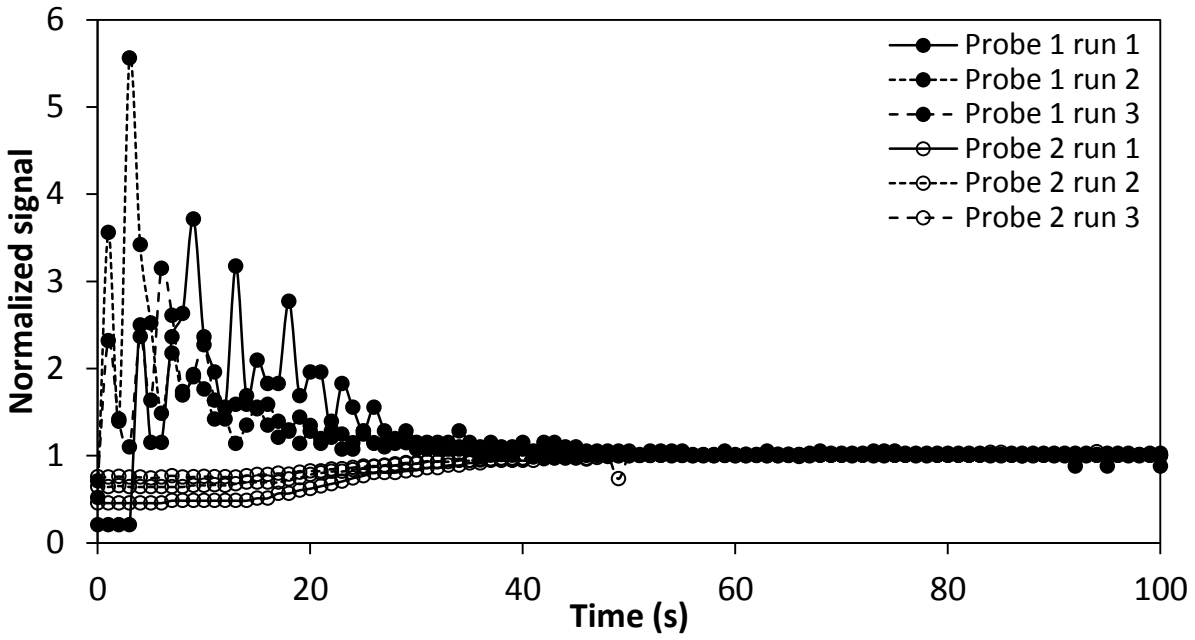

Figure B.5: Tracer response for configuration 1; gas flow switched off

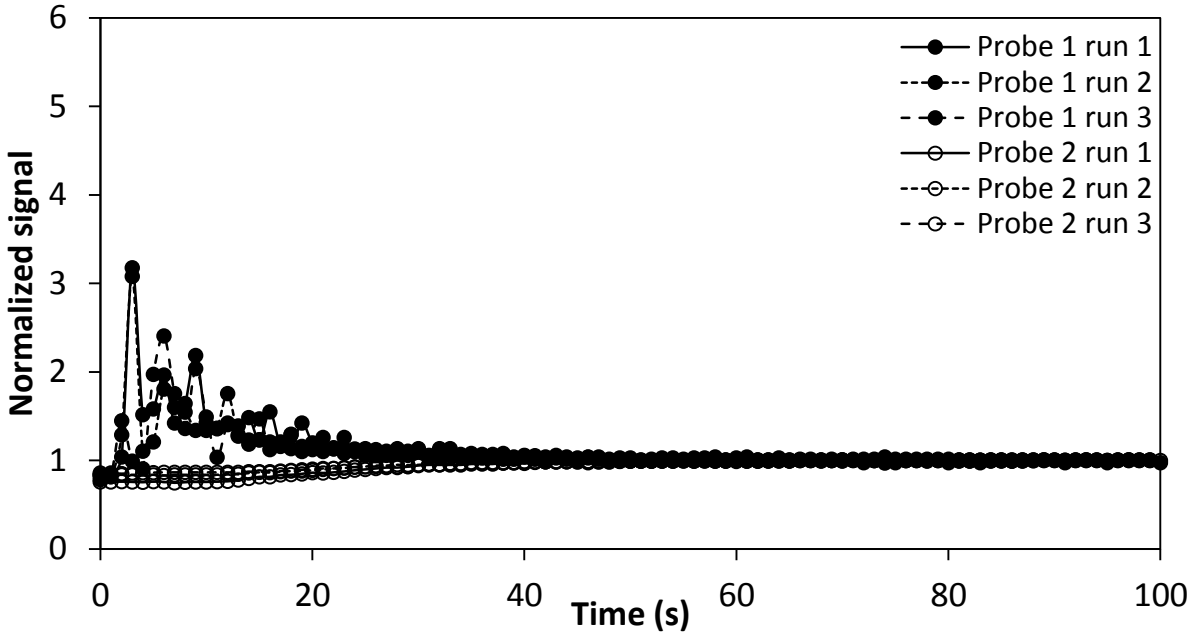

Figure B.6: Tracer response for configuration 1; gas flow 30 L h^{-1}

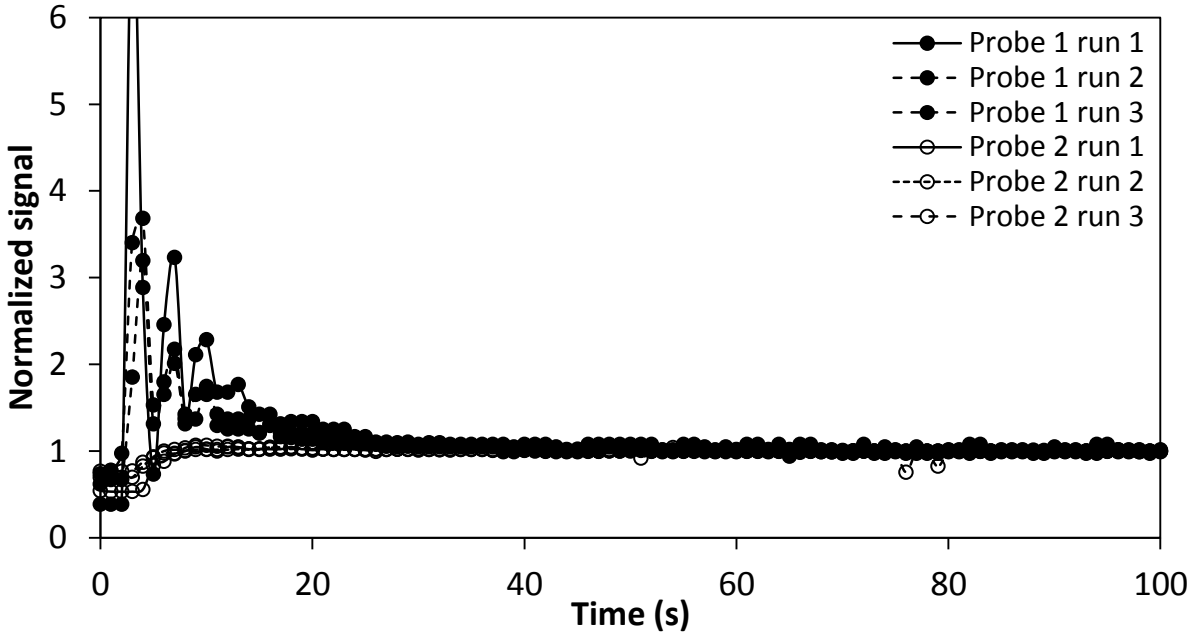

Figure B.7: Tracer response for configuration 2; gas flow switched off

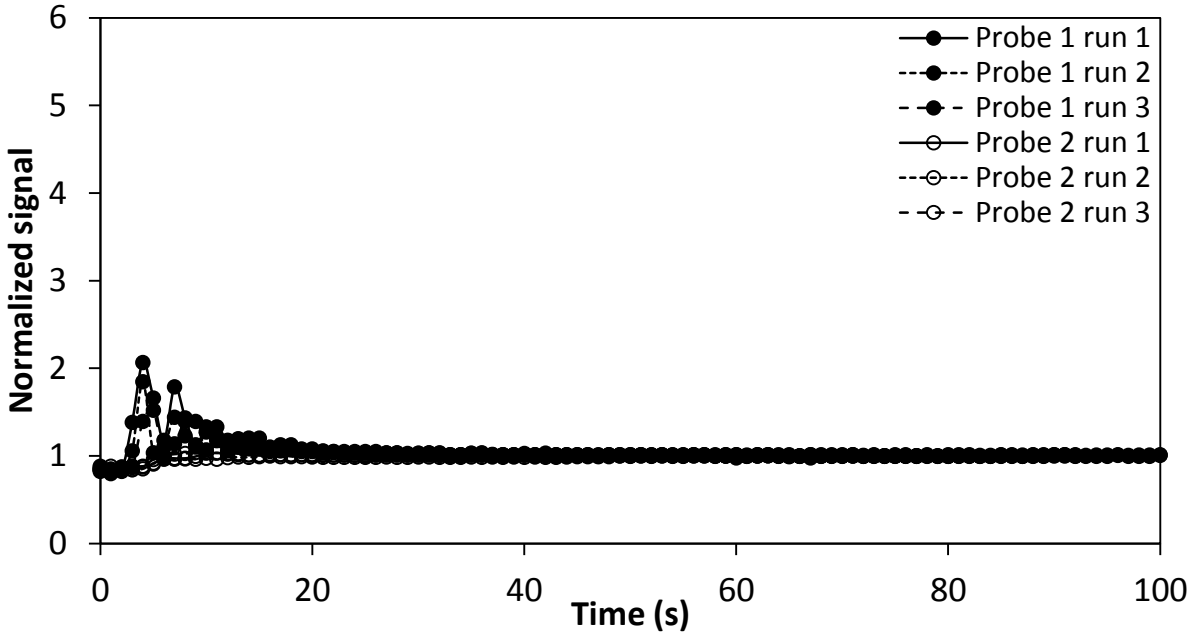

Figure B.8: Tracer response for configuration 2; gas flow 30 L h^{-1}

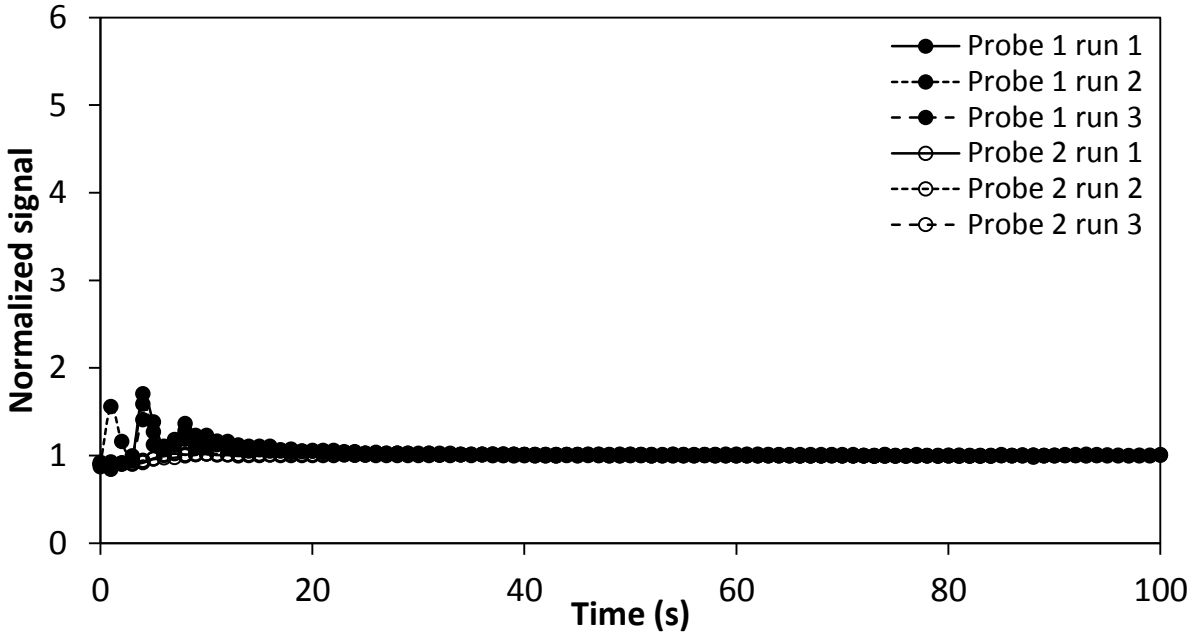

Figure B.9: Tracer response for configuration 2; gas flow 50 L h^{-1}

B.4. Quenching of hydrogen peroxide

B.4.1 Methods

Samples from UV/H_2O_2 experiments were quenched by adding 0.2 mg L^{-1} bovine liver catalase (Sigma), according to Liu et al. (2003). However, some preliminary tests were performed in order to confirm the suitability of this method for the oxidation experiments performed in this work.

The aim of these tests was to:

- get an estimate of the time required to remove all hydrogen peroxide
- study the influence of time on the activity of catalase stock solution
- investigate if catalase interferes with COD measurements

These tests were performed at different temperatures (0 and 25°C) and catalase concentrations (0.1 and 0.2 mg L^{-1}). A 30% hydrogen peroxide stock solution (Perhydrol®, VWR) was spiked to 100 mL of tap water in order to obtain a final concentration of 6 mM. After the desired temperature was reached, 50 or 100 µL of a freshly prepared 0.2 g L^{-1} catalase stock solution (in tap water) was added to the sample. The hydrogen peroxide concentration was studied as function of time. The experiment in which 0.1 mg L^{-1} catalase was added at 25°C was repeated with 2 hours and 1 day old stock solution.

To check whether catalase interfered with the COD measurement, the COD of surface water was determined before and after the addition of 0.2 mg L^{-1} catalase. A statistical independent samples t-test was used to analyse the results.

B.4.2 Results

Hydrogen peroxide decay profiles are given in Figure B.10. A freshly prepared catalase solution (0.1 or 0.2 ppm) is able to completely remove residual hydrogen peroxide within 20 min. The quenching activity rapidly decreases with time. More than one hour is needed to remove all hydrogen peroxide using a 0.1 ppm catalase concentration and 2 h old stock solution. Complete removal is impossible to achieve with a 1 day old stock solution. The hydrogen peroxide decay rate drastically decreased at low temperature.

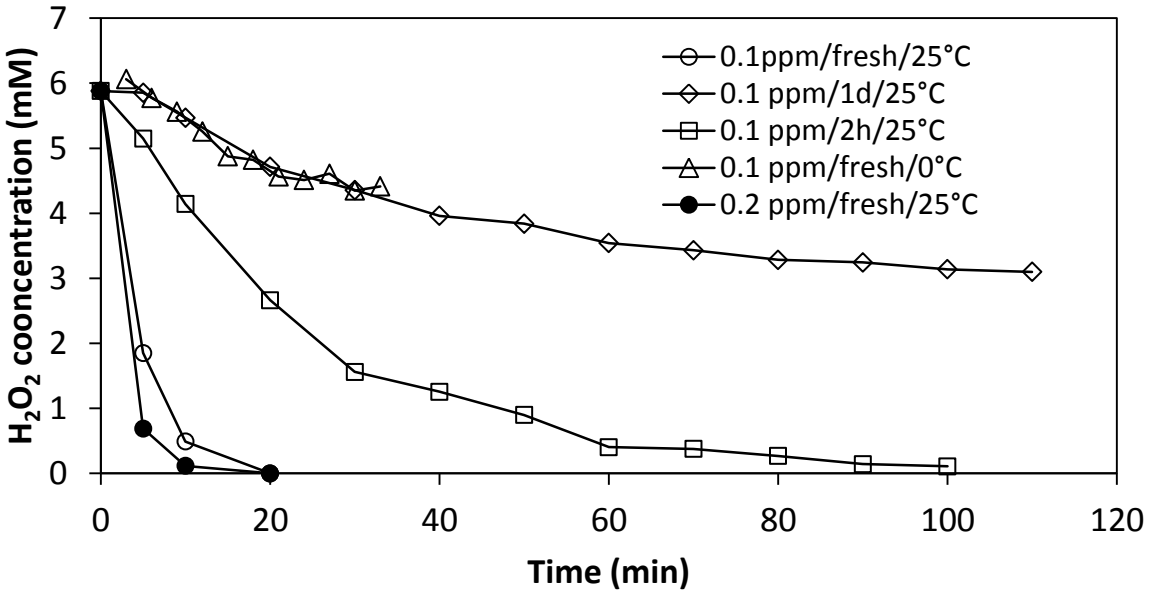

Figure B.10: hydrogen peroxide decomposition at different conditions (catalase concentration/age of stock solution/temperature)

COD values of a surface water sample before and after the addition of 0.2 ppm catalase are given in Table B.2. The COD was not significantly higher after catalase was added at a 95% confidence level as the calculated t statistical value (0.224) was lower than the critical value (2.571) of an independent samples t-test.

Table B.2: COD values before and after the addition of 0.2 ppm catalase

	COD (mg L^{-1})	
Replica No.	**Sample water**	**Sample water + catalase**
1	29.8	30.2
2	32.5	29.8
3	30,7	30.4
4	29.6	30.4
5	30.3	30.4
6	29.3	30.3

As such, 0.2 ppm freshly prepared catalase was added to all samples containing residual hydrogen peroxide. Prior to catalase addition, samples were brought to room temperature.

Curriculum vitae

Personal data

Name:	Wim T.M. Audenaert
Address:	Hulstbaan 63, 9112 Sinaai-Waas, Belgium
Nationality:	Belgian
Date of birth:	September 12, 1986
Place of birth:	Lokeren
Civil status:	Married with Katrien Van Buynder
E-mail:	wim.audenaert@howest.be; wim.aud@gmail.com

Education

2009-2012	Doctoral Training Programme in Applied Biological Sciences, Ghent University
2004-2008	Master of Science in Industrial Engineering: Environmental Sciences, University College West Flanders Master thesis: 'Zuivering van het douchewater van het Dranouter Festival' ('Purification of the shower wastewater of the Dranouter Music Festival'), promoter: Prof. Stijn Van Hulle

Additional courses with examination

2009	Modelling and simulation of biosystems (UGent) Integral environmental care (UGent) Chemometrics (UGent) Modelling and control of wastewater treatment plants (UGent) Water treatment techniques (UGent) Environmental technology: biological processes (UGent)
2010	Environmental technology: physical chemical processes (UGent) Water quality management (UGent)

Additional courses without examination

2010 Disinfection and oxidation techniques (Delft University of Technology)

Professional activities

2009-2012 Teaching assistant and doctoral researcher; Department of Mathematical Modelling, Statistics and Bioinformatics (BIOMATH), Ghent University; Department of Industrial Engineering and Technology (ENBICHEM), University College West Flanders. PhD thesis: 'Model-based study of ozonation and UV/hydrogen peroxide treatment for water and tertiary wastewater treatment', promoters: Prof. Ingmar Nopens and Prof. Stijn Van Hulle

2008 (Oct.-Dec.) Researcher within the research project 'Implementation of autotrophic nitrogen removal', partly funded by the Institute for Encouragement of Innovation by means of Science and Technology in Flanders (IWT) (TETRA Project); Department of Industrial Engineering and Technology (ENBICHEM), University College West Flanders

Teaching activities

2009-2012 Applied Chemistry, practical course at University College West Flanders

2009-2012 Organic Chemistry, practical course at University College West Flanders

2009-2012 Modelling and Simulation of Biosystems, practical course at Ghent University

MSc. theses supervised

2008-2009 M. Callewaert, 'Analyse van een volle-schaal ozoninstallatie: wiskundige modellering en studie van het transferrendement', University College West Flanders, Belgium

2009-2010 Y. Vermeersch, 'Analyse, modellering en optimalisatie van een volle schaal UV/H_2O_2 reactor voor waterhergebruik', University College West Flanders, Belgium

2010-2011 M. Degryse, 'Experimentele opzet van AOPs voor afvalwater- en waterbehandeling: combinaties van ozon, UV en waterstofperoxide', University College West Flanders, Belgium

2010-2011 M. Vandevelde, 'Modelmatige studie van de invloed van scavengerconcentraties op ozondecompositie in water: software-implementatie, dynamische simulatie en sensitiviteitsanalyse', University College West Flanders, Belgium

2011-2012 D. Vandierendonck, 'Invloed van ozonisatie en UV/H_2O_2 geavanceerde oxidatie op eigenschappen van opgelost organisch materiaal in secundair effluent', University College West Flanders, Belgium

Conferences/Symposia/Workshops attended

Co-organizer

- 1st IWA BENELUX Regional Young Water Professionals Conference, 1-2 September 2009, Eindhoven, The Netherlands (member of organizing committee)

- 2nd IWA BENELUX Regional Young Water Professionals Conference, 20-22 September 2011, Leuven, Belgium (member of organizing committee)

- 3rd IWA BENELUX Regional Young Water Professionals Conference, to be held in 2013 (member of organizing committee)

- 4th IWA/WEF Wastewater Treatment Modelling Seminar (WWTmod2014), to be held in 2014 (member of organizing committee)

Oral presentation

- WEST user group meeting, April 27-28 2009, Copenhagen, Denmark

- 1st IWA BENELUX Regional Young Water Professionals Conference, 1-2 September 2009, Eindhoven, The Netherlands

- 4th IWA Specialist Conference on Natural Organic Matter: From Source to Tap and Beyond, 27-29 July 2011, Irvine, California, USA

- 2nd IWA BENELUX Regional Young Water Professionals Conference, 20-22 September 2011, Leuven, Belgium

- International Ozone Association (IOA) International Conference on Ozone and Related Oxidants to Meet Essential Human Needs, 4-6 June 2012, Toulouse, France

Poster presentation

- PhD symposium of Faculties of Bioscience Engineering of Ghent University-Catholic University of Leuven, 20 December 2010, Ghent, Belgium

- 8th IWA Leading Edge Conference on Water and Wastewater Technologies, 6-10 June 2011, Amsterdam, The Netherlands

- 6th International Conference on Oxidation Technologies for Water and Wastewater Treatment, 7-9 May 2012, Goslar, Germany

Participant

- 5th International Conference on Oxidation Technologies for Water and Wastewater Treatment, 30 March-4 April 2009, Berlin, Germany

Publications

Peer-reviewed

- Audenaert, W.T.M., Vandierendonck, D., Van Hulle, S.W.H. and Nopens, I. Comparison of Ozone and HO• Induced Conversion of Effluent Organic Matter (EfOM) Using Ozonation and UV/H_2O_2 Treament, Water Research, submitted

- Audenaert, W.T.M., Vandevelde, M., Van Hulle, S.W.H. and Nopens, I. Influence of DOM Concentration on Parameter Sensitivity of a Mechanistic Ozone Decomposition Model, Ozone: Science and Engineering, submitted

- Audenaert, W.T.M., Vermeersch, Y., Van Hulle, S.W.H., Dejans, P., Dumoulin, A. and Nopens, I., 2011. Application of a mechanistic UV/hydrogen peroxide model at full-scale: Sensitivity analysis, calibration and performance evaluation, Chemical Engineering Journal 171(1), 113-126

- Van Hulle, S.W.H., Vandeweyer, H., Audenaert, W.T.M., Monballiu, A., Meesschaert, B., 2011. Influence of the feeding regime on the start-up and operation of the autotrophic nitrogen removal process, Water SA 37(3), 289-294

- Audenaert, W.T.M., Callewaert, M., Nopens, I., Cromphout, J., Vanhoucke, R., Dumoulin, A., Dejans, P. and Van Hulle, S.W.H., 2010. Full-scale modelling of an ozone reactor for drinking water treatment, Chemical Engineering Journal 157(2-3), 551-557

- Veys, P., Vandeweyer, H., Audenaert, W.T.M., Monballiu, A., Dejans, P., Jooken, E., Dumoulin, A., Meesschaert, B. and Van Hulle, S.W.H., 2010. Performance analysis and optimization of autotrophic nitrogen removal in different reactor configurations: a modelling study, Environmental Technology 31(12), 1311-1324

- Decostere, B., Daels, N., De Vrieze, S., Dejans, P., Van Camp, T., Audenaert, W.T.M., Westbroek, P., De Clerck, K., Boeckaert, C and Van Hulle, S.W.H., 2010. Initial testing of electrospun nanofibre filters in water filtration applications, Water SA 36(1), 151-156

- Decostere, B., Daels, N., De Vrieze, S., Dejans, P., Van Camp, T., Audenaert, W.T.M., Hogie, J., Westbroek, P., De Clerck, K. and Van Hulle, S.W.H., 2009. Performance assessment of electrospun nanofibres for filter applications, Desalination 249(3), 942-948

- Van Hulle, S.W.H., Audenaert, W.T.M., Decostere, B., Hogie, J. and Dejans, P., 2008. Sustainable wastewater treatment of temporary events : the Dranouter Music Festival case study, Water Science and Technology 58(8), 1653-1657

Not listed in the ISI Web of Knowledge

- Decostere, B., Daels, N., De Vrieze, S., Dejans, P., Van Camp, T., Audenaert, W.T.M., Hogie, J., Westbroek, P., De Clerck, K. and Van Hulle, S.W.H., 2008. Waterfiltratie met Electrogesponnen Nanovezels, Afvalwaterwetenschap 7(4), 17-28

- Van Hulle, S.W.H., Audenaert, W.T.M., Decostere, B., Hogie, J. and Dejans, P., 2008. De Folk Festival Dranouter Case: Duurzame waterbehandeling op tijdelijke evenementen, Afvalwaterwetenschap 7, 150-159

- Audenaert, W.T.M., Decostere, B., Van Hulle S.W.H., Dejans, P. & Hogie, J. (2008). Waterzuivering op het Dranouter Festival, Technology Upgrade, juni 2008, 10-11.

Conference proceedings

- Decostere, B., De Vrieze, S., Dejans, P., Van Camp, T., Audenaert, W.T.M., Hogie, J., Westbroek, P., De Clerck, K. and Van Hulle, S.W.H., 2008. Analyse van de performantie van nanovezels voor waterfiltratie, Congres Water en Klimaatverandering, 14-15 October 2008, Antwerp, Belgium

- Kiekens, P., De Vrieze, S., Van Camp, T., Decostere, B., Audenaert, W.T.M., Hogie, J., Westbroek, P., Van Hulle, S.W.H. and De Clerck, K., 2008. Electrospinning based nanofibrous structures for water filtration, 8th Autex Conference, 24-26 June 2008, Biella, Italy

- Van Hulle, S.W.H., Audenaert, W.T.M., Decostere, B., Hogie, J. and Dejans, P., 2008. Sustainable water treatment of temporary events: the Dranouter Music Festival case study, 5th IWA Leading-Edge Conference, 1 - 4 June 2008, Zurich, Switzerland.

- Decostere, B., De Vrieze, S., Dejans, P., Van Camp, T., Audenaert, W.T.M., Hogie, J., Daels, N., Westbroek, P., De Clerck, K. and Van Hulle, S.W.H., 2008. Performance assessment of electrospun nanofibres for filter applications, Membrane symposium and 12th poster day membrane technology, 26 November 2008, Antwerp, Belgium.

- Audenaert, W.T.M., Callewaert, M., Nopens, I., Cromphout, J., Vanhoucke, R., Dumoulin, A., Dejans, P. and Van Hulle, S.W.H., 2009. Full-scale modelling of an ozone reactor for drinking water treatment, 1st IWA BENELUX Regional Young Water Professionals Conference, 1-2 September 2009, Eindhoven, The Netherland.

- Decostere, B., Daels, N., De Vrieze, S., Dejans, P., Van Camp, T., Audenaert, W.T.M., Hogie, J., Westbroek, P., De Clerck, K. and Van Hulle, S.W.H., 2009. Performance assessment of functionalized electrospun nanofibres for removal of pathogens, 82nd Annual WEF Conference and Exposition, 10-14 October 2009, Orlando, USA.

- Daels, N., Decostere, B., De Vrieze, S., Dejans, P., Van Camp, T., Audenaert, W.T.M., Hogie, J., Westbroek, P., De Clerck, K. And Van Hulle, S., 2009. Performance Assessment of Functionalized Electrospun Nanofibres for Removal of Pathogens, 1st IWA BENELUX Regional Young Water Professionals Conference, 1-2 September 2009, Eindhoven, The Netherlands

- Vandeweyer, H., Van Hulle, S., Audenaert, W.T.M., Monballiu, A., Meesschaert, B., Dumoulin, A., 2010. Influence of hydraulic conditions on the start-up and operation of the autotrophic nitrogen removal process, 6th European Meeting on Chemical Industry and Environment (EMCHIE IV), 17-19 May 2010, Mechelen, Belgium

- Daels, N., Decostere, B., De Vrieze, S., Van Camp, T., Audenaert, W.T.M., Westbroek, P., De Clerck, K. And Van Hulle, S., 2010, 10th Flemish Youth Conference on Chemistry 1-2 March 2010, Blankenberge, Belgium

- Audenaert, W.T.M., Vermeersch, Y., Nopens, I. And Van Hulle, S.W.H., 2010. Integrated modelling of advanced oxidation processes : modelling of a full-scale UV/H_2O_2 reactor for horticultural water reuse, 22nd International ICFMH Symposium (Food Micro 2010): Microbial behaviour in the food chain, 30 August-3 September 2010, Copenhagen, Denmark

- Daels, N., Decostere, B., De Vrieze, S., Dejans, P., Van Camp, T., Audenaert, W.T.M., Hogie, J., Westbroek, P., De Clerck, K. and Van Hulle, S.W.H., 2010. Performance Assessment of Functionalized Electrospun Nanofibres for Removal of Pathogens, 7th IWA World Water Congress and Exhibition, 19-24 September 2010, Montreal, Canada.

- Daels, N., Decostere, B., De Vrieze, S., Van Camp, T., Audenaert, W.T.M., Westbroek, P., De Clerck, K. andVan Hulle, S.W.H., 2010. Performance assessment of functionalized electrospun nanofibres for removal of pathogens, Membranes in drinking and industrial water treatment, 27 – 30 June 2010, Trondheim, Norway.

- Audenaert, W.T.M., Vermeersch, Y., Nopens, I. and Van Hulle, S.W.H., 2010. Integrated Modelling of Advanced Oxidation Processes: Modelling of A Full-Scale UV/H2O2 Reactor for Horticultural Water Reuse, Ghent University-Catholic University of Leuven Faculty of bioscience engineering PhD symposium, 20 December 2010, Ghent, Belgium.

- Audenaert, W.T.M., Vandevelde, M., Van Hulle, S., Nopens, I., 2011. Influence of NOM concentration on parameter sensitivity of a mechanistic ozone decomposition model, 4th IWA Specialist Conference on Natural Organic Matter, 27-29 July 2011, Irvine, California, USA

- Audenaert, W.T.M., Vermeersch, Y., Van Hulle, S., Dejans, P., Dumoulin, A. and Nopens, I., 2011. Application of a mechanistic UV/hydrogen peroxide model at full-scale: Sensitivity analysis, calibration and performance evaluation, 8th IWA Leading Edge Conference on Water and Wastewater Technologies, 6-10 June 2011, Amsterdam, The Netherlands

- Audenaert, W.T.M., Vandevelde, M., Van Hulle, S., Nopens, I., 2011. Influence of NOM concentration on parameter sensitivity of a mechanistic

ozone decomposition model, 2nd IWA BENELUX Regional Young Water Professionals Conference, 20-22 September 2011, Leuven, Belgium

- Van Hulle, S.W.H., Vandeweyer, H.J.P., Audenaert, W.T.M., Monballiu, A. and Meesschaert, B.D., 2011. Influence of the feeding regime on the start-up and operation of the autotrophic nitrogen removal process, 2nd IWA BENELUX Regional Young Water Professionals Conference, 20-22 September 2011, Leuven, Belgium

- Audenaert, W.T.M., Vermeersch, Y., Van Hulle, S.W.H, P. Dejans, A. Dumoulin & Nopens, I., 2011. Application of a mechanistic UV/hydrogen peroxide model at full-scale: sensitivity analysis, calibration and performance evaluation, 8th IWA Symposium on System Analysis and Integrated Assessment (WATERMATEX 2011), 20-22 june 2011, San Sebastian, Spain.

- Audenaert, W.T.M., Vandierendonck, D., Van Hulle, S., Nopens, I., 2012. Assessing WWTP effluent organic matter conversion during ozone and UV/H_2O_2 treatment using multiple surrogates, International Ozone Association (IOA) International Conference on Ozone and Related Oxidants to Meet Essential Human Needs, 4-6 June 2012, Toulouse, France

- Audenaert, W.T.M., Vandierendonck, D., Van Hulle, S., Nopens, I., 2012. Assessing WWTP effluent organic matter conversion during ozone and UV/H_2O_2 treatment using multiple surrogates, 6th International Conference on Oxidation Technologies for Water and Wastewater Treatment, 7-9 May 2012, Goslar, Germany

MSc. Thesis

- Audenaert, W.T.M., 2008. Zuivering van het douchewater van het Dranouter Festival, University College West Flanders, Belgium

Miscellaneous

- Member of International Water Association (IWA) since 2008
- Member of B-IWA (Belgian IWA division) since 2010
- Member of International Ozone Association (IOA) since 2010
- Member of International UV Association (IUVA) since 2011
- Reviewer for Water Science and Technology, Water Science and Technology: Water Supply and various international conferences
- Responsible for websites of BIOMATH (updates), YWP BENELUX Conference (updates), WWTmod2014 Conference (design and updates) and ENBICHEM (design and updates)

In my opinion, the secret of happiness is the recognition of luck